NASA Conference Publication 3233

1993 Shuttle Small Payloads Symposium

Proceedings of a conference held
at the Holiday Inn
Annapolis, Maryland
October 4 - 7, 1993

National Aeronautics and
Space Administration

**Scientific and Technical
Information Branch**

1993

CONTENTS

CONTENTS (CONTINUED)

CONTENTS (CONTINUED)

CHARACTERIZATION OF FLUID PHYSICS EFFECTS ON CARDIOVASCULAR RESPONSE TO MICROGRAVITY [G-572]

George M. Pantalos, M. Keith Sharp, Stewart J.Woodruff, Richard D. Lorange
University of Utah
Salt Lake City, Utah 84103

Thomas E. Bennett
Bellarmine College
Louisville, Kentucky 40205

Jan J. Sojka, Mark W. Lemon
Utah State University
Logan, Utah 84322

ABSTRACT

The recognition and understanding of cardiovascular adaptation to spaceflight has experienced substantial advancement in the last several years. In-flight echocardiographic measurements of astronaut cardiac function on the Space Shuttle have documented a 15% reduction in both left ventricular volume index and stroke volume with a compensatory increase in heart rate to maintain cardiac output. To date, the reduced cardiac size and stroke volume have been presumed to be the consequence of the reduction in circulating fluid volume following diuresis and other physiological processed to reduce blood volume within a few days after orbital insertion. However, no specific mechanism for the reduced stroke volume has been elucidated. The following investigation proposes the use of a hydraulic model of the cardiovascular system to examine the possibility that the observed reduction in stroke volume may, in part, be related to fluid physics effects on heart function. The automated model is being prepared to fly as a GAS payload.

The experimental apparatus consists of a pneumatically actuated, elliptical artificial ventricle connected to a closed-loop, hydraulic circuit with compliance and resistance elements to create physiologic pressure and flow conditions. The ventricle is instrumented with high-fidelity, acceleration-insensitive, catheter-tip pressure transducers (Millar Instruments) in the apex and base to determine the instantaneous ventricular pressures and ΔP_{LV} across the left ventricle (LVP_{apex} - LVP_{base}). The ventricle is also instrumented with a flow probe and pressure transducers immediately upstream of the inflow valve and downstream of the outflow valve. The experiment will be microprocessor controlled with analog signals stored on an FM data tape recorder. By varying the circulating fluid volume, ventricular function can be determined for varying preload pressures with fixed afterload pressure. Pilot experiments on board the NASA KC-135 aircraft have demonstrated proof-of-concept and provided early support for the proposed hypothesis. A review of the pilot experiments and developmental progress on the GAS version of this experiment will be presented.

INTRODUCTION

The objective of the proposed research is to clarify the role of fluid physics effects on cardiovascular response to the microgravity environment using physical and analytical modeling techniques. Specifically, the role of the gravitationally-dependent, intraventricular hydrostatic pressure difference in ventricular filling will be investigated. The proposed investigation is stimulated by the results of in-flight echocardiographic measurements of astronaut cardiac function on the Space Shuttle[1]. These echocardiographic measurements have documented a 15% reduction in both left ventricular volume index and stroke volume with a compensatory increase in heart rate to maintain cardiac output. To date, the reduced cardiac size and stroke volume have been presumed to be the consequence of the reduction in circulating fluid volume following diuresis and

other physiologic processess to reduce blood volume within a few days after orbital insertion.[2,3] However, no specific mechanism for the reduced stroke volume has been elucidated. The following investigation proposes the use of a hydraulic model of the cardiovascular system to examine the possibility that the observed reduction in stroke volume may, in part, be related to fluid physics effects on heart function.

Many biophysical factors influence the filling of the heart during diastole. These factors include (1) the atrial pressure, (2) the inertia energy of the blood as it enters the ventricle, (3) the transmural pressure gradient, (4) the diastolic compliance of the myocardium and the passive, elastic recoil attributed to the "parallel elastic element" connective tissue mesh around the myofibrils,[4,5] and (5) a factor recently recognized,[6] a gravitational acceleration-dependent hydrostatic pressure difference, ΔP, that exists in the ventricles due to their size and anatomic orientation to the local gravitational axis. This investigation is limited to an examination of left ventricular function although the same concepts apply to right ventricular function. Hence, only the hydrostatic pressure difference in the left ventricle, ΔP_{LV}, will be considered in the proposed research. This hydrostatic ΔP_{LV} linearly increases the intraventricular pressure when progressing from the ventricular base to apex (Figure 1). Consequently, the linearly increasing ΔP_{LV} acts to augment the diastolic filling of the heart by increasing the elongation of the elastic, contractile, and viscous elements of the ventricular wall. The hydrostatic ΔP_{LV} is the product of the blood density ($\rho_{blood} = 1.06$ gm/cm^3), gravitational acceleration constant ($g = 980$ cm/sec^2), and the change in fluid column height from the reference point (Δh_{LV} cm). MRI scanning data has indicated that a typical Δh_{LV} for an average adult male left ventricle is approximately 7 cm. This Δh_{LV} results in a ventricular base-to-apex ΔP_{LV} of $\approx$ 7300 dynes/cm^2 ($\approx$ 5.5 mm Hg) for an average effect of between 2 to 3 mm Hg. Consequently, based purely on fluid physics considerations, in the absence of gravity where ΔP_{LV} becomes zero one would predict a reduced ventricular filling and therefore reduced stroke volume resulting in a rightward shift of the ventricular function curve (output vs. ventricular filling pressure) of 2 to 3 mm Hg. Hence, the investigators have hypothesized that the absence of ΔP_{LV} in the microgravity environment of spaceflight may account, in part, for the 15% reduction in stroke volume reported for astronauts while in orbit. An experimentally observed shift of ventricular function curve to the right during exposure to the microgravity environment would support the hypothesis of this experiment.

The objective of this research program will be addressed by the collection of cardiac performance data from a flight-worthy hydraulic model of the cardiovascular system in the extended duration, higher quality microgravity environment of orbital flight as a Get Away Special payload for the anticipated follow-up program. The results will influence the conduct and direction of future investigations into cardiovascular response to microgravity by recognizing the role of fluid physics effects. The investigators anticipate that the development of a three-dimensional, anatomically consistent hydraulic model will expand into other areas of investigation, such as changes in regional hemodynamics and fluid shifting with changes in posture (e.g. vertical vs. launch position). This study will advance the understanding of cardiovascular response to the environments experienced in manned spaceflight.

DEVELOPMENTAL PROGRESS AND METHODS

REVIEW OF THE PILOT EXPERIMENT CARDIOVASCULAR MODEL

Proof-of-concept for the proposed GAS payload was achieved by flying a pilot experimenton board the NASA KC-135 aircraft. The results and lessons learned from the pilot experiments have guided the development of the GAS version of the experiment. The hydraulic model of the cardiovascular system for the pilot experiment consisted of a pneumatically actuated, elliptical artificial ventricle (UTAH-100 human version left ventricle,[7,8] 5cm x 6cm x 10cm) with prosthetic

mitral and aortic valves (Medtronic Hall™, Medtronic, Inc.) and a highly compliant, pumping diaphragm. The inflow and outflow ports were located at the superior end of the long-axis of the ventricle to approximate the anatomy of the natural left ventricle (Figure 2). A compliant artificial atrium was attached upstream of the inflow port of the ventricle. The ventricle was connected to a closed-loop, hydraulic circulation simulator (an adapted version of the Penn State mock circulation[9]) with compliance and resistance elements to create physiologic pressure and flow conditions (Figure 3). The mock circulation was filled with a blood-analog fluid of 40% glycerin in water to approximate the viscosity of whole blood (3.4 cP @ 115 sec^{-1}). The mock circulation was fixed to a stainless steel tray (1m x 1.5m x .1m) which, in turn, was bolted to a floor-mounted support frame secured to the floor of the NASA KC-135 research aircraft.

The ventricle was instrumented with high fidelity, acceleration-insensitive, catheter-tip pressure transducers (Millar Instruments) in the apex and base to determine the instantaneous ventricular pressures and ΔP_{LV} across the left ventricle (LVP_{apex} - LVP_{base}). When the ventricle was positioned at 45° to the horizon to mimic the anatomic orientation of the human left ventricle, the Δh_{LV} for the UTAH-100 left ventricle was 6.3 cm, resulting in a calculated base-to-apex ΔP_{LV} of 4.9 mm Hg. The ventricle was also instrumented with flow probes (Transonic Systems) and pressure transducers (Millar Instruments) immediately upstream of the mitral valve (inflow) and downstream of the aortic valve (outflow, see Figure 2). Pressure transducers and flow probes and their calibration signals were calibrated against reference standards prior to shipment of the hardware to Ellington Field and upon return to Salt Lake City. The electrical calibration reference signals were used for in-plane checks of probe calibration. The shearing rate profile of the glycerin/water blood-analog fluid was also verified prior to departing Salt Lake City using a cone-and-plate viscometer (Brookfield Engineering, Model LVTDV-IICP).

The associated recording equipment and heart controller was rack-mounted in a chassis that was fixed to the aircraft floor. The equipment in the chassis included: a sixteen-channel digital data tape recorder (TEAC, Model RD-200T); a two-channel flow meter (Transonic Systems); eight transducer pre-amplifiers (Gould); an eight channel thermal pen recorder (Gould); and an artificial-heart controller (CardioWest Technologies) with a regulator and two tanks of compressed air. Accelerometers (PCB Piezotronics, Kistler) to measure the vertical axis (G_z) acceleration were mounted on the instrumentation chassis and the circulation simulator tray. The instrumentation chassis was five feet tall and weighed 441 pounds; the hydraulic simulator of the cardiovascular system with mounting tray and cart was three feet tall and weighed 160 pounds.

The in-flight test protocol specified the examination of ventricular function with the heart rate fixed at 90 beats per minute to correspond to the elevated heart rates reported for orbital flight.[2,3] The percentage of the cardiac cycle spent in systole was 43% and the ventricular driveline pressure delivered to inflate the diaphragm was 190 mm Hg. This driveline pressure was sufficient to fully eject whatever stroke volume the preload conditions created while the ventricle pumped against a mean afterload pressure of 95 mm Hg during stable, 1-G flight. Since this mode of artificial ventricular control (referred to as partial-fill, full eject) results in the same end-systolic volume at a fixed heart rate, any changes in the cardiac output are due to a change in stroke volume and, therefore, diastolic function. The circulating fluid volume of the mock circulation could be adjusted to create different preload conditions on the ventricular function curve. In-flight, the initial circulating fluid volume was adjusted to establish a stable, 1-G baseline near the peak of the ventricular function curve. After each set of 10 parabolas, 60 ml of the blood-analog fluid was withdrawn from the circulating fluid volume to establish a new, lower preload condition. The pressure, flow, and acceleration signals were continuously recorded to document the hemodynamic changes during the transition from 1-G to microgravity, during the period of microgravity, and during the transition from microgravity back to 1-G (including the period of ≈ 1.8-G hypergravity). The mock circulation system stabilized at a new operating condition in approximately 5 seconds, so steady system function was achieved for the majority of the 20 second duration microgravity exposure period. Data from 10 consecutive beats at equilibrium test

conditions were used to create ventricular function curves for each of the test conditions as well as to examine the end-diastolic pressure difference between the left ventricular base and apex.

The pilot experiments on board the NASA KC-135 have demonstrated proof-of-concept and provided early support for the proposed hypothesis as the predicted rightward shift of the ventricular curve was observed[6]. However, it was learned from the initial KC-135 experiments that (1) the ability to test over a range of preload conditions was limited, (2) aircraft vibration artifact diminished the quality of the data obtained, and (3) the hydraulic model needed refinement as indicated by the lack of rigorous physiologic authenticity of the instantaneous pressure and flow waveforms. All of these lessons learned have indicated the need for additional model development for the GAS version of the experiment.

GAS PAYLOAD DEVELOPMENT

The proposed research program requires the performance of three main tasks: (1) refinement of the cardiovascular system hydraulic model using both analytical modeling and physical testing (2) automating the function of the cardiovascular system hydraulic model, and (3) modifying the experimental apparatus to be compatible with the weight, space and operational specifications for a GAS payload.

The tasks pertaining to the refinement of the cardiovascular system hydraulic model are driven by two criteria:

(1) improving the dynamic response of the model and the physiologic authenticity of the instantaneous outflow pressure and flow waveforms (as validated by comparing the resulting input impedance spectra to the human spectra[10]); and

(2) accommodating the elements of the hydraulic model within the space limitations (19.75" diameter x 28.25" height) and weight limitation (200 pounds) for a Get Away Special payload canister.

Improving the dynamic response of the model and the physiologic authenticity of the instantaneous outflow pressure and flow waveforms will be accomplished by:

(1) reducing the inertance in the hydraulic model by shortening the circuit length as much as possible and eliminating bends with small radii;

(2) addition of more circuit elements, such as a characteristic resistor in the proximal section of the outflow conduit; and

(3) changing the systemic resistance element from a static to a dynamically varying elements with feedback and control so as to maintain a constant mean outflow pressure regardless of the test condition.

Proposed changes to the hydraulic model will first be evaluated using an analytical modeling method described below which will predict whether the physiologic authenticity will be improved. Ground-based tests will then acquire outflow pressure and flow waveforms for the computation of the input impedance spectrum[10] to verify the prediction of the analytical modeling assessment.

Accommodating the elements of the hydraulic model within the space and weight limitations for a Get Away Special payload canister will be accomplished by:

(1) reducing the length of the hydraulic circuit;

(2) reducing the size of the compliance chambers;

(3) integrating the compliance and resistance elements, and other components when possible; and

(4) automatic changes of the circulating fluid volume with a microprocessor controlled, miniature infusion/withdrawal pump

The feasibility of approaches 1 and 2 has recently been demonstrating by (1) reducing the length of the circuit used in the pilot project hydraulic simulator (shown in Figure 3) and eliminating bends with small radii and (2) reducing the size of the compliance chambers as shown in Figure 4. By reducing the length of the hydraulic circuit, the physiologic authenticity of the outflow pressure and flow waveforms was dramatically improved as shown in Figure 5 and verified by a comparison of the input impedance spectra. Significant weight and size reduction of the compliance chambers was achieved by substituting the leaf spring mechanism with a coil spring mechanism while maintaining the desired physiologic compliance. The weight was reduced from 13.6 pounds to 7.7 pounds and the size was reduced from approximately 18x7x12 inches to 7x7x12 inches.

Analytical Modeling of the Hydraulic Model

Candidate changes to the cardiovascular system hydraulic model will be represented by lumped parameter models. These lumped parameter models will be tested by computer to find the best match of impedance to the human circulation. The strategy for choosing model configurations will be to optimize the response of the model, not to duplicate existing mock circulation systems. This will ensure that authenticity will be achieved. In general, for each element in the analytical model, one point on either the impedance modulus or phase plot may be matched exactly. The more elements in the model, the more perfect the match, but each matching point chosen represents an additional nonlinear algebraic equation which must be solved for the values of the elements. Poles and zeros are the easiest points for which to solve since many solutions of this type are available from the field of electrical engineering. However, modulus and phase at harmonics of the heart beat frequency are more relevant matching points for models of the circulation because these are the points for which data are available or can be calculated with Fourier analysis. Solutions derived preliminary to this proposal used the latter method. For models with more than a few elements, an iterative solution becomes necessary. A multi-dimensional Newton-Raphson iteration algorithm has already been written and verified for solution of element values for models with up to five elements[12]. This method has the advantage of fast convergence if a good initial estimate for the solution can be input. The number of dimensions which the algorithm will accommodate is not limited, although the solution becomes unstable for poor initial estimates on systems with many elements. Bounds on the solution were imposed and the magnitude of the incremental steps was controlled to promote stability. The Downhill Simplex method was used to provide good initial guesses and to verify the final solution. This method has the advantage of good stability, but the disadvantage of slow convergence. These two algorithms will form the basis for solutions for more complex models.

Solutions are not needed for extremely large numbers of elements, since physical systems representing complex analytical models would become difficult to adjust and operate. It is anticipated that a good impedance match can be attained with less than ten elements. Arriving at the optimum configuration of elements is largely a trial and error process, guided by experience. For each trial configuration, descriptive simultaneous algebraic equations must be written. Solutions are then obtained iteratively.

A numerical model will also be developed of the actual performance of the improved mock circulation system after it is finalized. Ideally, the mock circulation system response will conform to that of the lumped parameter model derived above, although small deviations are to be expected. This as-built computer model will be useful for simulation and prediction of device performance

when connected to the mock circulation system. The same solution algorithms as discussed above will be used for this task. Again, the common goal of the proposed research plan is to utilize measured human vascular input impedance as a standard for the development of advanced analytic and hydraulic models. This approach has proven successful for the Co-P.I.[11,12] and has recently be corroborated by other investigators.[13]

GAS Payload and Protocol Description

Experimental methods to be employed for the proposed GAS payload will build on the methods developed for the pilot experiments. The revised hydraulic model of the cardiovascular system will use the same pneumatically actuated artificial ventricle used for the pilot experiment (Figure 4). A compliant artificial atrium will be attached immediately upstream of the inflow port of the ventricle. The ventricle will be connected to revised compliance and resistance elements (as mentioned in the previous section, Figure 4) to create improved physiologic pressure and flow conditions. The mock circulation will be filled with a blood-analog fluid of 40% glycerin in water to approximate the viscosity of whole blood (3.4 cP @ 115 sec^{-1}). A microprocessor-controlled peristaltic pump will infuse or withdraw fluid on command to create difference levels of circulating fluid volume and ventricular preload conditions to allow the generation of a ventricular function curve from the in-flight data.

The ventricle will be instrumented with high fidelity, acceleration-insensitive, catheter-tip pressure transducers (Millar Instruments) in the apex and base to determine the instantaneous ventricular pressures and ΔP_{LV} across the left ventricle (LVP_{apex} - LVP_{base}). The ventricle will also be instrumented with pressure transducers (Millar Instruments) immediately upstream of the mitral valve (inflow) and downstream of the aortic valve (outflow) and a flow probe (Transonic Systems) downstream of the outflow valve. Pressure transducers and flow probes and their calibration signals will be calibrated pre and post-flight against reference standards and the shearing rate profile of the glycerin/water blood-analog fluid will also be verified prior to filling the hydraulic model of the cardiovascular system.

Analog data will be recorded on a data tape recorder (TEAC, Model HR-30). A flow meter signal conditioning board (Transonic Systems) and pressure transducer pre-amplifiers (Millar) will be incorporated into the payload. A miniaturized artificial-heart driver (Heimes™ Portable Heart Driver, Symbion) will control the funcition of the artificial ventricle. An accelerometer (Endevco) to measure the vertical axis (G_z) acceleration will be mounted on the hydraulic model chassis.

The experiment package will be turned by a switch in the aft flight deck during a quiescent period of dead-drift gravity gradient mode. The in-flight test protocol will specify the examination of ventricular function with the heart rate fixed at 90 beats per minute to correspond to the elevated heart rates reported for orbital flight. The percentage of the cardiac cycle spent in systole will be 43% and the ventricular driveline pressure delivered to inflate the diaphragm will be 190 mm Hg. This driveline pressure will be sufficient to fully eject whatever stroke volume the preload conditions create while the ventricle pumps against a regulated mean afterload pressure of 95 mm Hg. Since this mode of artificial ventricular control (referred to as partial-fill, full eject) results in the same end-systolic volume at a fixed heart rate, any changes in the cardiac output are due to a change in stroke volume and, therefore, diastolic function. The circulating fluid volume of the mock circulation will be adjusted to create different six different preload conditions on the ventricular function curve by graded withdrawals and infusions of circulating fluid. In-flight, the initial circulating fluid volume will be adjusted to establish a stable baseline near the peak of the ventricular function curve. After three minutes of functioning at the established preload condition, a predetermined amount of the blood-analog fluid will be withdrawn from the circulating fluid volume to establish a new, lower preload condition. The pressure and flow signals will be continuously recorded to document the hemodynamic changes during the transition from one preload condition to the next. A brief "on-off-on" sequence of hydraulic model operation will be

used to document the mean circulatory filling pressure of the model in the different acceleration test environments. The ventricular function test will be repeated pre and post-flight on the ground so that a the 1-G data set can be compared to the in-flight data.

Data Reduction and Analysis

Analog pressure, flow, and acceleration signals from all ground and in-flight experiments will be recorded on FM data tape cassettes. Data reduction and analysis will proceed by two methods. First, the temporal changes in the recorded variables will be presented in chart recording format achieved by playing the tape back into a high fidelity, thermal array chart recorder (Graphtec Mark 12 Data Management System DMS1000). Second, mean and dynamic values of recorded signals will be determined by first playing back the tape back into an analog-to-digital converter and storing the digitized waveforms on a computer (GW Instruments MacADIOS ADPO A/D Converter, Macintosh IIci Computer, sampling rate of 716 Hz.) and then recalling the stored digital signals for subsequent manipulation to calculate desired values. Mean values to be determined from the stored digital signals include inflow pressure, left ventricular end-diastolic pressures (LVEDP) at the base and apex, the difference between the LVEDP at the base and apex, the mean outflow pressure, the mean outflow, and the stroke volume. These values will be determined for ten consecutive beats which occur after the response of the system to a change in gravitational acceleration has decayed The mean and standard deviation of the values will then be determined. A t-test will be used to assess the presence of statistically significant differences ($p<0.05$) between corresponding variables from the 1-G and μ-G test environments.

A linear regression, including correlation coefficient and significance level, will be determined for the ventricular function curves (stroke volume vs. $LVEDP_{base}$) from the 1-G and μ-G test environments. Tests of statistical significance of the differences between the zero-intercepts and the slopes of the regression lines will also be conducted.

The digitized outflow pressure and flow signals will also undergo harmonic decomposition using Fourier analysis to determine the input impedance spectrum (i.e., frequency dependent fluid resistance to fluid flow, where Z = oscillatory pressure/oscillatory flow) from the 1-G and μ-G test environments. The presence of statistically significant differences between impedance spectra will be tested using analysis of variance with repeated measures techniques.

REFERENCES

1) Bungo MW, Charles JB, Riddle J, Roesch J, Wolf DA, Seddon R. Echocardiographic Investigation of the Hemodynamics of Weightlessness. *J Am Col Cardiol* 1986; 7(2): 192A.

2) Bungo MW. The Cardiopulmonary System. In Nicogossian AE, Huntoon CL and Pool SL (ed): *Space Physiology and Medicine*. 2nd Ed. Lea & Febiger, 1989, 179-201.

3) Charles JB, Lathers CM. Cardiovascular Adaptation to Spaceflight. *J Clin Pharmacol* 1991; 31:1010-1023.

4) Yellin EL, Sonnenblick EH, Frater RWM. Dynamic Determinants of Left Ventricular Filling: An Overview. in J Baan, AC Arntaenius and EL Yellin (ed): *Cardiac Dynamics*, Martinus Nijhoff Publishers, 1980.

5) Sonnenblick EH. The Structural Basis and Importance of Restoring Forces and Elastic Recoil for the Filling of the Heart. *Euro Heart J* 1980; 1(A Supplement); 107-110.

6) Pantalos GM, Bennett TE, Bennett BS, Sharp MK, Schurfranz T, Everett SD: The effect of gravitational acceleration on ventricular filling. Diastolic ventricular function in microgravity and 1-G: Preliminary results. in NASA Publication: Recent Advances In Life Sciences, ed by FA Kutyna (in press) 1993.

7) Robison P, Pantalos G, Olsen D. Pneumatically Powered Blood Pumps Used as a Bridge to Cardiac Transplantation. *Critical Care Nursing Clinics of North America* 1989; Vol. 1, No. 3, pp. 485-494.

8) White RK, Pantalos GM, Olsen DB. Total Artificial Heart Development at the University of Utah: The Utah-100 and Electrohydraulic Cardiac Replacement Devices. in S Quaal (ed): *Cardiac Mechanical Assistance Beyond Balloon Pumping*, Mosby-Year Book, 1992, 181-193.

9) Rosenberg G, Phillips WM, Landis DL, Pierce WS. Design and Evaluation of the Pennsylvania State University Mock Circulatory System. *ASAIO J* 1981; 4(2):41-9.

10) Nichols WW, Conti CR, Walker WE, Milnor WR. Input Impedance of the Systemic Circulation in Man.*Circulation Research* 1977; 40(5):451-458.

11) Forbes L, Sharp MK. Preliminary Validation of a Model of Human Systemic Circulation. *Abstracts of First World Congress of Biomechanics*, 1990.

12) Sharp MK. Physical Modelling of the Human Circulatory System for Cardiovascular Device Testing. *Abstracts SIAM App Dynamical Systems*, 1992.

13) Ruchti TL, Brown RH, Jeutter DC, Feng X. Identification Algorithm for Systemic Arterial Parameters with Application to Total Artificial Heart Control. *Annals of Biomedical Engineering* 1993; 21:221-236.

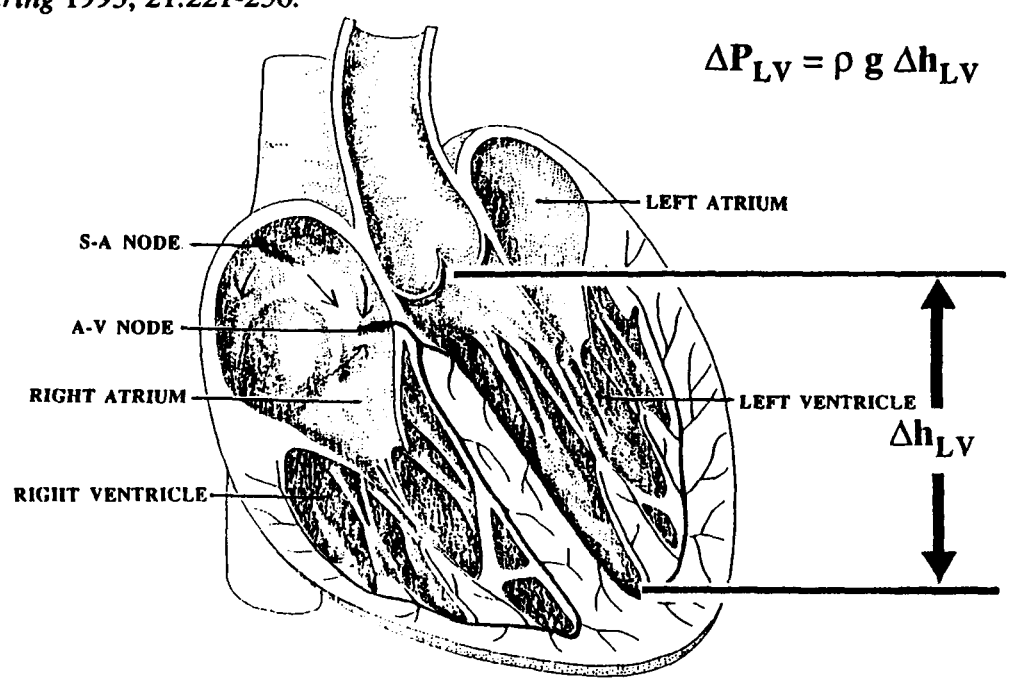

Figure 1. The intraventricular hydrostatic pressure difference, ΔP_{LV}, arises from the difference in height between the left ventricular base and apex as indicated by Δh_{LV}. This pressure difference is calculated using the equation: $\Delta P_{LV} = \rho g \Delta h_{LV}$, where ρ is the blood density (ρ_{blood} =1.06 gm/cm^3), g is the gravitational acceleration constant (g = 980 cm/sec^2), and Δh_{LV} is the change in fluid column height from the reference point in cm.

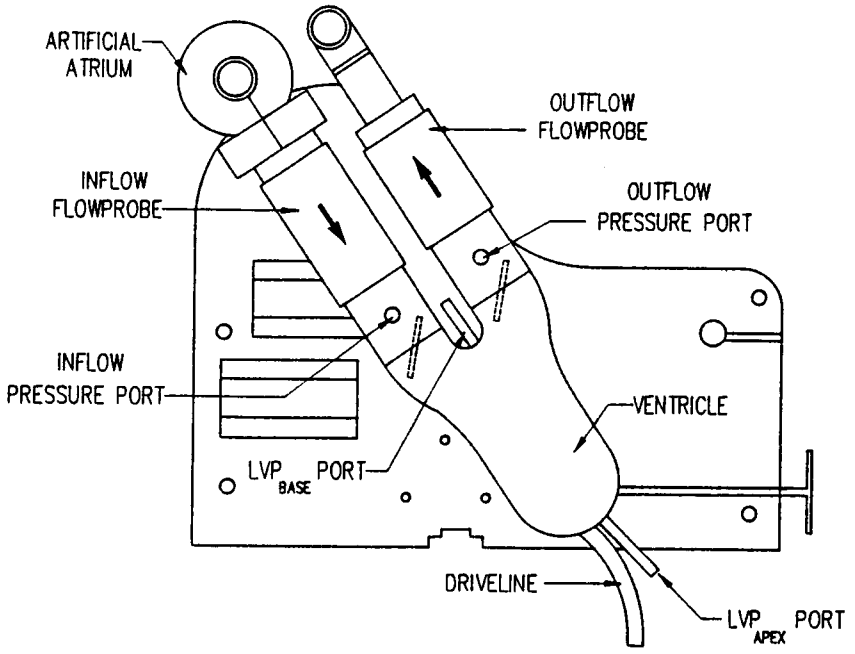

Figure 2. The artificial left ventricle used in the pilot experiments is shown positioned in the 45°, "1-G anatomic" orientation. The schematic indicates the location of the flow probes, pressure catheter introducer ports and other details. The arrows indicate the direction of flow through the ventricle.

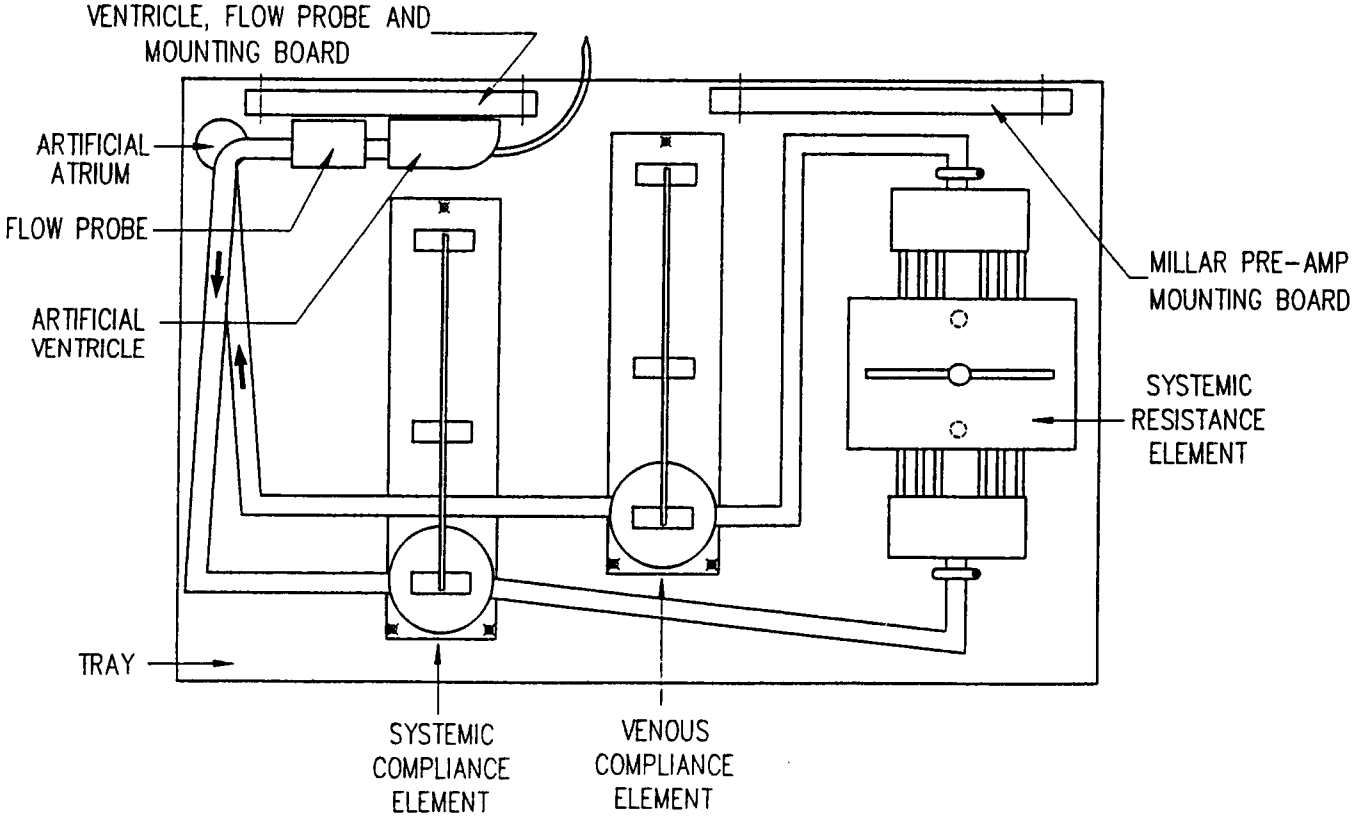

Figure 3. The hydraulic model of the cardiovascular system used in the pilot experiments is shown. The schematic indicates the location of the resistance and compliance elements as well as the artificial atrium and ventricle. The arrows indicate the direction of flow through the circulation simulator.

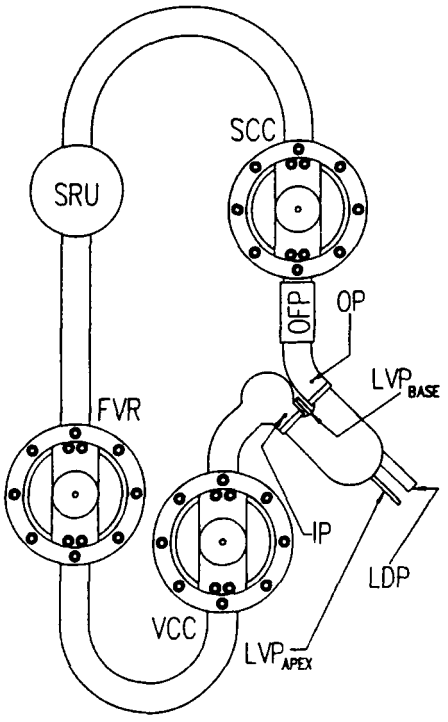

GAS PAYLOAD G-572 CONTENTS

COMPONENT	MAX POWER REQ.	WEIGHT LBS/(KG)
SCC=SYSTEMIC COMPLIANCE CHAMBER	- 0 -	7.7/(3.5)
SRU=SYSTEMIC RESISTANCE UNIT	TBD	2.0/(0.9)
PHD=PNEUMATIC HEART DRIVER	13.2V, 4A	13.2/(6.0)
FVR=FLUID VOLUME RESERVOIR	TBD	7.7/(3.5)
VCC=VENOUS COMPLIANCE CHAMBER	- 0 -	7.7/(3.5)
AH =ARTIFICIAL HEART	- 0 -	0.4/(0.2)
PRESSURE PRE-AMPS (5)	5.4V ea, 3.8 A 27V total	0.9/(0.4) ea 4.5/(2.0) total
FLOW PROBE	±5V, 200 mA	0.2/(0.1)
FLOW PROBE INTERFACE BOARD	±15V, 650 mA	0.5/(0.2)
DATA TAPE RECORDER	9V, 80 mA	1.3/(0.6)
EXPERIMENT CONTROLLER	TBD	TBD
BATTERIES	TBD	TBD
PRESSURE CATHETERS (5)	- 0 -	0.1/(.05)ea 0.5/(.25)total
AH DRIVELINE	- 0 -	0.2/(0.1)
CIRCULATING FLUID	- 0 -	2.2/(1.0)
CIRCUIT CONDUITS	- 0 -	1.1/(0.5)
CIRCULATION CONTAINMENT CHAMBER	- 0 -	TBD
ACCELEROMETER	TBD	TBD
A/D CONVERTOR & DIGITAL STORAGE	TBD	TBD
TEMPERATURE SENSOR	TBD	TBD
PASSIVE THERMAL INSULATION	TBD	TBD
INFUSION/WITHDRAWAL PUMP	TBD	TBD
FLUID RESERVOIR CONTAINER	TBD	TBD
STEPPER MOTOR	5V, 2A	TBD
HEATING ELEMENT	TBD	TBD
GCD INTERFACE	TBD	TBD
ELECTRICAL PLUMBING	- 0 -	TBD
BUMPERS	- 0 -	TBD
MOUNTING HARDWARE	- 0 -	TBD

Figure 4. The modified hydraulic model to demonstrate the feasibility of improving the physiologic authenticity and reducing the size of the pilot experiment hydraulic model is present along with the estimated weight and power budget for the GAS version of the experiment.

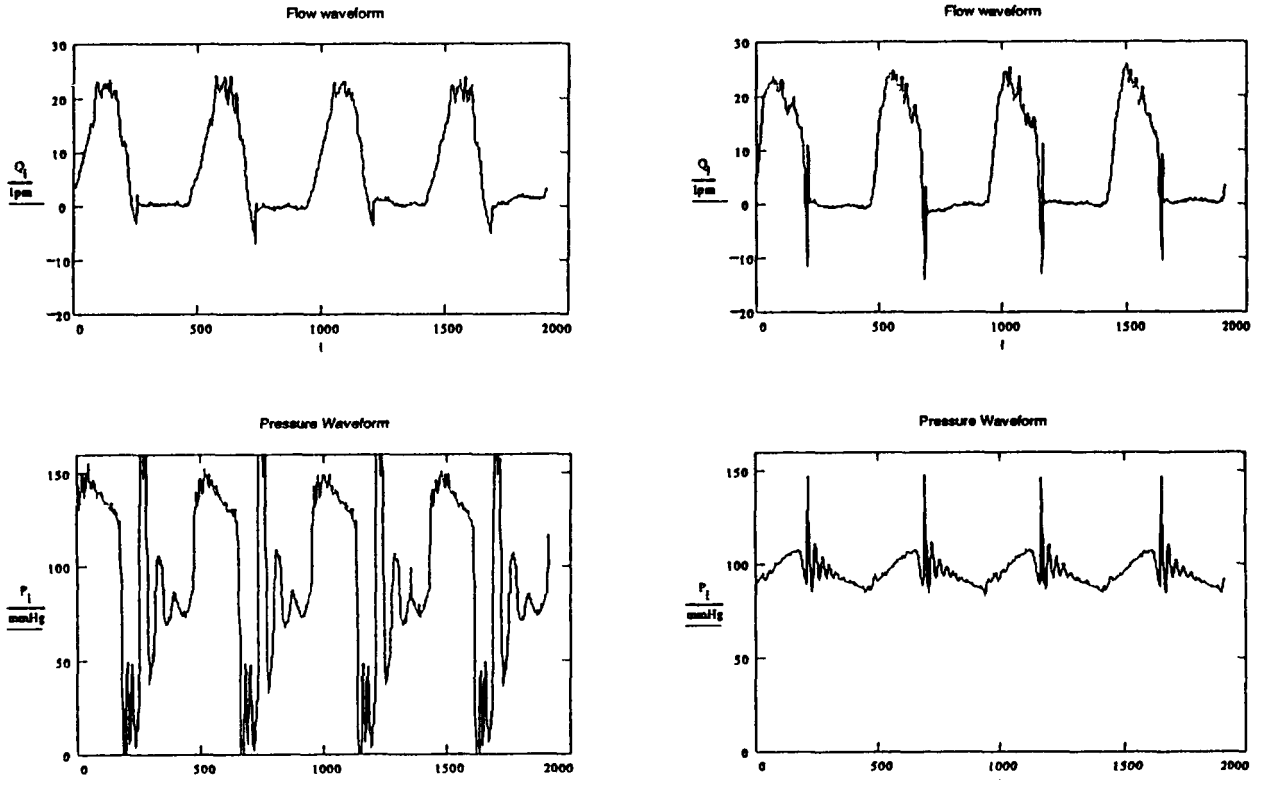

Figure 5. An example of the pilot experiment hydraulic model outflow pressure (bottom) and flow (top) waveforms are presented on the left for comparison to the improved outflow pressure and flow waveforms of the refinement feasibility hydraulic model presented on the right. The waveforms on the right are much more physiologic in appearance.

CALIFORNIA STUDENT GET AWAY SPECIAL PAYLOAD GAS-450

presented at

1993 Shuttle Small Payload Symposium, Goddard Space Flight Center
4-7 October 1993

Space Information Laboratories
P.O. Box 5090
Vandenberg AFB, CA 93437

A non-profit company dedicated to student "hands-on" education. Consists of professional engineers, scientists and technicians at Vandenberg AFB and the California Central Coast Community.

Authors

Glen Ray, GAS-450 Payload Manager
Edmund Burke, GAS-450 Technical Director & SIL Founder
Marty Waldman, GAS-450 Program Manager

1.0 ABSTRACT

The California **Student** Get Away Special Payload GAS-450, recently went into orbit on the STS-57 Mission, Space Shuttle Endeavour, 21 June 1993, 6:14 AM and landed on the 29 June 1993 at Kennedy Space Center (KSC). Fifty students (Figure 1, Ages 7 to 18) from 13 California Central Coast Schools and one in San Francisco designed and built 13 active experiments (6 modules) for this mission. Preliminary analysis of our **completely reusable payload bus system** indicated that the structure, power system, microprocessor and sensor systems in each experiment module worked flawlessly. The experiments themselves performed exceptionally well with a 60 % success ratio. The students are thoroughly documenting their own experiments and results via a standard research paper guideline generated by the GAS-450 technical staff. If you would like to review any one or all of these papers (13) please write to the SIL address above. Lessons learned (program management and technical) are documented at the end of the paper. If any other organization needs payload/experiment development or NASA documentation assistance, then please contact us. We can help make your idea a space tested reality.

Three years of intense effort culminated on 3 February 1993, the GSFC field operations team at Kennedy Space Center performed the final pressure decay and electrical tests upon the fully integrated GAS-450 flight canister. Subsequently, the payload was integrated with its parent GAS Bridge Assembly in mid-February and the bridge was transfered to the KSC orbiter team in late February 1993. The STS-57 mission orginally scheduled to launch on the 29 April 1993 slipped until 21 June 1993. Our Payload shared the cargo bay with ten other GAS Canisters, the EUREKA experiment, the SHOOT experiment, and the SPACEHAB-1 module. The SIL technical staff retrieved the GAS-450 payload after flight from the NASA Spin Test Facility at KSC and shipped it back to California on the 22 July 1993 for student analysis at Allan Hancock College this summer.

2.0 INTRODUCTION

This payload was conceived to encourage young people's growth through practical problem

solving. The challenge is to enclose several thousand pounds of space science into a two hundred pound canister. Sixty percent of the GAS-450 payload is dedicated to the necessary hardware, structures, and electrical systems required to support fifteen science packages. Six science modules with their enclosed microgravity experiments represent the remaining forty percent of the payload mass. Thirteen science teams were recruited three years ago via a short video and application form circulated through K-12 schools in Santa Barbara and San Luis Obispo County. Forty proposals were chosen from the hundreds of applications submitted. Each of the forty team leaders gave an oral presentation to an assemblage of parents, peers, and payload technical staff - who then selected the thirteen flight science packages. Thirteen experiment teams accomplished the design, development, and test schedules required to meet NASA's hardware and paperwork requirements. The following miniaturized masterpieces of basic space science are now flight tested.

Exp. No.	Experiment Title	Responsible School
01	Benzoic Acid Crystals	Cabrillo High School
02	On Orbit Fluid Transfer	Cathedral School for Boys
03	Bacteria Growth	Lompoc High School
04	Magnets in Space	Arroyo Grande High School
05	Bacteria, Radiation affects	Fesler Elementary School
06	Zero Point Energy	Lompoc High School
07	Electrolysis in Space	San Luis Obispo High School
08	Adhesives in Space	San LuisObispoHigh School
09	Osmosis	Pine Grove Elementary School
10	Seeds in Space	Paulding Middle School
11	Rock Crystals	Orcutt Junior Middle School
12	Fluid Behavior in space	Vandenberg Middle School
13	Silver Crystals	May Grisham Elementary School
14	Radiation Detector	SIL Staff
15	Accelerometer	SIL Staff

Four of the science modules contain two experiments each, the other two modules contain three and four experiments, respectively. Each module contains a locally designed and fabricated microprocessor to activate and sequence experiment functions, while simultaneously collecting and storing sensor data. The microprocessors and experimental apparatus in each of the six modules are connected to the GAS-450 power distribution system via umbilical cables.

3.0 EXPERIMENT DESCRIPTIONS

The GAS-450 payload is composed of thirteen experiments packaged into six self-contained modules (Fig. 2). The experiments are designed and developed by California Central Coast elementary, middle, and high schools. A technical staff of SIL engineers, scientists and technicians at Vandenberg AFB and the local community invented the GAS-450 payload bus system and are supporting the student experimenters.

Our principle objective of flying this payload is to educate young students about space science and engineering through hands-on experience. These young people are excited and have expended an enormous amount of energy developing their scientific and engineering skills.

The experiments are contained within a standard sealed GAS Canister purged with one atmosphere dry nitrogen. This payload has been classified Class B (Benign) in accordance with policy set forth in JSC TA-91-029.

3.1 EXPERIMENT OBJECTIVES

The scientific objectives of each experiment follows.

MODULE 1 - Cabrillo High School & Cathedral School for Boys
"BENZOIC ACID CRYSTAL GROWTH" & "ON-ORBIT FLUID TRANSFER EXPERIMENT"

EXPERIMENT 1
"BENZOIC ACID CRYSTAL GROWTH"

The objective of this experiment is to investigate the solidification/crystallization process of a Benzoic Acid Crystal. An earth grown Benzoic Acid crystal was heated to it's melting point once in microgravity, then allowed to reform and cool. The resulting "SPACE CRYSTAL" will be compared to earth grown crystals after recovery. Because convection and buoyancy effects are essentially eliminated in space, it should be possible to produce more perfect crystals.

EXPERIMENT 2
"ON-ORBIT FLUID TRANSFER EXPERIMENT"

The experiment plans to demonstrate the feasibility of on-orbit transfer of cryogens using an ullage exchange technique. Ullage exchange is the process of transferring gases from a receiver tank to a supply tank while the receiver tank is being filled with liquid (Freon 113) from the supply tank. The ullage exchange technique allows vent filling of a tank which results in lower energy requirements for on-orbit fluid transfer. Heating of the fluid will take place on orbit. Ullage exchange is achieved by connecting the receiver tank and supply tank in a closed fluid circuit. Liquid is pumped from the supply tank to the receiver tank, while either liquid or gas can return to the supply tank. As the process continues, liquid tends to accumulate in the receiver tank and the ullage gas collects in the supply tank. Benfits of this experiment include providing effective technology for cryogenic and other fluid transfers between spacecraft, and reducing power consumption, fluid losses, and contamination risks over competing techniques. The applications to future space missions are many.

MODULE 2 Lompoc High School & Arroyo Grande High School
"THE EFFECTS OF A SPACE ENVIRONMENT ON BACTERIAL CHEMICAL RESISTANCE" & "MAGNETS IN SPACE"

EXPERIMENT 3
"THE EFFECTS OF A SPACE ENVIRONMENT ON BACTERIAL CHEMICAL RESISTANCE"

In the near future we could be exposed to higher levels of cosmic radiation if depletion of the Ozone layer continues. The purpose of this experiment is to determine effects of unfiltered radiation upon growth, propagation and mutation of common Earthside bacteria. Space grown bacteria was subjected to selected household chemicals and antibiotics. The increased radiation experienced outside the atmosphere provide an environment similar to earth's should we allow our Ozone layer's continued degradation.

EXPERIMENT 4
"MAGNETS IN SPACE"

The purpose of this experiment is to study the effects of zero gravity on magnets and friction properties as magnet travels along a horizontal shaft. The interaction of magnetic forces between permanent magnets was investigated.

MODULE 3 - Fesler Elementary School, Lompoc High School
"BACTERIA IN SPACE" & "ZERO POINT ENERGY"

EXPERIMENT 5

"BACTERIA IN SPACE"

The purpose of this experiment is to investigate the survival rates and mutation rates of bacteria sent into orbit and exposed to higher radiation levels than found on Earth. The hypothesis is that the bacteria exposed to higher energy short-wave radiation (gamma and x-rays) when sent up into space, will suffer significantly higher morbidity and higher mutation rates than bacteria grown under identical conditions beneath the protection of the ionosphere of Earth.

EXPERIMENT 6
"ZERO-POINT ENERGY"

The purpose of this experiment is to study the Zero Point Energy (ZPE) process while in a high velocity microgravity environment. The ZPE hypothesis suggests a basic state of electromagnetic flux exists throughout all space. This experiment tests for this basic flux. The ZPE test cell is designed to concentrate deuteron nuclei about the central palladium electrode. A caduceus coil about the test cell is pulsed simulataneously to bias the nuclei. The biased nuclei are theorized to couple with the ZPE flux to yield a measurable amount of heat within the reaction cell.

MODULE 4 - San Luis Obispo High School
"BUBBLES IN SPACE" & "SPACE ADHESIVES"

EXPERIMENT 7
"ELECTROLYSIS IN SPACE"

The objective of this experiment is to investigate the electrode occlusion and bubble formation in electrolysis cells. In an electrolysis reaction, gas molecules accumulate at the electrodes. Small bubbles of these molecules form on the surface of the electrode until their attraction for the surface is overcome by the buoyancy of the gas. In microgravity, however, the factor of buoyancy is negated. Our hypothesis is that the bubble will envelop the electrode in microgravity and end the reaction. Data was recorded with respect to voltage and time for the electrolysis cells.

EXPERIMENT 8
"SPACE ADHESIVES"

The goal of this experiment is to investigate the strength of aluminum material bonded with various adhesives. Samples bonded in microgravity will be compared with gravity bound control. Adhesive grain structure and bond strength are principle objectives of the study. The study of this experiment was proposed for space structure and space flight repair applications.

MODULE 5 - Pine Grove Elementary and Paulding Middle School
"OSMOSIS IN SPACE" & SEEDS EXPOSURE TO RADIATION"

EXPERIMENT 9
"OSMOSIS "

The purpose of the osmosis experiment is to examine the effects of microgravity on diffusion of fluids through a membrane. The basic hypothesis is to determine if there is a difference in the rate of diffusion and/or osmotic pressure in space versus the Earth. This will be determined by a pressure transducer and logged in microcontroller memory. Knowledge will be gained in osmosis and membrane technology and it's uses in the medical field and the advancement of desalinization in space.

EXPERIMENT 10
"SEEDS EXPOSURE TO RADIATION"

Radish seeds will be exposed to the exoatmospheric cosmic radiation environment. Upon return, the seeds will be germinated and grown to maturity. Comparison will be made to Earthside grown controls. These seeds will be shared with students in grades K-12 in both the Santa Barbara and San Luis Obispo counties who were not able to participate in developing active experiments.

MODULE 6 - Orcutt Junior Middle School, Vandenberg Middle School, May Grisham Elementary

"ROCK CRYSTALS IN SPACE", "FLUID SEPARATION AND SURFACE TENSION EXPERIMENT", & "SILVER CRYSTALS IN SPACE"

EXPERIMENT 11
ROCK CRYSTALS IN SPACE

The purpose of this experiment is to determine the effects of microgravity on the growth of rock crystals. The crystals were grown by placing a seed crystal in a supersaturated solution of Sodium Oxide, Silicon Dioxide and water. The crystal growing process occurs at ambient temperature.

EXPERIMENT 12
"FLUID SEPARATION AND SURFACE TENSION"

The purpose of this experiment is to study separation of fluids of varying specific gravities in a microgravity environment. The surface tension is studied by observing the interaction of a benign sphere suspended within the fluids.

EXPERIMENT 13
"SILVER CRYSTALS IN SPACE"

The purpose of this experiment is to grow silver crystals in microgravity. Normally, gravity dominates the behavior of fluids, with undesirable effects on the quality of crystals. The silver crystals grown without convection should be less compact and cohesive (more powdered) than those produced on Earth.

3.2 EXPERIMENT FLIGHT RESULTS

Since the Goddard Symposium payload paper due date is 2 August 1993, and the GAS-450 payload arrived back in California on 22 July 1993, we did not have time to adequately analyze experiment flight results for inclusion in this paper. Preliminary results show that all forty-three payload experiment sensors (thermistors (24), pressure (11), photo (2), voltage (5), radiation (1)) worked and were successfully stored in the microprocessor system (EPROM) for post flight analysis and graphing. The only sensor that did not work was the Instrument Sensor Technology 3-axis accelerometer, the 2 month launch delay drained the internal batteries. Preliminary analyze indicates that most of the experiment failures are mechanical in nature. For example, a syringe plunger did not pull in or a linear actuator did not pull a membrane card. Each of the student groups (13) will be documenting their own experiment development and flight results via a research paper (10-15 pages). These will be available at the October 1993 Symposium. During the 1993 Symposium presentation, we will share some of the experiment flight results. Student experiment papers can be obtained by contacting Space Information Laboratories.

3.3 OPERATIONAL SCENARIO

As the Space Shuttle ascends through 70,000 ft., the orbiter baroswitch activates Relay A, initiating the 12 Vdc Power System which distributes power to each module. The microcontrollers in

each module activated the experiments shortly after the Space Shuttle orbital circularization and attitude maneuvers were complete. At launch plus one hour, the module microcontrollers started the experiment sequences. All experiments which require power and control initiated simultaneously. The microcontroller initiated a power down of all experiment support systems and components within each module upon experiment completion. Each module microcontroller system has preloaded software commands to sequence, control and store data from each experiment. The 12 Vdc Power Bus System is deactivated by an astronaut prior to descent.

4.0 GAS-450 Payload Bus System

The GAS-450 Payload is composed of three principle systems (SIL, patents pending): 1). Structural Support System 2). The Power Distribution System 3). Science Module System. (Fig. 3).

The **Structural Support System (SSS)** provides the hardware interface to the NASA experiment mounting plate, reacts battery inertial loads, locates the lateral support bumpers, restrains the six science modules, and establishes a sealed payload containment cylinder within the GAS canister. A layer of Soundfoam HT is bonded to the inner surface of the aluminum SSS stressed skin to increase experiment module energy containment capability and vibration isolation. The payload upper and lower bulkheads complete the containment on each end of the SSS cylinder. Reference paragraph 2.1 for further detail.

The **Power Distribution System (PDS)** provides payload electrical access to the NASA interface equipment plate and supplies 12 VDC to the science modules.

The **Science Module System (SMS)** consists of six sealed modules which enclose all payload experimental apparatus. All power and control leads are routed thru an "O"-ring style bulkhead connector. Each module contains a dedicated microcontroller to sequence the experiments and store data. Ambient air at atmospheric pressure was present inside the module. Experimental apparatus volume utilization is designed so that void space does not exceed thirty percent of total volume. Per requirements of NSTS 22648 the **SMS** is defined as a sealed container which will not propagate a fire from the interior.

Each of the six aluminum modules have an identical microcontroller system. The locally invented microcontroller system is made so that it can be reused in the future. The system is capable of sequentially controlling up to 20 electrical devices (Sink, 0 to 15 Amps) and storing 11 sensor channels. Each module utilizes the first four channels for temperature sensors (thermistor circuitry, -40 C to + 100 C). The microcontroller system is made up of two boards connected together using a 96 pin din plug and socket connector. The first board can download all data (EPROM) collected from experiments into a PC via an RS232 cable. Sensor information is placed into engineering units and plotted via ground PCs. The second board is a breadboard for special circuitry needed to run experiments. All chips are CMOS and perform over harsh environmental performance specifications.

The GAS-450 Payload Bus System is unique. No other GAS canister in the history of the program has ever flown 15 active experiments in one canister. The payload bus system is also completely reusable. The GAS-450 payload is something our technical staff is very proud of!

5.0 PEOPLE CONSIDERATIONS

The California Student "GAS #450" Space Shuttle Program has something for everyone in the local community. The heart of the project consists of the student experimenters. They are all young, talented and very excited about working on their experiments. These people are full of the stuff of youth and eager for directions in which to channel their energy. The GAS opportunity has provided hundreds of people of all sorts, an avenue to apply their creative energy into space research. Directly supporting the forty students are the teachers and advisors at the schools they attend and the technical staff of engineers, scientists and technicians from the local community.

Even with this kind of support, the project could not be successful unless other people pitched in and helped. The parents are supporting the experimenters by providing transportation, helping on experiment designs at home, attending meetings, and altering their own schedule during conflicts to insure the experimenters enough time to work on experiments. The sponsors help provide the equipment it takes to complete the experiment. They are the unsung heroes because many of the experiments use

specialty items that are not available at local stores and are not available as "off the shelf" items anywhere. The sponsors work hard to provide the item needed or to recommend a substitute. The student experimenters and technical advisors are thankful for the support from the 100 local and national sponsors of the California Get Away Special program.

NASA has been very supportive. The GAS-450 technical coordinated every design change through NASA to insure that a dangerous experiment was not inadvertently packaged in the GAS canister. The NASA personnel have responded to the SIL's efforts in a timely manner and a good working relationship has been established between the two organizations.

Last but not least, is the community at large. Community media was important as it told the local community what positive things a few of its citizens were doing and accomplishing. Newspaper, magazine articles, and television time spots were critical to the success of our payload by giving us credibility with potential sponsors. Three press conferences with the local media and newspapers were scheduled, one at the outset of the program, one after Phase II development was complete and one before shipment to Kennedy Space Center for final checkout and installation on the Space Shuttle. One individual in the GAS organization should be totally dedicated to fundraising.

An organization chart which describes the GAS #450 project in a humanistic way is shown in Figure 4. NASA Goddard, Parents, Family, SIL, Contractors (Sponsors), Schools, Friends and Teachers are veins feeding the heart of the project, "the young students". As long as everybody keeps the heart pumping, excited and willing to work hard, the project stays alive and on schedule.

6.0 STUDENT SCHEDULES AND MEETINGS

One of the guided objectives is to provide the students with an experience similar to the aerospace industry at large. Meeting organization, action item discipline, scientific procedures, and schedule milestones processes are utilized to enhance the program. The GAS-450 program used a 3 phase development approach. Under Phase 1, a preliminary experiment design paper, drawing and prototype model is due. Phase 2 development consists of producing a final experiment paper and drawing and a functional prototype model. Documenting experiment evolution and ground testing results with professional laboratory notebooks donated by Scientific Notebook, Co. is also part of Phase II development. The laboratory notebook is a written record of the student experiments. It is broken into the following scientific method categories: Purpose, Procedure, Experiment Apparatus, Observations and Data, Calculations and Conclusions. The experiment notebook is a vital tool in explaining to NASA in a final report how microgravity and space environmental factors effect the experiment. Plenty of ground testing is needed to prove the purpose of the experiment and draw a final conclusion. Phase 3 development consists of producing the final flight ready experiment module and interfacing it into the payload bus system. The students meet with the SIL Technical Staff once a week (3 hrs, June 1990, Program Inception) at Allan Hancock Community College (Santa Maria, California) to develop and test experiments. It has become apparent that regularly scheduled meetings are crucial for any GASCAN program. We have found that these reviews identify problems in designs, can help find flaws in basic system approaches to experiments, allow one to make changes to systems before they become difficult to change, help identify safety related issues and provide a good educational experience for the students. The technical staff monitors all three phases of the project each month with a progress chart.

7.0 LESSONS LEARNED

TECHNICAL

1. Utilize batteries with a very low self discharge rate (2-3% a month). Two battery types serve this purpose very well: Sealed Lead-Acid Gell Cell and Alkaline Batteries. The GAS-450 Payload used five Johnson Control Lead Acid Batteries (JC12150, 12V, 15AH each). We fully charged the batteries at the NASA Spin Test Facility at KSC five months prior to the launch. The GAS-450 payload batteries were 85% fully charged for the STS-57 mission. Count on a three to six month time frame from payload turnover to NASA at KSC and an actual launch date. Read the 1992 Shuttle Small Payload Symposium Papers, "Battery Selection for Space Experiments", by David R. Franciso and "Proper

Battery System Design for GAS Experiments", Stephen A. Calogero for further knowledge on battery selection and power system design. Utilize the electricity payload hazard report format in Mr. Calogero's paper for your Safety Data Package.

2. Building a battery box with a removable lid (NASA safety inspection of fuses and electrolyte resistant material inside (Conap) in the field) to pass a proof pressure test of 22.5 psi (Safety Paperwork, 24 hour test) is no easy task. Make sure you consult with an engineering company or individual who has experience in building pressure vessels before you develop your own. Leave plenty of excess room in power system area for your battery boxes.

3. Think about how to install fuses inside your battery boxes so that you do not have mechanical damage to them during launch. Plastic batteries with sunk-in terminals and areas to place fuses into are critical.

4. Include an acoustic and vibration dampening system in your payload system design. This will reduce the risk of experiment mechanical failures. If you hard mount components directly to the canister structure, then experiments and payload systems must be able to handle the acoustic and metal vibration during launch and landing.

5. Provide fans in experiments that use heaters to reduce hot spots. Remember, there is no convection in orbit. Make sure you utilize adequate heat sinks (conduction) for items such as regulators, transistors and diodes that dissipate significant power.

6. Develop a structure that is not excessively heavy and overdesigned. You may need this weight for experiments and batteries. Remember, you must be within the 200 lb limit for a 5 cubic ft. canister. Perform a basic classical structural analysis (X,Y,Z load of 10g's with factor of safety of 2.0) on your design idea before building it. Read the 1992 Shuttle Small Payload Symposium paper, "Structural Verification for a GAS Experiment", by Mark Peden for further knowledge on structural and vibration design and analysis. Utilize the structure hazard report format in this paper for your Safety Data Package.

7. Don't underestimate the time it takes to complete NASA's paperwork requirements: Payload Accommodation Requirement (PAR) and Safety Data Package (SDP) documents. We revised the PAR three times and the SDP five times before the documents were approved. This alone took over 2500 man-hours. The good part is that once you qualified your payload system, it's much easier to refly the same canister on future missions. Make sure you develop a payload bus system that can be reused.

PROGRAM MANAGEMENT

1. Provide a straightforward approach to soliciting students and teachers such as a video tape and application forms so that K-12 schools can be involved from the start of the program. Have the students submit experiment proposals for evaluation.

2. Interview the best individual or student group proposals for final acceptance into the program.

3. It is crucial to hold regularly scheduled meetings at least twice a week initially and once a week when the experiments are adequately researched and designed. Keep the pressure on the students to perform with experiment action items and design feedback, part procurement, and constant engineering drawing and prototype improvements. The students learn the most if they design and build their own experiments. Effort and curiousity is the key to significant learning.

4. It's crucial to obtain a tax-write off number (501C (3)) for parts, materials and funding. The only way to obtain this tax exempt status is to form partnerships in your local community so you can use their tax exempt status. Schools, colleges and universities, and non-profit organizations are prime candidates. Parts and materials are much easier to obtain than funding if you contact the company via letter and

describe the goals of your program and specific need. Send newspaper and magazine articles and any video information about your program. It usually takes much longer to obtain money. In our experience, companies or individuals will not donate parts, materials or funding unless you approach them via letters, presentations, grant proposals, etc. This all takes valuable time. Organizations that obtain grants without doing anything are few and far between. Do something and then start asking for parts, materials and funding. Administrative costs such as travel expenses, telephone calls, copies, video tapes, momentos, mailings, etc. add up. Partnerships in the local community can help to reduce this significant cost.

5. If your organization wishes to support an educational payload, please see NASA interim final rule amending 14 CFR Part 1214. NASA offers lower prices for SSCP's sponsored by domestic educational institutions (5.0 cu. ft.-$10,000, 2.5 cu. ft.-$5,000). Unfortunately, the current policy definition of a domestic educational institution excludes some educational GAS users. The definition includes only the following institutions: universities, colleges, elementary or secondary schools, or university- affiliated research foundations. If you are truely an educational payload and do not fit this rule, then contact Dr. Malcom V. Phelps (NASA HQ., NASA Educational Division, Code FET, Washington D.C. 20546, 202-358-1540) with a 2-3 page proposal discussing why you are an educational payload. Dr. Phelps will study proposals on a case by case basis and make a ruling. We think that the new policy should include any 501 (C) (3)- public charity or organization such as AIAA, IEEE, NSS, etc. that are developing canisters for students.

By reading the above lessons learned, you now realize that your organization must be extremely dedicated and do whatever it takes to finish the payload. The individuals organizing your program must realize the commitment and skills necessary to design and build a "GAS" payload for the Space Shuttle. You need professional engineers, scientists and technicians on your team to help.

8.0 CONCLUSION

The Get Away Special GAS-450 Payload successfully flew on the STS-57 mission, Space Shuttle Endeavour, 21 June 1993. The GAS-450 payload bus system (power, structure, microprocessors, sensors) enjoyed a 100% success rate and the student experiments were 60% successful. We are planning to refly our unsuccessful experiments and a few new ones on the STS-64 mission (GAS Bridge, Late 1994) and apply lessons learned in order to achieve success. Concurrently, SIL will be starting another program with a new group of K-12 students and experiments for a flight opportunity in mid 1996. This approach will allow us to have a GAS Payload in Space every 1 1/2 years. Special thanks to the Special Payloads Division of Goddard Space Flight Center, Mr. Mark Anderson our GSFC Technical Manager, Mr. Steve Calogero our NASA Safety Officer, and Mr. Russell Griffin our KSC/GSFC GAS Field Operations Manager, for their technical expertise, attention to detail, and assistance. NASA's Get Away Special program offers an unique opportunity for communities to provide **"hands-on"** experiences for children, as well as their adult helpers, opening their minds to the world of science and space, as well as the joy of learning. Many of the students involved in our program now express a desire to pursue scientific careers and have learned real skills such as electronics, metal fabrication, computer aided design, etc., that will help them reach their goals in life. The founders of Space Information Laboratories hope others will be inspired to start "hands-on" programs similar to the California Space Shuttle Program for our Children.

If you would like to contribute funds to this or **future California student "Get Away Special"** programs please contact Edmund D. Burke or Marty Waldman, Space Information Laboratories, P.O. Box 5090, Vandenberg AFB, CA 93437. Phone Number: 805-735-1155. Your contribution is tax deductible through the Allan Hancock College Foundation or Space Information Laboratories.

FIGURE 1

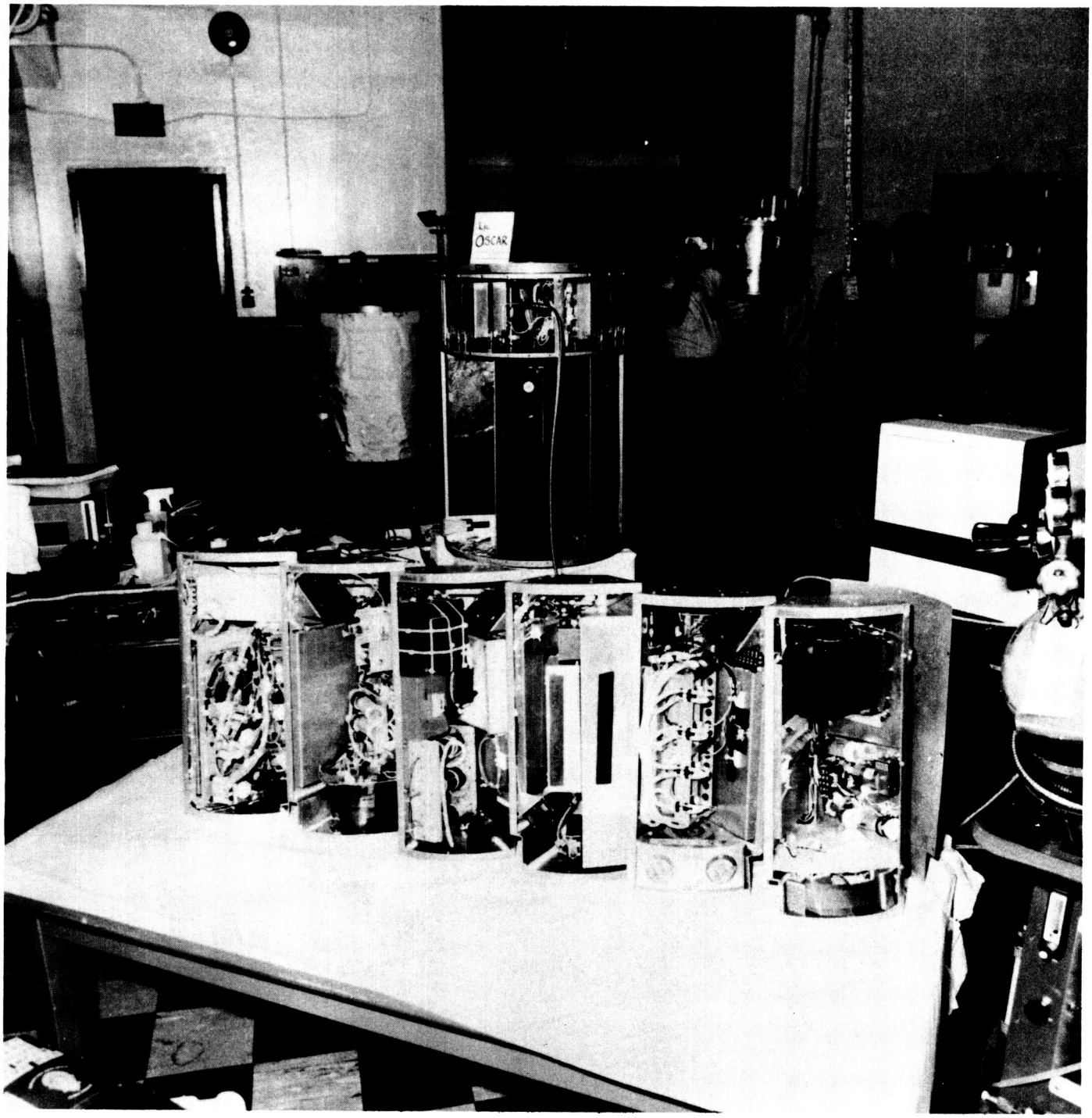

FIGURE 2

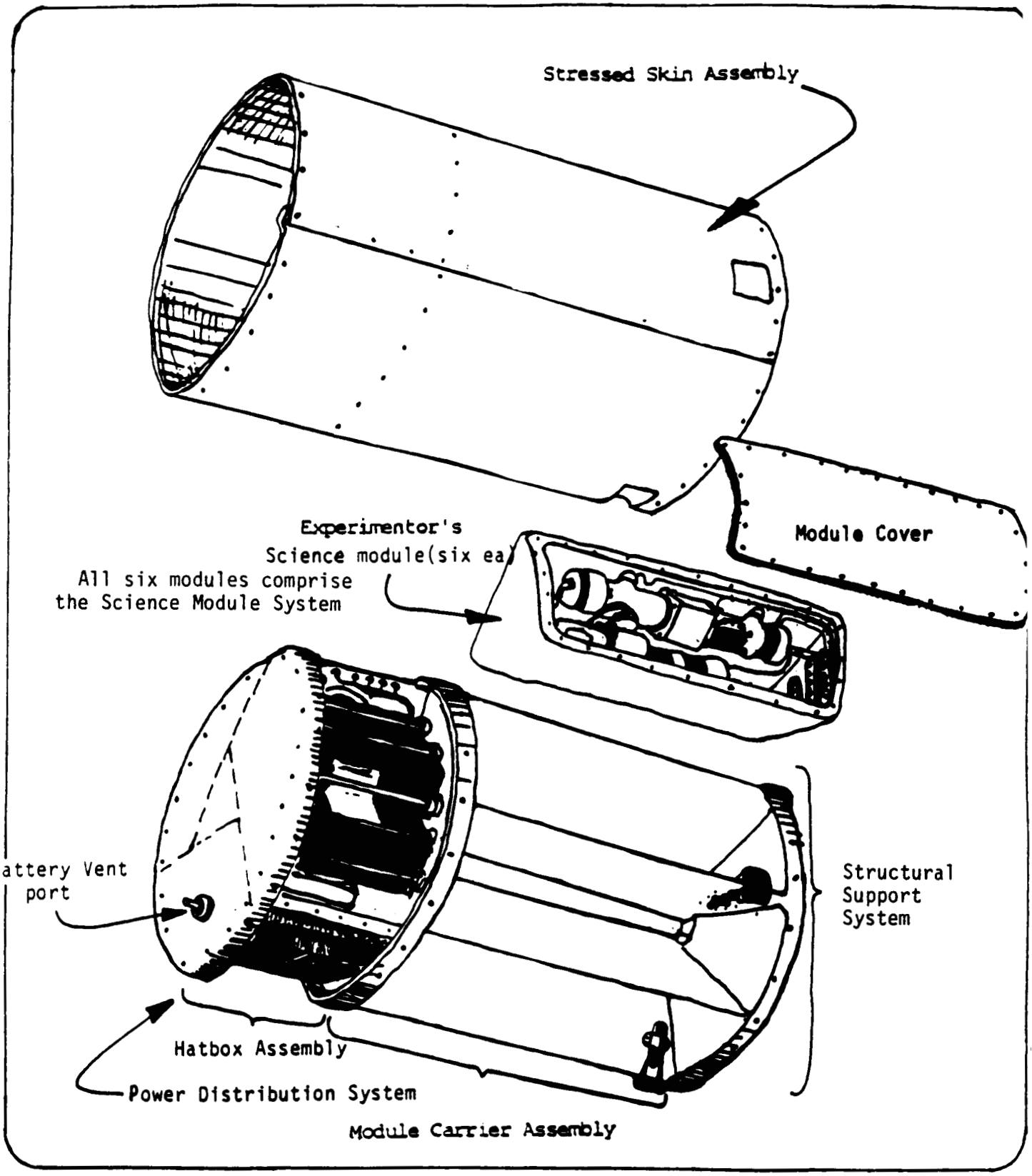

FIGURE 3

Payload Principle Systems

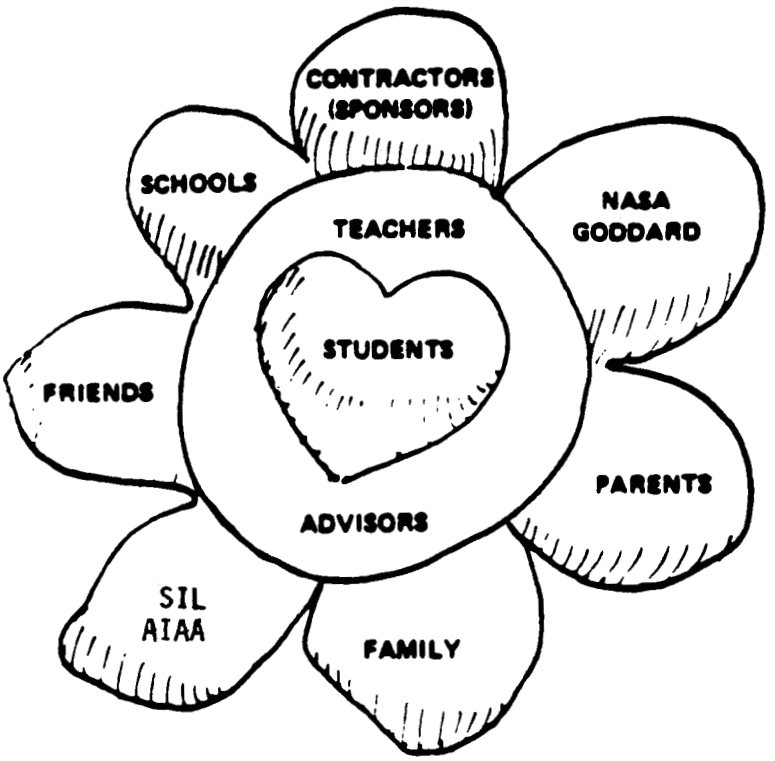

FIG. 4
ORGANIZATION CHART

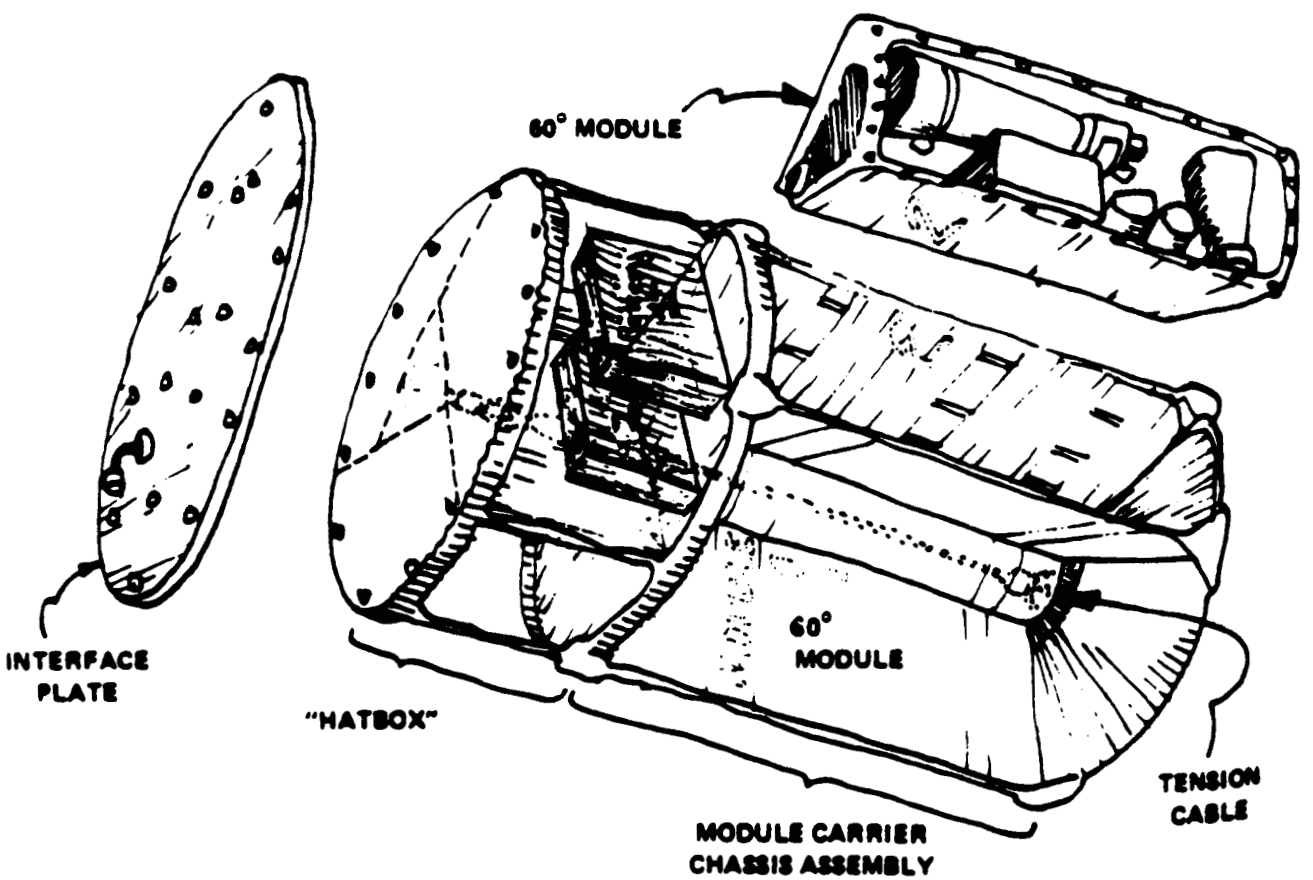

PAYLOAD CHASSIS LAYOUT

New Room Temperature High Resolution Solid-state Detector (CdZnTe) for Hard X-rays and Gamma-rays

AmyElizabeth C. Stewart
University of Maryland
College Park, MD 20740-3328

Upendra D. Desai
Goddard Space Flight Center - Code 682
Greenbelt, MD 20771

Abstract

The new CdZnTe high "Z" material represents a significant improvement in detectors for high energy photons. With the thicknesses available, photons up to 100 keV can be efficiently detected. This material has a wide band gap of 1.5 - 2.2 eV which allows it to operate at room temperature while providing high spectral resolution. Results of resolution evaluations are presented. This detector can be used for high resolution spectral measurements of photons in x-ray and gamma-ray astronomy, offering a significant reduction in the weight, power, and volume of the detector system compared to more conventional detector types such as scintillation counters. In addition, the detector will have the simplicity and reliability of solid-state construction. The CdZnTe detector, as a new development, has not yet been evaluated in space. The Get Away Special program can provide this opportunity.

Semiconductor Detectors

The most commonly used materials for semiconductor detectors are silicon (Si), germanium (Ge), mercury-iodide (HgI_2) and cadmium-telluride (CdTe). The energy resolution of these detectors is dependent on the

number of electron-hole pairs generated and the loss of charge during collection. The resolution can be improved by "doping" the detector material with the appropriate elements so that resistivity and the product of mobility and lifetime (μT) of the carriers will both be increased. Increasing resistivity will decrease the reversed bias leakage current which is the most significant cause of noise. Although silicon has the best mobility-lifetime product of any material currently studied, its low atomic number and small band gap result in relatively poor detection efficiency for energies above 20keV. Germanium provides good resolution with good detection efficiency, but cannot be used at room temperature due to its very small band gap. CdTe is a useful combination of elements because it combines relatively high atomic numbers (Z) with higher density and large band gap energy (E_g). The high Z and high density give the detector a higher efficiency of absorption than Si or Ge while the wide band gap allows the CdTe detector to be operated at room temperature with decreased probability of thermal excitation. A comparison of these three materials is provided in Table 1.

material	z	$\rho(g/cm^3)$	$E_g(eV)$
Si(300K)	14	2.33	1.12
Ge(77K)	32	5.32	0.74
CdTe(300K)	48/52	6.06	1.47

Table 1

The electronic properties of CdTe can be further improved, which has led to the development of ternary materials such as the new CdZnTe . The high resistivity (~10^{11} Ω-cm) of this material results from the increased band gap, thereby improving resolution through lower leakage currents. The CdZnTe detector has good collection efficiency for energies up to 100

keV and has good energy resolution without cooling. While the CdZnTe detector's energy range is not as large as that of the APD/scintillator combination, its solid-state construction gives it the advantages of reliability, reduced weight and reduced volume. A comparison of CdZnTe to some other commonly studied binary and ternary materials is presented in Table 2.

material	atomic #	$\rho(g/cm^3)$	$E_g(eV)$	resistivity(Ω-cm)	$\mu T(cm^2/V)$ (electrons)
CdZnTe	48/30/52	~6	1.5 - 2.2	10^{11}	$1X10^{-3}$
CdTe	48/52	6.2	1.44	10^{9}	$3.5X10^{-3}$
ZnTe	30/52	5.72	2.26	10^{10}	$1.4X10^{-6}$
HgI_2	80/53	6.4	2.13	10^{13}	$1X10^{-4}$
HgBrI	80/35/53	6.2	2.4 - 3.4	$5X10^{13}$	$2X10^{-7}$

Table 2

Results

We are currently evaluating four 4 mm X 4 mm and four 8 mm X 8 mm CdZnTe detectors manufactured by Aurora Technologies Corporation. All of these detectors are 1.5 mm thick. Results achieved with these detectors are summarized in Table 3.

detector #	bias voltage (V)	FWHM resolution (@59.6 keV)
732 (4mm)	250	7.0%
328 (4mm)	250	8.1%
736 (4mm)	350	8.0%
739 (4mm)	300	8.1%
540 (8mm)	350	9.8%
181 (8mm)	250	7.6%
788 (8mm)	280	9.0%
431 (8mm)	350	9.1%

Table 3

The average energy resolution of the smaller set of detectors at 59.6 keV is ~7.8%. For the 8 mm detectors, the average resolution goes up to ~8.9%. Figure 1 shows an energy spectrum for a 8 mm X 8 mm CdZnTe detector at room temperature with a ^{241}Am source. Figure 2 is a comparison of the spectra generated by a silicon avalanche photodiode(APD) and a CdZnTe detector, both 4 mm X 4 mm . In the CdZnTe spectrum, the 59.6 keV line and the lower energies are detected with comparable efficiency. In the APD spectrum, however, the 59.6 keV line is noticeably weaker than the low energy lines (logarithmic scale).

Conclusion

CdZnTe detectors offer great potential for the future of x-ray and γ-ray detection. Their low leakage current and good collection efficiency make them superior to the semiconductor detectors currently in use. We hope that the evaluation of CdZnTe detectors in space will demonstrate their reliability and usefulness.

CdZnTe Detector #700431
Length: 8mm
Width: 8mm
Thickness: 1.5mm

Figure 1

Taken at room temperature with ^{241}Am source and bias voltage at 350V.

CdZnTe Detector	#700732
Length:	4mm
Width:	4mm
Bias Voltage:	250 V

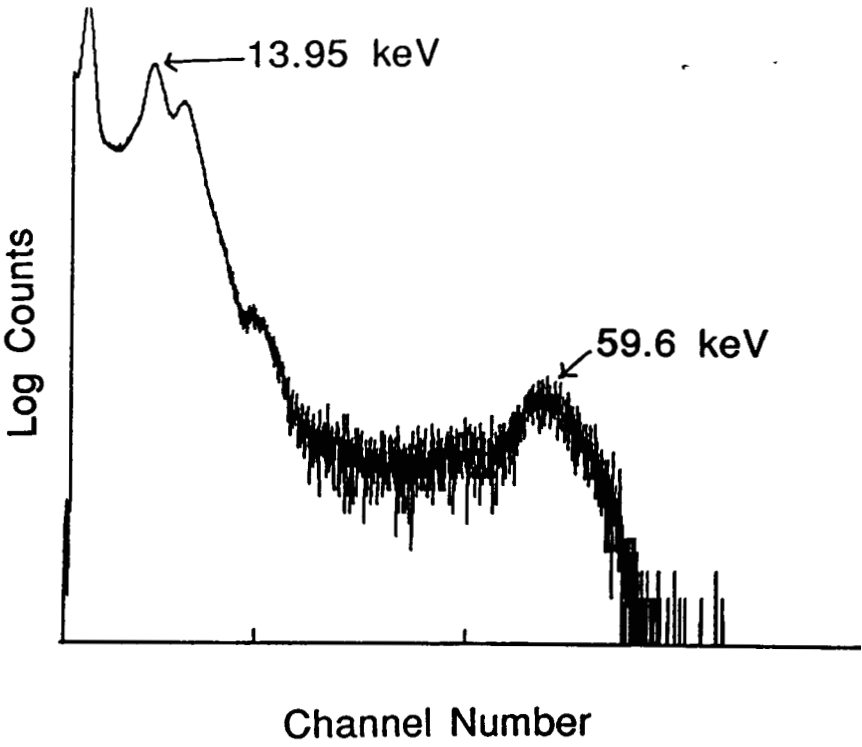

Silicon APD	#ND1231-3
Length:	4mm
Width:	4mm
Bias Voltage:	1.18 kV

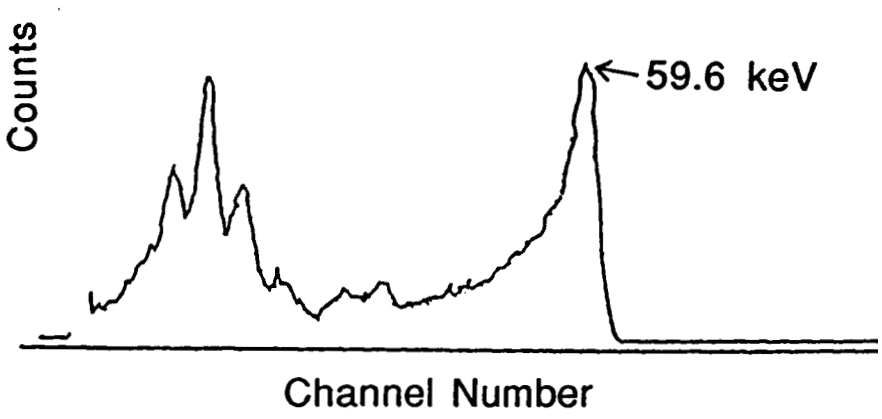

Figure 2: A Si avalanche photodiode (APD) and a CdZnTe detector of the same dimensions. Both spectra were taken at room temperature with a ^{241}Am source. (The APD also used a ^{55}Fe source.) The APD spectrum is logarithmic. As shown by the figure, the detection efficiency of the APD is poor at the 59.6 keV line, which cannot be seen in a linear plot. The CdZnTe spectrum is a linear plot.

References

G. Knoll, Radiation Detection and Measurement. Wiley & Sons, New York (1979), p.372-502.

G. Fraser, X-ray Detectors in Astronomy. Cambridge, New York (1989), p.179-228.

M. Hage-Ali, P.Siffert, Nuclear Instruments and Methods in Physics Research. A322 (1992) 313-323.

J. Butler, C. Lingren, F. Doty, IEEE Transactions on Nuclear Science. NS-39 (1992) 605-609.

M. Squillante, J. Zhang, C. Zhou, P. Bennett, L. Moy, *New Compound Semiconductor Materials for Nuclear Detectors.* Presented at: Spring 1993 Materials Research Society Meeting, San Francisco, CA. April 1993.

Telescope for X-ray and Gamma-ray Studies in Astrophysics

W. D. Weaver
Arkansas State University
State University, Arkansas 72467

U. D. Desai
National Aeronautics and Space Administration
Goddard Space Flight Center
Greenbelt, Maryland 20771

ABSTRACT

Imaging of X-rays has been achieved by various methods in astrophysics, nuclear physics, medicine, and material science. A new method for imaging X-ray and gamma-ray sources avoids the limitations of previously used imaging devices. Images are formed in optical wavelengths by using mirrors or lenses to reflect and refract the incoming photons. High energy X-ray and gamma-ray photons cannot be reflected except at grazing angles and pass through lenses without being refracted. Therefore, different methods must be used to image X-ray and gamma-ray sources. Techniques using total absorption, or shadow casting, can provide images in X-rays and gamma-rays. This new method uses a coder made of a pair of Fresnel zone plates and a detector consisting of a matrix of CsI scintillators and photodiodes. The Fresnel zone plates produce Moiré patterns when illuminated by an off-axis source. These Moiré patterns are deconvolved using a stepped sine wave fitting or an inverse Fourier transform. This type of coder provides the capability of an instantaneous image with sub-arcminute resolution while using a detector with only a coarse position-sensitivity. A matrix of the CsI/photodiode detector elements provides the necessary coarse position-sensitivity. The CsI/photodiode detector also allows good energy resolution. This imaging system provides advantages over previously used imaging devices in both performance and efficiency.

INTRODUCTION

In recent times, the need for X-ray imaging devices has been realized in astrophysics, solar physics, nuclear physics, medicine, and material science. In astrophysics, X-ray images can be used to study transients and X-ray bursts, as well as allowing broad spectrum maps of the skies. These high energy images can be matched with images in the optical range to give researchers more data for the study of the astrophysical phenomena. In solar physics, good X-ray images will allow the phenomena of solar flares to be studied more closely. X-ray crystallography is a valuable tool in material science. Good X-ray imaging devices would be beneficial in this field. The medical field also can benefit greatly from efficient X-ray imaging systems.

In the early 1960's, it was suggested that X-ray imaging could be done by shadow casting using coded masks.[1] The coded masks cast shadows of their patterns which can then be looked at to determine the arrangement of the sources. The coded mask should be such that the shadows cast by two sources have a low cross-correlation. The simplest of coded mask systems is a mask with a single hole[2]. This system directly provides an image of the

illuminating sources, but to achieve good resolution, the hole must be small. This does not allow many photons to pass, thus causing count rates to be low. In order to solve the problem of low photon numbers, more random holes must be added.[3] Extracting an image then becomes more difficult.

Multiple plane imaging systems have also been suggested by various authors. [4,5] These systems have larger apertures and thus allow higher photon numbers. The shadows cast by bi-grid systems are also confused, but they lend themselves to easy deconvolution methods such as an inverse Fourier transform. Two types of bi-grid systems are rotating modulation collimators and phased stationary systems.[6] Rotating modulation collimators provide both good spatial resolution and can have a large aperture. However, they do not provide good time resolution. For the rotating modulation collimators to provide the sine and cosine components needed for the inverse Fourier transform, the grids must be rotated. This means that sources which vary rapidly with time will have some of the detail lost. The amount of spatial resolution depends on the spacing of the parallel bars of the grid and the distance between the grids.[7,8,9]

Two zone plates in tandem do not require rotation to provide the modulation of the sources. One example of a zone plate which can be used is a Fresnel zone plate. A Fresnel zone plate consists of concentric rings of alternating opaque and transparent material all having equal area. When this system is illuminated by a source, the zone plates cast shadows on the detector. These shadows form Moiré patterns which are parallel lines whose separation is proportional to the distance the source is located off the axis of the system.[1,5]

Methods and Materials

The use of Fresnel zone plates in a bi-planar imaging system requires several choices depending upon angular resolution needed, field of view, etc. The zone plates can be constructed to various specifications.(See table) The thickness of the plates is the first variable to be chosen. The thickness of the plate is somewhat dictated in certain energies by the requirement that alternate zones must absorb the incident photons. When considering the plates for use with X-rays, the thickness of the material must be such to stop these high energy photons.

Fresnel zone plate specifications
Radius of innermost zone r_1 = 1 cm
Number of zones in plate N = 100
Radius of n^{th} zone $r_n = r_1 \sqrt{n}$
Diameter of zone plate d = 20 cm
Width of outer zone $\Delta r_N = r_1^2/d$ = 0.05 cm

The plate can be flat with a uniform thickness for all absorbing zones, or the plate can be tapered with the innermost zone being thicker than the outer zone. If the zones are of uniform thickness, the inner zones which have larger radii will allow photons to pass the zone plate at greater angles than the outer zones will allow. This will cause an unequal contribution to the

coded image by the various zones. If the thickness of the plate varies, however, the angle at which each zone allows a photon to pass will be equal. A tapered design will allow the outer zones to contribute to the production of the coded image by limiting the angle of incidence which the inner zones will allow the photons to pass. Greater thickness for the middle zones will allow the zones on the edge to contribute equally. The thickness at the edge of the zone plate should be chosen such that a photon passing though the outermost zone of the top plate is able to interact with any of the zones in the lower plate. The thickness of each zone can be determined using the following relation to the thickness of the innermost zone:

$$h_n = \frac{[h_1 (\sqrt{n} - \sqrt{n-1})]}{\sqrt{2} - 1}$$

where h_n is the thickness of the n^{th} zone and h_1 is the thickness of the innermost zone.

It is important to have the outermost zones of the plate contribute to the formation of the image because the angular resolution is a function of the size of the smallest zone.

$$\theta = \tan^{-1} (\Delta r_N / D)$$

where D is the separation between the two zone plates. Therefore, for the specifications given above, an angular resolution of approximately 1 arcminute is possible. It is not necessary for the detector to resolve the smallest zone of the zone plates as is necessary in single zone plate imagers. In bi-planar systems, the detector must only be capable of resolving the produced Moiré patterns. Since the size of the smallest zone determines the angular resolution, the value of the tandem Fresnel zone plate system is that it is not necessary for the detector plane for this system to have high spatial resolution capabilities. A course resolution detector plane can be used to detect the Moiré patterns.

The Moiré patterns are then deconvolved. A stepped sine wave fitting can be used for this purpose. An inverse Fourier transform is also an option in the reconstruction of the image from the Moiré patterns. To use an inverse Fourier transform, two Fresnel zone plate pairs must be used. To get the cosine component of the transform, both plates must be identical where $r_n = r_1\sqrt{n}$. The other pair of plates will give the sine component if one plate has its zones defined by $r_n = r_1\sqrt{n}$ and the other plate is phase shifted by having its zones defined by $r_n = r_1\sqrt{(n-1/2)}$.

The major advantage of this system over one using a rotating modulation collimator is that the images produced are not time-averaged. The Moiré patterns are produced instantaneously, thus providing a "snapshot" of the sources. This is particularly useful in the study of solar flares where the source of X-rays changes in a short time.

Using a matrix of CsI scintillators coupled to photodiodes as the detector will provide the course position sensitivity required to provide images with sub-arcminute resolution. This type of detector will also provide good energy resolution.

Conclusion

This system is capable of providing images with sub-arcminute resolution and energy resolution. The images produced are not time-averaged. Due to the symmetry of the zone plates, the need for careful rotational alignment, as is necessary for the grids of rotational modulation collimators, is avoided. The use of CsI scintillators coupled to photodiodes reduces the weight and volume of the instrument considerably when compared to a similar system using photomultiplier tubes to view scintillators. This system will provide improved images over those provided by currently used systems and will do so with significant savings on bulk and weight.

References

1. L. Mertz and N.O. Young, "Fresnel Transformations of Images", Proc. Int'l Conf. on Optical Instruments and Techniques, Ed. K.J. Habell, (1961) 305-312.

2. Gerald K. Skinner, "X-Ray Imaging with Coded Masks", Scientific American (August, 1988) 84-89.

3. R.H. Dicke, "Scatter-Hole Cameras for X-rays and Gamma-rays", Ap. J. **153** (1968) L101-L106.

4. H. Bradt, et al., "The Modulation Collimator in X-ray Astronomy", Space Sci. Rev. **8** (1968) 471-506.

5. L. Mertz, "Ancestry of Indirect Techniques for X-ray Imaging", Proc. SPIE **1159** (1989) 14-17.

6. K. Makashima, et al., "Modulation Collimator as an Imaging Device", Space Astronomy **XX** (1978) 272-289.

7. H.W. Schnopper, R.I. Thompson, and S. Watt, "Predicted Performance of a Rotating Modulation Collimator for Locating Celestial X-Ray Sources", Space Sci. Rev. **8** (1968) 534-542.

8. D. Cardini, et al., "A Fourier-Bessel Telescope for Hard X-ray Astronomy", Astron. Astrophysics **257** (1992) 824-830.

9. L.N. Mertz, G.H. Nakano, and J.R. Kilner, "Rotational Aperture Synthesis for X Rays", J. Opt. Soc. Am. A **3** (1986) 2167-2170.

MUZO
FLIGHT EXPERIENCE WITH THE PROGRAMMABLE MULTI ZONE FURNACE

Christian Lockowandt, Kenneth Loth
Swedish Space Corporation
P.O. Box 4207
S-17104 SOLNA, SWEDEN

ABSTRACT

The MUlti ZOne (MUZO) furnace has been developed for growing Germanium (Ge) crystals under microgravity in a Get Away Special (GAS) payload. The MUZO furnace was launched with STS-47 Endeavour in September 1992. The payload worked as planned during the flight and a Ge sample was successfully processed. The experiment has given valuable scientific information. The design and functionality of the payload together with flight experience is reported in this paper.

INTRODUCTION

The MUZO furnace together with the temperature control system was originally developed for Bridgman crystal growth experiments with Ge crystals in a GAS canister. The ability to adapt the furnace to shorter microgravity times, typically the 7-14 minutes in sounding rockets, was a design criterion. Another criterion was the capability of processing samples in both gradient and isothermal modes.

The core of the furnace is a ceramic tube with 5 heaters and cooling gas channels. The control system can control all the heaters, the cooling gas flow and the Peltier pulses independently.

A successful experiment was performed with the GAS 330 that was flown on the Shuttle flight STS-47 in September, 1992. A reflight of the MUZO furnace with GAS 541 onboard STS-59 in March/April -94 is planned.

PAYLOAD DESCRIPTION

Furnace

The MUZO furnace is shown in figure 1. The furnace structure is built with two end plates, which contain the inlets for cooling gas and Peltier pulsing. The thermal expansions of the crucible and the sample are absorbed by springs in the end plates of the aluminum outer structure. The 15 thermocouples are pressed towards the sample by springs for optimal thermal contact. All structural parts are made of aluminum.

The centre of the MUZO furnace is the ceramic tube, which holds the resistive heating wires and is equipped with cooling channels which

run along the sample length. The heating wires are divided in five heaters that can be controlled individually. A crucible is placed inside the tube, and the material of the crucible can be selected to be compatible with each specific sample. For growth of Ge crystals, quartz is used. The nominal sample size is 10 mm diameter and 100 mm long. Insulation between the ceramic furnace tube and the outer aluminum structure ensures reduced energy consumption as well as reduced structure temperatures. The maximum temperature in the furnace is 1300°C and the maximum heating rate is exceeding 3.5°C/s. The furnace is equipped with Peltier pulsing (25 A) at variable frequencies for tracking of the solid/liquid interface.

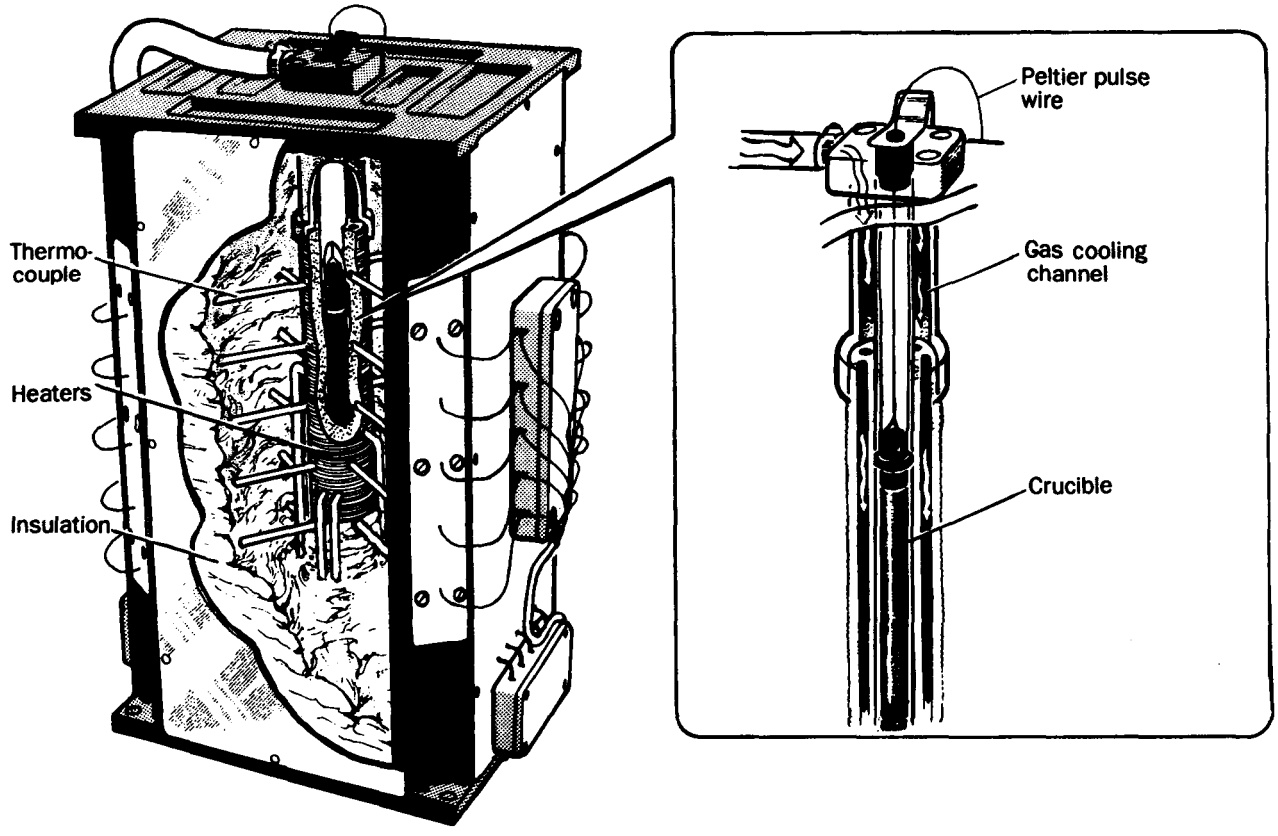

Figure 1: Cut away view of the MUZO furnace.

The design of the MUZO furnace makes it possible to change the sample in 15 minutes.

The unique feature of the MUZO furnace is the advanced temperature control system which allows for a variety of materials processing techniques ranging from isothermal to gradient growth, including rapid quench. The following growth techniques can be conceived:

- Isothermal growth
  (In-situ composite growth, High Temperature Solution Growth, Liquid Phase Epitaxy, etc.)

- Zone melting
  (Travelling Heater Method, etc.)

- Directional solidification
  (Gradient Freeze, Bridgman, etc.)

Several independently controlled heaters and a gas cooling system controlled by the furnace microprocessor, makes it possible to program:

- velocity and acceleration of solidification
- temperature gradients and profiles

Power System

The payload is powered with a battery unit consisting of sealed-lead batteries of standard type (which makes it a low cost design). Two sizes of cells are used (22 cells of 25 Ah, 2 V and 11 cells of 12.5 Ah, 2 V) arranged in three packages of 22 volt to optimize the total size of the power unit. A sealed compartment with venting pipes is used to accommodate the battery cells. The temperature of the batteries is monitored during the flight before the experiment starts. If the temperature is to low, a small heater that is incorporated in the battery unit is switched on to increase the temperature of the batteries to ensure maximum power delivery from the batteries. The whole battery unit holds a total capacity of 1.5 kWh.

During the vibration test of the payload some problems with the battery cells not withstanding the vibration levels occurred. The inner section of the cells containing the electrolyte moved and a fracture between the inner and outer connectors occurred. This was solved by putting three hose clamps around the cells and fixating the inner section better by pinching the cells. This rather crude method worked flawless and the battery cells capacity is still in accordance with the specification one year later.

Control System

The control system comprises a programmable microprocessor system. This includes thermocouple preamplifier, A/D converter, microprocessor, on board memory and power distributors for DC power to the heaters (DC power is used instead of AC to avoid the generation an oscillating magnetic field in the sample).

The software is designed for real time operation system. This makes each module independent and simplifies its adaption to a new experiment. The on board control system software is compatible with the software in the Ground Support Equipment (GSE). This facilitates the collection of data from experimental runs during testing. It also makes possible the dumping of on board memory data to the GSE. During testing, it is possible to change the experimental parameters of the control system in real time, thus decreasing the time needed

to adapt to a new experiment. In addition, the GSE allows for the construction of graphs of all data collected by the system.

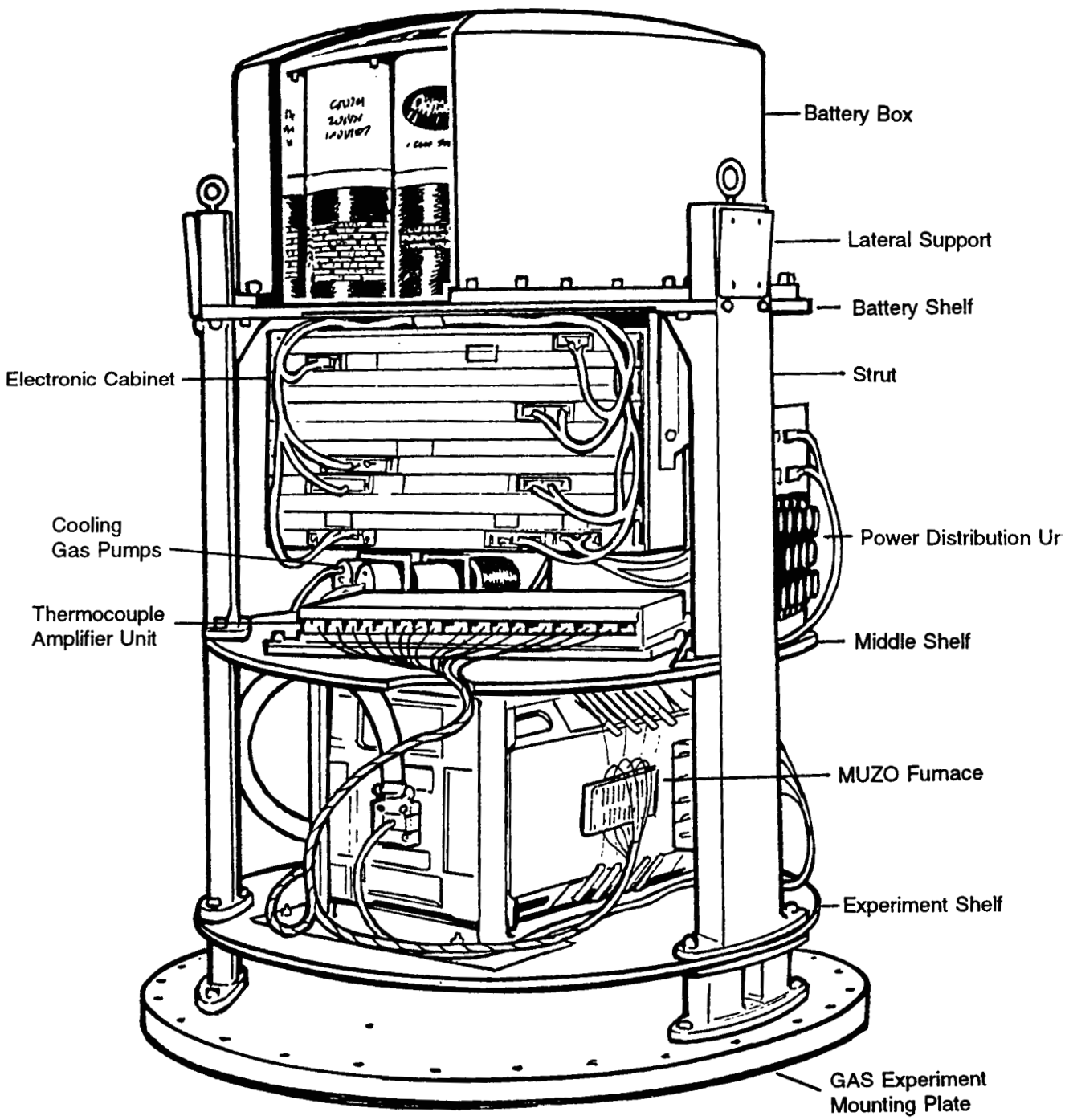

Figure 2: The GAS 330 Payload

The control system collects information from 15 thermocouples and uses the information to regulate the temperature in the sample. The control system has a software regulator for each heater. Each regulator uses different thermocouples during an experimental sequence depending upon the position of the solid/liquid interface.

During the development phase, much effort has been put into solving the problem of energy dissipation at the solid/liquid interface during solidification. Having taken the latent heat of fusion of Ge into account, the control system allows crystal growth rates and sample temperature gradients in accordance with preset values.

It is important to keep a constant temperature gradient in the molten part of the sample during the whole experiment sequence. In figure 3, temperature readings from the solidification phase of the experiment sequence are shown.

Figure 3 shows that the experiment sequence starts with a period of constant velocity (the first 10 lines from the top are separated with equal distance, each line is separated by 100 sec) and then the velocity is increasing. The sample has a melting point of 938°C. The diagram shows that the temperature gradient in the liquid part of the sample is very close to the required 2°C/mm during the whole experiment sequence.

The temperature readings in figure 3 are collected during the flight experiment. The coordinate axes are showing temperature and sample position. Each special mark in the figure indicates a position and a temperature of a thermocouple. Every 100 seconds, a line is drawn to show the temperature inside the sample, starting with the line on top.

Cooling System

The furnace core is equipped with longitudinal cooling gas channels that makes it possible to quench the sample or to achieve steep temperature gradients. The cooling system is of an open loop type and the atmosphere in the canister (argon to protect the sample from oxidation) is used as cooling medium. The gas is circulated through the furnace by two pumps. The gas flow is controlled by changing the speed of the pumps.

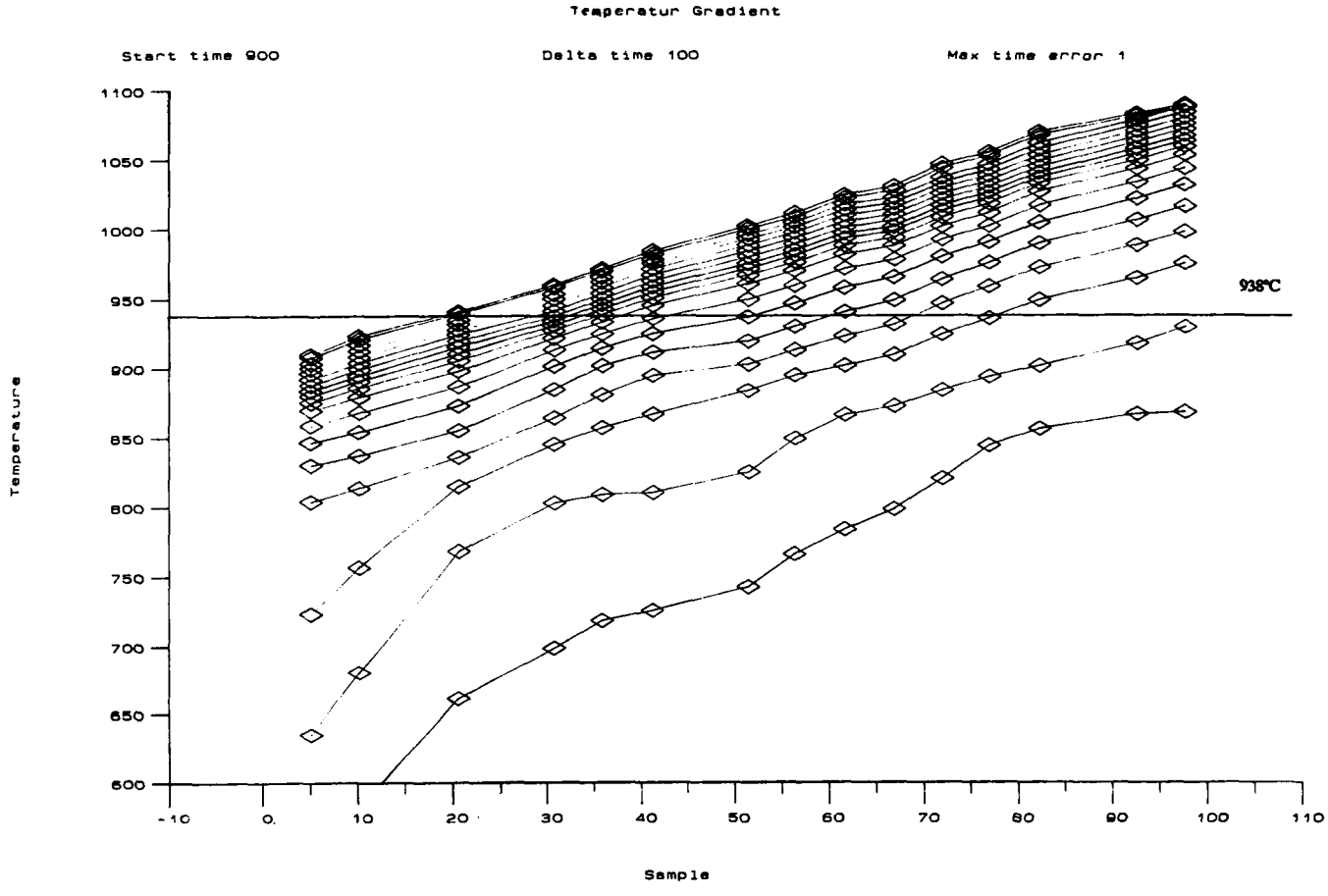

Figure 3: Axial temperature distribution in the sample at every 100 seconds, starting from top of diagram.

MICROGRAVITY EXPERIMENTS WITH Ge CRYSTALS

The first space experiments, for which the MUZO furnace has been used, was designed to study the morphological stability of a planar solid/liquid interface. Accurate control of temperature gradients and growth rates are therefore necessary. A growth rate profile starting with a period of constant rate, to obtain steady state conditions, and followed by a period with acceleration have been chosen.

The growth rate could be followed by interface demarcations obtained by Peltier pulsing every third second. The demarcations also revealed the interface shape, which was slightly concave, i.e. the centre growing about 0.5 mm behind the periphery. Of course the development of the morphological instability can also be followed by the demarcations.

A way to characterize the furnace performance, in terms of convection level in the melt, is to study axial concentration profiles. This has been done in 10 mm diameter Ge crystals doped with Ga. Results from 9 crystals grown under different convection conditions are shown

in figure 4. The growth rate profiles are for all samples identical. The space sample shows a segregation typical for totally diffusion controlled growth, i.e. negligible convection. The crystal, grown in a vertical, thermally stabilizing condition, shows a segregation behaviour typical for mixed convective-diffusive transport. At about 13 mm the concentration starts to increase as a result of increased growth rate. At the same position in the space sample the initial transient was not ready and steady state was never reached.

As a summary of the tests it can be concluded that the furnace is well suited for studies of convective effects on segregation, on ground as well as in space.

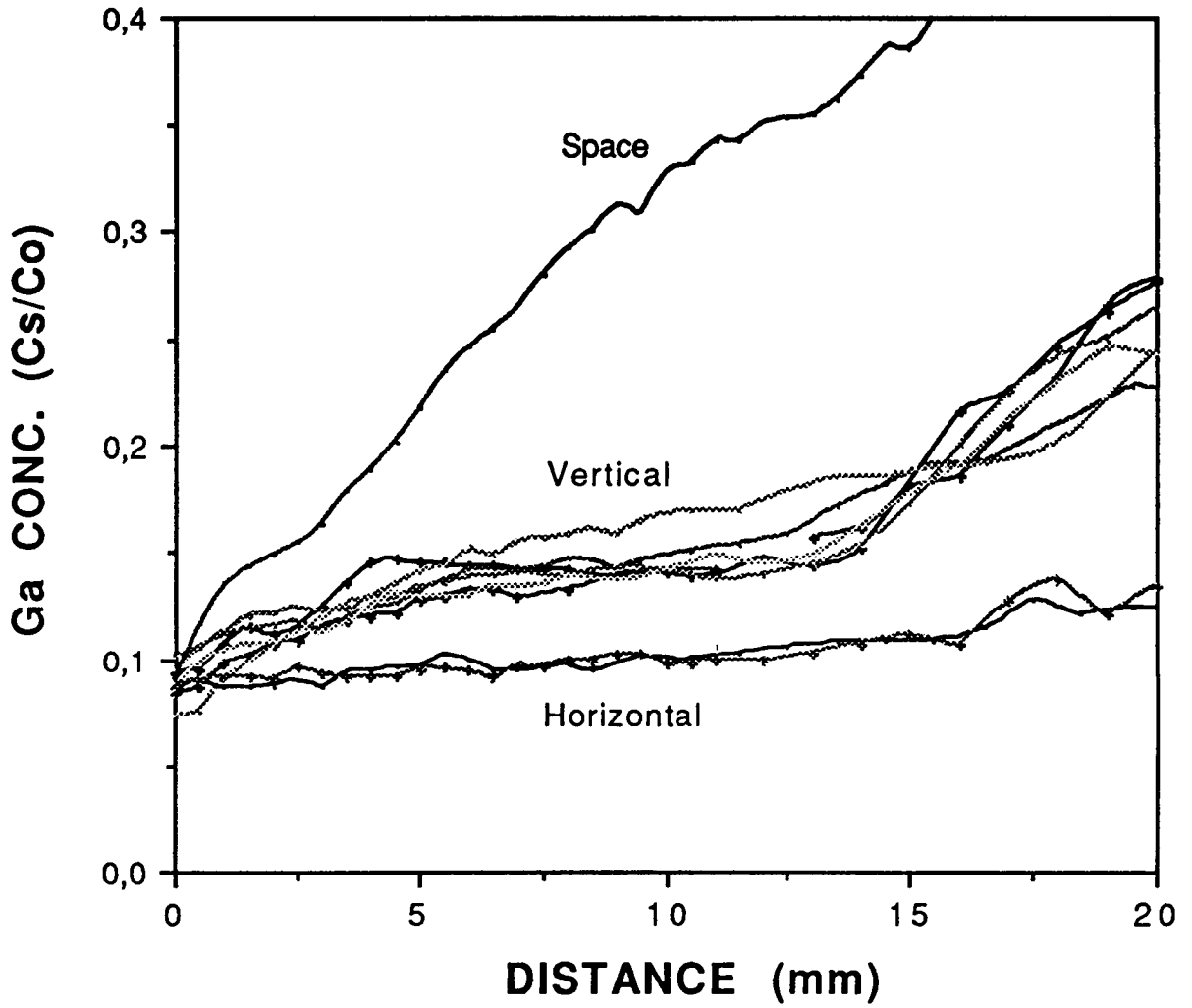

Figure 4: Normalized concentration profiles from the centre line of Ge crystals grown under different convection conditions. One crystal was grown in space. Six crystals were grown on ground in vertical, thermally stabilized with hot end up, position. The remaining two crystals were grown in a horizontal position.

ALTERNATIVE EXPERIMENT APPLICATIONS

Liquid Phase Epitaxy

The Liquid Phase Epitaxy (LPE) technique is a method of significant importance for the growth of advanced semiconductors. Microgravity experiments with the LPE technique is of major scientific and technological interest. However, the LPE technique poses severe thermal requirements on the experiment equipment and has rarely been applied in microgravity.

The thermal requirements of the LPE technique should be fulfilled by the MUZO furnace which is designed, inter alia, for high-temperature isothermal applications such as high temperature solution growth.

In-Situ Produced Composite Material

Metal Matrix Composite (MMC) is used in many applications today and one such is carbides bounded by a metal matrix. This material can be produced by in-situ precipitate carbides in a metallic liquid. This could be done by letting two materials with different composition react with each other. A precipitation of small crystals can occur at this reaction, which will give the composite.

The reaction between the two materials in liquid form often give rise to concentration and temperature gradients. The caused convection in the melt will influence the precipitation process.

In-situ produced composite material experiments requires an isothermal furnace for medium to high temperature applications. This should be fulfilled by the MUZO furnace.

CONCLUSIONS AND RESULTS

The MUZO furnace has so far demonstrated very interesting results during an experiment under microgravity conditions and will therefore be utilized for a new experiment in a GAS canister in 1994.

The batteries that were reinforced due to problems during the vibration tests functioned perfectly during flight and there has been no reduction in battery capacity one year after the flight.

The maximum temperature in the payload during flight due to internal and external heating has been between 40-50°C depending on the location inside the payload.

REFERENCES

[1] M. Lichtensteiger, A.F. Witt and M.C. Gatos;
J. Electrochem.Soc. 188 (1971) p. 1013.

[2] U.E. Holmes and H.C. Gatos;
J. Electrochem.Soc. 128 (1981) p. 429.

[3] A. Rouzaud, D. Camel and J.J. Favier;
J. Crystal Growth, 73, (1985) p. 149.

[4] M. Adornato and R.A. Brown;
J. Crystal Growth, 80, (1987) p. 155.

[5] S.R. Coriell and R.F. Sekerka;
J. Crystal Growth, 46, (1979) p. 479.

THE GAMCIT GAMMA-RAY BURST DETECTOR

Benjamin J. McCall, John M. Grunsfeld, Srdjan D. Sobajic
Chinley Leonard Chang, David M. Krum
Albert Ratner, Jennifer E. Trittschuh
California Institute of Technology
Pasadena, California 91125
for the GAMCIT Team

ABSTRACT

The GAMCIT payload is a Get-Away-Special payload designed to search for high-energy gamma-ray bursts and any associated optical transients. This paper presents details on the design of the GAMCIT payload, in the areas of battery selection, power processing, electronics design, gamma-ray detection systems, and the optical imaging of the transients. The paper will discuss the progress of the construction, testing, and specific design details of the payload.

In addition, this paper will discuss the unique challenges involved in bringing this payload to completion, as the project has been designed, constructed, and managed entirely by undergraduate students. Our experience will certainly be valuable to other student groups interested in taking on a challenging project such as a Get-Away-Special payload.

SCIENTIFIC OBJECTIVES

The first report of gamma-ray bursts (GRBs) occurred in 1973 from earth orbiting satellites. GRBs are highly energetic events, that are characterized by a rapid increase in the observed gamma-ray flux, at energies from tens of keV to several MeV's. The decline of such events may be a simple exponential or quite complex non-linear decay. Three gamma-ray bursts observed by the BATSE detector on the Compton Gamma Ray Observatory are depicted in Figure 1.[1]

It soon became evident that gamma-ray bursts represent one of the most energetic and violent events in the observable universe. Ever since the first detection of these phenomena, many experiments, including the BATSE experiment, have been designed to monitor them, yet their origin is still one of the great enigmas of modern astrophysics. The BATSE observations have yielded important data on the possible origin of these events. By determining the coarse location of these bursts, BATSE researchers have observed an isotropic distribution of GRBs. Furthermore, from studies of the intensities of these bursts, researchers have deduced that the bursts are not distributed homogeneously, but have a definite boundary. [2] The distribution of a sample of gamma-ray bursts, observed by BATSE, and showing their isotropy, is shown, in Figure 2. These facts indicate that the bursts are either local to the solar system, distributed in a large halo around the Galaxy, or at cosmological distances.

One theory suggests that neutron stars in binary systems are the cause. In this scenario, a normal companion star transfers material into an extremely strong gravitational potential well near the neutron star. The energy gained by this matter is converted into gamma-rays near the surface of the neutron star producing a gamma-ray burst. Other models predict that comets, or other material is accreted by an isolated neutron star of black hole producing a GRB. An interesting prediction of these theories is that as the gamma-rays strike the atmosphere of the companion star, some of the gamma-ray energy may be converted to visible light. If these theories are correct, then a GRB may be accompanied by an optical transient. [3]

OVERALL SYSTEM DESIGN

GAMCIT uses two standard NaI(Tl) scintillation gamma-ray detectors, combined with a 35mm film camera and film sensitive to visible electromagnetic radiation. GAMCIT is the first experiment to search for gamma-ray bursts and their associated optical transients truly simultaneously. An intelligent micro-controller triggers the camera when a burst is detected by the scintillators. Two detectors are used to require a multiple coincidence between independent units, reducing the possibility of a non-gamma-ray burst triggering the payload. The time and location of the burst are determined by using an on-board Global Positioning System (GPS), which provides extremely accurate information. This information is needed to correlate the results of GAMCIT with other experiments, namely BATSE and the Pioneer Venus Orbiter. If we detect an optical flash we should be able to localize the source to within a radius of less than 10 arc minutes. To discriminate against solar flares and other anomalies, we incorporate a small silicon charged particle detector. Solar flares resemble gamma ray bursts, however, they are usually accompanied by a large flux of charged particles. The charged particle detector will detect such events and allow us to veto them.

STRUCTURAL DESIGN

The three major structural components of the GAMCIT experiment are the user lid, the main supporting structure, and the battery box. The GAS lid is the attachment interface between the can and the NASA mounting plate. Since we are using a Motorized Door Assembly (MDA), a major task was designing a space facing pressure vessel lid. The concerns that were dealt with during the design process were structural integrity, thermal insulation, and maximization of gamma-ray penetration. All structural components (not including fasteners) are 6061-T6 aluminum.

This was accomplished using a composite lid, composed of a thermally insulative inner core of Kevlar (manufactured by E. I. du Pont de Nemours & Co., Inc.) and high-density foam, and an exterior of aluminum which provides structural integrity and mounting. The regions above the scintillator crystals have the aluminum removed for greater gamma-ray penetration. The area above the camera lens

is replaced by an optically transparent quartz window assembly. (See Figure 3.)

The main structure partitions the center region into three sections - two for gamma-ray detection and one for the optical camera and electrical system. The cross-section of this structure is a modified "Y." To avoid welding and maintain strength, this structural configuration is fabricated by taking three plates, bending them to the desired angles, and bolting them together back to back. Aluminum shelves are bolted normal to the partition surface to provide structural stability and allow the mounting of components. (See Figure 4.)

The main supporting structure bolts directly to the top of the battery box. The battery box consists of a top and bottom plate connected by aluminum bars. The bars act to both strengthen the box and to hold in or provide mounting for the battery cases. The individual battery packs consist of ten batteries (or, a few special packs of five) soldered and epoxied together. To allow for efficient replacement, each pack is then housed in a cage of two aluminum plates held together with metal spacers. The interior of the battery packs is coated with an electrically isolating gel to prevent premature discharging of batteries.

DETECTOR DESIGN

There are two major components of the detector system: the gamma-ray detector system and the optical transient detection system. The gamma-ray detector is comprised of two NaI(Tl) scintillator crystals, 16 cm in radius and spanning an angle of 115 degrees each. This provides GAMCIT with a gamma-ray viewing area of approximately 650 square centimeters. Each scintillator crystal is optically coupled to an 7.6 cm (3 inch) diameter eight-stage photo-multiplier tube (PMT) by the use of a light integration cone, the interior of which is coated with a highly reflective barium sulfate paint. (See Figure 5.) The PMTs collect the photons emitted by the crystals and convert them into an amplified electrical signal. This signal is then passed on to the electronics system.

The other major system is the optical camera system. The system is comprised of a professional 35mm film camera with a 250 exposure data back. The lens system is a standard 50mm f/1.2 lens available from the camera manufacturer. Since the image to be photographed is at infinity, and the depth of field is unimportant, the lens may be stopped down to the lowest setting (f/1.2). The focus ring, however, must be fixed so that vibrational stress does not cause the camera to de-focus. The data back holds 250 exposures, and each burst triggers the camera for five one-minute exposures, indicating that we will have sufficient film for 50 bursts. This is an over-estimate of the number of real bursts that are statistically expected, however, false triggerings may significantly increase this number.

The film used is standard 35mm Technical Pan film with a

resolution of 320 lines per mm, sensitive to visible light. With an exposure of one minute at the 50mm f/1.2 setting we can expect to see up to seventh magnitude astronomical objects. Although the manufacturer suggests hypersensitizing the film prior to usage in astronomical applications, we find that such a task would be logistically daunting, and have found acceptable results without any such process.

ELECTRONICS DESIGN

At the heart of the electronics system lies a 16-bit CMOS, high-reliability, low-power micro-controller. The micro-controller is in charge of all instrument control, data handling and system maintenance functions. Figure 6 shows the block diagram for the payload.

The primary function of the micro-controller is to identify and record a gamma-ray burst. This is accomplished by having the output current from the PMT pass through the amplification and detection electronics.

The signal from the PMT will pass through a charge sense amplifier that will convert the current pulse into a voltage spike. This signal is then fed through two discriminators, a low level one that has a threshold level set to 15 KeV, and a high level one with a threshold set at 1000 KeV. Using the signals from the high and low level discriminators it is possible to determine whether an event (a burst) has actually occurred or if it is outside our mission specifications. This event signal passes through a series of 16 bit counters implemented in a field programmable gate logic array (FPGA). The counters determine the number of events that occur in a time bin. The time bins will correspond to durations of 50 microseconds, 100 microseconds, 1 millisecond, 10 milliseconds, 100 milliseconds, 1 second, 10 seconds, and 100 seconds. The outputs are multiplexed onto the data bus. The signal from the charge sense amplifier also passes through a pulse shaping amplifier. The pulse shaping amplifier lengthens the pulse creating a "flat top" for the analog-to-digital converter. The 8-bit A/D converter is activated by an event signal that is delayed by 500ns, so that the A/D converter digitizes the peak of the pulse shaping amplifier output. The A/D converter is set so that 0 KeV corresponds to chanel 0 and 1 MeV is channel 255.

A 5.5 sigma (where sigma is the standard deviation of the date in a given time bin) detection scheme is implemented in the software. A running average and sigma is kept over the last 17 time periods in each of the eight time bins. If in a given time bin a counter value exceeds the running average by more than 5.5 sigma, a burst is detected and the system will record the time and the A/D converter will be activated and will begin recording pulse heights. The charged particle detector output is monitored by the micro-controller and it serves as a veto in deciding to send the system to Burst Mode, (i.e. if we detect a charged particle simultaneously with a gamma-ray we will not enter Burst Mode).

In addition, the electronics system must communicate with the Global Positioning unit (GPS) to record the time and position of the Orbiter. This operation is performed every second. The data is buffered by Flash RAM and written to the hard disk drive through the IDE interface.

Camera operation is also controlled by the electronics system. When a burst is detected, and the system goes into Burst Mode, a relay is triggered that closes the shutter contacts on the camera body. The contact is kept closed for one minute, upon which it is opened and closed again immediately for the next exposure, until five exposures have been attempted. Furthermore, the electronics also has to monitor the level from a photodiode in the optical light path, so that the shutter can be closed (or not opened at all) in the event that the camera rotates into an extremely bright object, (e.g. the sun).

Finally, the electronics system is in charge of some elementary housekeeping. The electronics monitor the temperature, pressure, current and battery voltage sensors. The temperature and pressure sensors are polled by an A/D converter every minute, and are stored every five minutes. The current and battery voltage are monitored so that the micro-controller manager will send an interrupt if power begins to drop, allowing the system to save vital data.

POWER MANAGEMENT

One of the primary concerns of the GAMCIT Team was the power source selection, since all Get-Away-Special (GAS) payloads must be totally autonomous from the Space Shuttle Orbiter except for the crew activated relays. Thus, upon drawing up a power budget, it was our task to determine which type of power source was most appropriate to our application requirements. After a careful consideration of the products currently available on the market, and of those that fell within the NASA safety margins, we decided on standard commercially available alkaline D-size cells. The cells have a nominal voltage of 1.5 V with a rated capacity of 14.25 Amp-hours.

The major problem one encounters with alkaline cells is their less than ideal discharge characteristic. In general, such cells discharge linearly with time from their nominal voltage (1.5 V) to the rated cut-off voltage (0.8 V). In order to overcome this difficulty, we were forced to consider a DC-DC converter. The DC-DC converter we chose has an input voltage range from 7-35 VDC, and three output terminals: two at 12 VDC and 0.7 Amperes maximum current, and one terminal at 5.1 VDC and 5.0 Amperes maximum current.

The actual battery setup is configured as 27 packs of 10 batteries each, for a total of 270 batteries. Each pack of batteries provides 15 VDC nominally, discharging to the cut-off voltage of approximately 8 VDC. Each parallel leg of the total

battery power supply is protected by a Schottky diode to prevent circulating currents which would lead to mission failure. In addition, the whole power supply is protected by a 6 Amp fuse, chosen in accordance with NASA regulations, on the ground leg.

The electronic system is fully powered through the DC-DC converter, except for a clock that is powered continuously and is supplied with its own power source, a small lithium watch type battery.

The two photo-multiplier tubes are powered by a -1500 VDC power supply. The voltage is reduced to the appropriate stage using a resistive voltage divider. The current is extremely low (< 1 microA) so that the resistive power dissipation can be kept low. The power supply will receive a +12 VDC signal from the DC-DC converter and will convert it to the -1500 VDC needed by the PMTs.

Finally, the optical camera system is powered by its own set of 6 alkaline D-cells. An adapter available directly through the camera manufacturer allows us to use 6 D-cells rather than 6 AA-size cells. The camera data back clock also has its own lithium watch type battery that will maintain the clock accurately for an extended period of time.

CONSTRUCTION AND TESTING

Currently GAMCIT is still in the early stages of construction. A prototype of the support structure has been constructed, and the battery box has been designed and one 10-battery pack has been built. The user lid has been designed but no construction has yet begun. The electrical system has been finalized and some prototyping has begun.

Most of the preliminary testing has been completed. We performed a battery test, the results of which were positive. The batteries lasted for a full day longer than anticipated. Another battery test will be attempted before the actual flight to ensure the validity of the first one. Two film tests were performed, which are yet to be carefully analyzed, but the results are positive as well. The primary concern is that because of the Orbiter's significantly higher velocity, we will not be able to see as deep as from earth. This effect occurs because the Orbiter's angular velocity is 16 times greater than the earth's, and the light that hits an area of 1 square millimeter on earth will spread over an area of 16 square millimeters in space. Effectively, the exposure is cut by a factor of 16.

One further test that needs to be done is the shake test on the PMT. A shake test involves mounting the PMT to a standard mounting plate, and actuating the plate via a motor operating at a certain frequency. The shake test will range from 20 Hz to 2000 Hz, increasing the magnitude of the oscillation from 20 Hz to 100 Hz, keeping it constant from 100 Hz to 1000 Hz, and decreasing the magnitude from 1000 Hz to 2000 Hz. A ruggedized model of the PMT is

available from the manufacturer, however, it will not be known until after the test whether the ruggedized version will be needed. After the construction is complete we will run a full test on the entire experiment simulating the entire Orbiter flight, including Orbiter thermal and mechanical conditions, such as vibration, etc.

CHALLENGES

The GAMCIT project at Caltech has been driven entirely by undergraduate students since its beginning. GAMCIT is actually a spin-off of the Caltech Students for the Exploration and Development of Space (SEDS), a student group with over one hundred members (over 6% of the student body, graduate and undergraduate). The sponsorship of Caltech SEDS has been essential to the success of the project, in terms of drawing in interested students, facilitating support from Caltech's administration, and bringing in start-up funds from aerospace corporations.

While the sponsorship of a large student group is very beneficial, our experience has proven that projects such as ours cannot succeed without faculty and staff support. Dr. John M. Grunsfeld served as our first advisor for the GAMCIT project, and was instrumental in obtaining recognition and laboratory space for the project, as well as in the preliminary design work. After Dr. Grunsfeld left Caltech to become an astronaut candidate, the students of GAMCIT approached Dr. Maarten Schmidt of the astronomy department to serve as a faculty advisor. Dr. Schmidt's assistance has proven invaluable in securing financial support from Caltech and outside organizations to continue the project. It is also worth noting that securing course credit for work on the project has been very helpful in recruiting new members to the project team, and our thanks go to Dr. Joel Burdick of the mechanical engineering department at Caltech for assisting us in this respect.

However, the challenges involved in the GAMCIT project go far beyond those of politics. Because our "engineers" are all undergraduates, the project's participants have faced quite a learning curve in all areas of the science and engineering of the payload. While this makes for a much slower timetable than projects in industry might enjoy, it also serves to provide hands-on experience for undergraduates that is seldom available in standard university curricula.

As in any other workgroup, leadership, responsibility, and personal relations are critical issues to the success of a project such as ours. However, these problems are exacerbated by having an all-undergraduate working group - students are students first and space experimenters only in their "spare time." Offering course credit can serve as a limited incentive to "get things done," but ultimately the motivation must come from the students' own sense of involvement in the project, which is in turn dependent in large part on the leadership and group dynamics of the project.

In the end, most of the hard work on a project staffed by undergraduates must, unfortunately, be done during the school year. In the summer of 1993, GAMCIT was able to offer stipends to five students to work for ten weeks on the project (many thanks to Ms. Joanne Clarey of Corporate Relations and to Ms. Carolyn Merkel of the Summer Undergraduate Research Fellowship Board). While most of the design details were hammered out over the summer, much of the construction is left to the full project team this fall, and as before all students are sure to be pressed for time.

The challenges and pitfalls involved in a project such as ours, staffed entirely by students, are indeed distinct from those faced in similar projects in industry or the military. While the pitfalls are many, the rewards of a student-run project are even more plentiful. We welcome correspondence from present, past, or potential student groups who are interested in Getaway Special projects.

CONCLUSIONS

The GAMCIT experiment has been a rewarding experience for all involved in its design and construction. GAMCIT also provides an almost guaranteed return, because any gamma-ray data collected can be correlated with similar observatories currently on ULYSSES, the Pioneer Venus Orbiter and the Compton Gamma Ray Observatory. A single optical transient correlated with a gamma-ray burst would provide a stringent constraint on burst theories.

REFERENCES

1. Fishman, G.J., Meegan, C.A., Wilson, R.B., Paciesas, W.S., Pendleton, G.N., The BATSE Experiment on the Compton Gamma Ray Observatory: Status and Some Early Results, NASA Conference Publication 3137, 1992, pp. 26-34.

2. Meegan, C.A., Fishman, G.J., Wilson, R.B., Paciesasm W.S., Pendleton, G.N., Hornack, J.M., Brock, M.N., and Kouveliotou, C., Spatial Distribution of Gamma-ray Bursts Observed by BATSE, Nature, 1992, vol. 355, pp. 143-145.

3. Surka, D.M, Grunsfeld, J.M., Warneke, B.A.: GAMCIT - A Gamma-Ray Burst Detector. Shuttle Small Payloads Symposium NASA CP-3171, 1992. (Paper 15 of this compilation.)

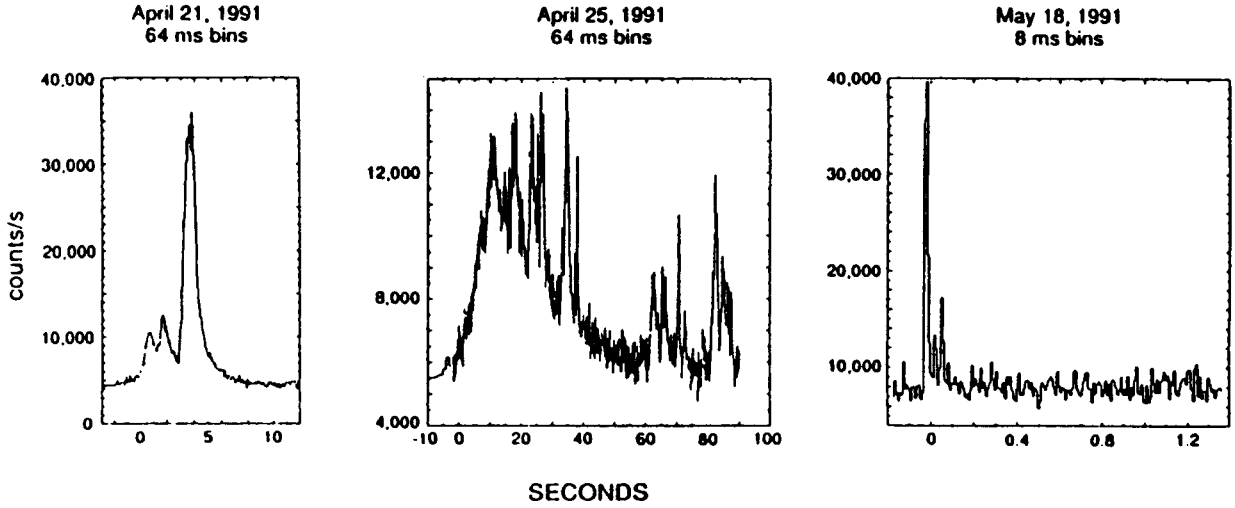

FIGURE 1. A sample of gamma-ray bursts as observed by the BATSE instrument on the Compton Gamma Ray Observatory (reproduced from [1]). These burst profiles show the wide variety of structure and varying time durations of gamma-ray bursts, from milliseconds to 100s of seconds. The energies of the gamma-rays in these plots range from 60 keV to 300 keV.

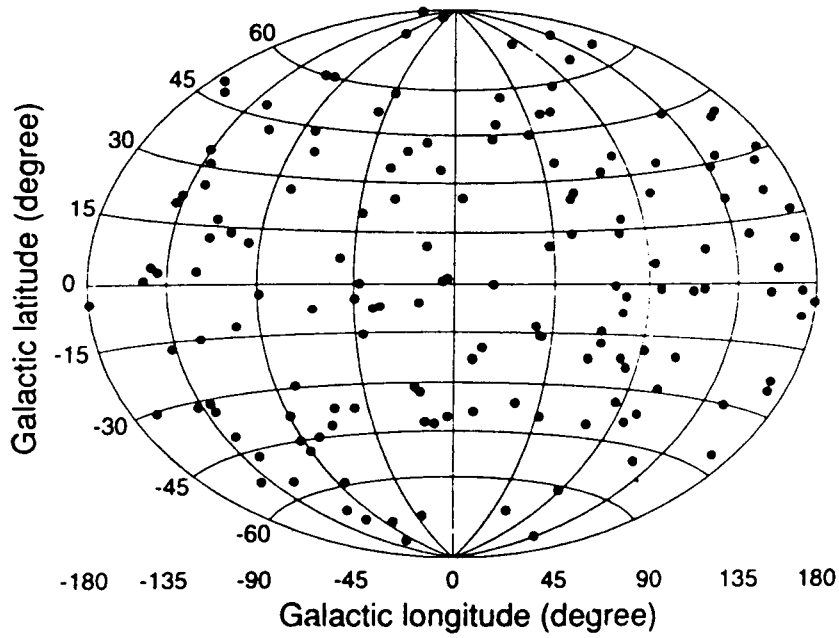

FIGURE 2. The angular location of gamma-ray bursts in Galactic coordinates as observed by the BATSE instrument on the Compton Gamma Ray Observatory (reproduced from [2]). The observed distribution shows no significant deviation from isotropy. In particular no enhancement along the Galactic plane (latitude=0) is seen, as would be expected if the sources of gamma-ray bursts had the same distribution as the stars in the Galaxy.

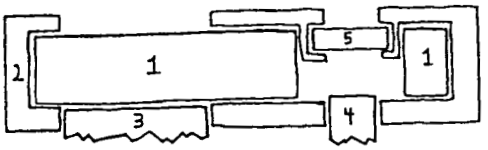

FIGURE 3. A cross section of the user lid. 1. Kevlar and foam insulation. 2. Mounting brackets. 3. Scintillator Crystal. 4. Camera Lens. 5. Quartz Window.

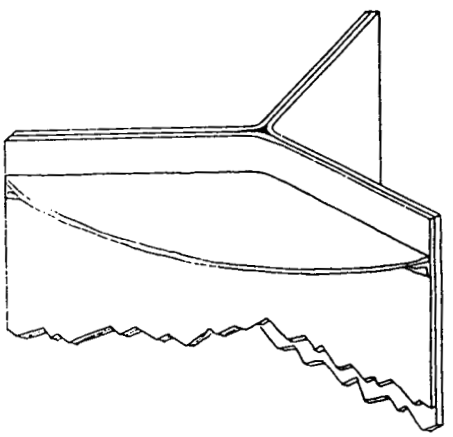

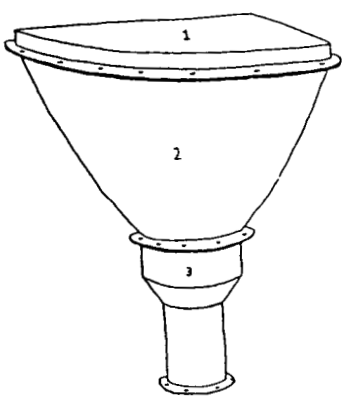

FIGURE 4. A cut-away view of the "Y" shaped supporting structure, with one shelf in place.

FIGURE 5. The gamma-ray detector assembly. 1. Scintillator Crystal. 2. Light Integration Cone. 3. Photo-Multiplier Tube.

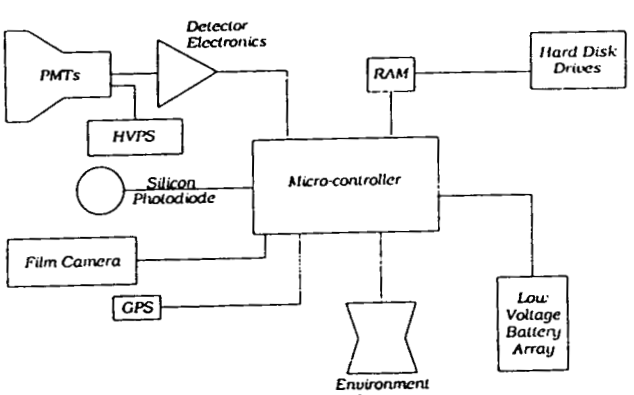

FIGURE 6. Block diagram of the Caltech GAMCIT experiment.

STATIC COMPUTER MEMORY INTEGRITY TESTING (SCMIT)
An experiment flown on STS-40 as part of
GAS Payload G-616

Thomas Hancock
Private Research
Huntsville, AL USA

ABSTRACT

This experiment investigated the integrity of static computer memory (floppy disk media) when exposed to the environment of low earth orbit. The experiment attempted to record soft-event upsets (bit-flips) in static computer memory. Typical conditions that exist in low earth orbit that may cause soft-event upsets include: cosmic rays, low level background radiation, charged fields, static charges and the earth's magnetic field. Over the years several spacecraft have been affected by soft-event upsets (bit-flips), and these events have caused a loss of data or affected spacecraft guidance and control.

This paper will also describe a commercial spin-off that is being developed from the experiment.

INTRODUCTION

Over the years several different spacecraft have suffered soft event upsets (bit-flips) of their onboard memory. The most famous instance occurred in 1986 when the Voyager 2 spacecraft was encountering the planet Uranus. The spacecraft suffered soft-event upsets in its Flight Data Subsystem that caused a loss of guidance and control for several hours and resulted in the spacecraft pointing its cameras and other instruments out into deep space and away from the planet.

Today as larger, more complicated systems are planned (United States Space Station Freedom, etc.) the possibility of soft-event upsets may become more of a concern. Large space systems may not rely on mass uplinks (for reloading of their command and data, attitude control and experiment work station subsystems) due to the size and complexity of the uplink files, but carry back-ups of the flight software (operating systems) onboard as static memory.

Goal

The goal of this experiment was to:

1. Observe soft-event upsets
2. Determine the frequency of soft-event upsets
3. Determine the characteristics of soft-event upsets
4. Determine the possible effectiveness of different types of shielding material
5. Evaluate the possibility of using static memory as a type of Passive detector.

EXPERIMENT

Methods and Materials

The experiment consisted of 40 floppy disks of a standard commercial type. Each contained a text file that functioned as a bit-map. Each text file/bit-map was of an identical size and format (see Figure 1). This method made it simple to determine when a soft-event upset had occurred by observing a change in the logic state (the character representation) of any area on the bit map during post flight analysis (see Figure 3). Each text file filled the disk to capacity.

Groups of 10 disks were inserted into each of four storage containers. Several of the disks were covered in one of three types of shielding material. The three types of shielding material were:

normal anti-static nylon
aluminized mylar mesh
field dispersing (electrically neutral) nylon.

Procedure

The experiment was constructed by:

1. Developing a large text file/bit-maps
2. Copying identical bit-maps on all 40 disks
3. Covering a number of the disks with one of 3 types of shielding material
4. Testing to assure the integrity of the disks
5. Inserting disks in groups of 10 into storage boxes

The experiment was integrated into the GAS canister in July of 1990. The experiment was stored in the GAS canister on the GAS bridge until early 1991 and was launched in June 1991 as part of STS-40. The experiment remained in orbit for 9 days.

Post flight recovery of the experiment took place in July of 1991 and detailed analysis was started shortly thereafter.

Post Flight Analysis

Each disk was analyzed for evidence of soft-event upset. Currently single event, soft-event upsets have not been observed. However, 10 disks did exhibit characteristics that may or may not be attributable to massive numbers of soft-event upsets. As each disk was verified prior to launch, errors of the type observed normally would have been detected during testing. Unfortunately the experiment lacks the fidelity to accurately measure massive changes to the logic state at this time, as these were not anticipated prior to flight. The disks that exhibited these characteristic were not shielded during the flight.

CONCLUSIONS

In general, the experiment was successful. The type of soft-event upset (single events) anticipated prior to flight were not observed. However, a massive number of changes observed in the logic state of 10 disks does indicate the possibility that events had occurred and were recorded on the disk media. The experiment should be repeated with a greater level of fidelity and if possible, flown several times to establish a baseline.

COMMERCIAL SPIN-OFF

INTRODUCTION

During the development of this experiment, a new method for measuring levels of exposure to or detecting numbers of events (bit-flips) caused by radiation, cosmic rays or other energetic sources was identified. This product uses a method similar to that employed in the experiment.

Methods and Materials

This product will use standard size 3.5 inch floppy disks. Each disk will have its magnetic media made of a material that is more susceptible to soft-event upsets (see Figure 2). Each disk will contain a standard text file/bit-map (similar to Figure 1.).

Procedure

A user can carry the disk(s) or place them within the environment that is to be monitored. This product also has a potential use as a static detection array. Several disks can be placed on the surface of a small retrievable satellite or other structure for long term monitoring of the associated environment (earth or space).

When desired, the dosage or number of events recorded can be determined by using a standard statistical algorithm. This method makes it possible for a user to determine the relative dosage or number of events recorded by inserting the disk into any standard Personnel Computer and starting the associated program.

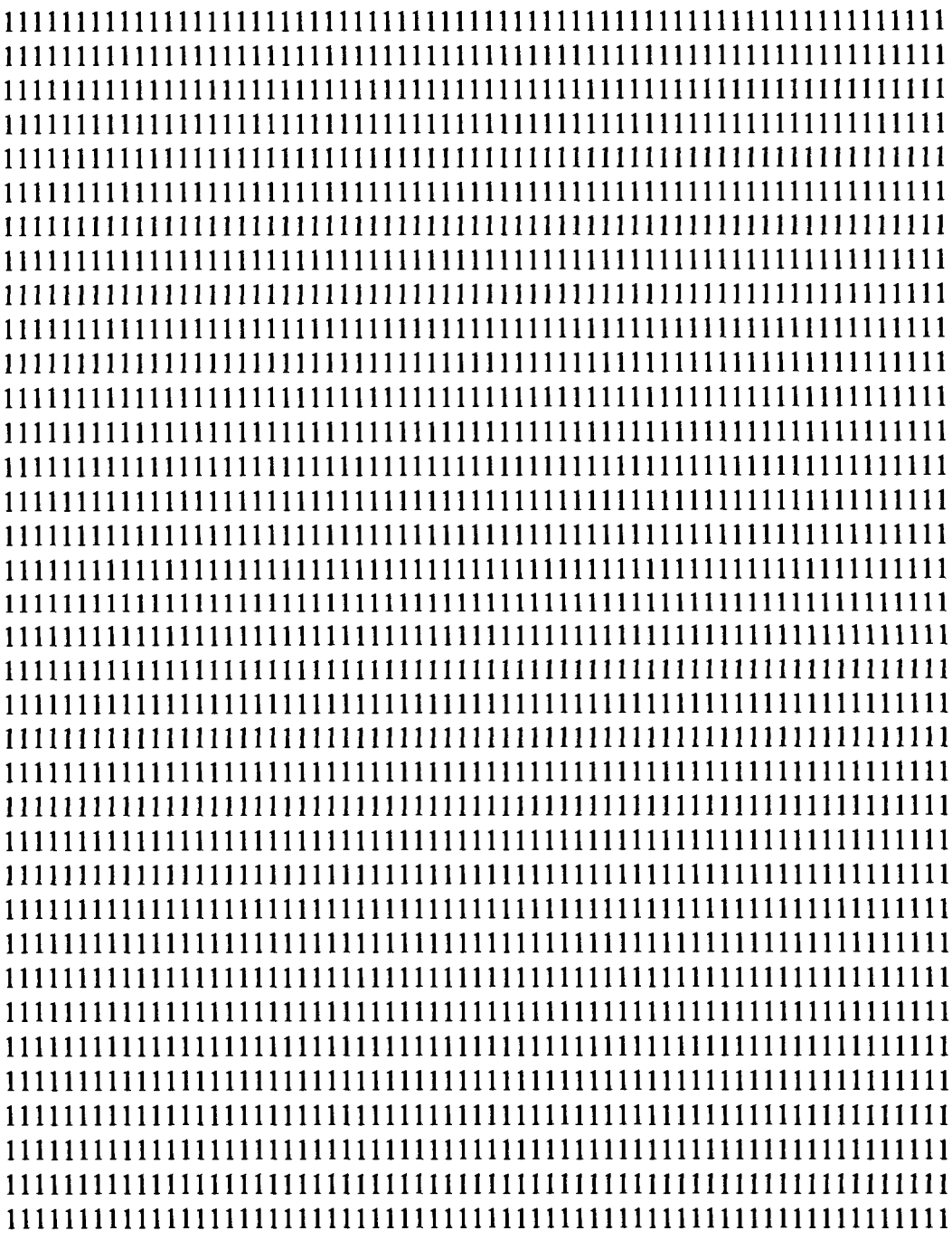

Figure 1. Sample of Text File/ Bit-map

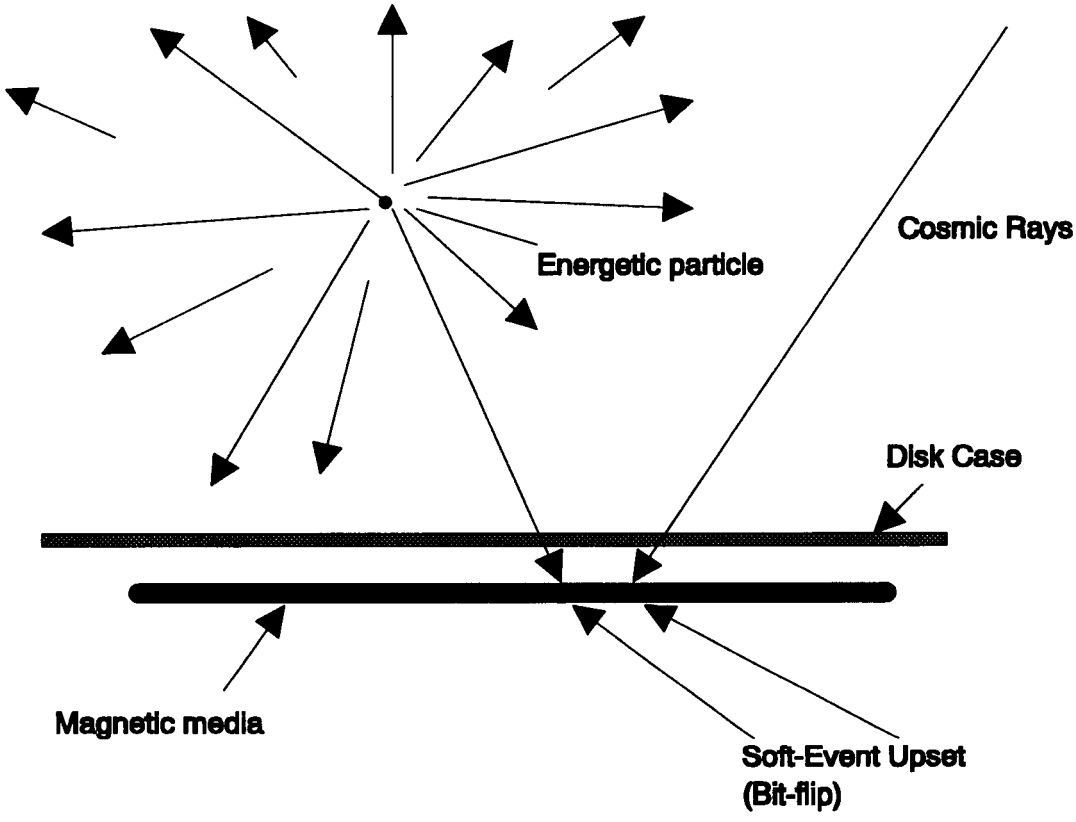

Figure 2. Soft-Event Upset

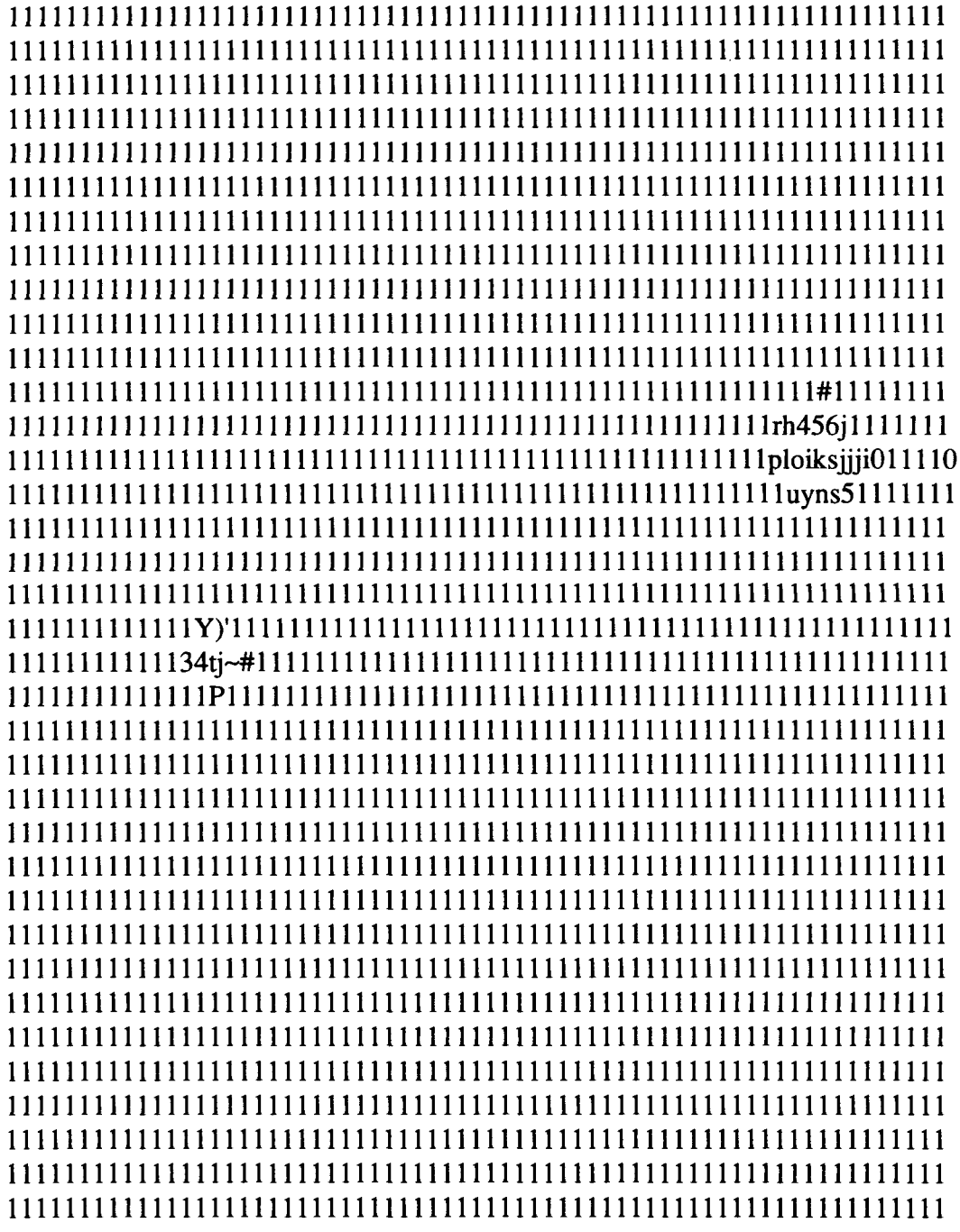

Figure 3. Example of soft-event upsets anticipated before flight

THE FIRST FLIGHT OF THE QUESTS GAS PAYLOAD, G-521

Darrin Gates, Electrical Systems Engineer,
Bristol Aerospace, Winnipeg, Manitoba

ABSTRACT

An overview of all of the phases of the QUESTS Get Away Special project is presented in this paper. Details from the early phases of the project; design, manufacture and test, through to the first flight results are provided. The handling of safety issues, payload capabilities, the experiment complement, payload integration and de-integration and interfacing with NASA is also discussed.

INTRODUCTION

The QUESTS (Queen's University Experiment aboard the Space Transportation System) project originally started as a Canadian Space Agency (C.S.A.) competition to come up with a microgravity materials processing experiment. Prof. Reg. Smith (Queen's University) won the competition and was tasked to design the furnaces and to define the experiments that would fly on a Shuttle based Get Away Special (GAS) payload. Bristol Aerospace was then contracted by the C.S.A. to design, manufacture, test and integrate the GAS payload to accommodate Queen's University science and to satisfy all NASA safety requirements. During the design phase it was realized that more furnaces could be accommodated. This led to the invitation of Dr. Kedar Tandon at the University of Manitoba to participate in this GAS project.

DESIGN, MANUFACTURE AND TEST

The QUESTS payload hardware and software were designed to act as a flexible platform for material experimentation and research in a microgravity environment. The payload was designed to handle the initial experimenter requirements and to accommodate future science as well. The philosophy of the design approach included the following considerations;

- a modular hardware design for easy removal and replacement of experiments and subsystems,
- design of flexible controller software that would allow for simple experiment parameter changes,
- large contingencies in the available stored energy to handle future experimentation.

NASA safety requirements and proper material selection were of foremost concern during design and manufacture. Wire and fuse sizes were selected such that the wire temperature would remain below vacuum rated limits under maximum current conditions. A structural analysis was performed to ensure payload integrity during launch and landing loads. Maximum furnace temperatures during thermal runaway conditions were determined to ensure compatibility with payload materials. Pressure of the heatsink container was determined for maximum thermal input conditions.

Flight environment concerns were also addressed during payload design and manufacture. Environmental testing activities included;

- vibration (3-axis, 15g on components, 3g on the entire payload),
- temperature (-40 to +85°C),
- full flight simulation test (real time operation simulating the actual flight operations).

SAFETY

All three phases of the NASA safety document submissions were without any major problems. The Preliminary Safety Data Package (SDP) was submitted early during the design of QUESTS. Preliminary parts lists, drawings and test results were supplied in this SDP. Early hazard assessments were made and controls were proposed.

During manufacture as some of the safety concerns were addressed, the Final SDP was submitted. The Final SDP included more detailed parts/material lists and drawings that reflected the as built payload. Testing results were also included in the Final SDP. Hazard assessments and controls were also refined. After this submission NASA requested that an Energy Containment Analysis be performed. The containment analysis, in QUESTS case, was a detailed thermal analysis that showed all of the stored energy in the battery system could be contained within the payload structure and support systems without raising the temperature to hazardous levels. This analysis simplified the safety documentation. A number of the hazard assessments and controls could be removed, after the analysis results showed that the hazards were no longer probable.

The Phase III SDP was submitted after payload testing was completed. All of the To Be Determined (TBD's) were answered and the documentation reflected the actual as built, as tested QUESTS GAS payload. No outstanding items were in the Phase III SDP, and it was this document that was used at the Kennedy Space Center (KSC) during integration to approve the payload for flight.

PAYLOAD CAPABILITIES

The QUESTS payload is capable of carrying 12 isothermal diffusion and 3 gradient crystal growth/directional solidification material processing experiments. Each furnace is capable of temperatures of up to 1000°C.

Each isothermal furnace contains 1 winding and an integral motor/quench block assembly for sample insertion, extraction and cooling (Figure 1).

Each gradient furnace contains 3 windings and the stationary sample is internally fastened to an aluminum foam/paraffin wax heatsink (Figure 2). The heatsink assembly removes heat from the sample to create a temperature gradient.

The payload controller and flight software provide the timing, experiment control, data acquisition and storage functions for QUESTS. A flexible PID algorithm is used to control the furnace temperatures. Time and temperature profiles for each experiment are individually programmable. Experiment temperatures are saved once per minute along with the diagnostics. A 1 Mbyte memory cartridge is used to store experiment temperature and diagnostic data. Expansion of the memory cartridge to 4 Mbytes is being examined for future flights.

Associated electronics provide the interface to thermocouples, power windings, stepper motors, diagnostic sensors, power system and ground support equipment.

Power for the payload is provided by 2 packs of silver-zinc cells, capable of about 2.2 kWatt-hours.

Diagnostic data parameters are measured and saved periodically during the flight. Parameters measured include: acceleration, payload temperatures, pressures, bus voltages and current. These parameters are saved to the memory cartridge along with date, time, status flags and messages for postflight processing.

Low level accelerometers ($\pm$10mg full scale) are used to measure the microgravity environment. The readings are filtered above 0.6 Hz and can resolve to 1.2 μg.

Ground support equipment hardware and PC-based software provide tools to test experiment concepts and verify payload operation prior to flight.

A picture of the QUESTS GAS payload is shown in Figure 3.

EXPERIMENTS

The experiment complement on the first flight of QUESTS was made up of directional solidification and diffusion experiments. Professor Reg Smith and Steve Goodman (Queen's University, Kingston) had 14 samples and Kedar Tandon (University of Manitoba) had 1 sample. Table 1 provides a description for each of the experiments.

The results of the solidification of the Bi-BiMn eutectic at small growth rates will assist Queen's in the development of the theory of anomalous eutectic freezing. Previous work by Queen's and others suggest an anomalously low value for the interphase spacing when the eutectic is frozen slowly.

The University of Manitoba is studying the effect of microgravity on the segregation, phase morphology and the phase distribution of Al-38%(wt)Cu hypereutectic.

Queen's diffusion experiments are designed to measure diffusion coefficients for a number of alloy systems to provide data from which to further develop our understanding of the structure of liquids. The diffusion experiments include the materials; Pb, Au, Bi, Ag and Mn.

PAYLOAD INTEGRATION

Payload integration took place in June 1992, about 3 months before launch. The facilities on the Cape Canaveral Air Force Station (CCAF) were excellent and the GAS integration team was very helpful. Preparation of QUESTS for flight included the following activities;

- battery top-up charging (the batteries were fully charged prior to shipment),
- sample installation (the flight samples were hand carried by the experimenter to the integration facility),
- hardware securement (all fastening hardware was checked),
- payload operation (all systems were checked, verified in the flight configuration and given a GO status),

- NASA interface verification (payload operation using interface plate),
- installation into the flight canister,
- purge and leak checks.

FLIGHT CHARACTERISTICS

The QUESTS GAS payload flew on STS-47. The published flight characteristics for STS-47 are;

Launch	-	12 Sept. 1992, 10:23
Shuttle	-	Endeavour
Orbit	-	163 nm x 57° inclination
Attitude	-	gravity gradient
Landing	-	20 Sept. 1992, 8:53

The QUESTS payload flew on the GAS bridge assembly (Figure 4) and the final measured weight was exactly 200 lbs.

PAYLOAD DEINTEGRATION

The same facilities were used for deintegration as for integration. Deintegration took place in October 1992, about 1 month after the flight. Deintegration activities included;

- canister leak check (to verify integrity of the seal),
- payload removal from the flight canister,
- payload operation (to ensure functionality after the flight),
- data extraction (the memory cartridge with experiment and diagnostic data was downloaded to the PC),
- sample removal (all samples were removed and hand carried back to the scientist for processing).

FIRST FLIGHT RESULTS

All of the experiments on the first flight of the QUESTS payload operated as planned. The directional solidification flight samples have been analyzed and the results were good. Queen's eutectic samples showed no difference between the micro-g and ground based processing. This result was proposed by Queen's prior to flight and verified by KC-135 and drop tower processing. The University of Manitoba observed excellent long crystals in their sample processed on the shuttle. A more homogeneous mixture was obtained with no precipitates due to gravity.

A typical flight temperature profile for a gradient furnace is shown in Figure 5.

The diffusion samples have not been sectioned yet, therefore science results specific to these experiments are not available at this time.

Diagnostic data was extracted from the memory cartridge and analyzed on the PC. Temperatures inside the payload ranged from about 41°C steady state to about 85°C peak on a deck near one of the operating furnaces (Figure 6). The payload temperatures were higher than expected possibly due to the gravity gradient (tail pointed toward earth) attitude used for this flight. Discoloration of the external GAS can cloth and the yellowing of the GAS bridge assembly itself were other indications of the

extreme thermal environment experienced during the flight.

Filtered acceleration data indicated peaks of about 140 μg during experimentation. The acceleration data for each axis did exhibit offsets from zero-g during flight. Typical acceleration perturbations from these offsets were in the order of 50 μg (Figure 7).

CONCLUSIONS AND FUTURE ACTIVITIES

Payload operations were as planned. The scientists were pleased with the results of their experiments in the microgravity environment. The QUESTS GAS payload will be refurbished for re-flight with a new experiment complement. QUESTS 2 should be ready for flight about the middle of 1994.

Table 1 - QUESTS Experiment Complement

Expt Number	Furnace Type	Experiment Description	Times (minutes)
1	Gradient	Directional Solidification of Bi-MnBi (eutectic)	105
2	Gradient	Directional Solidification of Bi-MnBi (eutectic)	180
3	Gradient	Directional Solidification of Al-38% (wt) Cu (hypereutectic)	105
4	Isothermal	Diffusion of Pb-Au (363°C)	150
5	Isothermal	Diffusion of Bi-Ag (313°C)	120
6	Isothermal	Diffusion of Pb-Au (437°C)	120
7	Isothermal	Diffusion of Bi-Mn (313°C)	120
8	Isothermal	Diffusion of Pb-Au (538°C)	90
9	Isothermal	Diffusion of Pb-Ag (363°C)	90
10	Isothermal	Diffusion of Pb-Au (850°C)	60
11	Isothermal	Diffusion of Pb-Ag (517°C)	60
12	Isothermal	Diffusion of Bi-Ag (437°C)	60
13	Isothermal	Diffusion of Pb-Ag (850°C)	35
14	Isothermal	Diffusion of Bi-Ag (695°C)	30
15	Isothermal	Diffusion of Bi-Mn (695°C)	30

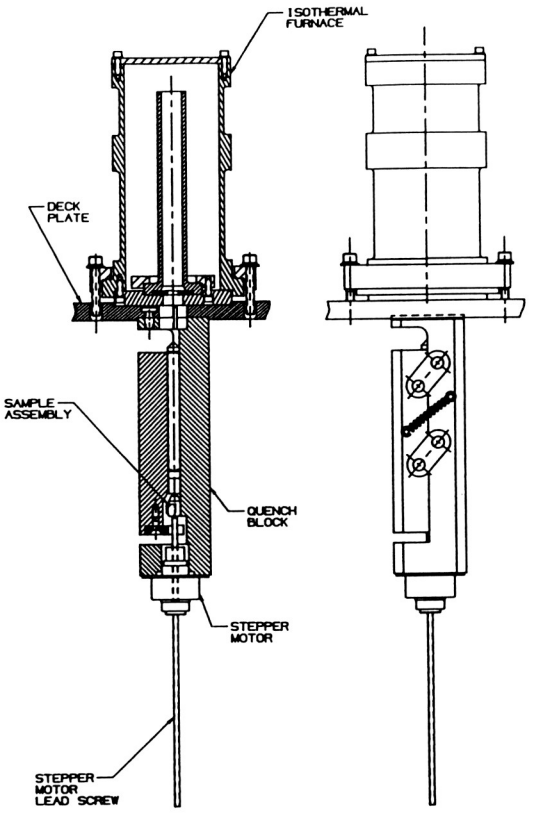

Figure 1 - Isothermal Furnace Assembly

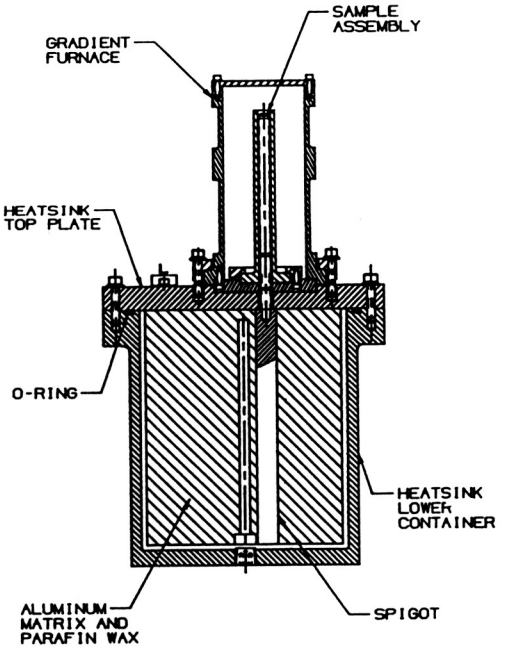

Figure 2 - Gradient Furnace - Heatsink Assembly

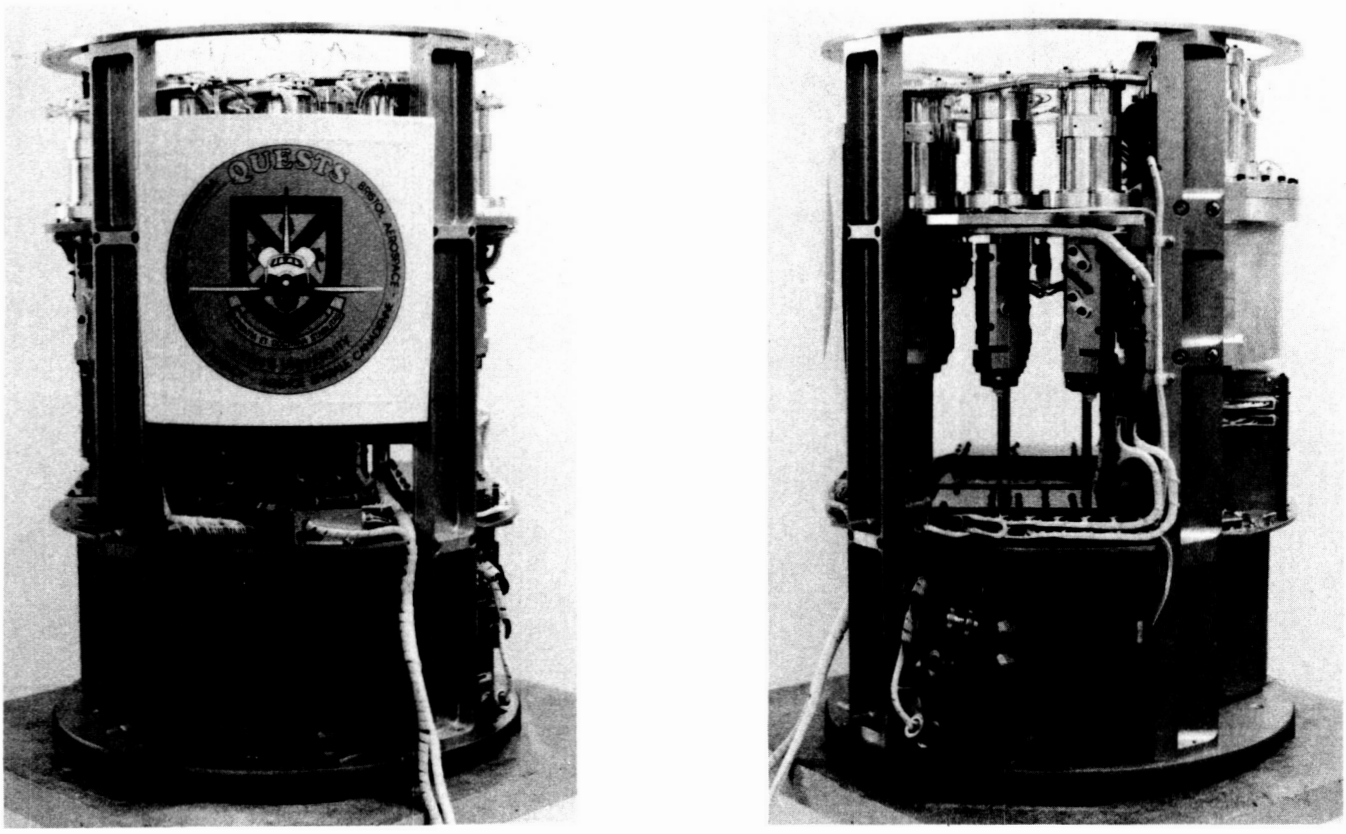

Figure 3 - QUESTS GAS Payload, 2 Views

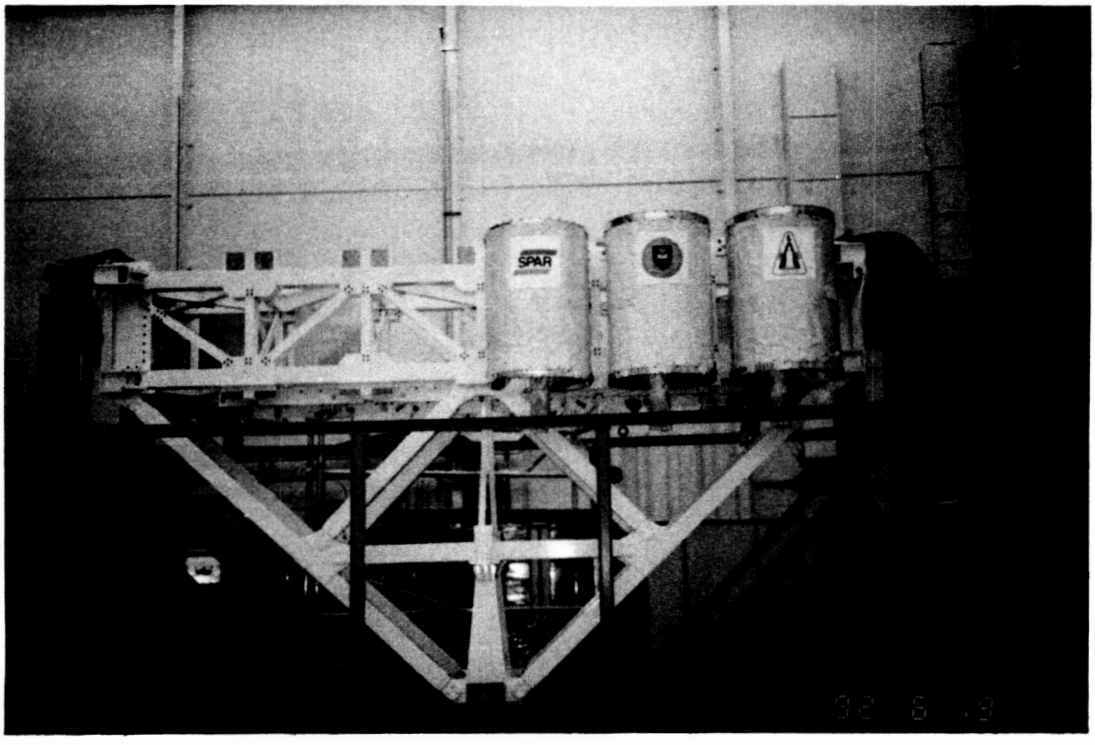

Figure 4 - QUESTS on the GAS Bridge Assembly

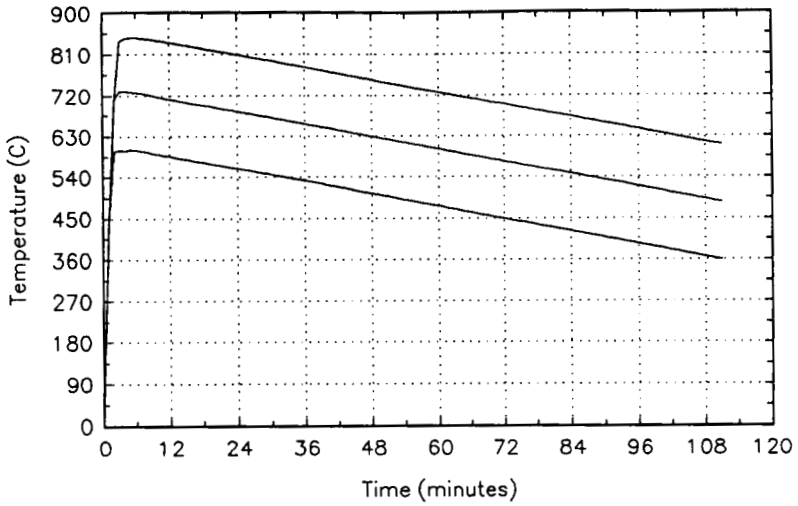

Figure 5 - Graph of Gradient Furnace Flight Temperatures

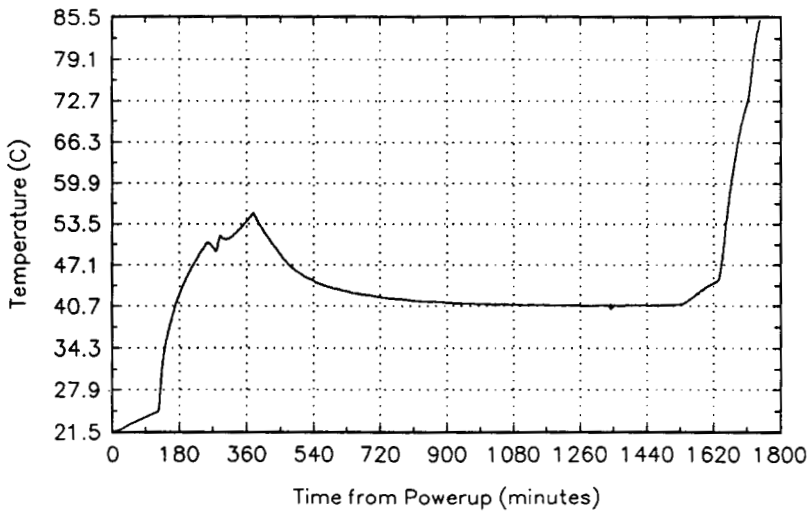

Figure 6 - Graph of Isothermal Furnace Deck Flight Temperature

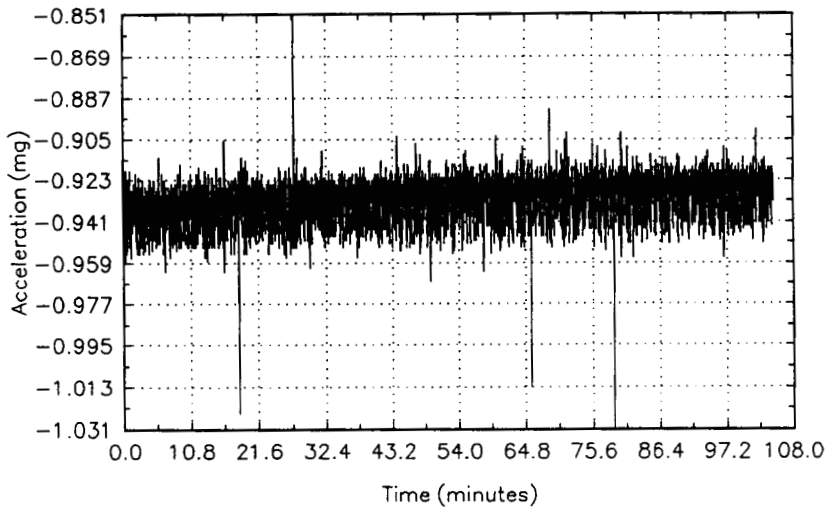

Figure 7 - Graph of Typical X-axis Acceleration During a Flight Experiment

VPU™ DEMONSTRATION MISSION
VICINITY PROCESSOR UNIT™ OVERVIEW

Loren Abdulezer
Evolving Technologies Corporation
One Wall Street Court
New York, NY 10005-3302

ABSTRACT

Evolving Technologies Corporation is designing a new type of computer called a *Vicinity Processor Unit™ (VPU).* The VPU is designed to monitor and control payloads using an operating system, control process and software environment that specifically takes into account the time delay associated with remotely controlling and monitoring a group of payloads in real time. This is a fundamentally different way of computing which has vast scientific implications for the design and implementation of data processing systems for future space flight missions.

As a demonstration misssion the VPU™ is expected to be flown aboard the Space Shuttle (Payload Identification No. G-700) as a part of NASA's Small Self-Contained Payloads (SSCP) Program. We believe this mission can greatly facilitate the development and validation of technology which may prove to be mission critical for many future space flight missions.

PAYLOAD DESCRIPTION AND MISSION OVERVIEW

Experiment Description:

The Vicinity Processing Unit™ (VPU) is composed of one or more microprocessors which has the ability to regulate or control one or more payloads either independently or in conjunction with an Earth based ground control site (i.e., Ground Support Equipment [GSE]) for normal operations of the respective payload(s).

Mission Overview

This mission is designed to be a demonstration mission which serves two purposes — to help validate the feasibility of the VPU concept and to identify areas for additional research. It is hoped that optimization of this demonstration mission will provide valuable scientific information and facilitate technological advances which could be readily incorporated into future space flight missions.

Specifically, we believe that we can demonstrate that an integral ground/vicinity control system, for remotely monitoring and managing of one or more experiments, can be conducted in "real time". i.e., the effective control of a remote experiment is not, per se, limited strictly by the time lag associated with transmission and processing time. More importantly, the load balancing features for the distribution of data processing in the operating system we are designing will largely be transparent to the design of the actual control system and software which operates the experiment.

To a degree which is not available today, the experimenters would be able to create a software program without having to be needlessly concerned with the effects of time lags. Of course there will be limits to how far this technology can be carried. It is our objective to demonstrate in actual fact that these limits lie well beyond what is commercially and economically achievable today. Even if such systems can only match the technical performance of conventional control systems it will still be cost effective because the cost of payload and software design will be considerably reduced.

MISSION OPERATIONS

Orbital Requirements & Payload Control Parameters

The nature of real time control from a remote location entails the need for telecommunications services between ground and experiment. For purposes of this demonstration mission we will select the control of sub payloads which only require a nominal level data being transferred. It has not been determined as to what telecommunications services is most suitable. As a minimum it is clear that telecommunications control can be achieved with low rate modem speeds.

Operational Requirements & Constraints

While there will be ground participation in the remote control of experiments, Shuttle Mission Specialists will only need access to Autonomous Payload Controller (APC) to start the experiment or otherwise interrupt its operations should it be required at any time during the mission.

The choice of experiments (sub assemblies of the GAS Can or other simple payloads associated with the mission) to be controlled by the VPU will be geared to address needs which will reflect operational requirements for an industrial strength implementation.

ATTITUDE SENSOR PACKAGE

R. Aceti, M. Trischberger, P.J. Underwood
European Space Agency (ESA)
European Space Research and Technology Centre (ESTEC)
Noordwijk, The Netherlands

A. Pomilia, M. Cosi, F. Boldrini
Officine Galileo
Campi Bisenzio, Italy

This paper describes the design, construction, testing, and successful flight of the Attitude Sensor Package. The payload was assembled on a standard HITCHHIKER experiment mounting plate, and made extensive use of the carrier's power and data handling capabilities. The side mounted HITCHHIKER version was chosen, since this configuration provided the best viewing conditions for the instruments. The combination was successfully flown on board Space Shuttle Columbia (STS-52), in October 1992.

The payload was one of the 14 experiments of the In-Orbit Technology Demonstration Programme (Phase I) of the European Space Agency.

PROJECT ORGANIZATION

The successful flight of the Attitude Sensor Package (ASP) payload was the result of the combined effort of 3 centers. Firstly, the Special Payloads Division (SPD) of the Goddard Space Flight Center (GSFC). Secondly, the In-Orbit Technology Demonstration Programme (TDP) of the European Space Agency (ESA). Thirdly, the companies Officine Galileo of Florence (I) and MACDIT of Lecco (I).

The companies worked under contract to the TDP. Officine Galileo is a European leader in the field of electro-optical instruments for ground and space applications. They have been active in the space market for over 30 years, and have supplied these systems for many European spacecraft. The company performed the system design, and was also responsible for most subsystems. MACDIT worked under subcontract to Officine Galileo, to provide their specific expertise, the mechanical design and manufacture and the thermal design.

ESA's TDP was instituted in 1987 to provide a means of establishing the viability of advanced technologies in the space environment. The first phase of the programme involved 14 different experiments, and the ASP was the most complex of these. With the help of experts of ESA's Technical Directorate, the programme funded and managed the design of the payload, and liaised with the SPD to ensure compatibility with the carrier.

The SPD of GSFC provided the HITCHHIKER carrier, an essential element to accommodate the payload on the Space Shuttle. The group also acted as an interface to other NASA centers to ensure that the payload is safe, and that its operational requirements are met. Extensive facilities are made available to the experimenter to communicate with the payload and the flight control team.

OBJECTIVES OF THE ASP PAYLOAD

The objective of the ASP payload was to test 3 independent spacecraft attitude sensors under realistic conditions in space. To combine the sensors in a single test was particularly attractive, in that they complemented each other and yielded high overall accuracy. The sensors were: the Modular Star Sensor (MOSS), the Low Altitude Conical Earth Sensor (LACES), and the Yaw Earth Sensor (YESS). Each sensor had a specific set of individual test objectives.

The overall accuracy of the MOSS sensor with respect to angular resolution had to be verified, combined with an investigation of sensitivity, the ability to track multiple stars, and the effect of integration time. The sensor was equipped with a baffle to attenuate light from bright celestial bodies, or reflections from orbiter structure. The flight test aimed to demonstrate the effectiveness of the baffle, by exploiting times at which the sensor was exposed to adverse stray light.

The LACES test was expected to determine the overall accuracy of the sensor. Due to its superior accuracy, the MOSS data was to serve as the attitude reference. It also determined the inaccuracies caused by the Earth's deviation from a perfectly round body. Since the sensor operates in the infra-red portion of the spectrum, seasons have an effect on the accuracy. This was to be checked by pointing the sensor to different portions of the horizon.

Also for the YESS, the MOSS served as primary attitude reference to determine the overall sensor accuracy. For the sensor to function, distinctive features on the surface of the Earth are required. This is impossible to simulate, and only a flight test provides adequate data. Featureless areas, such as deserts and oceans, were thought to make positive readings difficult or impossible. A flight test would provide an extensive map of the surface in the spectral range of the sensor, so that global performance can be predicted.

DESCRIPTION OF THE ASP PAYLOAD

The ASP payload consisted of the 3 sensor subsystems, the Interface Master Unit (IMU), the Payload Control Unit (PCU), and a support structure. The entire payload was wrapped in a multilayer insulation.

The purpose of the MOSS sensor is to provide input data to the attitude control system of three-axis-stabilised spacecraft, to provide high accuracy pointing of scientific instruments. It can acquire and track up to five stars simultaneously. The relative instantaneous position of each tracked star is computed with reference to the sensor's 3° x 4° field of view, with an accuracy of better than 2 arc-seconds. Within certain limits, the sensor's ability to detect faint stars can be traded for tracking speed. In the highest sensitivity mode, stars of magnitude 7.8 can still be detected. The ASP payload allowed mode selection to be made by telecommand. The star positions are measured in terms of X-Y pixel coordinates within the field of view, and the magnitude of each star target is also measured. The detector, cooled by a Peltier thermoelectric pump, is a CCD, and is placed in the focal plane of the cathadioptric optical system. The stray light coming from sources outside the MOSS field of view was attenuated with a baffle, which was designed to be effective for Sun and Earth minimum approach angles of 45° and 8° respectively.

The LACES is a two-axis (pitch and roll) infrared Earth sensor suitable for attitude control and Earth pointing of spacecraft and platforms operating at altitudes ranging from 100 to 2000 km. LACES performs a conical scan around its line of sight, analysing the 14 to 16.5 micron infrared band. A threshold system detects temperature changes typical of space/Earth transitions. The measurements yield the time it takes to scan from the space-to-Earth to the Earth-to-space transition, which is related to the pitch and roll angles of the spacecraft. A bolometer is the focal plane of the instrument act as the detector.

The YESS measures the yaw angle of the spacecraft with respect to the velocity vector. This is achieved by viewing the Earth through two mutually perpendicular reticles, consisting of parallel opaque bars, with transparent slits between them. The reticles are at an angle of 45 degrees to the zero-yaw direction. The images are projected onto two infrared pyroelectric detectors. A translating scene causes modulation on either detector output, with a frequency proportional to the yaw angle of translation and to the displacement speed of the image. In the processing electronics, the signal gathered by the two channels is converted into yaw attitude information. The sensor scans a field of view of 6 by 14 degrees, and has an accuracy of better than 0.5°.

Specific interface requirements of the application dictated the design of the electrical sensor interfaces. In this payload, a uniform adaptation to the requirements of the PCU was necessary, which was accomplished by the IMU. It acted as a buffer unit, with specific interfaces toward the sensors, and standard interfaces to the PCU. The IMU also included the power distribution and switching for the sensor boxes.

The PCU acted as the central on-board computer. On the one side it communicated with the IMU, and the other side with the Hitchhiker avionics. The primary data stream was channeled

through the HITCHHIKER Medium Rate Ku-Band channel. A fixed format of 30K-bit/second accommodated variable length data packets, which originated from the sensors. This approach provided the required time independence, since the operation of the sensors was unsynchronized. The HITCHHIKER asynchronous downlink channel held housekeeping and sensor summary information. Sensor on/off and MOSS mode commands could be dispatched through the HITCHHIKER asynchronous uplink. The command execution was either direct, or delayed, according to time information provided by the command.

The ASP structure was designed to mate with a side wall mounted HITCHHIKER configuration (see figure 1). It was roughly box shaped, and made up of six aluminum panels, each machined out of solid aluminum blocks. The panels were attached to the HITCHHIKER experiment mounting plate, so that it formed an integral part of the payload. The purpose of this structure was to elevate the sensors above the Orbiter sill level, to satisfy their complex field of view requirements. Electronic boxes were attached directly to the HITCHHIKER plate and to the lateral panels of the ASP structure. Except for the YESS, which was directly attached to the HITCHHIKER plate, the MOSS and the LACES were accommodated on the top plate of the structure. The total weight of the ASP payload was approximately 130 kg.

For thermal control reasons, the experiment was wrapped with multi-layer insulation blankets. Cooling was accomplished by radiating heat into space. Heaters controlled by thermostats were used on the electronic mounting plate to provide heat input during cold Orbiter attitudes.

FLIGHT RESULTS

The high angular accuracy of the MOSS, in the order of 2 arc-seconds, made it the natural lead instrument of the ASP. The LACES and YESS Earth sensors, by contrast, have a precision of only 4 arc-minutes and 0.5° respectively. Even the attitude measurement system of the Orbiter is less accurate than the MOSS, since it relies on gyro instruments that are periodically recalibrated, using star tracker data. The system accuracy is typically 30 arc-seconds.

Therefore, the MOSS was without comparison. However, while it was not possible to directly validate the absolute measurement accuracy of the MOSS, it was at times possible to make a relative assessment of the sensor's measurement performance. Often, more than one star was tracked by the MOSS simultaneous. In this case, with the help of the orbiter attitude data, the area of the celestial sphere being viewed by the sensor was identified. By correlation of the MOSS data with star catalog data, the relative accuracy and the stability of the sensor was determined.

Besides specific accuracies, the sensors measured attitudes in certain axes. The LACES provided roll and pitch information while the YESS only provided yaw information. The MOSS provided

information of both roll and yaw, thus permitting a cross comparison with, and calibration of the lower accuracy sensors.

MOSS DATA ANALYSIS

During the flight, certain planned sequences of the Space Transportation System (STS) maneuvers and sensor commands were carried out to test specific aspects of the MOSS performance. The main part of the processing of the MOSS sensor output was performed using coordinates of a spherical surface (a part of the celestial sphere referenced to the axes of the sensor), because this has made it easier to account for the movement of stars across the field of view, as well as matching entries in the star catalogue. The conversion from the sensor output took account of the optical distortion as well as the effect of projecting onto the planar surface of the CCD.

The post flight analysis showed that all the MOSS commands from the ground were correctly interpreted and executed. Operating sequences demonstrated the sensor's capabilities in terms of sensitivity, number of stars to be tracked, and integration time. The following sensitivities were observed:

$m_v = 5.89$	at 40 msec integration time
$m_v = 6.94$	at 90 msec integration time
$m_v = 7.91$	at 250 msec integration time

Consistently, the error in magnitude indication with respect to the catalogue data was within its theoretical limit of 0.25 m_v.

At various attitudes of the STS during the daylight portions of the orbits, the sensor behaviour, at different distances from the earth limb to the centre of the field of view, was analyzed. Full performance in terms of maximum detectable star magnitude was obtained when the angle between the earth's limb and the centre of the field of view was 15° or higher. For more acute angles, the illumination of the detector by stray-light decreases the capability to detect dim stars. Typically, at 10° the detectable limit magnitude was 7.01 m_v at 250 mseconds integration time. The reason for this is the limit of the baffle performance. Performance improvement would have been possible by lengthening the baffle. This was not possible due to space limitations.

The ability of the sensor to track fast moving stars was verified. During yaw maneuvers the sensor tracked stars moving through the field of view at a speed of about 300 arcsec/sec, which was well in specification.

Only relative accuracy evaluation could be performed due to the lack of a higher quality absolute attitude reference. At least 2 stars had to be in the field of view. An overall accuracy of 2 arcsec (1σ) was consistently observed.

LACES DATA ANALYSIS

The main objective of the LACES test was the correction of the mathematical mode of the Earth, taking into account the Earth's oblateness and the seasonal effects, and the overall accuracy test. As said before, the MOSS provided the attitude reference for the LACES sensor. The 0.07° overall accuracy approached theoretical predictions. Therefore, the mathematical model is considered valid, and no further refinements are necessary.

In the range of 170° to 360° the LACES sensing is inhibited to avoid false triggers caused by thermal gradients of spacecraft structure in the field of view. The test showed that the sensor regains full accuracy 10° past the inhibited zone. At 7.5° past the inhibition zone, the error increases to 0.1°. At 5° past the error is already 0.5°.

YESS DATA ANALYSIS

During the ASP mission, the YESS sensor showed subnominal behaviour in one of the measurement channels. Excessive noise was the assume cause. Tests carried out after the mission showed that this high level of noise was caused by a degradation of the associated detectors. Although this failure prevented direct yaw measurement, the test results are nevertheless very interesting. For extended periods of time the reading of the good channel provided signals that are proportional to the features on Earth. At the time of writing this article, the full data was not yet surveyed, but it is reasonable to assume that many measurements had been taken over oceans and deserts. The information will be evaluated theoretically, to provide the overall sensor performance.

GROUND INFRASTRUCTURE DESCRIPTION

The ground support equipment (GSE) had the task to support the payloads during the ground processing flow, and certain parts were used also during the flight.

The structure of the GSE allowed easy adaptation to the ground and flight environment. The change could be achieved with a single instruction at the startup of computer 1.

Mechanical Ground Support Equipment

The mechanical ground support equipment (MGSE) of the payload consisted of a transport container that could also be used as a work stand, after the top cover was removed. In the work stand mode, the payload was upright, and allowed easy access to all components.

Electrical Ground Support Equipment

The electrical ground support equipment (EGSE) was composed of three computers and a specially built unit, the 'HITCHHIKER Simulator and Monitoring' Unit (HHSIM).

Computer #1 was dedicated to experiment commanding and the display of housekeeping data. Computer #2 displayed and recorded the Medium Rate Ku-Band data. The initial de-commutation and de-packaging occurred in the HHSIM. Computer #3 displayed the celestial segment within the MOSS sensor's field of view. The primary data originated from a star catalogue, which was read according to the attitude provided by the Orbiter reference.

Payload commands were dispatched from computer #1, using predefined command templates. The commands had packet form, and included a time tag to allow delayed execution. In this way, several orbits were planned and the relevant commands uplinked ahead of time.

PAYLOAD GROUND FLOW

All the three sensors carried their own reflective alignment cubes, to relate their precise mounting orientations to a similar cube located on the experiment structure. Relative alignment was measured before and after the flight, with only small change being detected, demonstrating the high level of stability of the payload assembly.

With the exception of the PCU, most of the environmental tests were conducted on the integrated ASP payload, as opposite to testing at box or sensor level. The PCU was subjected to vibration, thermal-vacuum, and EMC tests. Random vibration test at qualification levels, thermal vacuum, and EMC were then repeated on the ASP payload assembly. The ASP integration with the HITCHHIKER Avionics and a subsequent EMI test was carried out at GSFC. To conduct these tests, GSFC provided the HITCHHIKER ground station and simulators of the Shuttle data link. These units were used in conjunction with the ASP sensors stimulator included in the ASP GSE.

At the Kennedy Space Center (KSC), the ASP payload was subjected to an electrical compatibility tests (CITE), and to an Interface Verification Test (IVT). The objective of these tests was to prove that the payload, connected to the Orbiter power and data system, could receive and correctly execute all the relevant commands.

About two weeks after the landing of STS-52 at KSC, the ASP payload was deintegrated from the Orbiter and transported to ASTROTECH. After carrying out post flight performance testing, the payload was packed and shipped to Italy.

FLIGHT OPERATIONS

The flight operations were conducted from the GSFC Small Payloads Flight Operations Control Center (POCC). The commands could be sent at every orbit of ASP data taking. Each packet set the MOSS in a particular configuration for one or more orbits. Each orbit of data taking corresponded to a test of a particular feature of the star tracker. One orbit, for example, was dedicated to testing the sensor's ability to detect and track dim stars, while another orbit was used to investigate the sensor's performance when set to track the maximum number of stars. Essentially, the YESS and the LACES had optimal operating conditions throughout the flight. A minimum of 16 orbits were needed to completely demonstrate all sensors features. ESA and Galileo personnel operated the ASP payload throughout the Shuttle ten day mission and the number of ASP orbits actually achieved was more than double the minimum required GSE during the 10 day long mission.

Part of the ASP mission was conducted with the Orbiter flying either nose or tail forward, and with the cargo bay facing the Earth. With the Shuttle in this attitude, the MOSS line of sight and the LACES scanning cone axis were directed toward the pole of the orbit. The YESS line of sight was directed toward the centre of the Earth. Then, the MOSS field of view rotates 360 degrees about the center, and essentially the same stars are detected.

The ASP was also operated with the Orbiter in a tail or nose forward attitude, with the cargo bay oriented toward the Earth, but with 5 degrees roll offset away from the Earth. In this attitude, during one orbit, the MOSS field of view described an angulus of 5 degrees radius, and thereby a wider portion of the sky was scanned, with more target stars available. The effect of the 5 degrees roll away from the Earth was also to attenuate the stray light into the star tracker.

The Orbiter also performed a planned flight maneuver with the cargo bay to Earth and the wing pointed along the velocity vector. In this attitude, the MOSS line of sight was tangential to the orbit and the star moved at higher speed through the sensor field of view. This attitude was requested to test the YESS sensor. Additionally, starting from this attitude, the Orbiter also performed a $\pm$ 15 degrees rotation about its yaw axis. Shuttle mission embody this concept of flexibility.

Many maneuvers and attitude changes occurred during the flight, most of them according to a previously established flight plan. We were offered the possibility to adjust the plan, to either accommodate difficulties, or to allow further investigation of phenomena observed during the mission. These ad-hoc plans were introduced during the daily operations replanning. This flexibility was experienced as a very valuable feature of the HITCHHIKER system.

CONCLUSIONS

A number of significant results have been achieved in this ASP flight test on board the Shuttle. The preparation of the payload was in itself a very valuable exercise. The optical sensors operated in its intended environment, under illumination and target conditions which cannot realistically be reproduced on ground. The fact that the experiment hardware was retrievable added extra value to the mission because we could perform post flight performance tests.

Although further evaluation of the ASP flight data will continue for some time, the results obtained from the flight are very satisfactory. The data analysis clearly indicates an extremely satisfactory performance by the two primary sensors, the MOSS star sensor and the LACES infra-red sensor. Both units performed in specification, and in particular the MOSS functioned well over a significant range of different observing conditions. In spite of the anomaly suffered by the YESS, enough data has been gathered to characterize the sensors. The future utilization of further development of all the sensors on the ASP will benefit substantially from the experience and results derived from the ASP mission. In fact, the MOSS and the LACES are already foreseen for European space missions.

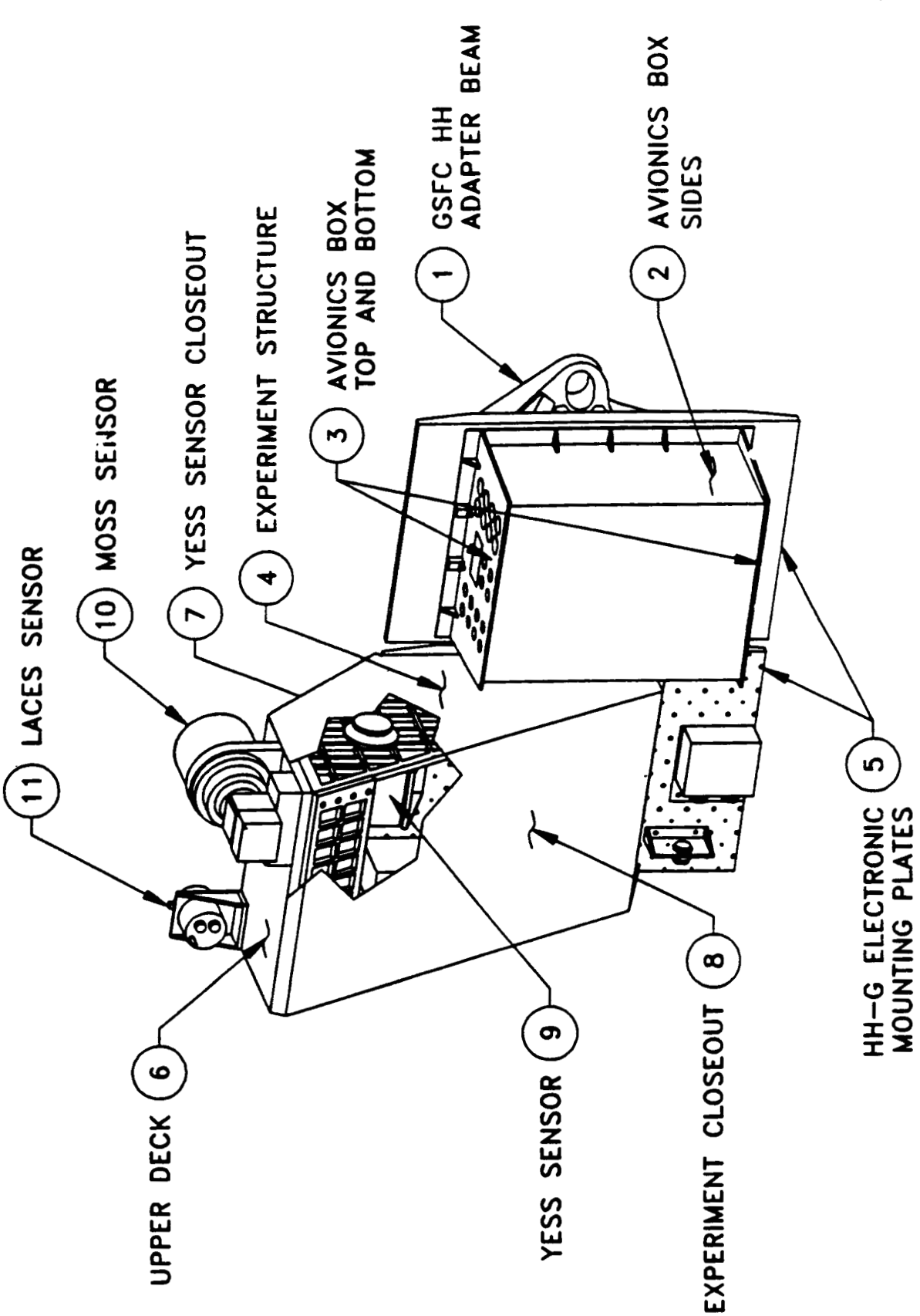

FIGURE 1 - ATTITUDE SENSOR PACKAGE PAYLOAD CONFIGURATION

FIGURE 2 - ATTITUDE SENSOR PACKAGE PAYLOAD ON-BOARD STS-52

Space Applications Industrial Laser System (SAILS)[1]

T.D. McCay, J.B. Bible, R.E. Mueller

The University of Tennessee-Calspan
Center for Space Transportation and Applied Research (CSTAR)
Tullahoma, TN 37388-8897

and

The University of Tennessee Space Institute (UTSI)
Center for Laser Applications
Tullahoma, TN 37388-8897

ABSTRACT

A program is under way to develop a YAG laser based materials processing workstation to fly in the cargo bay of the Space Shuttle. This workstation, called Space Applications Industrial Laser System (SAILS), will be capable of cutting and welding steel, aluminum and Inconel alloys of the type planned for use in constructing the Space Station Freedom. As well as demonstrating the ability of a YAG laser to perform remote (fiber-optic delivered) repair and fabrication operations in space, fundamental data will be collected on these interactions for comparison with terrestrial data and models.

The flight system, scheduled to fly in 1996, will be constructed as three modules using standard Get-Away-Special (GAS) canisters. The first module holds the laser head and cooling system, while the second contains a high peak power electrical supply. The third module houses the materials processing workstation and the command and data acquisition subsystems. The laser head and workstation canisters are linked by a fiber-optic cable to transmit the laser light.

The team assembled to carry out this project includes Lumonics Industrial Products (laser), Tennessee Technological University (structural analysis and fabrication), Auburn University Center for Space Power (electrical engineering), University of Waterloo (low-g laser process consulting), and CSTAR/UTSI (data acquisition, control, software, integration, experiment design).

This report describes the SAILS program and highlights recent activities undertaken at CSTAR.

INTRODUCTION

The UT-Calspan Center for Space Transportation and Applied Research (CSTAR) is one of 17 NASA Centers for the Commercial Development of Space (CCDS). The mission of CSTAR is to team with industry and academia in the development of new and innovation space technologies.

[1]This work is supported by NASA Code C under grant NAGW-1195, The University of Tennessee Space Institute, Lumonics Industrial Products Division.

The SAILS program has been developed under this mission because of its broad potential to benefit industry, academia, and government through advanced laser materials processing technology.

The project team consists of five organizations, headed by Professors Dwayne and Mary Helen McCay of CSTAR and the UTSI Center for Laser Applications, Professor Walt Duley of the University of Waterloo, Steve Llewellyn of Lumonics Corporation, Professor Richard Houghton of Tennessee Technological University, and Professor Ray Askew of Auburn University. Brice Bible of CSTAR is the program manager and Susan Olden of the Goddard Space Flight Center (GSFC) is the mission manager.

The long term space missions planned by NASA will require some form of machining and repair capability. The SAILS experiment will act as the proof-of-concept to firmly establish the YAG laser as a viable materials processing tool for space applications. Follow on phases to the program will develop the infrastructure necessary for implementation on long term space structures by the end of the century.

As the lifetime and complexity of space structures increase, our ability to construct, maintain and repair these structures in space must also be improved. The industrial laser represents a possible solution to the problem of conducting multiple task manufacturing and repair operations at remote, hostile locations such as an orbiting platform.

The purpose of the SAILS project is to demonstrate the capability to employ a YAG laser processing facility in space and to perform practical laser materials processing operations under microgravity conditions. The objectives of this project may be grouped under the following categories:

Science: Determine the effects of gravity on welding, drilling, cutting, brazing, and soldering. Compare experimental results with models to improve predictions of process behavior in 1 and 0 g.

Space Engineering: Demonstrate the viability of laser technology to perform repair and fabrication type operations in space. Applications include a laser repair kit for Space Station, manned Mars missions, a Moon base, and a laser-based factory in space.

Laser Engineering: Design refinement and demonstration of the industrial YAG laser to show that it has become a simple, compact, efficient and rugged tool capable of operating in any environment. It is of particular importance to show the advantages of fiber optic beam delivery, including ruggedness and the ability to operate in remote and harsh environments.

The 1996 flight, designated SAILS-01, is the first in a series of experiments designed to validate the YAG laser as a viable multipurpose energy workstation for space. Interest by the NASA Code C CCDS community as well as other industry, academia, and government organizations has resulted in plans for at least two follow-on flights. Figure 1 indicates the current flight strategy for the SAILS facility.

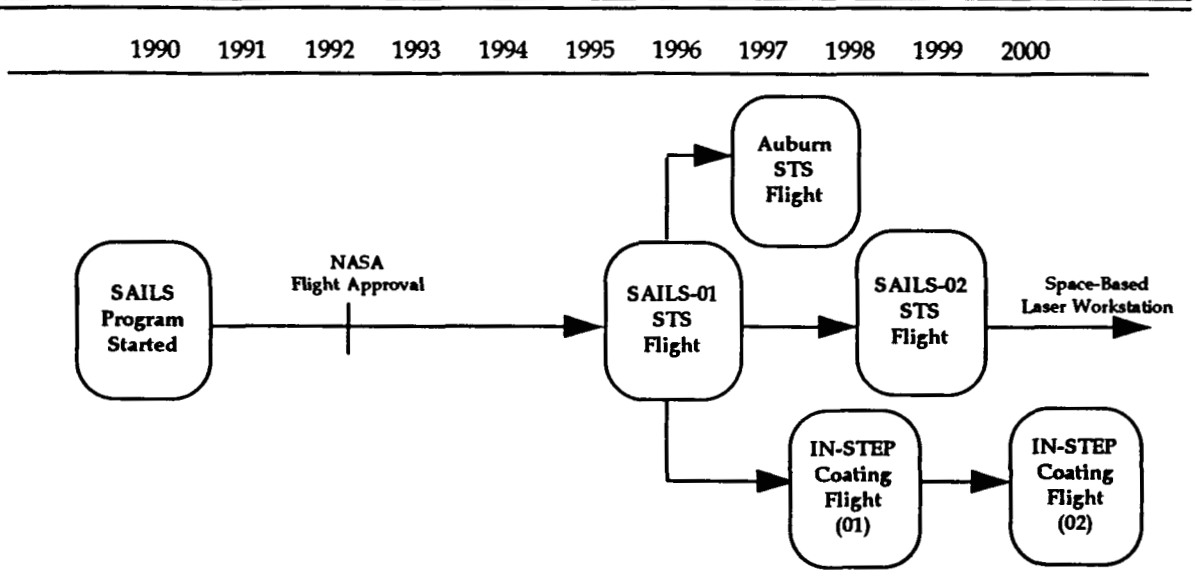

Figure 1 SAILS Facility Flight Plans

SAILS EXPERIMENT SELECTION

As the SAILS experiment is designed to demonstrate the viability and practicality of laser materials processing in space, the processes to be tested and the materials used should have some application in space systems. After initial trials to show that the materials could be processed with the laser power anticipated for the flight system, the materials and processes were selected as shown in Table 1.

Table 1. Materials and Processes Selected for Testing in the SAILS Experiment.

Material	Spot/Seam Weld	Drill/Cut	Braze	Solder
316L Stainless	✓	✓	✓	
2219 Aluminum	✓	✓		
6061 Aluminum	✓	✓		
Inconel 718	✓	✓		
Copper				✓
Kapton		✓		
Lead/Tin	✓			

The processes all have obvious practical applications, in space or on earth. Structural joining operations (welding and brazing) will be needed in the assembly and repair of man-rated habitats. Cutting will be required for removing damaged components for repair and in the recycling of space debris. Soldering of electrical and electronic components could be accomplished remotely using a dexterous manipulator and a fiber delivered laser beam, with much less heat input to nearby components than with a conventional solder iron.

GROUND EXPERIMENTATION

Preliminary studies were carried out during 1991-92 using a 400 W Lumonics JK701 YAG laser to show that the materials and processes under consideration could be processed with a relatively low power laser. Since that time, the operating characteristics of the flight laser have been made available with the introduction of the LUXSTAR laser by Lumonics Corporation, the industrial sponsor for the program (see Table 2). Detailed experiment studies will be completed in late 1993 at CSTAR using the LUXSTAR laser to produce the precise processing conditions anticipated for each of the flight experiment samples. As well as finding workable combinations of processing parameters, this study will determine scaling relationships (depth and width of weld vs power, metal structure) between the flight power level and presently available ground-based laser power levels. This will allow us to predict the performance of higher power lasers operating under space conditions.

Table 2. Flight Laser Operating Characteristics

Parameter	Value
Average power	50 W
Peak optical power	3000 W
Pulse length	0.5 - 20 ms
Pulsing rate	to 100 Hz
Pulse energy	to 30 J [10 J]
Fiber core diameter	400 μm
Minimum spot size	200 μm
Dimensions (Industrial unit)	86.5x56.5x77.5 cm
Weight (Industrial unit)	200 kg
Input voltage	200-240 VAC [28 VDC]
Output voltage to Flashlamp	660 V pulses
Power Consumption	5.5 kW

FLIGHT HARDWARE DESIGN

The SAILS flight experiment will be housed in three Get-Away-Special (GAS) canisters mounted on the HitchHiker cross bay carrier. These canisters will be interconnected via the top plates for experiment control and distribution of power and laser energy. Figure 1 shows this three-canister configuration and the major components in each module.

The first canister, CAN 1, will contain the laser head, output module (capacitor bank), and cooling system for generation of the laser energy necessary to conduct the experiments. The laser head and output module will be acquired and repackaged from the LUXSTAR Nd:YAG 50 W laser system, a new commercial product manufactured by Lumonics. The cooling system, consisting of a pump and heat exchanger, will be fabricated at CSTAR to provide transfer of the heat generated in the laser cavity

during processing.

The second canister, CAN 2, contains the electrical power supply for providing the high peak power necessary to generate the laser energy in CAN 1. This can will consist of Silver-Zinc battery cells housed in a vented container (power source), a DC-DC convertor for electrical power conditioning, and the laser control module. The DC-DC convertor will condition the battery energy to the proper voltage for transfer to the capacitors in CAN 1. The Auburn University Center for Space Power will design and fabricate the power conditioning system in this canister and the power source will be provided by CSTAR. Use of orbiter power was considered as an alternative to the batteries for laser power. However, the peak power requirements for the experiment is approximately 5 kW, which is greater than the maximum of 3.5 kW available to a HitchHiker customer.

CAN 1 and CAN 2 will be connected via an electrical cable for transfer of the high voltage battery power from the power supply to the laser head. The connectors, cable support structure, and canister modifications will be provided by GSFC and are currently under development. CSTAR will provide the electrical cable.

The combination of CAN 1, CAN 2, and the voltage interconnection produce a complete, self-contained, ruggedized Nd:YAG laser system for delivery of laser energy to the experiment workstation, CAN 3.

The third canister, CAN 3, contains the workstation for conducting the SAILS experiments. This canister consists of the experiment samples, workhandling, and command and data acquisition systems. The sixteen samples (2.5 cm X 5.5 cm each) will be rotated on a platen and located under the laser beam for processing. A given sample will be processed for approximately 15 seconds, followed by a monitoring period to allow each critical subsystem to return to the appropriate operating conditions before moving to the next sample. This will continue until all 16 samples have been processed. The internal laser beam will be delivered as a free-space beam with moving optics. This configuration mimics current industrial laser practice of using a moving optics end effector to achieve more motion flexibility. The data acquisition systems will include video storage of the actual process (coaxially and along the sample), recording of the environmental conditions before and during each process, and monitoring of the laser process parameters (pulse length, energy, and duration) for each sample.

CAN 3 will be linked to CAN 1 via a fiberoptic cable for delivery of the laser energy to the workstation. This cable will consist of a 400 micron fiber surrounded by a copper shield and control/continuity data lines all encompassed in a nylon outer cover. The connectors will be designed for a hermetic seal at the canister with lid modifications to be provided by GSFC and the fiber/connectors to be provided by CSTAR.

Each of the three canisters will be filled with Argon gas pressurized to one atmosphere and filled with inert gas. CAN 1 and CAN 2 will use dry N_2 while CAN 3 will use Argon to provide enhanced processing conditions for the flight hardware components.

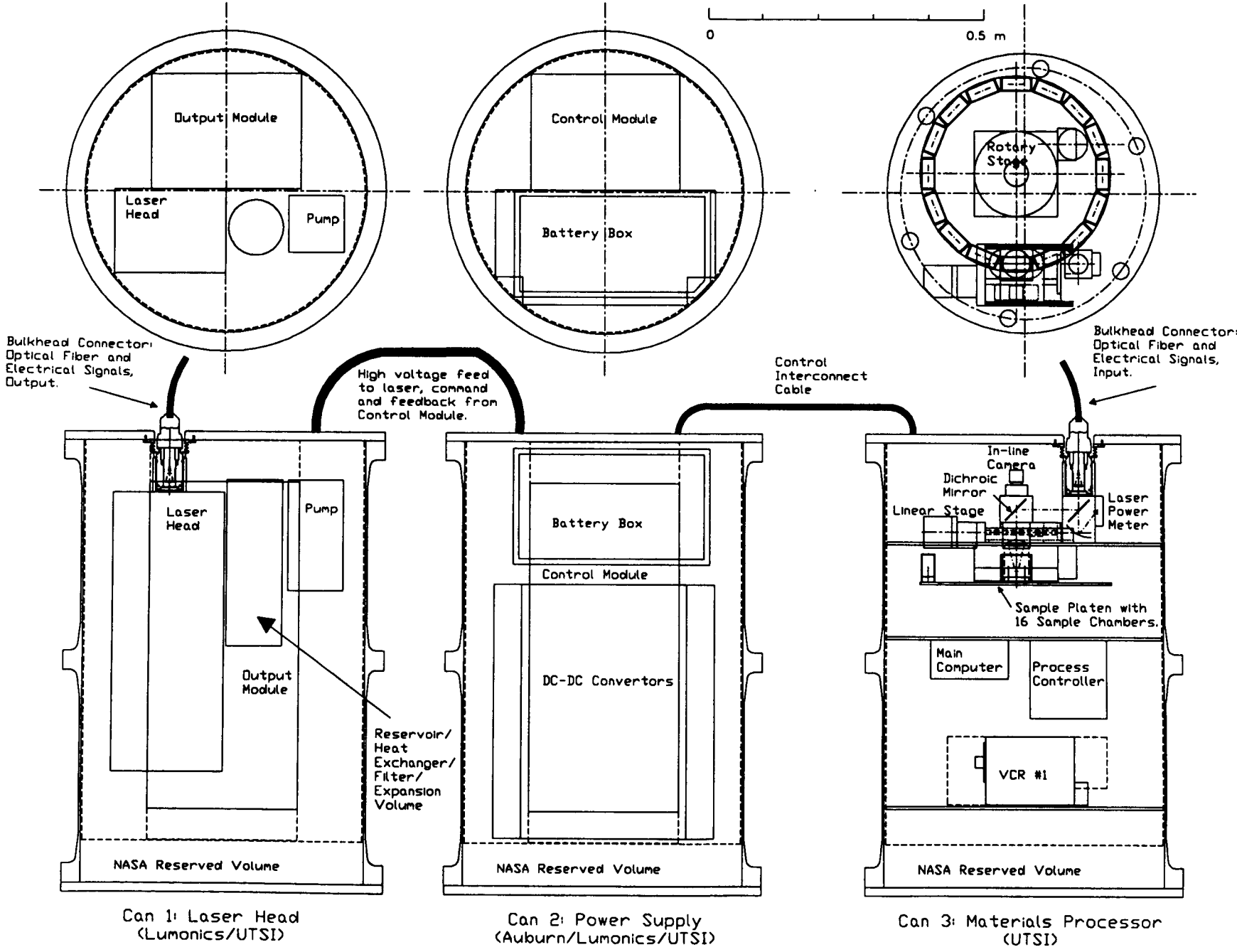

Figure 2 SAILS Canister Configuration

PROGRESS TO DATE

The SAILS program was proposed to NASA Code C in 1990 with funding and payload approval received in 1991. As described above, work through FY92 focussed primarily on establishing the operating envelope necessary to accomplish the experiment objectives of the program. FY93 has centered on design and development of the flight hardware required to accomplish these objectives. To date, the following activities either have been completed or are underway:

- Completion of preliminary design of the components in each of the three canisters, including the interconnecting fiberoptic and electrical systems.
- Candidate hardware systems for many of the components in the sample workstation canister, CAN 3, have been identified and several components have been procured. The computer/control, VCR, and camera systems have been purchased and are currently under development and integration at CSTAR. TTU has completed preliminary design of the internal experiment structure and a prototype test frame has been fabricated for vibrational testing.
- The Lumonics LUXSTAR laser, CAN 1, has been installed at CSTAR and is currently undergoing operations testing. A prototype cooling system has been developed and will be tested with the laser in early FY94.
- The electrical and fiberoptic interconnection systems have been discussed with GSFC. Design and fabrication of the external mounting hardware will be provided by GSFC and development of the cables will be provided by CSTAR.
- The Carrier Payload Requirements (CPR) document has been submitted to the GSFC Small Payloads Office with final approval anticipated by September 1993. The Safety Data Package has been initiated with the potential hazards identified in the Payload Safety Requirements Matrix. Submittal of the package to JSC for the Phase 0/1 safety review is expected shortly after the CPR is approved.

FY94 ACTIVITIES

Activities in FY94 will focus on continued development of the flight hardware with completion of procurement and fabrication of the sample workstation canister (CAN 3) modules and most of the laser (CAN 1) and power (CAN 2) canister components anticipated. Some of the major milestones planned for FY94 include:

- Procurement/fabrication of the experiment motion system, internal optics, sample carrier, and internal frame for CAN 3 will be completed. Integration and testing of the canister will be initiated.
- Development of the power supply, cooling system, batteries, and internal frames for CAN 1 and CAN 2 as well as integration of these modules into the LUXSTAR laser for operational tests will be initiated.
- Design of the fiber, voltage, and control interconnects will be completed and fabrication will be initiated.

- **Identification of the payload safety-critical items and safety verification procedures will be completed. The Phase 0/1 safety review will be completed and the Phase 2 review process will be initiated.**

The SAILS Program Schedule is shown on Figure 3 and illustrates the overall timetable planned to achieve the FY96 shuttle flight.

CONCLUSION

A program is well underway to develop the first laser materials processing workstation for use in space. As well as providing fundamental information on several laser-material interactions, this program will demonstrate the ability of laser processing to perform useful repair and fabrication operations in space.

SPACE APPLICATIONS INDUSTRIAL LASER SYSTEM (SAILS)

PROGRAM SCHEDULE

Task Name	Start Date	Due Date
Program Concept	Jul/01/91	Jul/01/91
SAILS Program Management	Jul/09/91	Apr/28/98
LIPP	Jul/02/91	Jan/13/97
Ground Experimentation	Oct/02/91	Jan/04/94
Computer Modelling	Dec/14/93	Jan/02/97
Flight Hardware Development	Aug/19/92	May/08/95
LUXSTAR Preparation	Aug/02/93	Jan/12/94
Laser Canister	May/03/93	Jan/03/95
Laser Head	Jun/01/93	May/19/94
Laser Cooling System	Jul/01/93	Jul/22/94
Laser GAS Can Structure	May/03/93	Jan/03/95
Laser Control Interfaces	Sep/01/93	May/18/94
Laser Beam Delivery	Jun/01/93	Apr/19/94
Power Canister	Mar/01/93	Jan/03/95
Laser Power Supply	Sep/01/93	Sep/01/94
Laser Batteries	Mar/01/93	Jun/21/94
Power Control Interfaces	Sep/01/93	Jul/21/94
Power GAS Can Structure	May/03/93	Jan/03/95
Process Canister	Aug/19/92	Jul/06/94
Computer System	Aug/19/92	Jan/21/94
Sample Materials /Carrier	Oct/01/92	Apr/01/94
Data Logger System	Aug/19/92	Mar/03/94
Sensor System	Aug/19/92	Jun/01/94
Control Interfaces	Nov/20/92	Apr/01/94
Beam Delivery	Dec/31/92	Jul/06/94
Visual Data System	Oct/01/92	Jan/03/94
Motion Drive/Control System	Jan/04/93	Mar/01/94
Process Gas Can Structure	Apr/01/93	May/20/94
Fiberoptic Interconnect	Mar/01/93	Sep/01/94
Voltage Interconnect	Sep/01/93	Sep/21/94
Control Interconnect	Sep/01/93	Jul/21/94
Software Development	Sep/01/93	Oct/03/94
Support Equipment	Apr/01/93	May/08/95
Integration and Testing	Oct/13/94	Sep/10/95
KC-135 Flight Experiments	Mar/06/95	Jun/06/95
Flight Preparation	Aug/08/95	Nov/13/95
Launch	Mar/21/96	Mar/21/96
Post Flight Analysis Complete	Sep/26/96	Sep/26/96

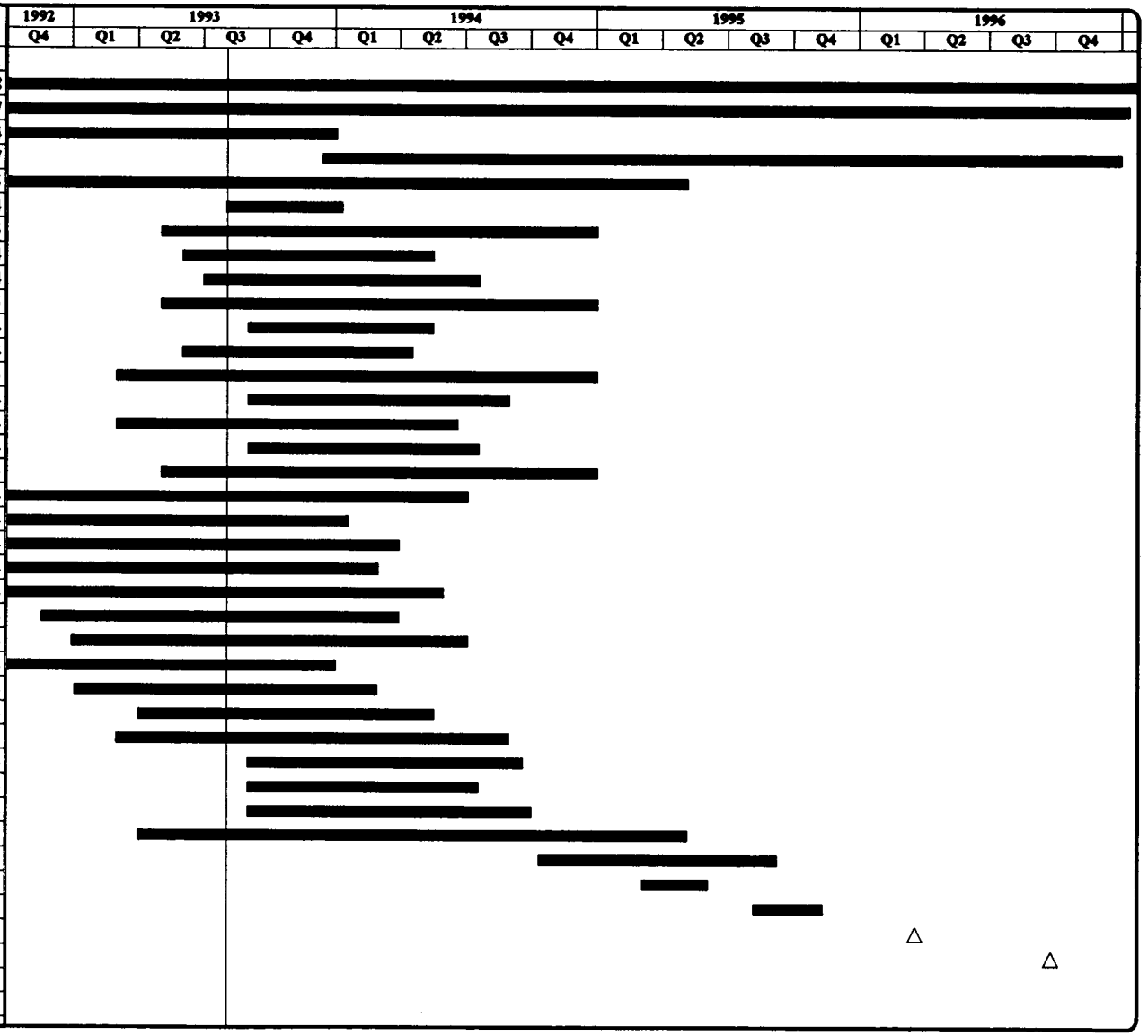

Last Update: 8/2/93

A HIGH RESOLUTION ULTRAVIOLET SHUTTLE GLOW SPECTROGRAPH

George R. Carruthers
E. O. Hulburt Center for Space Research
Naval Research Laboratory
Washington, DC 20375-5320

ABSTRACT

The High Resolution Shuttle Glow Spectrograph-B (HRSGS-B) is a small payload being developed by the Naval Research Laboratory. It is intended for study of shuttle surface glow in the 180-400 nm near- and middle-ultraviolet wavelength range, with a spectral resolution of 0.2 nm. It will search for, among other possible features, the band systems of excited NO which result from surface-catalyzed combination of N and O. It may also detect O_2 Hertzberg bands and N_2 Vegard-Kaplan bands resulting from surface recombination. This wavelength range also includes possible N_2^+ and OH emissions. The HRSGS-B will be housed in a Get Away Special canister, mounted in the shuttle orbiter payload bay, and will observe the glow on the tail of the orbiter.

INTRODUCTION AND BACKGROUND

Shuttle glow was first observed in the visible spectral range by astronauts on the STS-3 mission in 1982 (see Refs. 1 and 2). However, probably similar phenomena have also been observed by instruments on unmanned satellites[3-5]. The glow is observed only on surfaces of the shuttle orbiter (or other satellite vehicle) which face the direction of motion (ram). The glow intensity is observed to increase rapidly with increasing atmospheric density[2,6]. There have been several imaging and spectrographic studies of the visible shuttle glow[6-8], but only limited observations of shuttle glow in the ultraviolet and infrared wavelength ranges.

The leading contenders among reaction mechanisms proposed to explain the glow are various recombination processes, involving reactive gases in the upper atmosphere such as O, N, and NO[7,9-11]. For example, the visible glow is thought to be largely due to the reaction

$$NO + O \rightarrow NO_2 + h\nu \text{ (continuum)}.$$

Other possible recombination reactions which produce molecules in excited states, which can then subsequently radiatively de-excite (producing radiation in the ultraviolet), include:

$$N + O \rightarrow NO^* \rightarrow NO + h\nu \text{ (beta, gamma, and delta bands)}$$
$$O + O \rightarrow O_2^* \rightarrow O_2 + h\nu \text{ (Hertzberg bands)}$$
$$N + N \rightarrow N_2^* \rightarrow N_2 + h\nu \text{ (Lyman-Birge-Hopfield, Vegard-Kaplan bands)}$$

The ramming surface facilitates these reactions by compressing the gas, providing translational energy to the reacting atoms or molecules (by virtue of the 8 km/sec orbital velocity), and by providing temporary storage sites (on the solid surface) for reactive species.

Shuttle glow was imaged in the 180-200 nm far-UV wavelength range, for the first time, with NRL's Far Ultraviolet Cameras experiment during the STS-39 mission[12] (see Fig. 1). It is thought, but not proven, that the glow in this wavelength range is due to nitric oxide (NO) δ-band emissions, produced by N + O recombination. If so, there should be equal or stronger NO band emissions in the 200-400 nm wavelength range. NO and NO^+ emissions were observed in the infrared by the SKIRT experiment, also on the STS-39 mission[13].

Emissions due to N_2 and/or N_2^+ may also be present in the UV below 400 nm. Water vapor outgassing may give rise to the OH resonance emission near 310 nm. However, there have so far been no spectrographic observations in the 180-200 nm range imaged by the Far UV Cameras, and neither imaging nor spectrographic measurements of shuttle glow (with positive detections) in the 200-400 nm range. Therefore, there is a need for followon spectrographic measurements in the ultraviolet wavelength range below 400 nm to identify, and measure the intensities of, the spectral emission features in this wavelength range.

OBJECTIVES

The scientific objectives of HRSGS-B are to identify the chemical species and reactions which are responsible for producing shuttle glow in the 180-400 nm wavelength range. This requires the identification, and spectral intensity measurements of, emission features in this wavelength range with moderately high spectral resolution and high diffuse-source sensitivity. In addition, measurements of glow intensity vs. distance from the hard surface producing the glow (by ramming the ambient atmosphere) are required, particularly for determinations of the responsible reaction kinetics. These measurements will be compared with similar measurements of the visible glow. The UV measurements may also aid in understanding the surface glow observed at longer wavelengths, and in predicting intensities to be expected at shorter wavelengths in the far-UV.

INSTRUMENTATION

The HRSGS-B scientific instrument is a high resolution imaging spectrograph, incorporating a UV-sensitive image intensifier, whose data are recorded as film images. The instrument is mounted in a Get Away Special canister, with the view direction toward the tail of the shuttle orbiter (see Fig. 2). During the flight mission, the glow on the surface of the orbiter is observed when either the payload bay or the wing on the side where the GAS canister is mounted is facing the velocity vector, and the orbiter is in Earth shadow.

The instrument (see Fig. 3) consists of five major components: (1) folding mirror and entrance window; (2) objective lens; (3) main spectrograph assembly; (4) detector assembly (image intensifier and film transport); and (5) electronics and power subsystem. All but item (1) are housed in a sealed Get Away Special (GAS) canister, filled with dry nitrogen at 1 atmosphere pressure. Item (1) is mounted on the top surface of the GAS canister lid.

The folding mirror and objective lens form an image of the scene to be observed on the entrance slit of the spectrograph. This provides the instrument with "imaging spectrographic" capability, i.e. the spectral distribution of intensity is displayed in one dimension (the direction perpendicular to the spectrograph slit) and the spatial distribution of intensity (along the spectrograph slit) is displayed in the transverse dimension.

The main spectrograph module consists of the entrance slit, collimating mirror, folding mirror, plane diffraction grating, and Schmidt camera. The Schmidt optics include a fused silica corrector plate, a spherical mirror, and a fused silica field-flattening lens which is placed just in front of the image intensifier faceplate (the latter is located at the prime focus of the Schmidt optical system). This assembly produces an image of the spectrum at the focal surface of the Schmidt camera. Since the 25 mm diameter format of the image intensifier can only accommodate a spectral range of 50 nm in a single exposure, four separate exposure sequences are required (with different rotation settings of the plane diffraction grating) to cover the entire 190-400 nm range.

The detector assembly consists of a proximity-focused microchannel image intensifier and film transport. The image intensifier (made by Varo, Inc.) consists of a UV-transmitting window, UV/visible sensitive photocathode, microchannel plate, phosphor screen, and fiber optic output faceplate. Photoelectrons from the photocathode are proximity focused onto the front surface of the microchannel plate (MCP), where they are multiplied by a factor of several hundred (by secondary emission multiplication in the MCP channels). These electrons are then incident on a phosphor screen which emits visible light under electron bombardment. This phosphor screen is deposited on a fiber optic plate which conducts this light to its output face, where it can be recorded on film or coupled to an electronic imaging device such as a CCD. The film transport contains 35 mm roll film (Kodak T-Max P3200) which records the image produced by the image intensifier. The film is pressed into contact with the rear fiber optic window of the intensifier during exposures. The film transport has a capacity of 15 ft. of film, sufficient for about 60 exposures.

The electronics module (see Fig. 4) contains a microprocessor sequencer and relays to operate the spectrograph film transport and grating rotation drive, in accordance with pre-programmed exposure sequences (initiated by GCD relay

command). It is planned to take a sequence of three exposures, having durations of 12, 60, and 300 seconds (375 seconds total, including film advances), at each grating rotation setting. At the end of the sequence, the grating is returned to its starting position and the microprocessor is reset. The electronics box also provides high voltage power to the image intensifier.

The HRSGS-B experiment is classified as a Complex Autonomous Payload (CAP), because several of its special requirements (such as those on orbiter attitude and time of operation) are beyond the standard services available to Get Away Special customers. However, the hardware required for the investigation is compatible with a standard GAS canister as its housing.

CONCLUSIONS

The HRSGS-B instrument has been designed to provide moderately high spectral resolution measurements of shuttle surface glow in the 180-400 nm ultraviolet wavelength range, a hitherto little-explored spectral region. Detection and identification of the emission features responsible for the glow will allow identification of the participating chemical species and reactions. These identifications may also aid in understanding, or predicting the nature of, shuttle surface glow in other wavelength ranges not directly observed in this experiment. The HRSGS-B instrument provides a simple, low-cost means for obtaining the necessary observational data.

In addition to the author, several students have been involved (and will be involved) in the development of the HRSGS instruments, at both college and high school levels. They have worked at NRL as cooperative education (college) students and under DoD's Science and Engineering Apprentice Program for high school students.

REFERENCES

1. Banks, P. M., Williamson, P. R., and Raitt, W. J., "Space Shuttle Glow Observations", Geophys. Res. Lett., **10**, p. 118 (1983).

2. Mende, S. B., "Measurements of Vehicle Glow on the Space Shuttle", in Proceedings of the A.I.A.A. Shuttle Environment and Operations Meeting (AIAA CP 838), p. 79 (1983).

3. Yee, J. H. and Abreu, V. J., "Visible Glow Induced by Spacecraft-Environment Interaction", Geophys. Res. Lett., **10**, p. 126 (1983).

4. Huffman, R. E., LeBlanc, F. J., Larrabee, J. C., and Paulsen, D. E., "Satellite Vacuum Ultraviolet Airglow and Auroral Observations", J. Geophys. Res., **85**, p. 2201 (1980).

5. Conway, R. R., Meier, R. R., Strobel, D. F., and Huffman, R. E., "The Far Ultraviolet Vehicle Glow of the S3-4 Satellite", Geophys. Res. Lett., **14**, p. 628 (1987).

6. Mende, S. B., Banks, P. M., and Klinglesmith, D. A., "Observation of Orbiting Vehicle Induced Luminosities on the STS-8 Mission", Geophys. Res. Lett., **11**, p. 527 (1984).

7. Swenson, G. R., Mende, S. B., and Clifton, K. S., "Ram Vehicle Glow Spectrum; Implication of NO_2 Recombination Continuum", Geophys. Res. Lett., **12**, p. 97 (1985).

8. Green, B. D., Rawlins, W. T., and Marinelli, W. J., "Chemiluminescent Processes Occurring Above Shuttle Surfaces", Planet. Space Sci., **34**, 879 (1985).

9. Kofsky, I. L. and Barrett, J. L., "Spacecraft Glows from Surface-Catalyzed Reactions", Planet. Space Sci., **34**, 665 (1985).

10. Barrett, J. L., Kofsky, I. L., and Murad, E., "Ultraviolet Glows from Recombination on Spacecraft Surfaces", in Ultraviolet Technology (Vol. **687** of Proceedings of the S.P.I.E.), p. 28 (1986).

11. Kofsky, I. L., "Excitation of N_2 Lyman-Birge-Hopfield Bands Emission by Low Earth Orbiting Spacecraft", Geophys. Res. Lett., **15**, 241 (1988).

12. Carruthers, G. R., Morrill, J. S., Dohne, B. C., and Christensen, S. A., "The AFP-675 Far Ultraviolet Cameras Experiment: Observations of the Far-UV Space Environment", in Ultraviolet Technology IV (Vol. **1764** of Proceedings of the S.P.I.E.), p. 21 (1992).

13. Ahmadjian, M., Jennings, D. E., Mumma, M. J., Espenak, F., Rice, C. J., Russell, R. W., and Green, B. D., "Infrared Spectral Measurements of Space Shuttle Glow", Geophys. Res. Lett., **19**, p. 989 (1992).

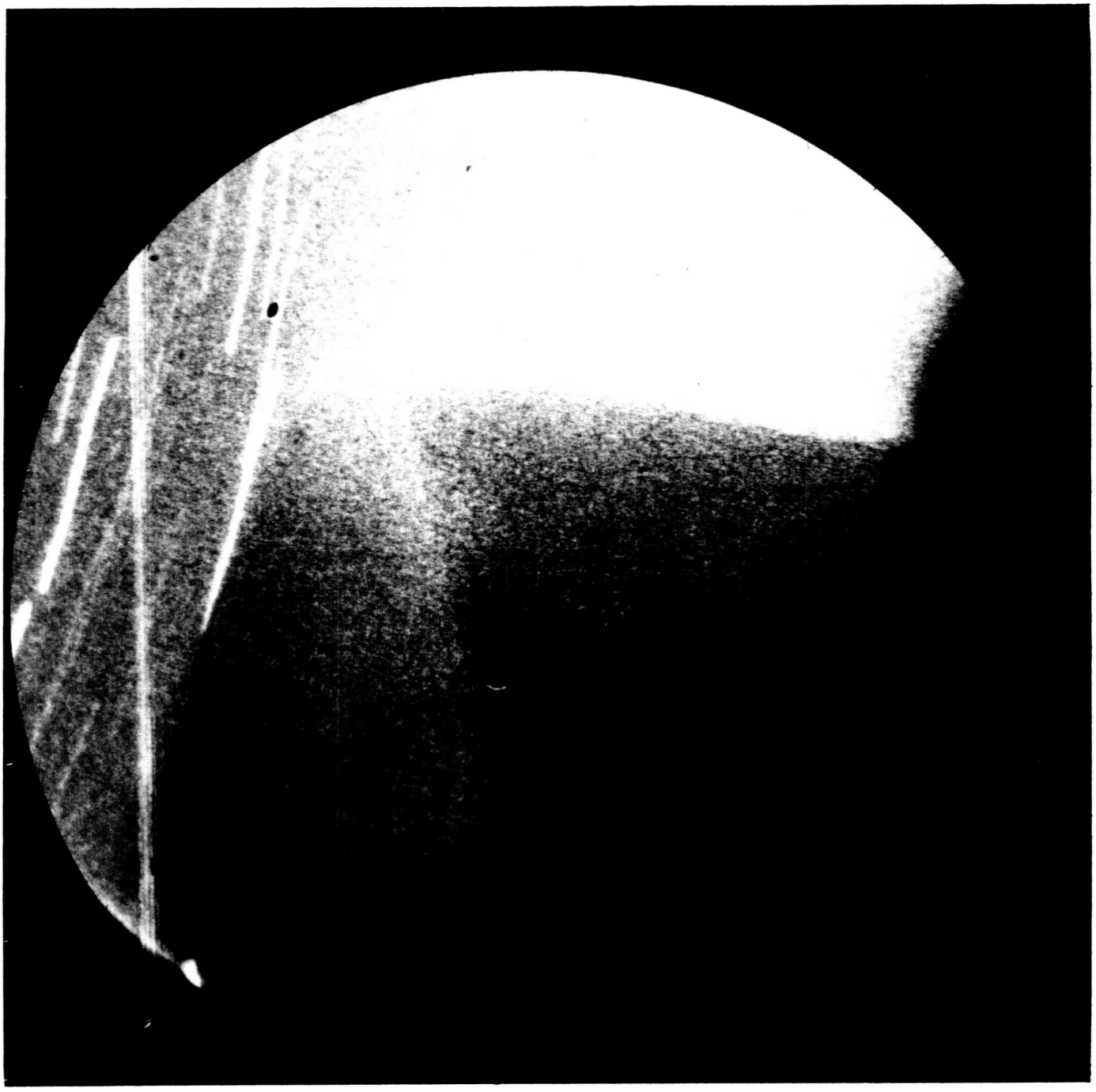

Figure 1. Far-UV (165-200 nm) image of the tail of the shuttle orbiter Discovery, obtained with the #2 Far UV Camera during the STS-39 mission (exposure time 100 seconds). Note that there is a definite "shuttle glow" in this wavelength range, and that the glow appears more diffuse (extends to a greater distance from the surface) than the corresponding visible shuttle glow.

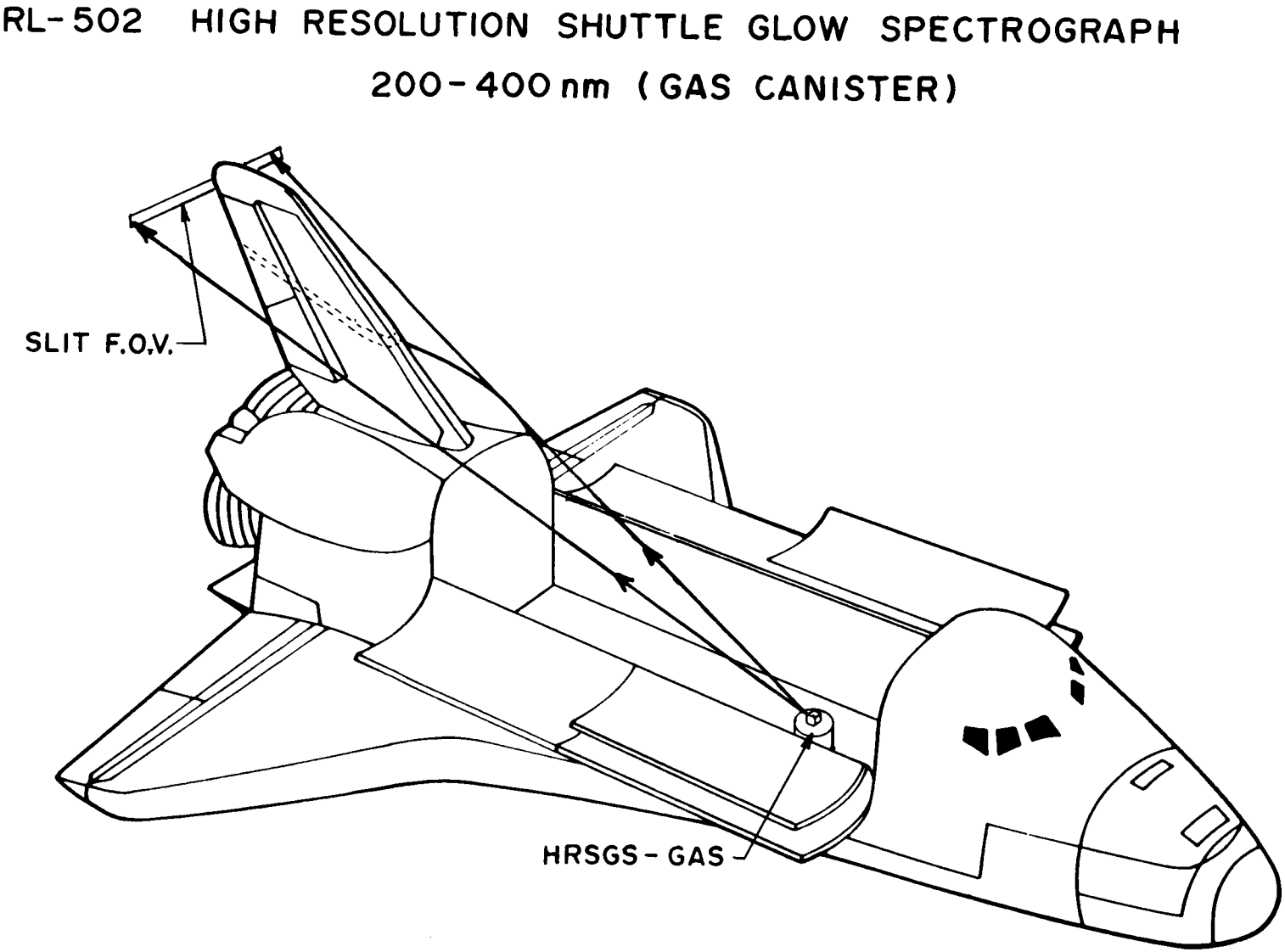

Figure 2. High Resolution Shuttle Glow Spectrograph-B (HRSGS-B) observing geometry for studies of surface glow on the orbiter vertical stabilizer and/or OMS pods.

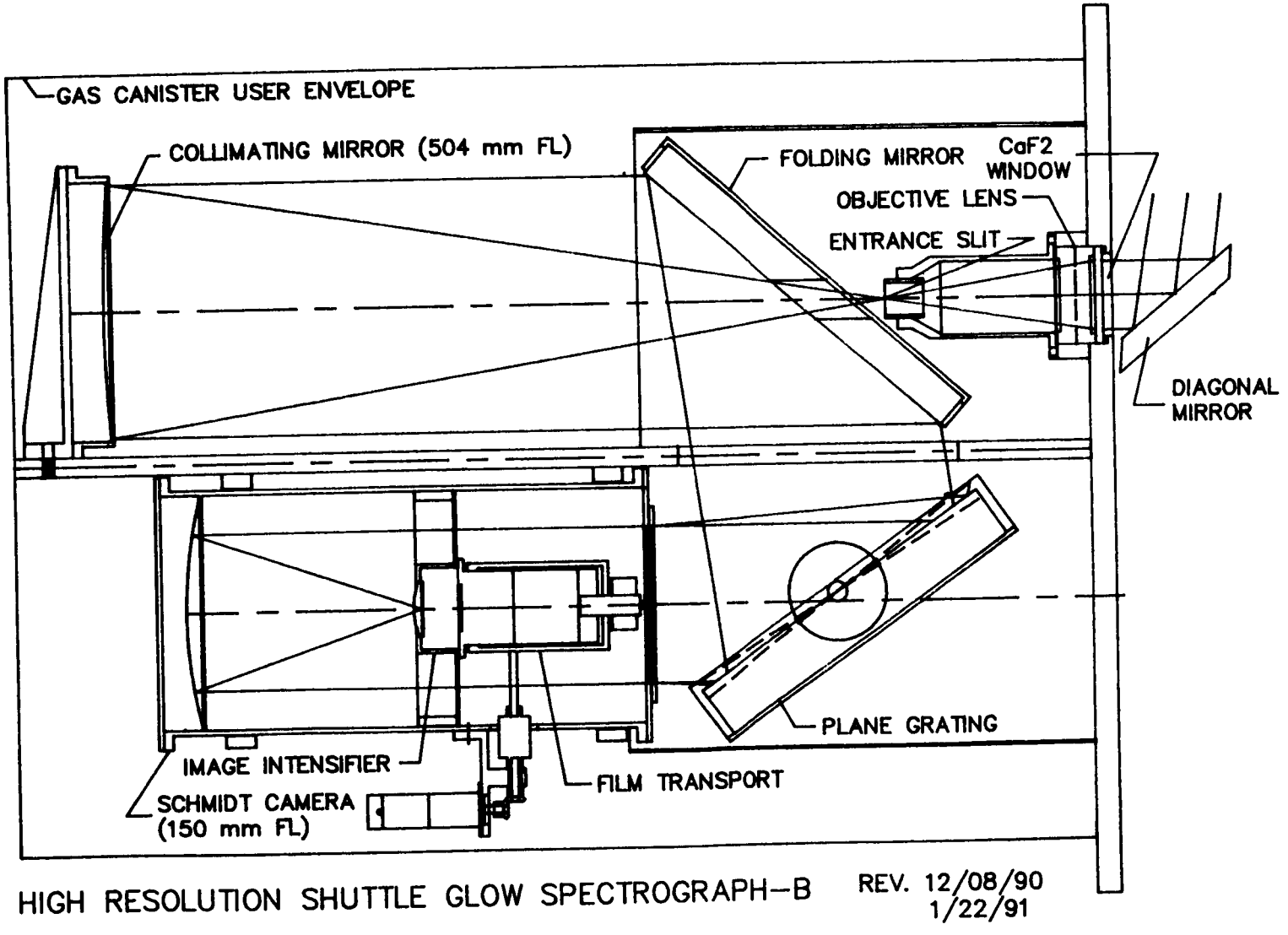

Figure 3. Diagram of the HRSGS-B optical instrumentation.

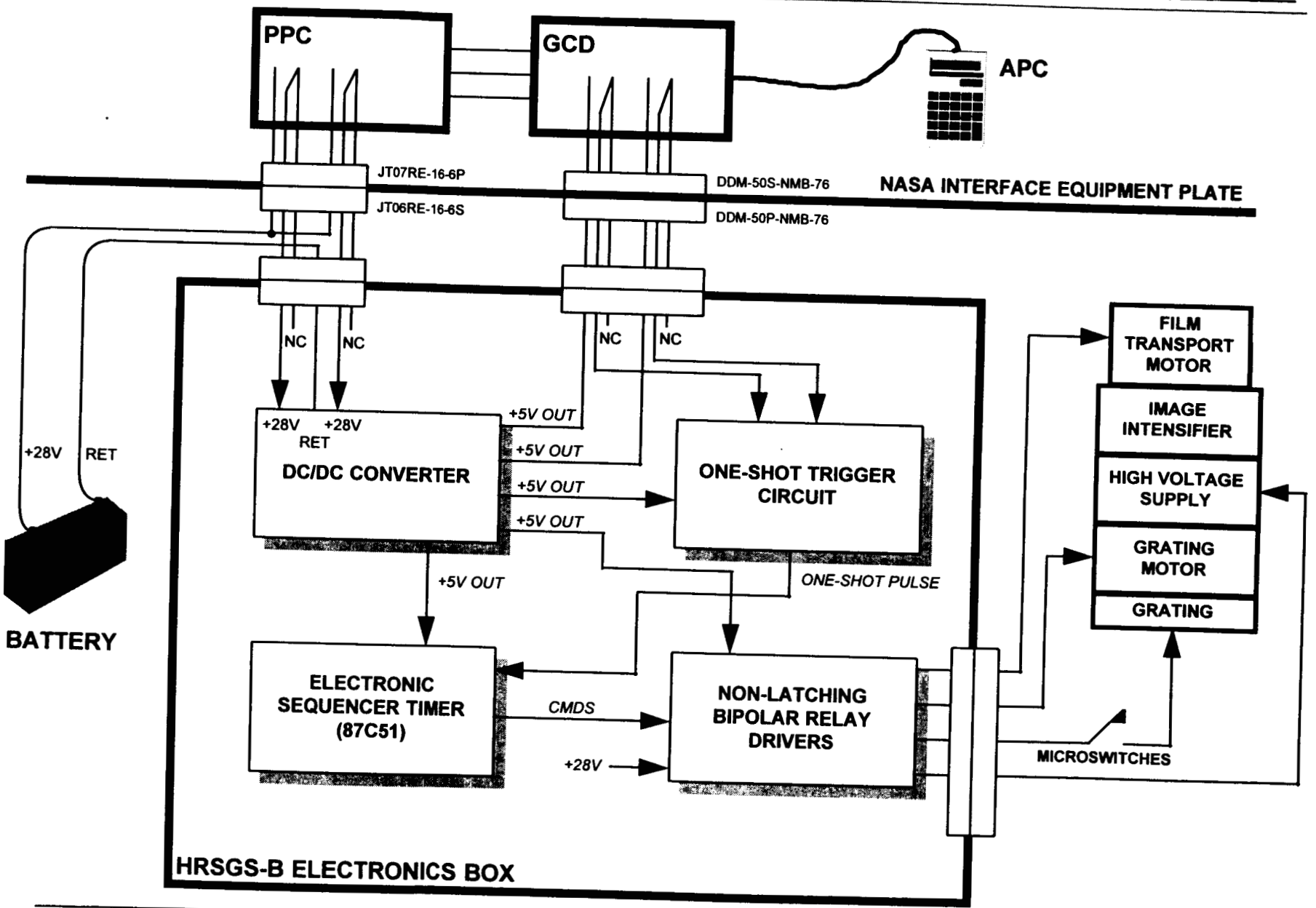

Figure 4. Block diagram of the HRSGS-B power and control electronics.

MATERIALS FLIGHT EXPERIMENT CARRIER CAPABILITY AND FUTURE FLIGHT EXPERIMENTS ON HITCHHIKER-M CARRIER PROGRAM

D. Davis
Center on the Commercial Development of Space (CCDS)
Center on Materials for Space Structures (CMSS)
Case Western Reserve University
Cleveland, Ohio 44106

ABSTRACT

The CMSS has designed, fabricated, and qualified a unique Materials FLight EXperiment (MFLEX) carrier. The MFLEX is a reusable materials experiment carrier designed to support a wide array of sensors that measure synergistic effects on candidate space materials in Low Earth Orbit (LEO). The MFLEX can be integrated on a variety of launch vehicles/carriers and multiple units can be networked to optimize the surface area of carriers such as the Hitchhiker-M currently being built by the Goddard Space Flight Center (GSFC).

INTRODUCTION

Advanced structural materials are being developed for the next generation of satellites and space stations. These materials have to withstand the harsh environment of space for long duration missions, with little or no maintenance. The major causes for degradation of materials are UV radiation, atomic oxygen, electron and proton radiation and thermal cycling (1). Atomic oxygen and vacuum thermal cycling (2) are the critical factors for LEO structures while radiation is critical in higher orbits. The evaluation of structural materials for LEO is done by a combination of ground based simulated exposure and space flight experiments.

The primary objective of the MFLEX is to introduce organic/inorganic materials and coatings to a flux of atomic oxygen in LEO, providing a variety of testing methods. The MFLEX has been designed to provide "real-time" data of the space effects on selected materials. The candidate materials will have undergone extensive ground-based testing prior to being integrated to the reusable space flight hardware designed for multi-mission Space Transportation System (STS) use.

HARDWARE DESCRIPTION

It is convenient to divide the MFLEX into three modules: 1) the Motorized Lid Unit (MLU), the first (top) module, 2) the Sensor Control Unit (SCU), the second module and 3) the Electronics Control Unit (ECU), the third module.

The three separate MFLEX housings are machined from 6061-T651 Aluminum and clear anodized MIL-A-8625 Rev. E, Type II, Class I. They are uniform in length and width for assembly. The assembled MFLEX (Figure 1) measures 12" X 15" X 9" and weighs approximately 52 lbs.

Power requirements are 28V and operates at .5 Amps, with a peak power of 4.5 Amps during lid operations. Communications are via an RS-485 serial interface bus.

Motorized Lid Unit

The MLU houses sensored (active) materials experiments and a retractable motorized lid assembly which protects the experiments from contamination of direct exposure to unfavorable environments. The lid assembly (tractor feed type mechanism) is operated during the mission by ground command. Once the lid is retracted, data will be recorded from the active area and transmitted via the host carrier to Earth, for real time observation.

Six active tray assemblies can be mounted onto the Tray Frame Assembly, contained in the MLU. The active tray assemblies consist of the material specimens, appropriate sensors, Daughter Printed Curcuit Board (PCB), and the Mother PCB. See Figure 2.

The Daughter PCB provides the electronic interface for the sensors. Resistance can be varied on this PCB to allow flexibility for each experiments requirement, which also allows flexibility for different types of sensors to be used other than currently defined. A Daughter PCB is assembled onto each active tray for ease of assembly and removal. The Daughter PCB connects to the the Mother PCB which provides electrical distribution from the Tray Specific PCB and routes the electronic signal to the Daughter PCB.

The MLU also accommodates passive (unsensored) specimens on the sides of the top surface; these are not protected by the motorized lid assembly.

Sensor Control Unit

The SCU houses two printed circuit boards, 1) the Tray Specific Board (TSB) which provides analog signal conditioning, analog to digital conversion and signal multiplexing; and 2) the Common Functions Board (CFB), which provides the driver for the stepper motor and both power supply filtering/conditioning for the TSB.

Electronics Control Unit

The ECU houses two printed curcuit boards; 1) the Electronics Control Board which provides the processing, communications link, and watchdog functions; and 2) the Acoustic Emissions Boards which supports acoustic emission experiments.

HARDWARE CAPABILITY

Experiment Area

The passive area currently accommodates two 0.50", thirty-six 0.75", and twelve 1.0" diameter specimens. Two passive experiments can be accommodated, sized up to 0.25" X 2.4" X 10.5" each.

The active experiment area currently accommodates forty-eight 0.5", and seventy-two 0.75"; or it can house experiments up to 1" X 9" X 10". These experiments and their trays can be customized to accommodate almost any configuration, not exceeding physical constraints.

Sensor Capability

The MFLEX can support a variety of sensors that provide accurate measurement of materials erosion that occurs in-flight. Measurement data that requires recording during the mission will consist of resistance, light transmittance, temperature, strain, and frequency emissions. In order to support these requirements, CMSS has designed in capacity to incorporate several sensor types; included are two types of actinometers, three types of thermal sensors, two ranges of strain gages, photo-diodes, and acoustic microphones. See Table 1 for sensor specifications and ranges.

SUMMARY

The MFLEX is a unique integrated materials testing facility that is now available for users to directly obtain data "real-time" for evaluating materials in space. The MFLEX can be used to conduct material experiments in LEO or deeper space, retrievable or non-retrievable, short or long duration missions. The MFLEX can also be used to monitor the health of spacecraft structures.

The unique capability of modifying the host of sensors used for each experiment provides flexible testing methods for materials evaluation in space. The MFLEX facilitates a network capability that can be integrated onto a carrier. It has been proposed as an expanded materials test facility as an attached payload for a long duration experiment on Space Station Freedom.

FUTURE WORK

Materials Laboratory Experiment-01 (MatLab-01)

The MFLEX is scheduled to launch its maiden flight on STS-60, November 1993. The MFLEX is integrated as a piggyback payload on the Wake Shield Facility, a free-flyer experiment carrier designed by the CCDS at the University of Houston. The MFLEX is mounted perpendicular to the velocity vector (RAM). Conclusions will be provided at the 3rd Annual Materials in Space Symposium, May 1994.

Candidate Materials Space Experiment (CMSE)

July 1995, multiple MFLEX's will be exposed to the space environment using a Hitchhiker-M (HHM) carrier currently being designed by the GSFC. This carrier will be held into RAM by the Orbiters Remote Manipulator System (RMS). This experiment can potentially support up to 1000 material experiments.

Long Duration Experiment

CMSS is currently investigating the possible manifest of a long duration experiment.

REFERENCES

1. B.A. Banks, "Atomic Oxygen Interaction with Materials on LDEF." Proc. LDEF Materials Data Analysis Workshop, NASA Conference Pubs. 10046, July 1990.

2. R.C. Tennyson, G.E. Mabson, W.D. Morison and J. Kleiman, "The LDEF/UTAIS Composite Materials Experiment." Proc. LDEF First Post-Retrieval Symposium, NASA Conference Pubs. 3134, June 1991.

Table 1
Current MFLEX
Sensor Specifications

Qty	Sensor/spec	Range
96	Actinometer	
	high resolution channel range	0 to 500Ω
	resolution	0.5Ω
	large channel expanded range	0 to 10kΩ
	resolution	10Ω
24	Photodiodes	
	input range	0 to 300mA
	resolution	300μA
	diode voltage	0.v max
2	Solar cells	
	input range	0 to 1.5mA
	resolution	1.5μA
	diode voltage	1mV max
5	Acoustic microphone	
	voltage out	1.4Vpp
	noise	3μV
	dynamic range	84dB
9	±500μ Strain gauge	
	resolution	1μ strain
16	±5000μ Strain gauge	
	resolution	10μ strain
16	Thermistors	
	temperature range	-50°C to +150°C
	resolution	0.5°C from 0°C to 100°C
72	Platinum resistance thermometer	
	temperature range	-50°C to +150°C
	resolution	0.25°C
48	AD590 (ic)	
	input range	-60°C to +150°C
	resolution	0.21°C

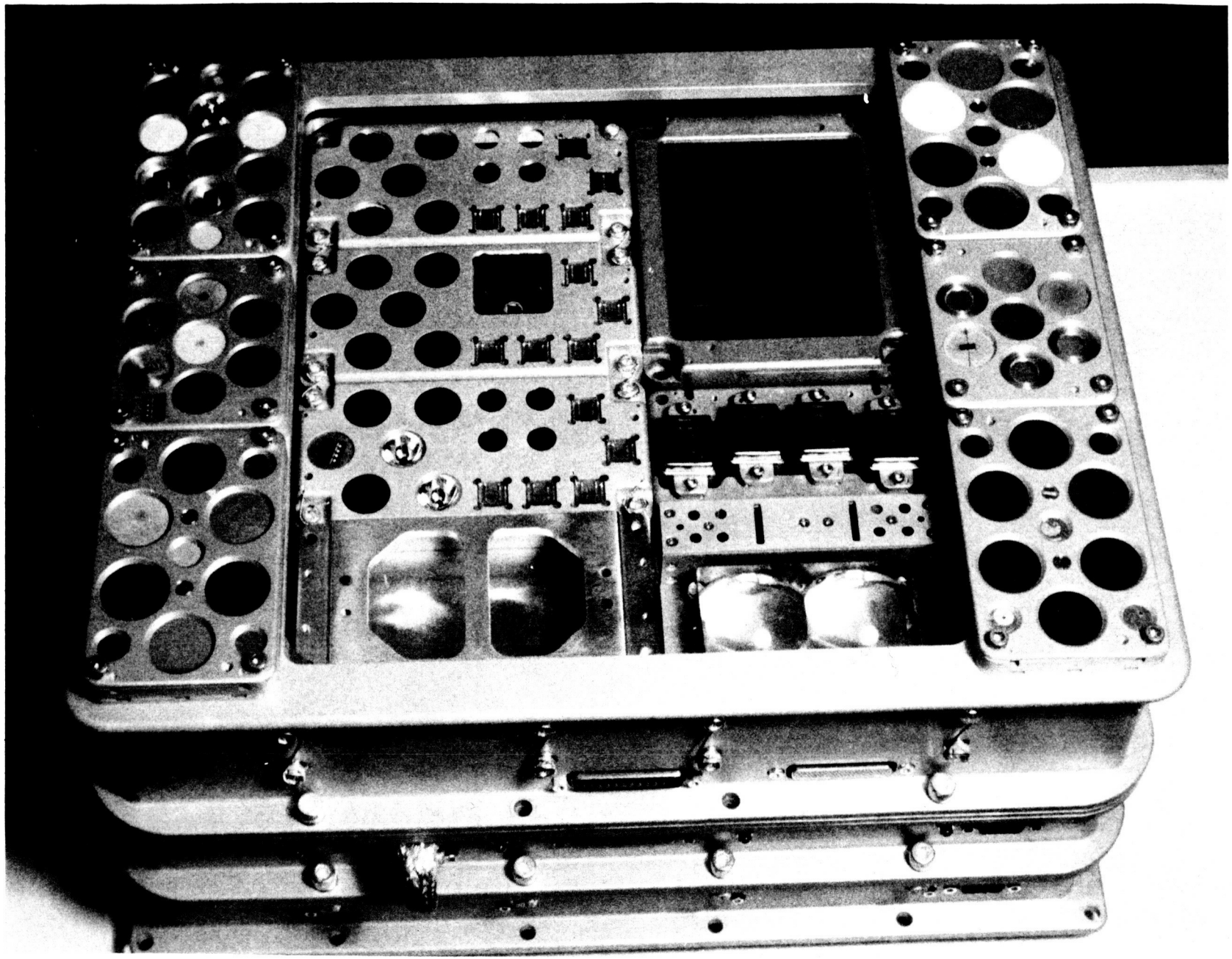

FIGURE 1
MATERIALS FLIGHT EXPERIMENT CARRIER CONFIGURATION FOR MATLAB-01

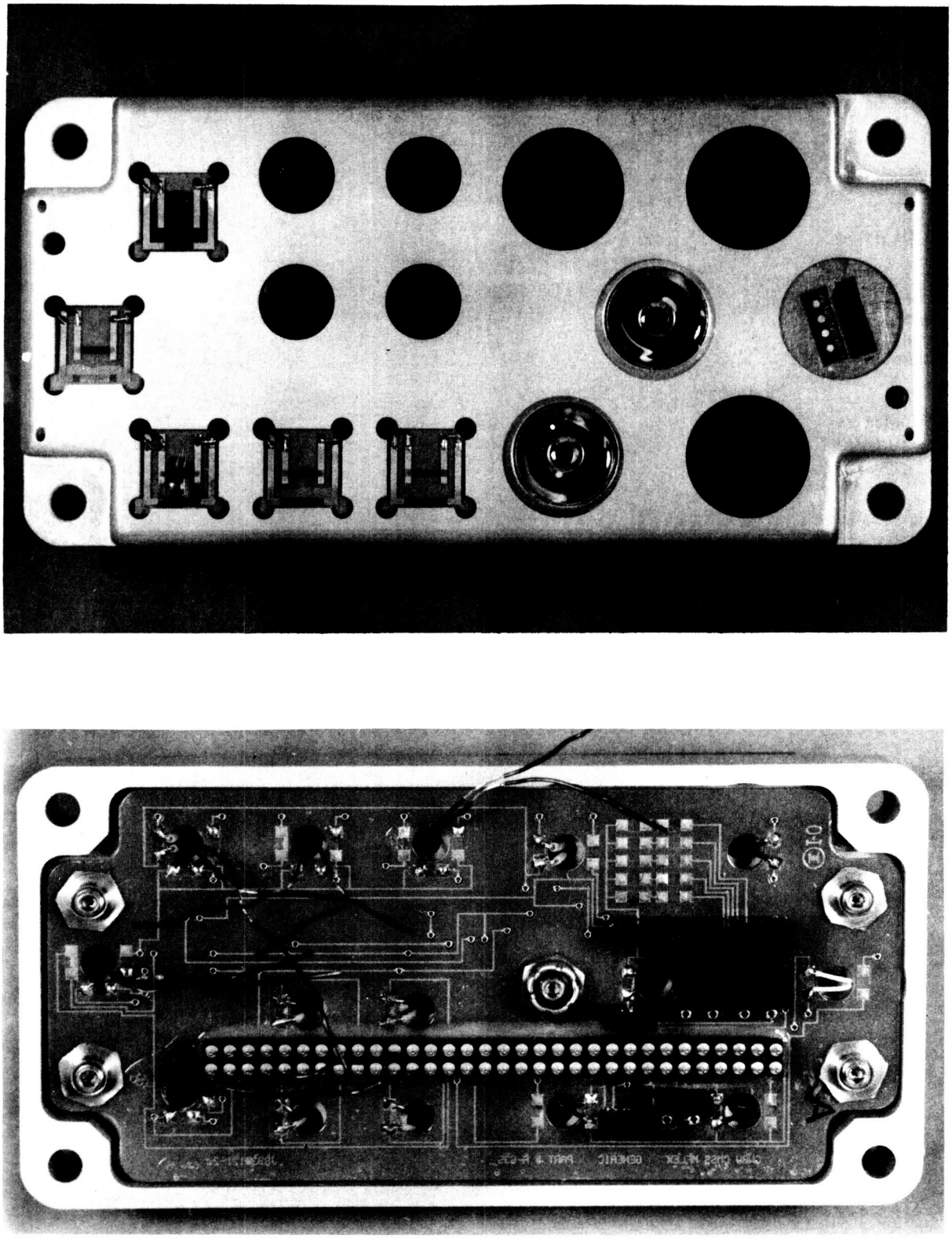

FIGURE 2

TOP - GENERIC ACTIVE TRAY ASSEMBLY WITH MATERIAL EXPERIMENTS

BOTTOM - DAUGHTER PRINTED CIRCUIT BOARD ASSEMBLY ON ACTIVE TRAY

LIMITED DURATION OF CANDIDATE MATERIALS EXPOSURE EXPERIMENT (LDCE): A COMPLEX AUTONOMOUS PAYLOAD (CAP) USING A GET AWAY SPECIAL (GAS) CANISTER

D. Davis
NASA Center on Commercial Development of Space Program (CCDS)
Center on Materials for Space Structures (CMSS)
Case Western Reserve University
Cleveland, Ohio 44106

ABSTRACT

CMSS has designed, fabricated, qualified and flown the LDCE payload as a cost effective space flight hardware to conduct exposure of materials to the space environment. The hardware has been qualified for 10 missions, utilizing a GAS Canister, supplied by Goddard Space Flight Center. Results of the first series of LDCE experiments have shown that the hardware performed as expected.

INTRODUCTION

Advanced structural materials are being developed for the next generation of satellites and space stations. These materials have to withstand the harsh environment of space for long duration missions, with little or no maintenance. The major causes for degradation of materials are UV radiation, atomic oxygen, electron and proton radiation and thermal cycling (1). Atomic oxygen and thermal cycling are the critical factors for low Earth orbit (LEO) structures while radiation is critical in higher orbits. The evaluation of structural materials for LEO is done by a combination of ground based simulated exposure and space flight experiments.

The primary objective of this LDCE payload is to introduce developmental organic/inorganic materials and coatings to a flux of atomic oxygen in low earth orbit. The candidate materials will have undergone extensive ground-based testing prior to being attached to reusable space flight hardware designed for multi-mission Space Transportation System (STS) use. Even though small shuttle payload GAS Canisters are used as the carrier, the LDCE experiment has been classified as a Complex Autonomous Payload (CAP) due to specific requirements for altitude, attitude and duration placed on the orbiter.

HARDWARE DESCRIPTION

The LDCE experiment assembly consists of the experiment disk, sample holders, and the high density center panel plus its attachment bracket. The sample holder assemblies are bolted onto the experiment disk, the attachment bracket bolts onto the high density panel and then onto the experiment disk, refer to Figure 1.

Sample Holder Assemblies

The LDCE experiment hardware consists of 8 sample holder assemblies to which material specimens are integrated. All 8 holders are designed to insure that no one component exceeds 0.25 lbs. (low release mass). This accounts for the difference in the number of specimens and thickness for each holder. Seven of the sample holders allow for the placement of 0.75" diameter material specimens accommodating different thicknesses of specimens (e.g., 1/32" up to 1/4" thick), refer to Figure 2. One sample holder allows placement of a thin film rectangular sample of 1.00" X 0.50".

In addition, the LDCE experiment disk provides a method for exposing eight 1.0" diameter specimens, these specimens are mounted in a slightly different manner. Instead of using a bolt top-down assembly, these specimens are mounted from the under side of the disk. A retainer plate then bolts to the underneath side of the disk, holding the 1.0" specimen in place, refer to Figure 3. Total weight of the holders, fasteners and samples is approximately 14 lbs.

High Density Panel Assembly

Located in the center of the support disk is an area termed the "high density panel." The configuration of this area is flexible, allowing each experiment configuration to differ to meet unique custom requirements. Figure 4 shows an example of different configurations. The high density sample holder panel is bolted to the high density support box. The high density box is attached to the support disk via the attachment bracket. The weight of the high density panel averages about 8-9 lbs. with the recent configurations.

All material samples are placed into their prospective holders and supported by spacers and wave springs to insure a positive upward force to seat them against the retainer plate. Sample holder assemblies are then bolted to the experiment disk, followed by the high density panel assembly.

Experiment Support Disk

Each experiment disk is 19.65" diameter with a 15.34" diameter section to which all sample holders, high density panel and bracket are attached, refer to Figure 5. The disk is capable of supporting 150 lbs., being held in place to the end plate of the GAS Can door assembly, using 24 #10 bolts.

Each disk is fabricated from a different aluminum alloy. Alloys selected for the LDCE series are 7075-T651, 7075-T7351, and Aluminum-Lithium alloy 8090-T8771. The first two alloys were selected based on past flight history. All three disks were clear anodized to spec MIL-A-8625 Rev. E., Type II, Class 1.

The Al-Li was selected as an experimental structural material, after extensive ground based evaluation. This is a much lighter alloy with superior mechanical properties. Using it in the fabrication of the LDCE flight hardware will help qualify it for other space related applications (2).

Internal GAS Can Experiments

CMSS has developed a method of utilizing the internal portions of GAS Cans for experiments that do not require atomic oxygen exposure. The protrusion on the under side of the experiment disk from the high density box provides a surface area with a bolt pattern for experiments to be attached, refer to Figure 6.

Summary and Conclusions

The CMSS experiment demonstrates that LDCE type experiments are a cost effective method of using the GAS Canisters for controlled exposure of materials to the space environment. The internal portion of the canister is dedicated to launch survivability studies that do not require atomic oxygen exposure.

Part of the flight hardware is fabricated of a developmental Al-Li alloy, thus supporting the flight qualification of this material.

All the objectives were accomplished on STS-46, July 1992, minimizing the utilization of the shuttle small payload accommodation capabilities. Results were reported at the 2nd Annual Materials in Space Symposium (3), May 1993 at CMSS.

FUTURE WORK

At the time of this writing, the second in a series of LDCE experiments are awaiting the launch of STS-51. Upon the return of the LDCE hardware, re-testing of the disks and re-integration will occur for the third experiment in the LDCE series. LDCE 6-7-8 will be launched on STS-62, February 1994. Results will be reported at the 3rd Annual Materials in Space Symposium, May 1994.

REFERENCES

1. B.A. Banks, "Atomic Oxygen Interaction with Materials on LDEF. Proc. LDEF Materials Data Analysis Workshop, NASA Conference Pubs. 10046, July 1990.

2. S. Zaat, Phd Thesis "The effects of ionized gas exposure on the toughness and fatigue properties of aluminum alloys and composites."

3. Proceedings 2nd Annual Materials is Space Symposium, May 1993.

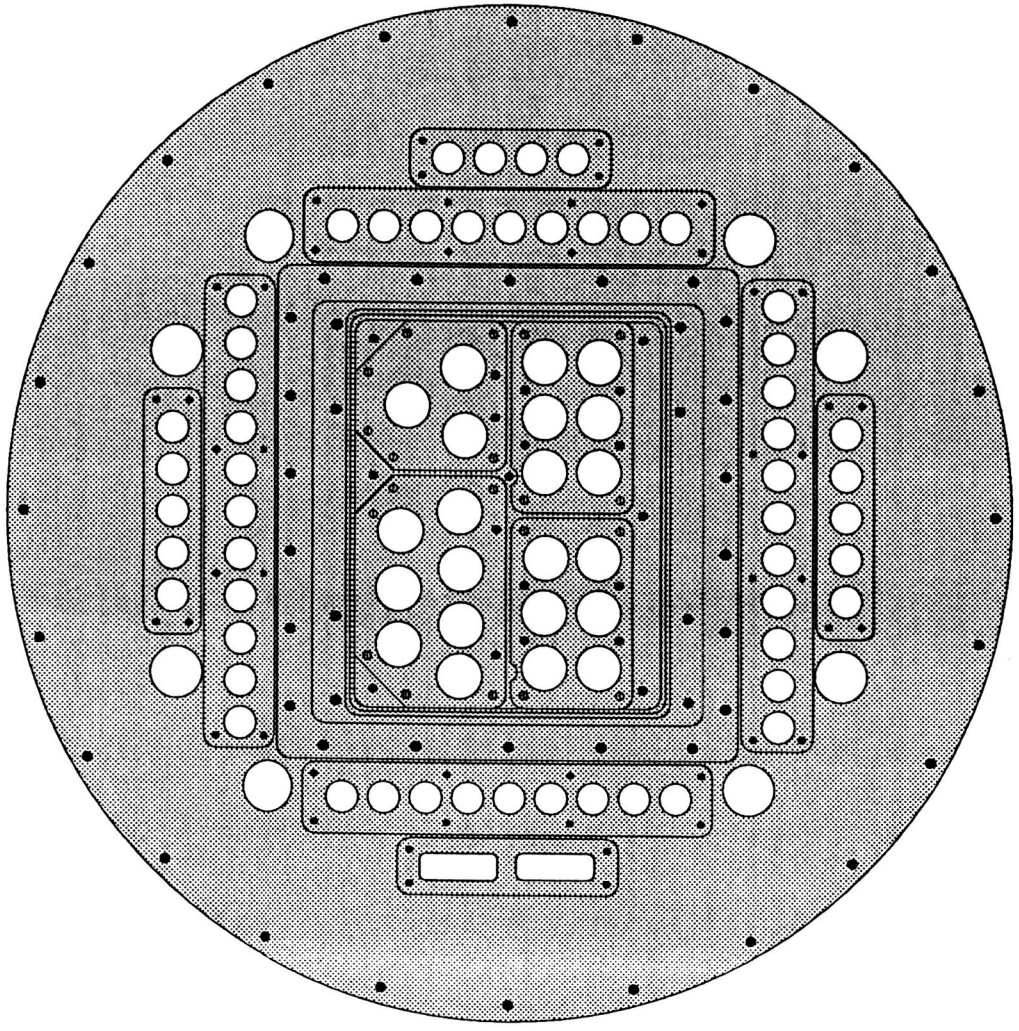

Limited Duration of Candidate materials exposure Experiment (LDCE) Assembly

Figure 1

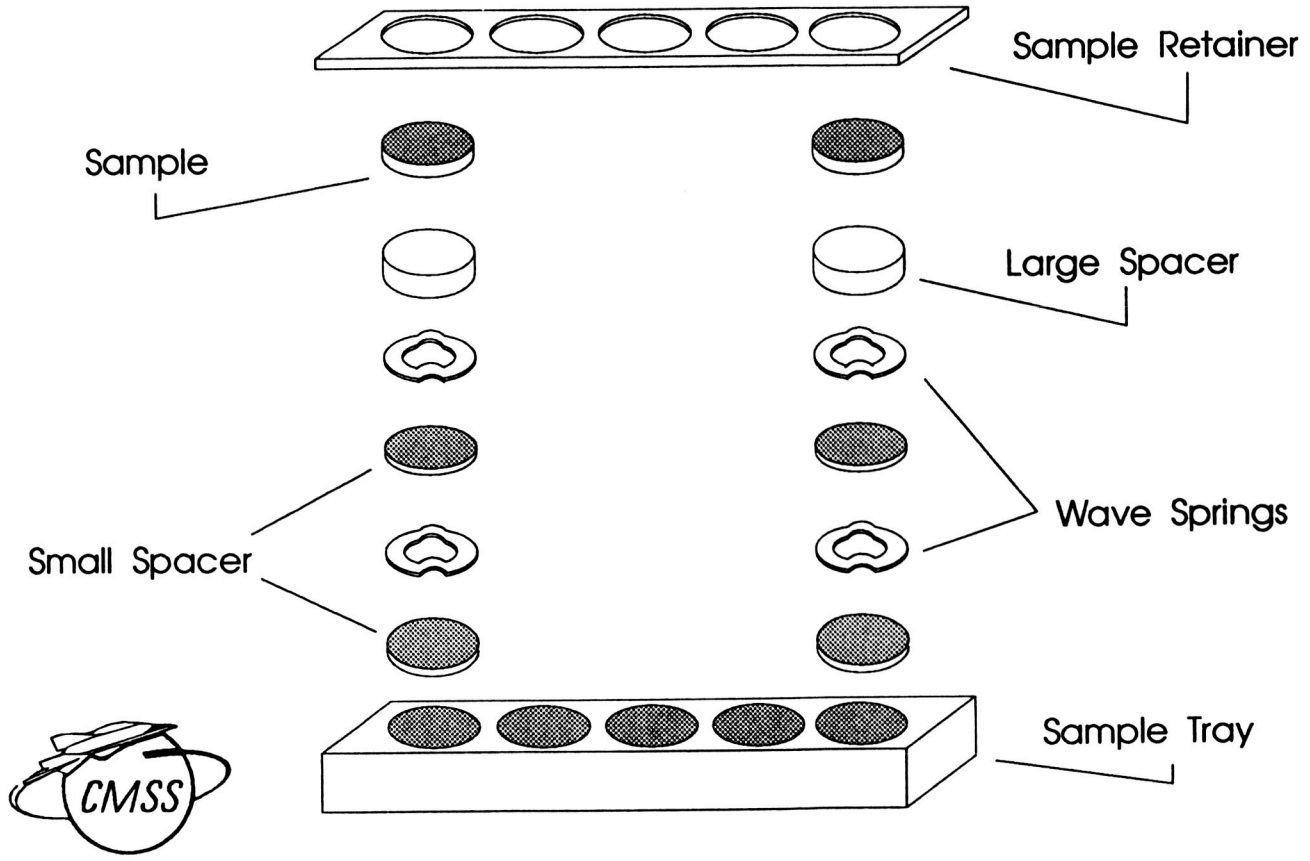

LDCE Sample Holder Assembly Illustration

Figure 2

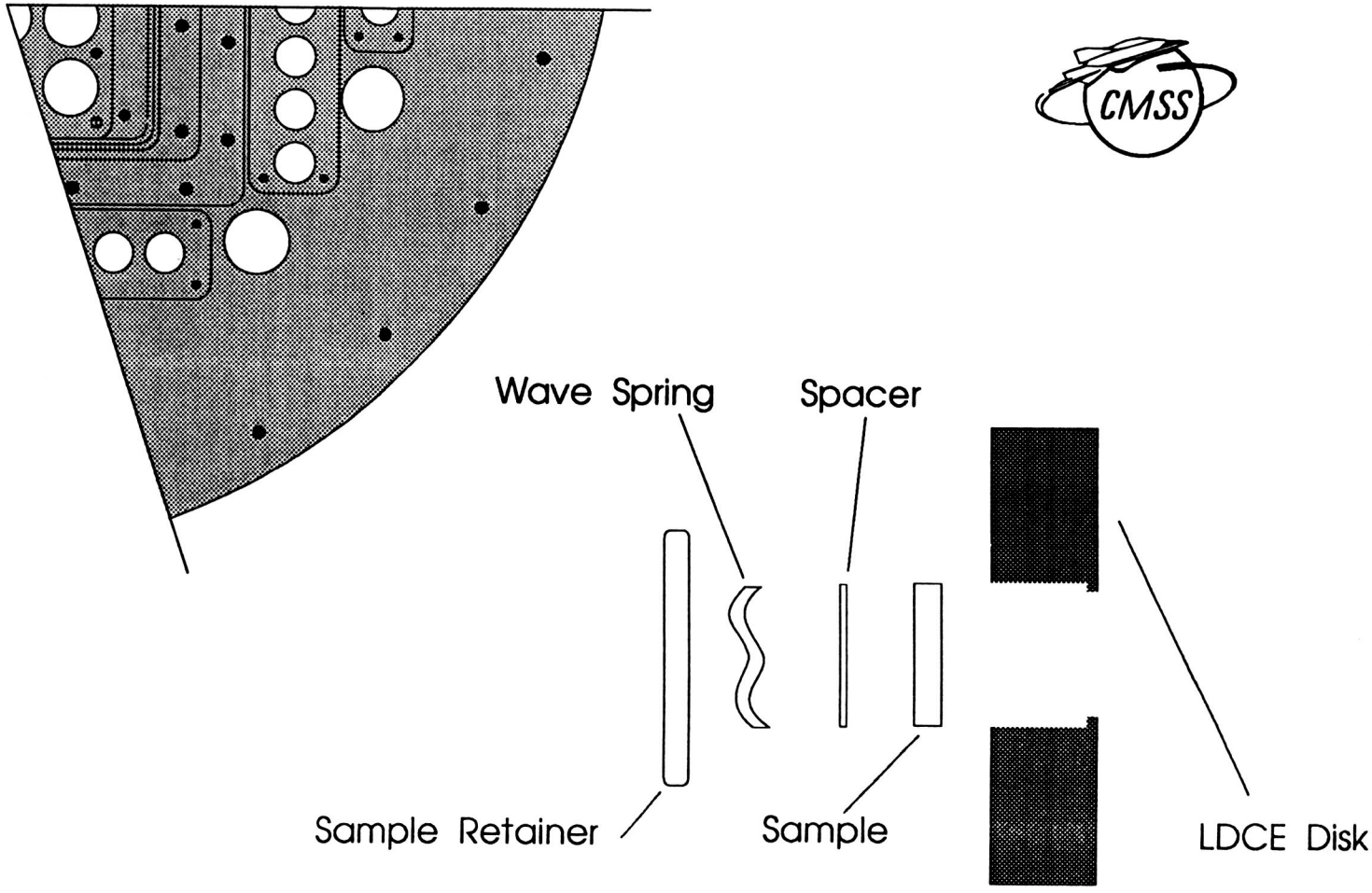

Method of Mounting 1.0" Specimens to LDCE Experiment Disk

Figure 3

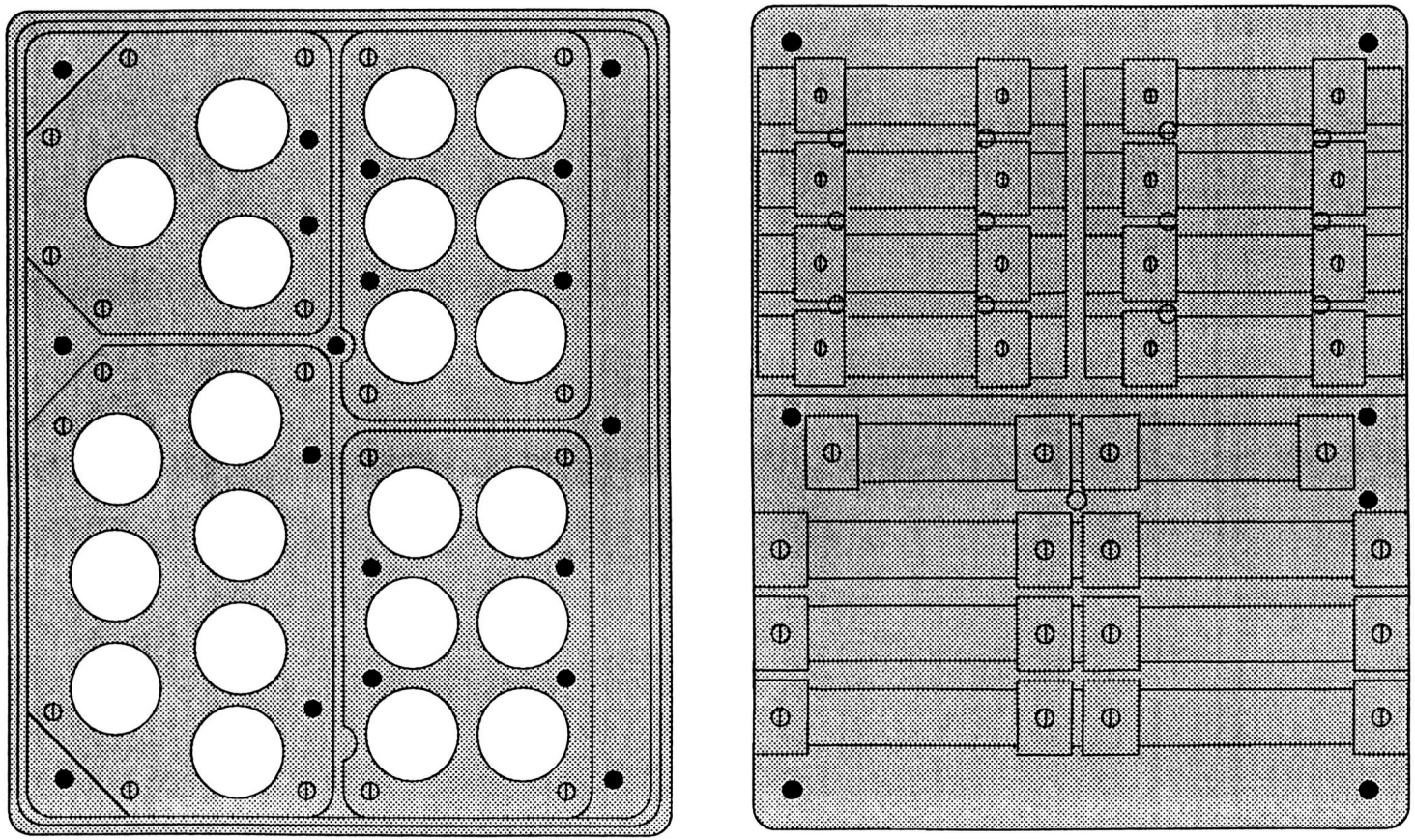

High Density Panel Assemblies used on LDCE 4 & 5

Figure 4

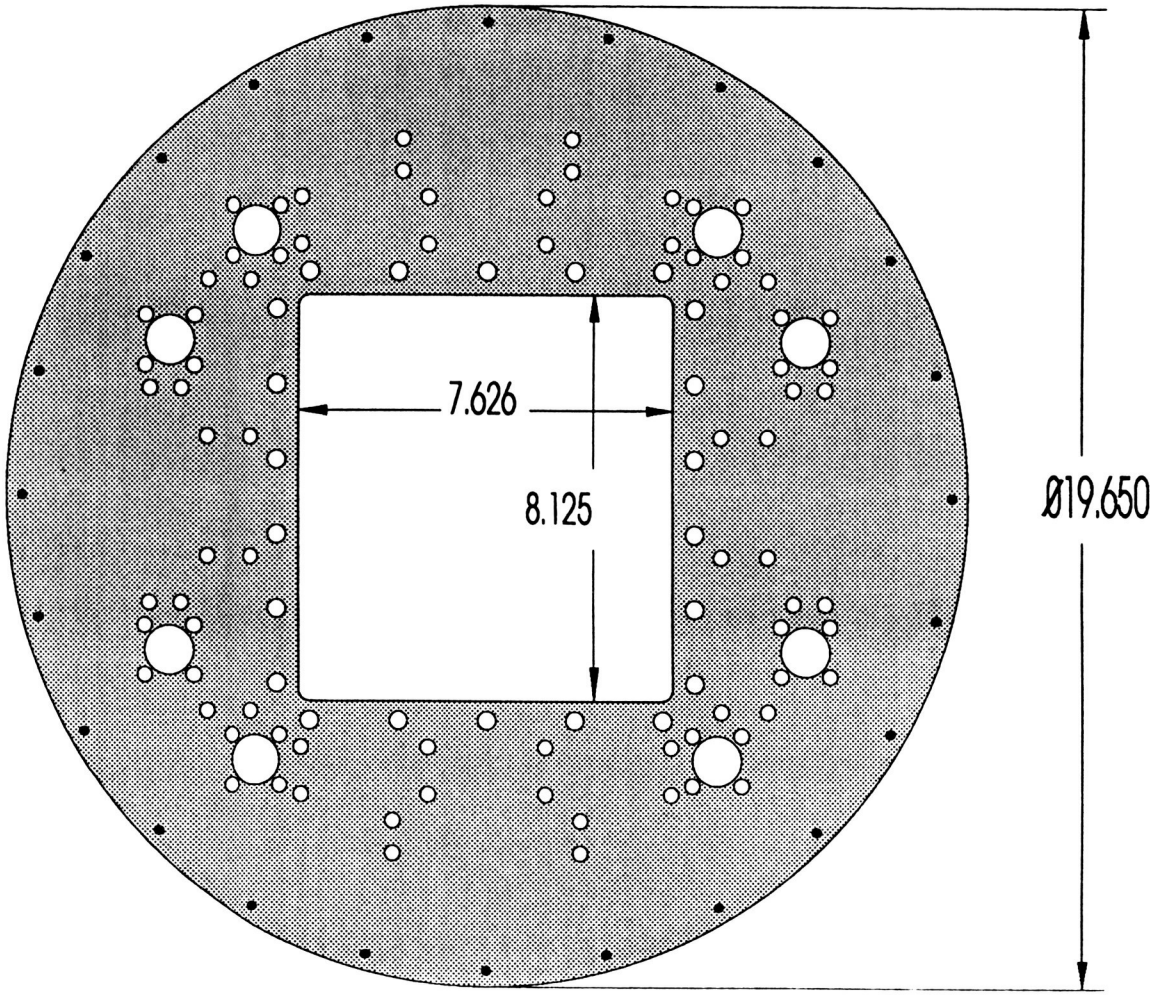

LDCE Experiment Support Disk

Figure 5

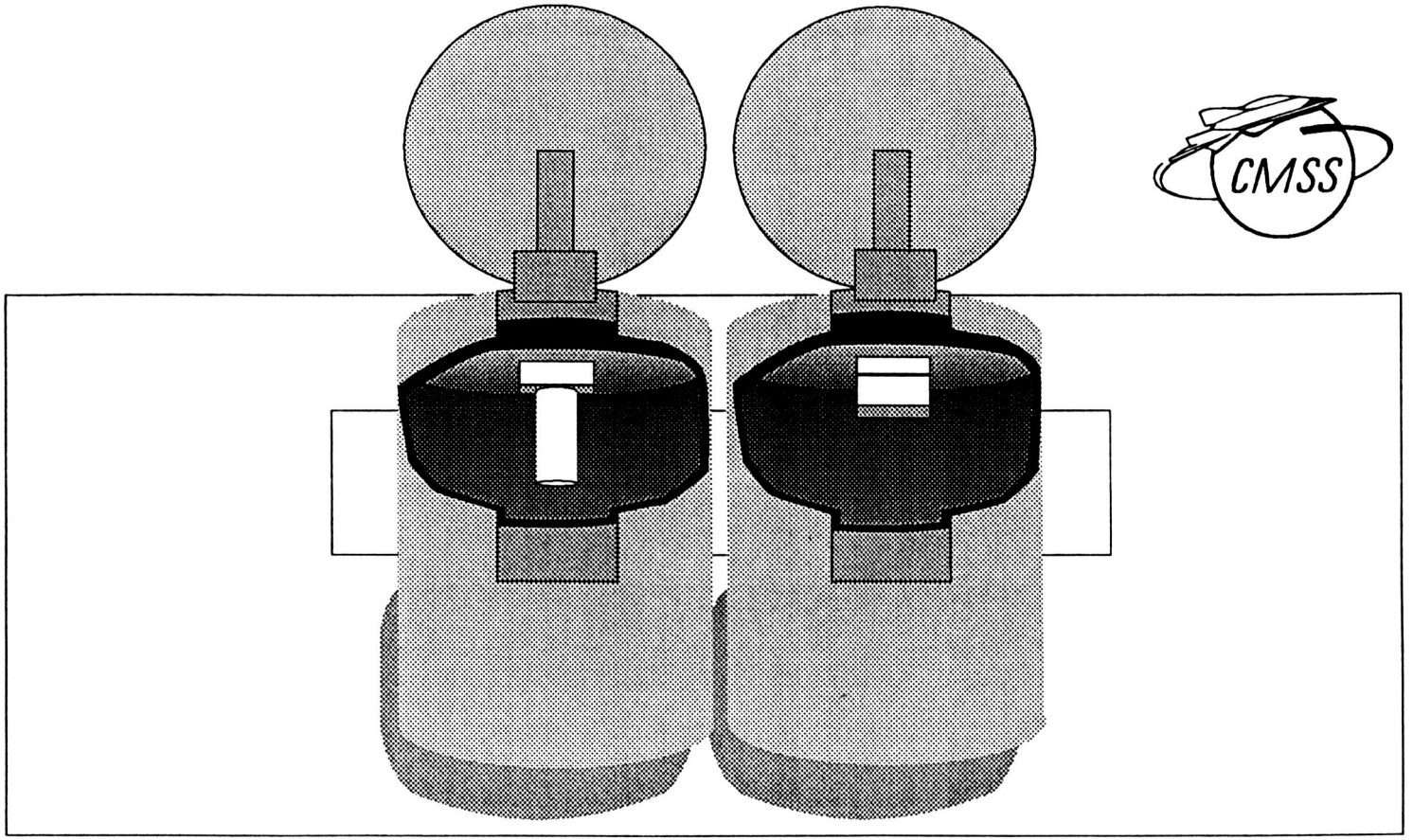

Internal GAS Can Experiments Mounted to the LDCE Experiment Disk

Figure 6

Kennedy Space Center Processing of Shuttle Small Payloads

Michael E. Haddad
National Aeronautics and Space Administration
Kennedy Space Center
Kennedy Space Center, Florida 32899

ABSTRACT

There are many steps involved in preparing a payload for a mission into space on the Space Shuttle. Operations at the John F. Kennedy Space Center (KSC) are the last of those steps for the hardware before the payload is launched. To assure a successful and efficient KSC processing flow, a great deal of planning between the Robert H. Goddard Space Flight Center (GSFC) and KSC personnel is required before the payload arrives at KSC. After arrival, pre-flight operations occur between payload personnel, GSFC and KSC personnel for integration of the payload into its carrier (if required), in preparation for installation into a Orbiter. Once installed into a Orbiter, final test(s), checkout, and close-out of the payload is performed by GSFC and KSC personnel before launch. Mission support varies depending on the payload flying, but once the mission is complete and the Orbiter has returned to KSC, post-flight operations begin. This usually involves a reverse flow of the pre-flight operations. KSC operations conclude when the payload, its ground support equipment (GSE), and personnel depart KSC. A list of lessons learned is generated at the end of each payload flow, to avoid repeating the same mistakes (if any) for the next payload or for multiple repeat flights of the same payload. Always monitored are planned changes that may affect the payloads, GSE, KSC facilities, payload personnel, GSFC personnel, and/or KSC personnel.

INTRODUCTION

This paper will discuss KSC processing of mostly the Get Away Special (GAS) payloads and Complex Autonomous Payloads (CAP's), with some mention of Hitchhiker type payloads. The STS-57 GAS Bridge Assembly (GBA) KSC operational flow will be used to demonstrate a normal flow of GAS/CAP payloads. The STS-57 GBA containing 11 GAS payloads and 1 CAP payload (CONCAP-IV) was launched on the Space Shuttle Endeavour, June 21, 1993 and landed at KSC on July 1, 1993. A general layout of facilities at KSC is shown on Figure 1.

PLANNING PHASE

The planning phase begins when a GAS, CAP, or Hitchhiker payload is manifested to fly on the Space Shuttle. This can be many years into the future, as shown in Figure 2, which reflects that KSC is planning well into the future to support many payloads. From this figure it can be seen how changes in the Space Shuttle manifest can cause major impacts to KSC facility utilization flow for payloads. The actual experiments may not yet be selected, but knowledge of the number of GAS, CAP or Hitchhiker payloads manifested for a certain STS mission is used to start preliminary planning. KSC personnel are involved early in the

design phases of Hitchhiker type payloads because of the extensive integration and testing that needs to be performed at KSC. The GAS/CAP payloads do not require this, but early knowledge of what each GAS/CAP payload contains and its function allows GSFC and KSC personnel to better prepare facilities and support. Design inputs from KSC will allow the designer to modify the payload design early enough to avoid any problem areas that may be encountered at KSC with the current design. An example may be the location of a connector required to support pre-flight testing. On a bench in the experimenter's laboratory, access to the connector is easy. Once the experiment is integrated with its carrier and the carrier installed into the Orbiter, access to that connector could be impossible.

As the payload matures, KSC personnel review all the documentation, drawings, schematics, and requirements associated with both the payload and the Shuttle. This assures the payload will be properly prepared for the Shuttle, that the Shuttle will be properly prepared for the payload, and that all the personnel, facilities and support are ready for payload operations at KSC. Many teleconferences, and working group meetings take place to solve any possible problems or conflicts. Again, this is performed well before the payload arrives at KSC. This STS-57 mission was the fifth flight of the GBA so much of the work that had been performed on past flights was repeated taking into account the different payload types. The planning phase ends and the operational phase begins once the payload, GSE, or personnel arrive at KSC. This does not mean "planning" ends because all through the processing flow planning continues to prepare for all upcoming activities.

OPERATIONAL PHASE

Figure 3 (reference 1) shows the standard processing flow of the GAS/GBA payload(s) at KSC. Each block represents a facility with operations performed at that facility listed below. Experiment personnel and GSE will usually arrive before the experiment in order to configure any equipment that may support the experiment. After the experiment(s) arrive at the GAS facility, the experimenter will spend between 1 to 4 days checking out the payload, Figure 4. At the same time, GSFC personnel are preparing the GAS canister for experiment installation. Then the installation of the experiment(s) into the GAS canister occurs. This is performed by using an overhead crane and GSFC lifting sling attached to the upper plate of the payload, Figure 5. The payload is raised from its work area and lowered into the GAS canister and secured. GSFC personnel electrically connect the lower plate GAS subsystem electronics to the experiment and perform a test. When the interface test is successful, GSFC secures the lower plate to the GAS canister, Figure 6. KSC personnel support as required. The GBA, some CAP, and most Hitchhiker payloads are not assembled in the GAS facility. A Payload Processing Facility (PPF) will be used because of the physical size of the payload or strict payload requirements like, special handling, servicing requirements, contamination concerns or use of a KSC control room is required.

The GBA missions require that the GAS/CAP payloads be installed on the GBA in a PPF. The PPF used is determined by the Facility Utilization Schedule, Figure 2, and payload requirements. While the payloads are being prepared, GSFC personnel are preparing the GBA for the payloads. The GAS/CAP payloads are then moved from the integration area to the PPF using KSC transportation (some payloads may be prepared in the same PPF as the GBA). From this point on, all transportation is performed using KSC equipment. Once in the PPF each payload is installed onto the GBA and final electrical connections are made. When all payloads are installed on the GBA, a final test of all payloads is performed, and the GBA is prepared for transportation to the Operations and Checkout (O&C) building, Figure 7.

If the GAS/CAP or Hitchhiker payload will be installed onto a GAS beam side mounted to the Orbiter sill it will be transported to the Orbiter Processing Facility (OPF) with payload GSE using KSC transportation. In the OPF, the payload is mounted onto the GAS beam that has been installed into the Orbiter by Shuttle personnel. Some Hitchhiker payloads may first go to the O&C and undergo an integrated test in the Cargo Interface Test equipment or CITE, before transportation to the OPF. This CITE test, under KSC control, is very extensive and requires a great deal of coordination between GSFC and KSC personnel. The CITE test emulates the Orbiter as closely as possible.

The PPF to O&C building move is performed using a security escort, due to the slow speed and flight hardware classification. Plus all security escort convoy operations can only be performed during non-peak traffic hours. This transport usually occurs 2 to 3 months before launch. Up to this point, GSFC has had the responsibility of the payload with KSC in the support role. After arrival at the O&C, the roles change and KSC is now responsible for the payload with GSFC in the support role. The GBA is removed from the KSC transporter and placed on the Highbay floor of the O&C building. The next operation at the O&C is a cleanliness check of the GBA before being installed into the Payload Canister. This is then followed by installation of the primary payload(s), Figure 8.

The Payload Canister is then moved to the OPF. Some missions require that the payloads be moved to the Vertical Processing Facility (VPF) to add more payload elements, for the launch, before the canister is moved to the launch pad for installation into the Orbiter. This will occur for the GBA on the STS-60 mission. Once at the OPF, all the payloads are installed into the Orbiter during one lifting operation, Figure 9 and Figure 10. This operation can take up to 16 hours with more than 200 persons involved. The electrical and mechanical connections are made between the payload and Orbiter and an Interface Verification Test (IVT) is performed on all payloads, with the primary payload(s) having priority. This is the last test performed on the GBA before launch. A sharp edge and cleanliness inspection of the GBA is performed by the Astronauts and Orbiter close-out operations are performed. If access to the payload is not planned on the launch pad, this will be the final inspection and last access of the GBA before launch. This can occur 1 to 2 months before launch. Again, this will be determined by the primary payload(s). All payload

access equipment is removed and the Orbiter payload bay doors (PLBD's) are closed. The Orbiter is then moved to the Vehicle Assembly building (VAB), Figure 11, for mating of the Orbiter to the External Tank (ET) and Solid Rocket Boosters (SRB's). Then the integrated Shuttle launch vehicle is moved to the launch pad. No GAS/CAP or Hitchhiker operations are performed in the VAB or during roll out to the pad.

If the PLBD's are opened at the launch pad, Figure 12, usually only a sharp edge and cleanliness inspection of the GAS/CAP payload(s) is performed. Hitchhiker payloads may require an extensive amount of servicing, testing and close-out operations. Access to the payloads in the payload bay must be completed 64 hours before launch (reference 2). This allows all the Orbiter operations to be completed before launch.

The Shuttle is launched, the mission takes place, and landing should occur at the Shuttle Landing Facility (SLF) at KSC. During this time, KSC is preparing for the payloads post-flight operations. If the Shuttle lands at Edward's Air Force Base (EAFB), it requires 5-7 days before the Shuttle returns to KSC. After arrival at KSC, no access to payloads is possible until 4-5 days after arrival, because of the time required to tow the Orbiter from the SLF to the OPF, jacking, leveling and deservicing of the Orbiter before the PLBD's are opened. Payload operations can then begin. All the payloads that span the width of the Orbiters payload bay are removed from the Orbiter in one lifting operation, Figure 13 and Figure 14, and installed into the payload canister, Figure 15. This occurs 5-7 days after the Orbiter arrives at KSC. The GAS/CAP and Hitchhiker payloads mounted to GAS beams are removed after the major payloads and installed into the experimenters GSE. From this point, post-flight GAS/CAP and Hitchhiker KSC operations are usually the reversal of pre-flight operations, except no CITE test is performed post-flight.

LESSONS LEARNED

A list of lessons learned, during ground processing, is generated after each Shuttle mission. Major lessons learned from all KSC operations that apply to GAS/CAP and Hitchhiker payloads are stated below:

1) COMPLETE THE SAFETY REVIEW PROCESS EARLY! The Flight safety review process is required for the on-orbit mission, but the Ground safety review process must be completed before any work can be performed at KSC. Most payloads should plan to complete the process 3-6 months before payload arrival. This allows time to satisfy concerns stated during the review process. Also, for GAS payloads, completing the safety review process early could be used to enhance the possibility of being selected as a back-up payload. Many GAS payloads have lost their chance to fly a scheduled mission because they did not complete the safety review in time. It should be noted that the KSC safety office considers GAS payload ground safety just as important as all other payloads. When it comes to safety, all payloads are treated the same. Please contact the GSFC safety office early!

2) Plan to have most of the preparation work on the experiment completed before arrival at KSC. The experiment should only require minimal checkout before integration into the GAS canister. Extensive work could be performed at KSC if required, but it is not desirable. It should be noted that a 12 hour/day work constraint is strictly imposed at KSC. Also use of any kind of chemicals is strictly controlled at KSC. Experimenters should plan to have all samples/chemicals installed on the experiment or contained in protective containers, with no planned work at KSC. Before payload arrival to the launch site, experimenters must provide the Launch Site Support Managers (LSSM), Process Waste Questionnaires (PWQ's) for "any" chemicals or materials brought to the launch site to support ground operations. Material Safety Data Sheets (MSDS) for these chemicals or materials must be maintained at their location of use. Contact GSFC representative for more details on these requirements

3) The experimenter should bring any required support or equipment with the experiment. KSC can supply almost any kind of support desired but the equipment may not be the same as used by the experimenter off-site and may not satisfy experimenters' requirements. If support from KSC is required, plan early! All experimenters need to coordinate through GSFC for any KSC support.

4) Experimenters should use long life batteries. If a launch slips, the experiments could sit for up to 5 months without access for battery changeout. Silver-Zinc batteries are recommended because they have been proven and flown inside may GAS cans. Nickel-Cadmium is not recommended because of their short life span.

FUTURE ACTIVITIES

The Autonomous Payload Controller (APC) is currently used to operate the GAS/CAP payloads. Future plans call for the use of the Payload Ground Support Computer (PGSC) to control operations. This will increase the time to perform pre-flight checkout due to use of this hardware.

Environmental requirements at KSC will become more strict in the future, so plans should be made to use the most benign chemicals possible if they are to be handled at KSC.

REFERENCES

1. Dean Zimmerman, "Get-Away Special Payloads Launch Site Support Plan", NASA K-PSM-11.3 Revision D, July 1991

2. System Description and Design Data-Ground Operations, NSTS 07700, Volume XIV, Appendix 5, Revision K.

3. Photographs, Bionetics Corporation, Kennedy Space Center, 1993

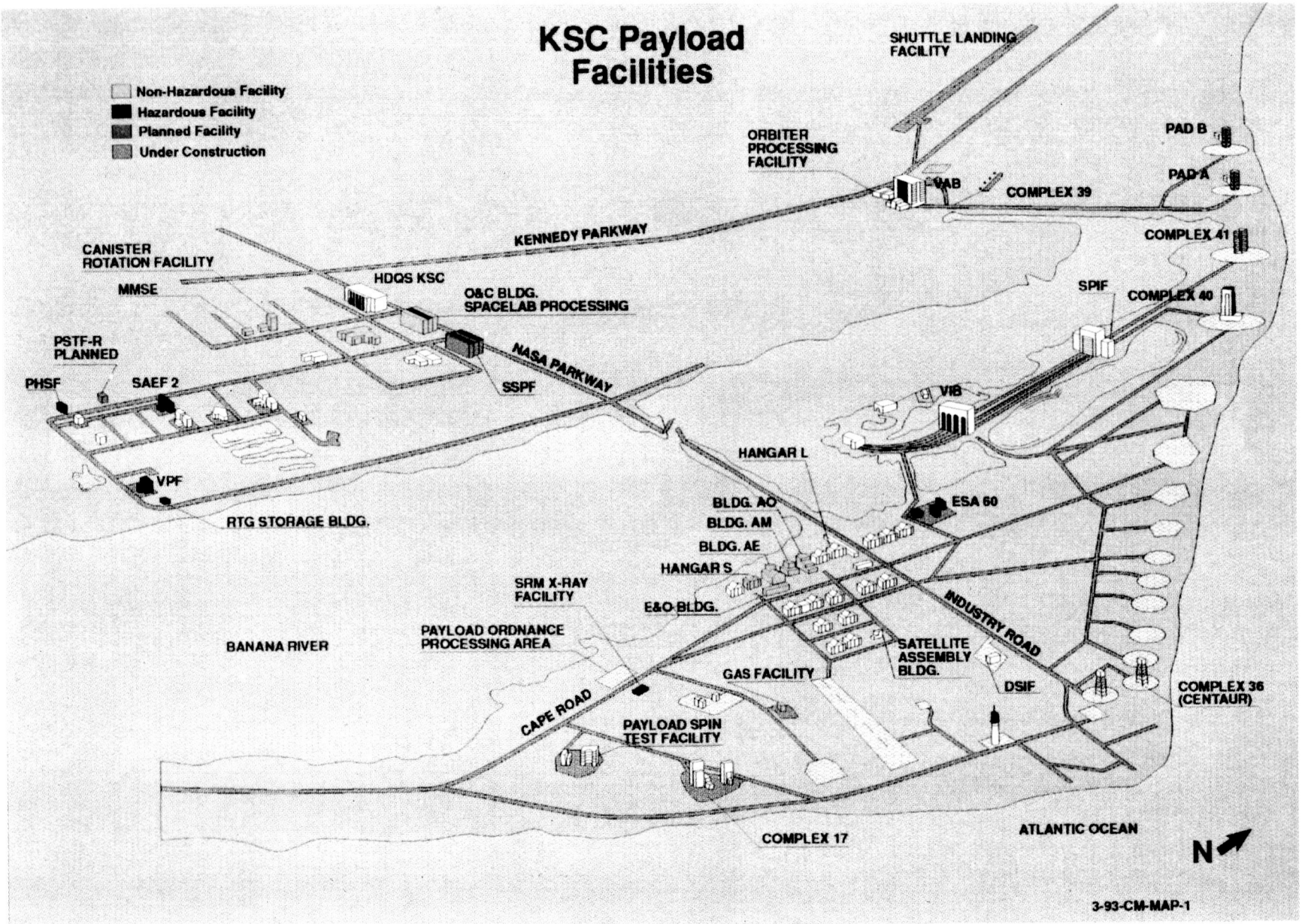

Figure 1 - Kennedy Space Center Facilities

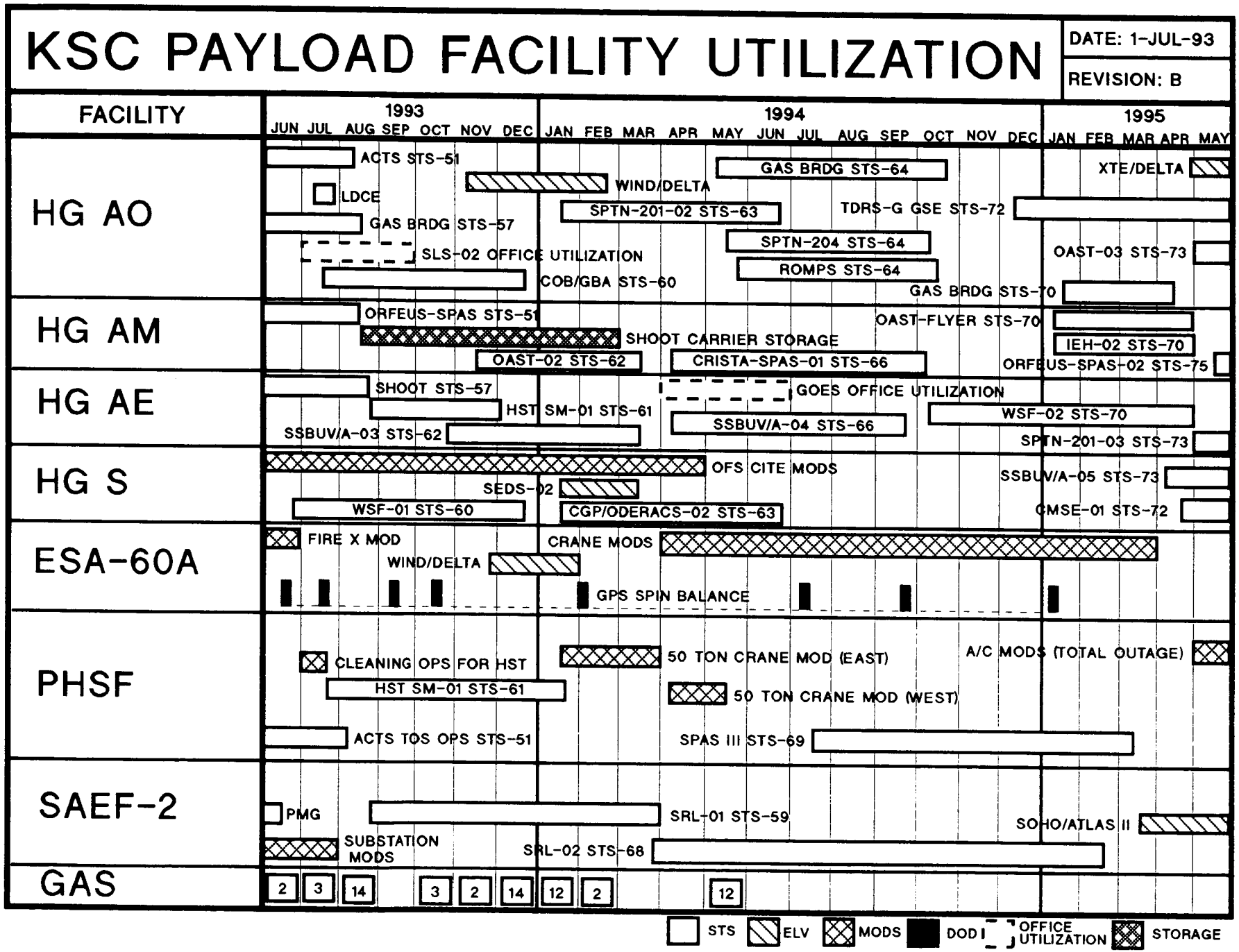

Figure 2 - KSC Payload Facility Utilization

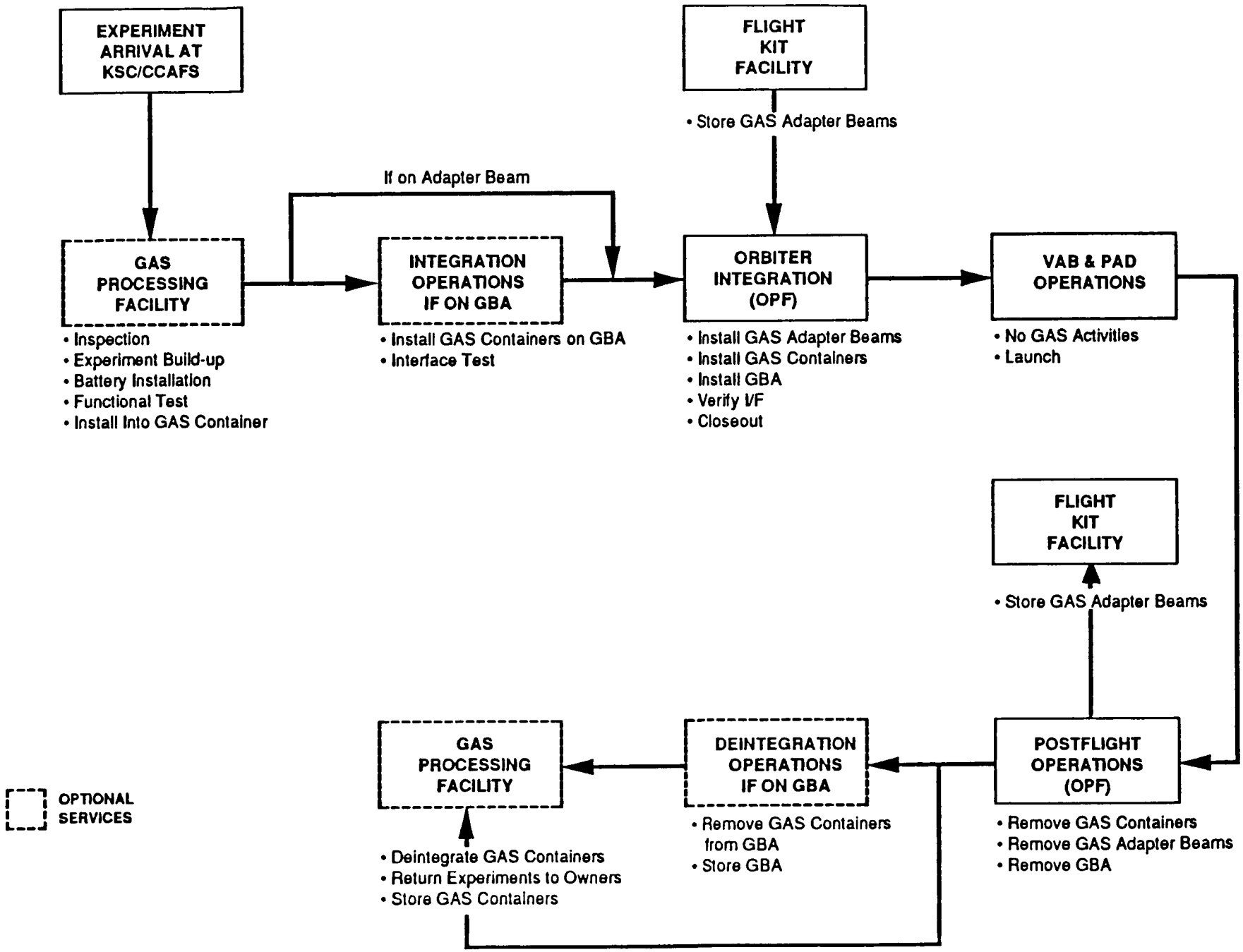

Figure 3 - Process Flow for Horizontally Installed GAS/GBA

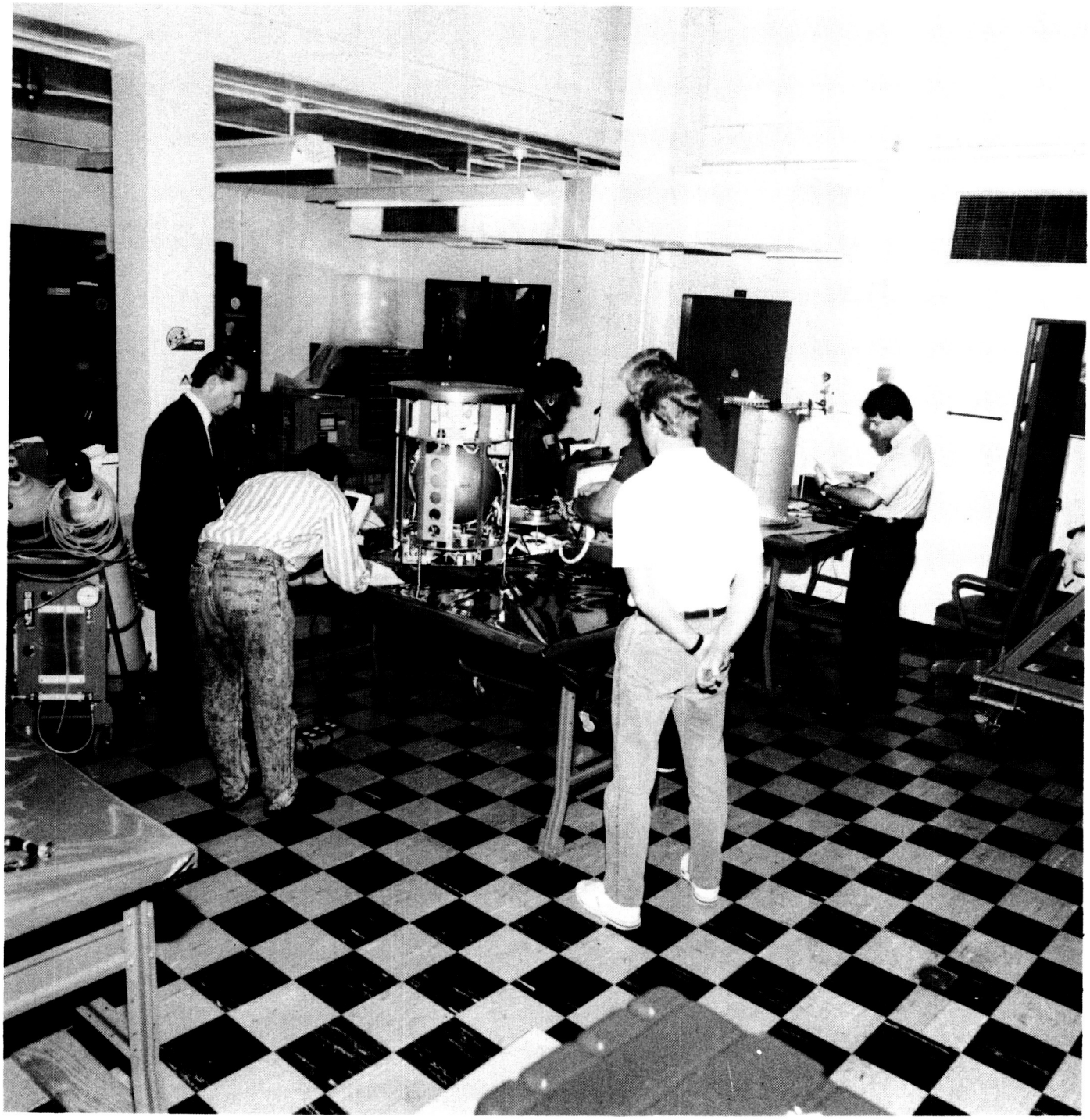

Figure 4 - STS-57 G-535, LERC Pool Boiling Experiment at GAS Facility

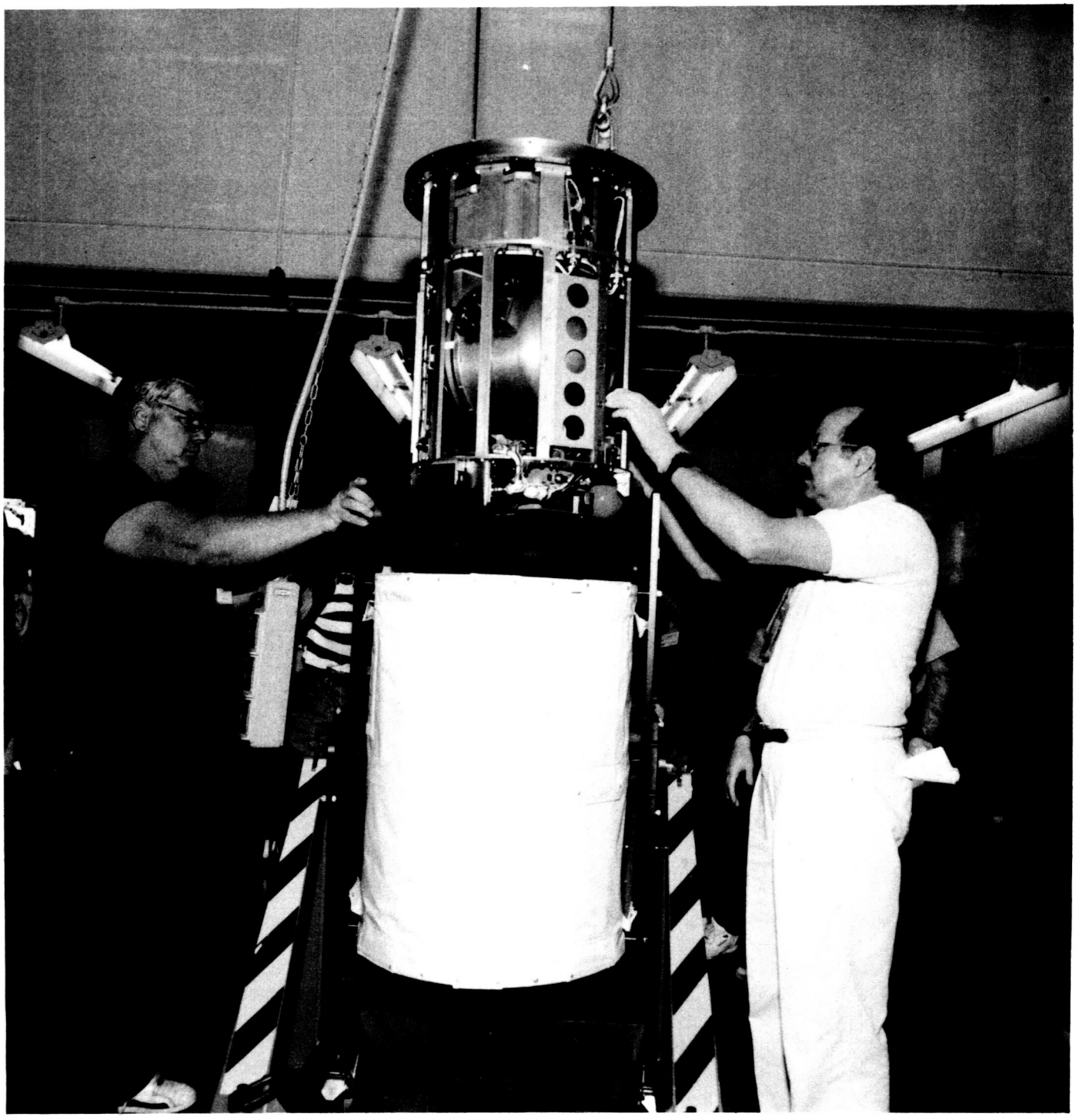

Figure 5 - STS-57, G-535 installation into GAS Canister at GAS Facility

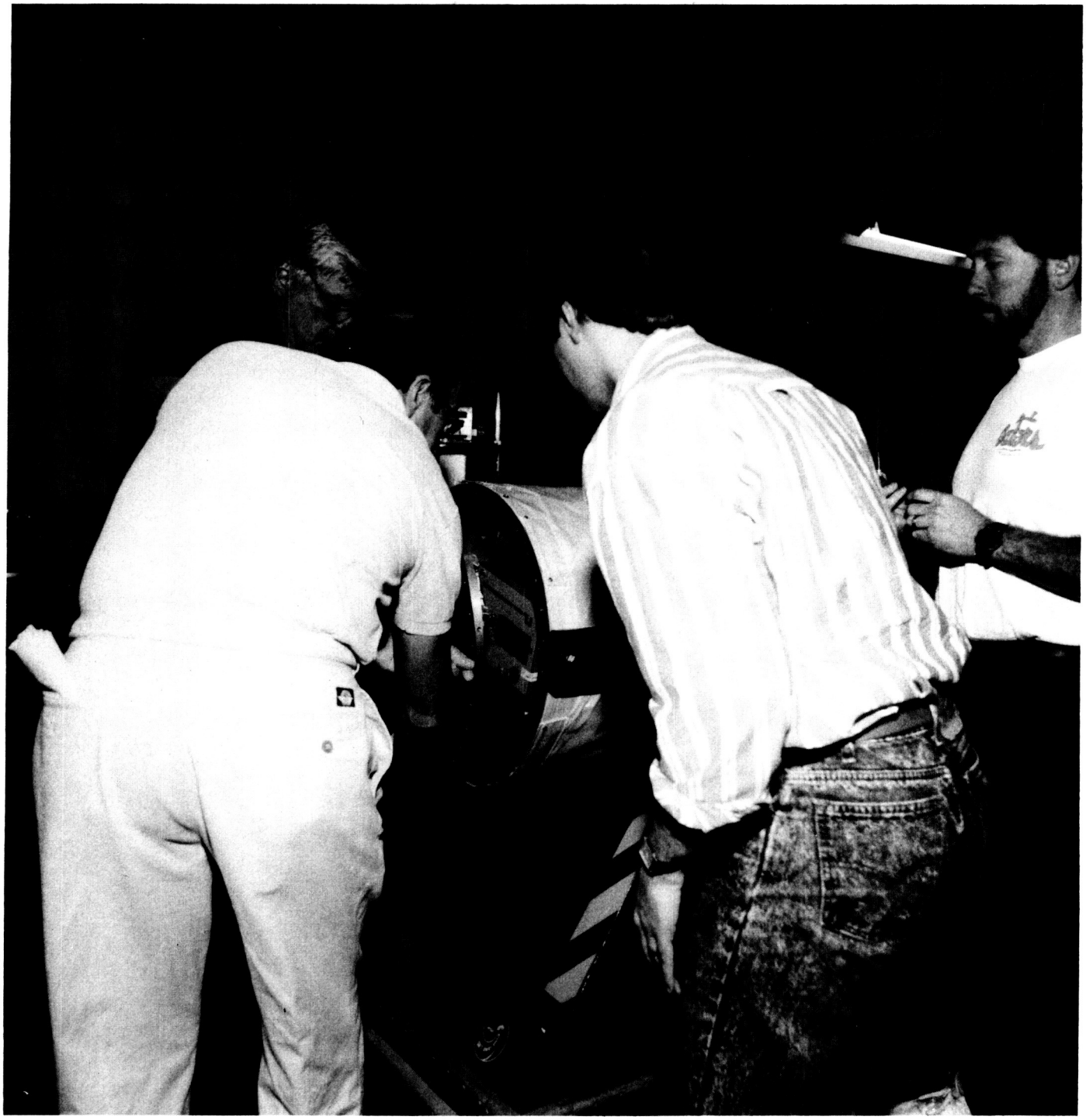

Figure 6 - STS-57, G-535 lower plate installation onto GAS Canister at the GAS Facility

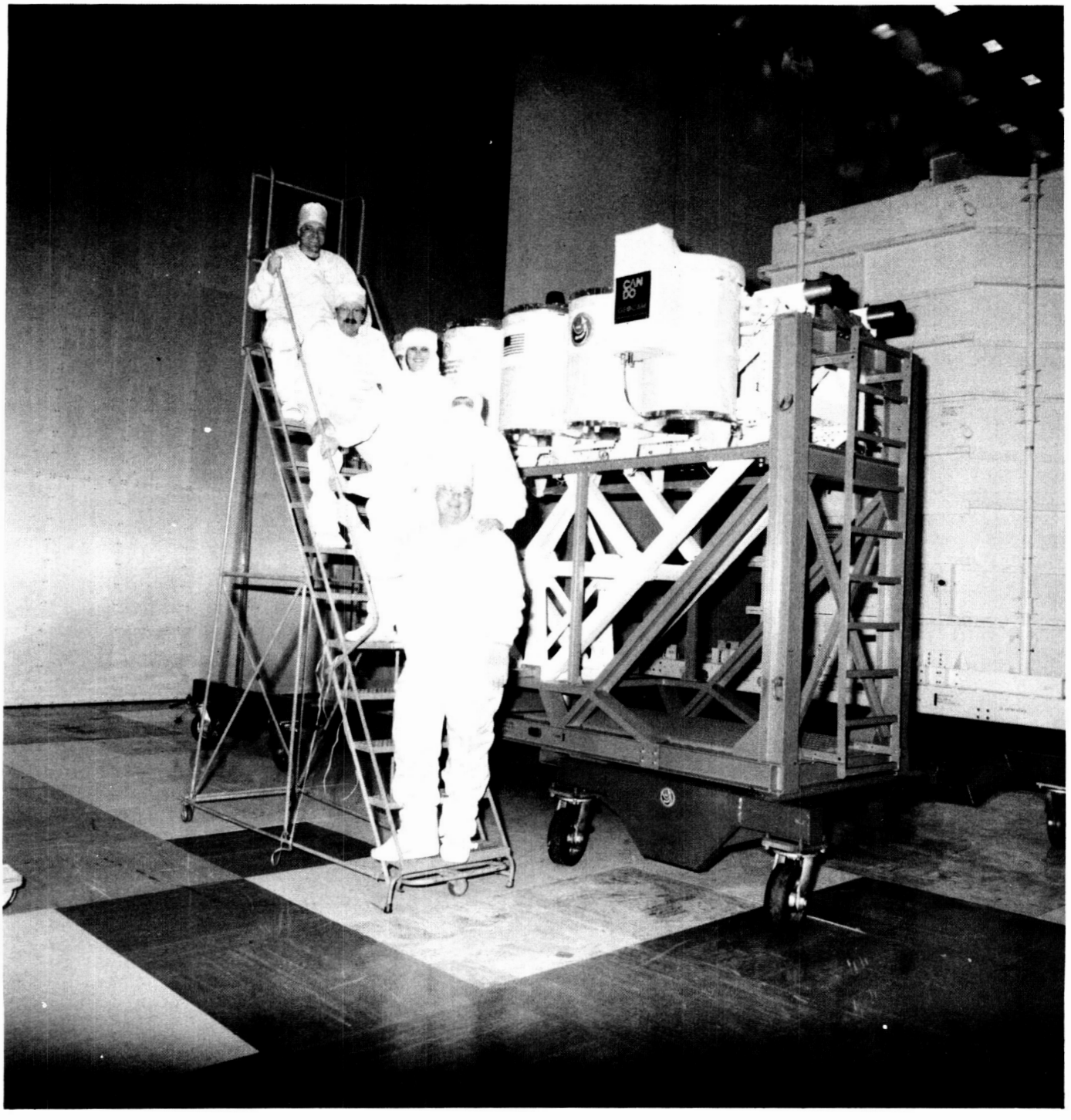

Figure 7 - STS-57 GBA Integration At Payload Processing Facility, Hanger AO

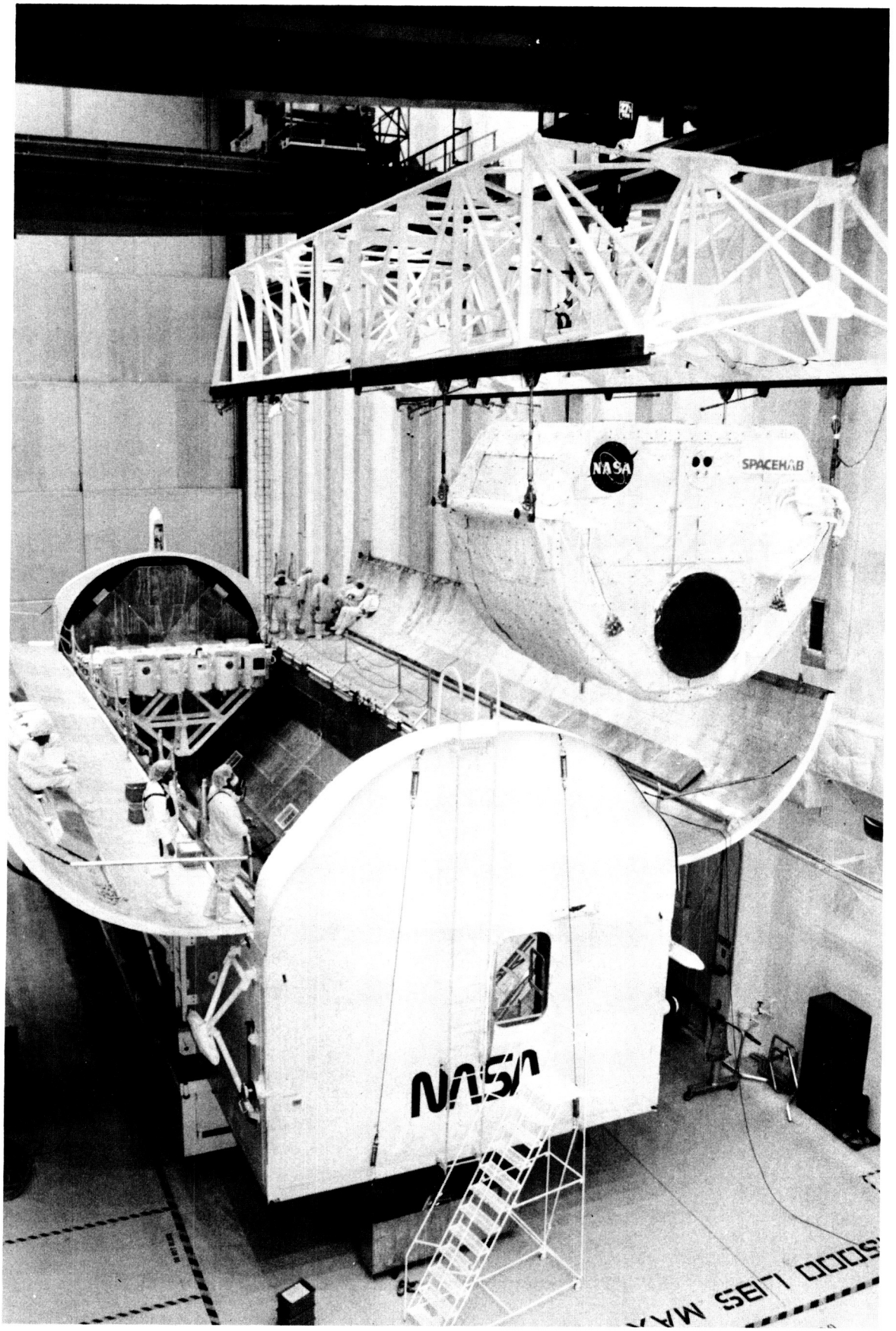

Figure 8 - STS-57 Spacehab-1 Installation into Payload Canister containing GAS Bridge Assembly

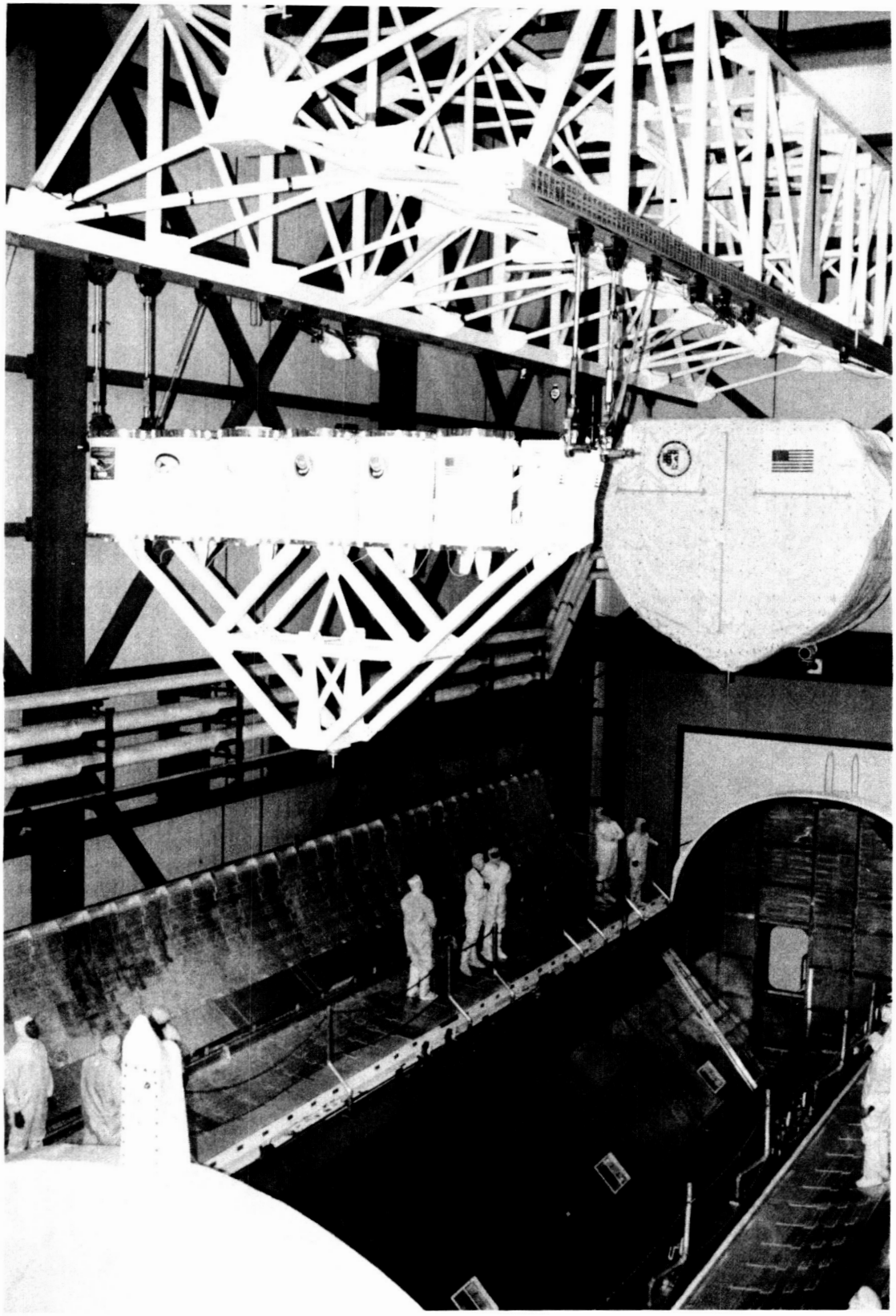

Figure 9 - STS-57 Payload Removal from Payload Canister for installation into Orbiter Endeavor, Orbiter Processing Facility

Figure 10 - Installation of STS-57 payloads into Orbiter Endeavor

Figure 11 - Rollover of STS-57 Endeavor from Orbiter Processing Facility to Vehicle Assembly Building

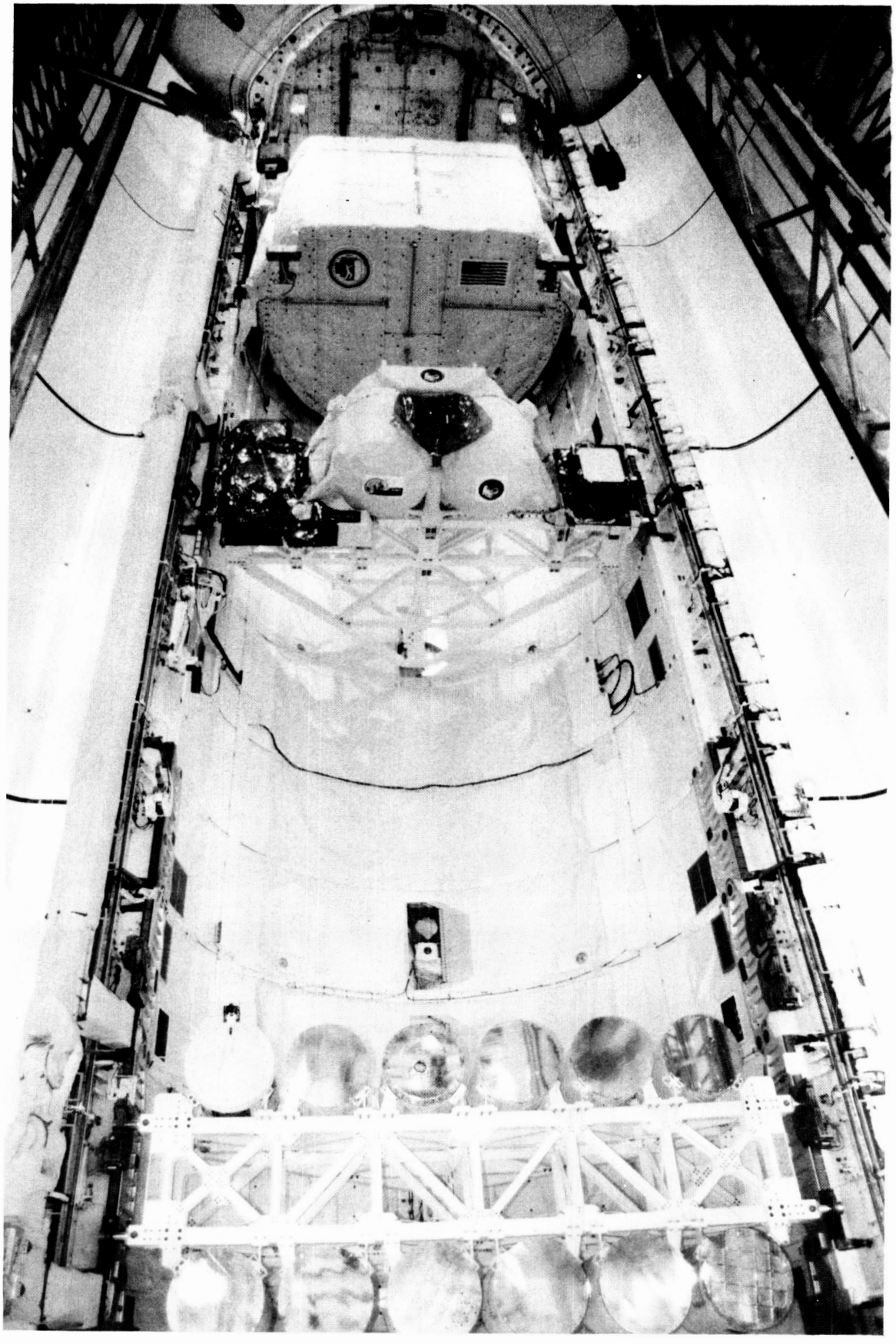

Figure 12 - STS-57 Payloads at Launch Pad 39B

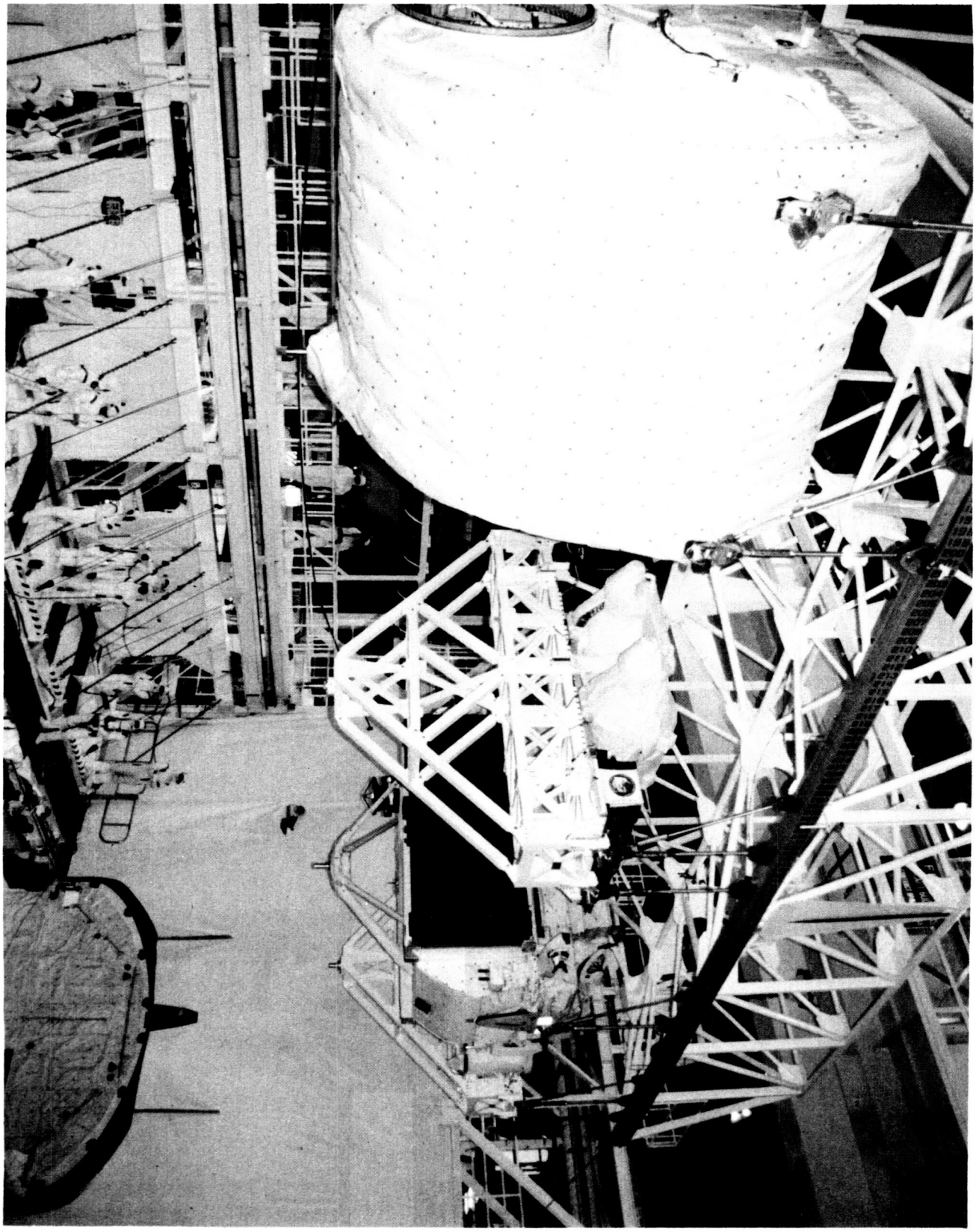

Figure 13 - STS-57 Payloads Removed from Endeavour at Orbiter Processing Facility, Post-Flight

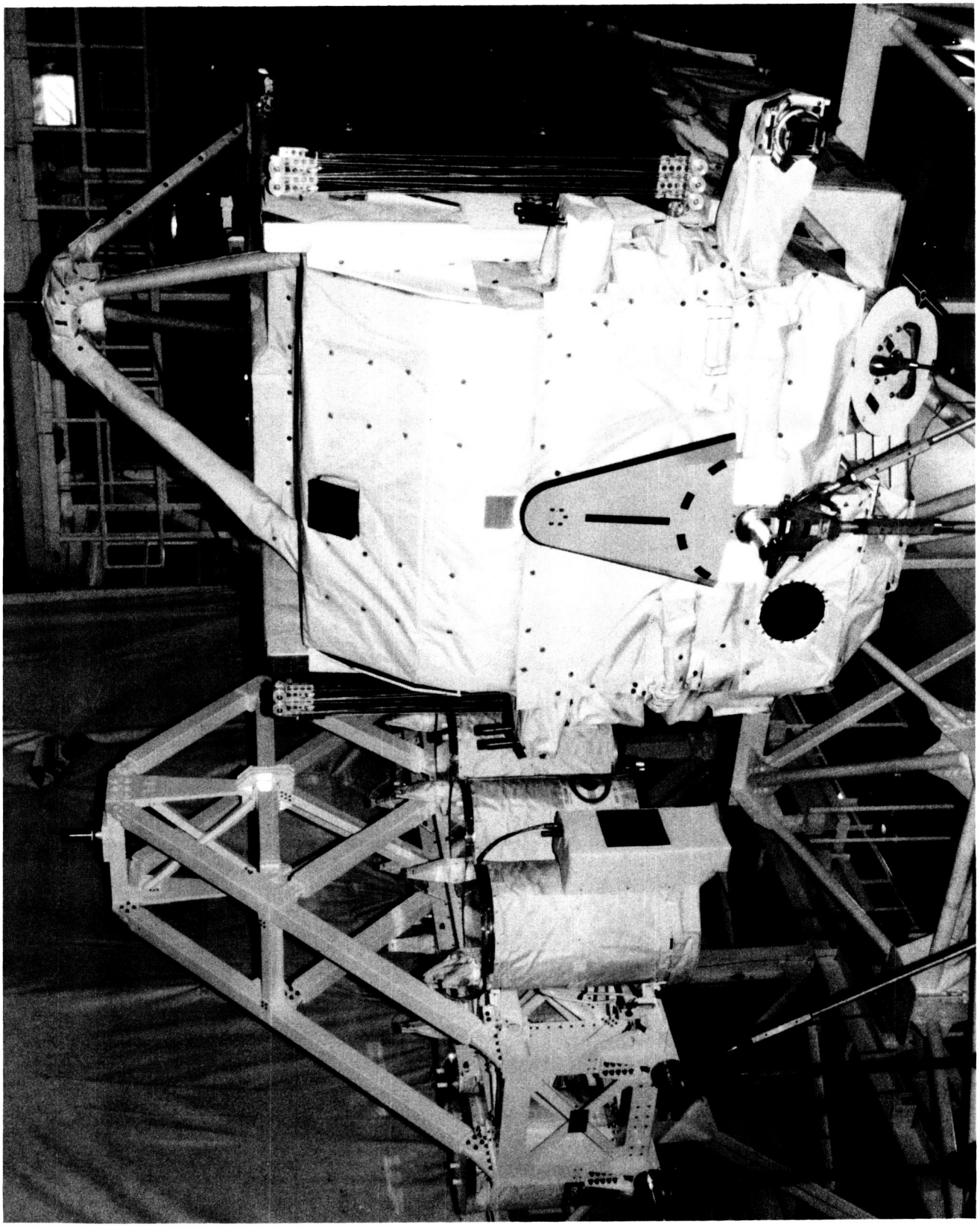

Figure 14 - STS-57 Payloads Removed from Endeavour, Close-up View of EURECA and GAS Bridge Assembly, at Orbiter Processing Facility, Post-Flight

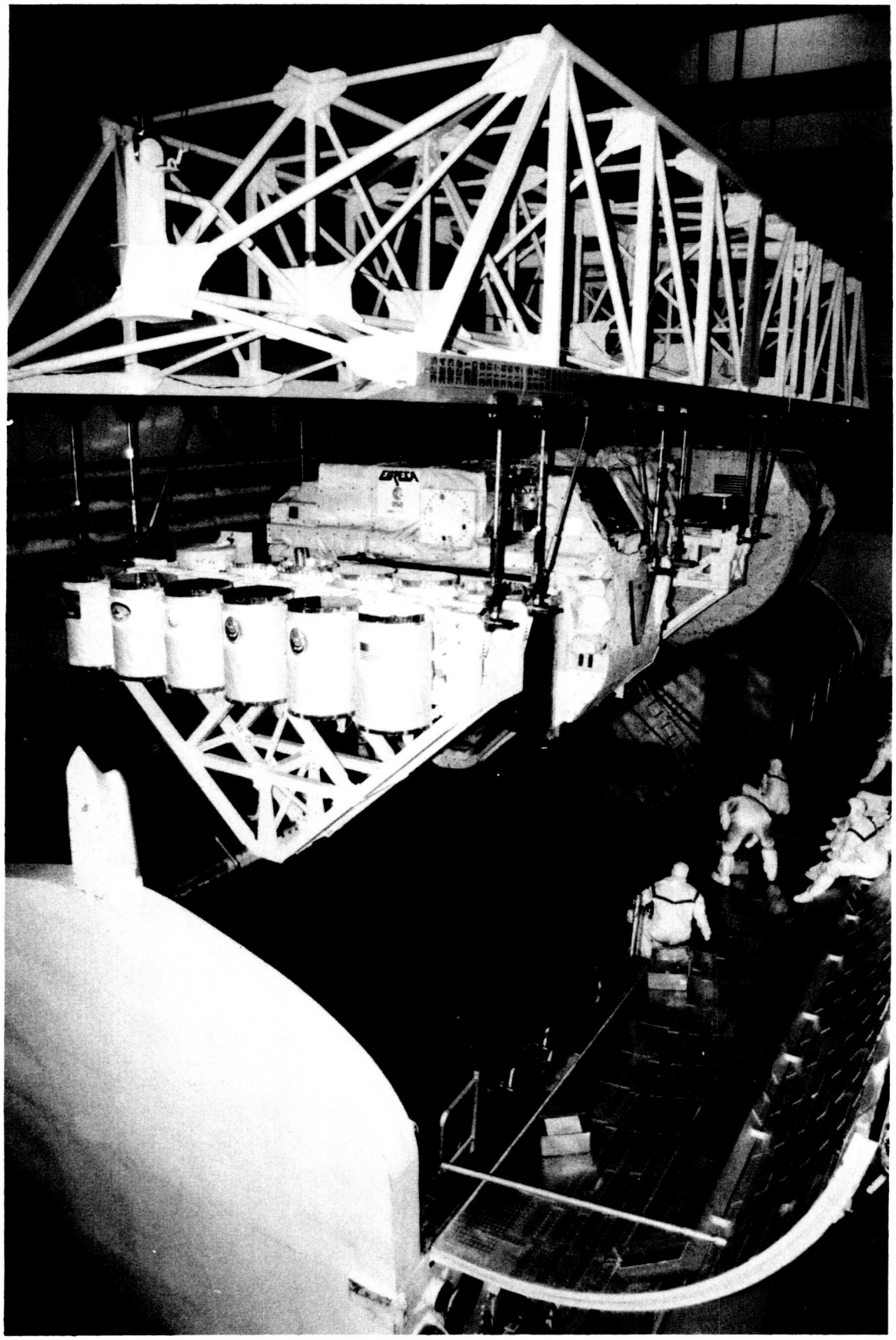

Figure 15 - STS-57 Payloads Installed into Payload Canister at Orbiter Processing Facility, Post-flight

UVSTAR, AN IMAGING SPECTROGRAPH WITH TELESCOPE FOR THE SHUTTLE HITCHHIKER-M PLATFORM

Roberto STALIO
Department of Astronomy, University of Trieste & Center for Advanced Research in Space Optics - Area Science Park, Padriciano 99, 34016 - Trieste

Bill R. SANDEL, A. Lyle BROADFOOT
Lunar and Planetary Laboratory, University of Arizona, Tucson, AZ 85721

ABSTRACT

UVSTAR is an EUV spectral imager intended as a facility instrument devoted to solar system and astronomy studies. It covers the wavelength range of 500 to 1250 Å, with sufficient spectral resolution to separate emission lines and to form spectrally resolved images of extended plasma sources. Targets include the Io plasma torus at Jupiter, hot stars, planetary nebulae and bright galaxies. *UVSTAR* consists of a pair of telescopes and concave grating spectrographs that cover the overlapping spectral ranges of 500 - 900 and 850 - 1250 Å. The telescopes use two 30 cm diameter off-axis paraboloids having focal length of 1.5 m. An image of the target is formed at the entrance slits of the two concave grating spectrographs. The gratings provide dispersion and re-image the slits at the detectors, intensified CCDs. The readout format of the detectors can be chosen by computer, and three slit widths are selectable to adapt the instrument to specific tasks. *UVSTAR* has internal gimbals which allow rotation of ±3° about each of two axes. Dedicated finding and tracking telescopes will acquire and track the target after rough pointing is achieved by orienting the Orbiter. Responsabilities for implementation and utilization of *UVSTAR* are shared by groups in Italy and the U.S. *UVSTAR* is scheduled for flight in early 1995, timed for an opportunity to observe the Jovian system.

INTRODUCTION

UVSTAR, UltraViolet Spectrograph Telescope for Astronomical Research, is a spectrographic telescope for observations of astronomical and planetary sources; it operates in the 500-1250 Å waveband at ≈ 1 Å resolution. The experiment has capability for long slit spectral imaging of extended cosmic sources such as planets, planetary nebulae, supernova remnants, H II regions, and external galaxies. *UVSTAR* will fly as a Hitchhiker-M payload on the Shuttle (Figure 1). The experiment complement includes an independent companion instrument that will be provided by Darrell Judge (University of Southern California) to measure the absolute solar flux in selected extreme ultraviolet bands. The two experiments form the IEH (International EUV/FUV Hitchhiker) mission.

UVSTAR consists of a movable platform and an optical system. The platform will provide fine pointing (±5 arcsec) within ±3° from the nominal view direction, which

is near the Shuttle +Y axis, i.e. perpendicular to the long axis of the Shuttle and in the plane of the wings. The optical system consists of a set of two telescopes and Rowland concave-grating spectrographs with intensified CCD detectors. The first spectrographic telescope (FUV) operates in the 850-1250 Å spectral range; the second (EUV) covers the 500-900 Å region. A number of pointed observations will be made of calibration targets, planets, ultraviolet stellar sources and extended objects. At any time the *UVSTAR* is pointed toward the hemisphere outward from the Earth and the Shuttle is on celestial lock, it is possible that a source of interest for UV astronomy will be within the pointing range. In this case, *UVSTAR* will operate in a ''serendipitous/target-of-opportunity'' mode; in this mode targets that will have been defined in advance will be acquired and observed.

UVSTAR has two nearly identical spectrograph channels (EUV and FUV) that will observe simultaneously the same target. Each channel consists of a telescope mirror, and a concave grating spectrograph with its own intensified CCD detector. The telescopes form images of the target at the entrance slit of the spectrographs. The concave gratings of the spectrographs both disperse and re-image the light from the target onto the 2-D detectors. Spatial resolution along the slit is preserved, so that in the cross-dispersion direction the detectors records many spectra corresponding to different part of the source simultaneously. The optical design is driven by the facts that at the EUV wavelengths of interest

- only reflective optics can be used,
- reflectivities are poor, which requires minimizing the number of reflections if weak sources are to be detected in a short period of time.

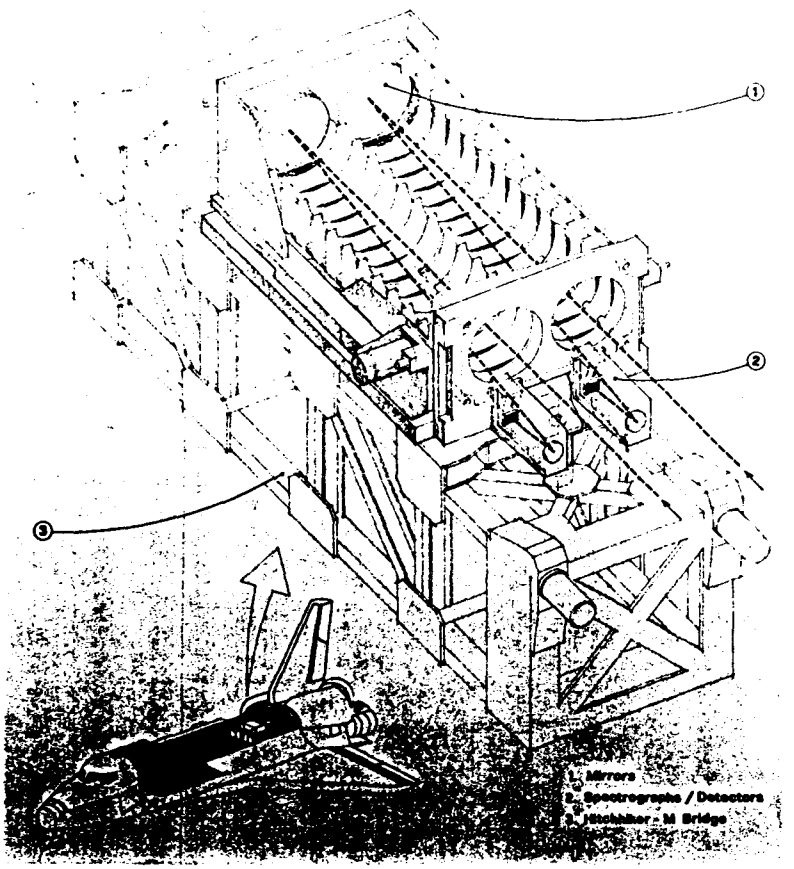

Figure 1: Sketch of the opto-mechnical configuration of *UVSTAR*

TELESCOPES

The telescope mirrors are off-axis paraboloids of 30 cm diameter and 1.5 m focal length. They are SiC coated for maximum reflectivity; are made by Zerodur to prevent defocussing due to thermal changes; are joined to the spectrographs by rods of a carbon composite material of about zero thermal expansion coefficient along its length.

SPECTROGRAPHS

Each spectrograph employs a single concave, holographic grating to disperse the radiation and focus it on the detector. Holographic ruled gratings can achieve aberration correction and a flat focal plane over a length of 8 mm in the cross-dispersion, and 15.4 mm in the dispersion directions. The 70 × 100 mm gratings have a radius of curvature of 275 mm. To maintain good focus over a range of temperatures, the gratings will be fabricated on Zerodur blanks. The grating cell is mounted to permit small motions relative to the spectrograph housing. The position of the grating relative to the entrance slit and detector is established by invar rods that extend from the grating cell to fixed positions near the entrance slit and detector.

The two spectrographs cover overlapping spectral ranges, 500-900 Å and 850-1250 Å. In each case the spectrum of about 400 Å is dispersed along 1152 pixels, giving a dispersion of ≈ 0.35 Å per pixel. The array is 298 pixels wide. In the image mode the spectral/spatial images are comprised of 2 ×1152 × 298 pixels, that is, nearly 7×10^5 pixels or 1.4×10^6 bytes if each pixel is digitized to 16-bit accuracy. The read out format is controlled by computer so that it can be matched to the needs of a particular experiment.

SLIT SELECTOR

Each of the spectrographs is equipped with a mechanism for selecting among three entrance slits. All slits have the same length of 0.25° but differ in width. The slits widths and their uses are:

- Narrow slit (3 pixels, 9 arcsec). This slit will provide about 1 Å resolution and will also have spatial resolution it.
- Medium slit (13 pixels, 39 arcsec). This slit will give global images of extended sources (planetary nebulae, SN remnants, Jupiter's disk) at the wavelengths of most intense emissions. Resolution is 4.5 Å.
- Wide slit (33 pixels, 100 arcsec). This aperture will allow the whole image of the Io plasma torus to be dispersed into its major emissions and re-imaged with a resolution of 12 Å.

DETECTORS

The intensified CCD (ICCD) detectors consist of standard proximity-focused image intensifier tubes that are fiber-optically coupled to CCDs. They have successfully flown in previous missions. Both image intensifiers are windowless. Charge from photoevents is amplified by the microchannel plate and electrostatically accelerated

to a phosphor screen on a fiberoptic window. The visible-wavelength image from the phosphor is transferred to the CCD by fiber optics for readout. A special position of the slit changing mechanisms seals the spectrograph enclosures to protect the detectors and gratings from contamination. Each spectrograph is equipped with a small ion pump to assure a satisfactory vacuum environment for operating the windowless intensifiers on orbit.

SENSITIVITY

The ICCD detectors of *UVSTAR* are 2-D detectors with photon-counting capability. Thus the overall instrument performance is related to the rate at which photoevents are generated at the photocathode of the detector. For the imaging spectrographs, Table I gives the sensitivity for two kinds of source, namely a point source of continuum emission, and an extended source of monochromatic emission. The wavelengths are in Å, the area of the telescope mirror (A) is in cm^2, Ω is the solid angle, measured in sr, corresponding to the field of view of a single pixel, δ (Å/pixel) is the spectral dispersion, σ is the reflective-dispersive efficiency of the grating, ε the quantum efficiency of the photocathode, μ the reflective efficiency of the telescope, R is the response for a point source in units counts/pixel/s per photon/cm^2/s/Å, S is the response for monochromatic emission of brightness I Rayleighs; the units are counts/pixel/s per Rayleigh.

GUIDING & OTHER CHARACTERISTICS

UVSTAR includes capabilities for independent target acquisition and tracking. The spectrograph package has internal gimbals that allow angular movement of ±3° from the central position. Rotations about the azimuth axis (parallel to the Shuttle Z axis) and elevation axis (parallel to the Shuttle X axis) will actively position the field of view to center the target of interest in the fields of the spectrographs.

Two dedicated visible imagers (Finder and Tracker) having different fields of view, and a quadrature diode, provide guiding information.The Finder has 60 mm focal length and f/1.4 optics giving a field of view of 6° × 8°. The system, fully planned and constructed at CARSO, works in two modes:

Finder mode:
From a coarse knowledge of the pointing direction (± 3°), the system recognizes autonomously the acquired stellar field and point to the chosen direction within ± 5''.

Tracker mode:
After having reached the wanted direction, it operates with three different techniques:

1) same as the finder mode: at every acquisition, the system repeats the star field identification routine. In this mode the algorithm requires, on the average, a processing time of 300 ms (on a 386/387 at 25 MHz).
2) Triangulation mode: the system chooses three stars out of the stars selected in the finder mode and by means of a triangulation procedure, calculates the position of the center of the sensor which concides with the chosen pointing direction. In this case the algorithm needs a few ms of processing time.
3) Star pointing mode: the target star is at the center of the sensor. We correct its position at every acquisition keeping it at the center. The algorithm takes only few ms of processing time.

As an alternative to the above mentioned routines we have developed another procedure (planet mode) which doesn't use any identification procedure, but simply searches for the brightest object in the FoV, brings it at the sensor center and tracks it with the algorithm 3.

The Tracker is a 75 mm diameter cassegrain telescope with a focal length of 1.5 m and a field of view of 0.24° × 0.32°. Finder and Tracker have their own ICCD detector, 384 × 288 pixel arrays. The tracker ICCD will have the same plate scale as the spectrograph. In addition the tracker telescope will also be equipped with an intensified quadrature diode which will track a 8-9 magnitude star with negligible processing time. The diameter of the photodiode is 3 mm and the star image will be 1 mm. The tracking accuracy will be better than ±5''.

SCIENCE PROGRAM

1 ASTRONOMY

The ''pointed'' observations from *UVSTAR* will be of 25±5 astronomical sources per flight. A similar number of pointed observations will be available to the planetary physics program. At the end of the program we will have observed 100 to 150 astronomy sources. About 40% of them will be 1) calibration, 2) EUV, and 3) extended sources.

Predicted sensitivity curves for point sources and examples of source observability are displayed in Figures 2, 3 and 4. The sensitivity curves are presented under the form of fluxes which can be observed in 25 minutes with S/N = 6 in the two channels, EUV and FUV. Two observing modes, full resolution and reduced resolution (about 6 Å, IUE-like), are considered. In Figure 2 are also displayed the energy distribution of two important UV sources: HZ 43, a nearby subdwarf, which is among the few stars observable in the 500 - 912 Å band and the bright quasar 3C273. Both are well observable from *UVSTAR*, even if, at the shorter FUV wavelengths, the signal to noise ratio of 3C273 will be slightly less than 6 using the "standard" exposure time of 25 minutes. Figure 3 gives compares the FUV sensitivity curves with energy fluxes of two representative cataclysmic variables; Figure 4 does the same for two important Seyfert galaxies. In this last case both continuum fluxes and line fluxes are reported.

The effects of interstellar extinction on exposure times are presented in Figure 5 for full resolution spectra. With the IUE-like resolution one gain a little bit less than 2 magnitudes. The effects also include the absorption for molecular hydrogen. The FUV interstellar reddening curve and the H_2 absorption have been discussed in a previous study of low resolution data from the Voyager UV Spectrometers (ref. 1).

The EUV program will be fundamentally different from that at longer wavelengths because of the opacity of neutral hydrogen in the interstellar medium. In general we will be able to observe only within a few tens of parsecs from the Sun; however, in those directions where the ISM has low density, we will go farther and possibly observe some stars. In general only a few hot white dwarfs are listed as candidates. However, the recent results by ROSAT and EUVE indicate that a substantial number of sources would be observable. As an example, among the EUV sources detected by ROSAT WFC (at 100 and 137 A) in a 60 x 60 degree field centered at $\alpha = 14^h$ and $\delta = 10°$ are the low X-ray binaries Sco X-1 and Her X-1, the FUV source Spica (B1V star), 3C273 (

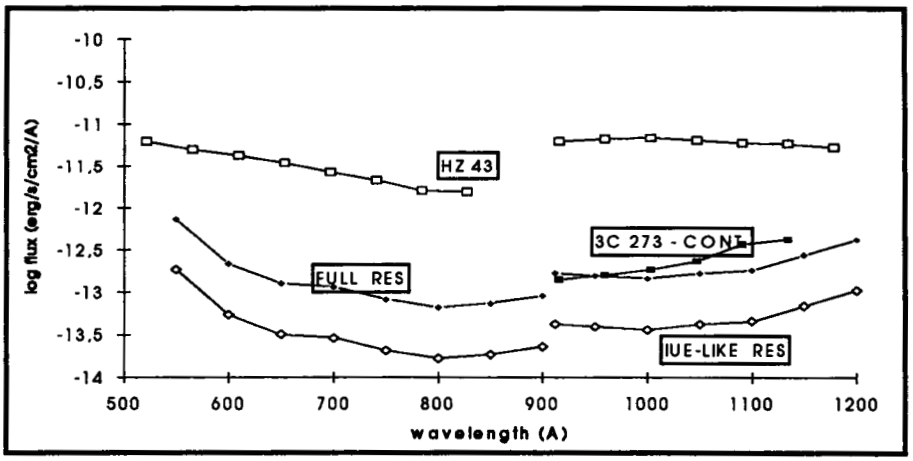

Figure 2: Sensitivity curves for point sources and EUV/FUV fluxes of HZ43 and 3C273

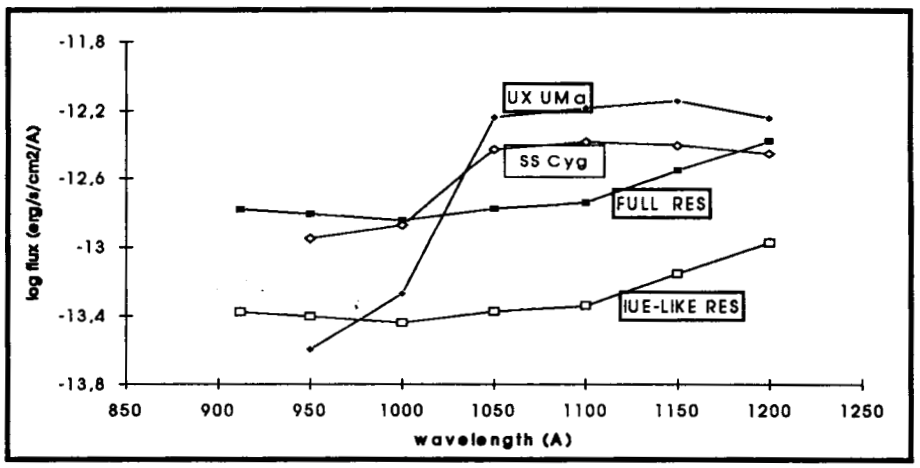

Figure 3: Same as Figure 2 for cataclysmic variables.

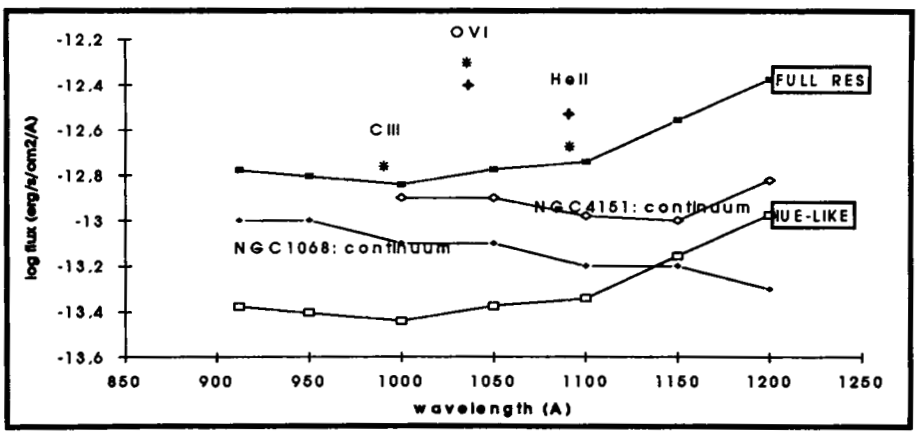

Figure 4: Same as Figure 2 for the Seyfert galaxies NGC 1068 and NGC4151. The symbol ✚ refers to line intensities of NGC 4151; the symbol ✱ to NGC 1068

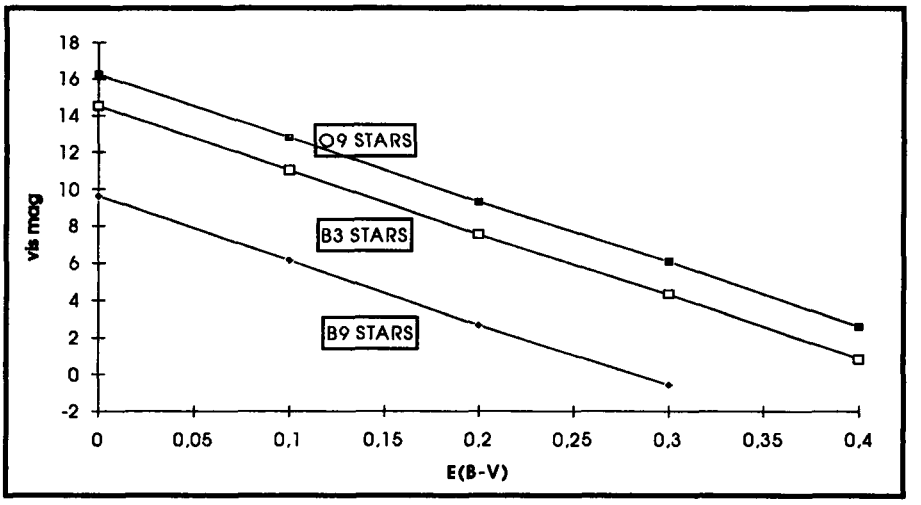

Figure 5: The diagram shows the limiting magnitude reachable for a S/N = 6 at full resolution in 25 minutes for different spectral types and different E(B-V). The effect of molecular hydrogen absorption is also included

(quasar), NGC 4152 and MRK 478 (Seyfert galaxies) and the EUV source HZ43. ROSAT list includes many other sources in the same general area: spiral galaxies, white dwarfs and late type stars. EUVE has recently observed intense EUV emission from the B2 II star ε CMa in the 500-740 Å and 345-605 Å bands (Ref. 2).

2 PLANETARY PHYSICS

Io's plasma torus is a natural laboratory for investigations of plasma physics. It is our best-studied example of an astrophysical plasma, having been probed by both in-situ and remote sensing techniques. The full implication of early measurements revealing neutral sodium and ionized sulfur near Io's orbit was not realized until the discovery, by the *Voyager UVS*, of an intense hot plasma ($T_e \approx 10^5$ K), forming a complete toroidal cloud about Jupiter, near Io's orbit. As a consequence of the high electron temperature, the dominant emissions from S II, S III, S IV, and O II are in the EUV and FUV spectral regions, the brightest feature being near 685 Å. About 2×10^{12} W is radiated in the EUV; this is the dominant mechanism for energy loss from the torus. Although ground-based studies of the visual wavelength torus emissions have added to our knowledge of this plasma, measurements in the EUV are a more direct method of studying processes in the torus. To date, studies of the plasma torus have demonstrated that measurement in the EUV spectral region is essential, full spectral coverage in this region is required, and morphological studies, i.e. imaging of the whole system are necessary.

UVSTAR will complement and extend observations of Jupiter and Io's plasma torus made by the *Galileo* spacecraft orbiting around Jupiter. *Galileo*'s orbital geometry limits its opportunities for viewing the plasma torus with the UV instruments, and especially with the EUV spectrograph, which is most diagnostic of torus conditions. *UVSTAR* will provide observations of the Jupiter system at improved spectral resolution. The imaging spectrographs will measure the intensity of several important emission lines of S II, S III, S IV, and O II as a function of position in the torus, measure the H_2 band emissions of Jupiter'sdayglow and aurora, and clarify the coupling of Jupiter's aurora and the torus. The H Ly-α dayglow intensity will be

correlated with the absolute solar flux measurements taken with the companion instrument of the University of Southern California. Spectral dispersion with simultaneous imaging makes the most efficient use of observing time and photon collecting ability. No photons within the bandpass of the instrument are wasted. These capabilities open the way for a far more thorough investigation of torus EUV morphology and dynamics than is possible with other existing or planned instrumentation.

The spectrographs, when operating in the wide-slit configuration, form two-dimensional images of a target within the slit. Images at different emission lines are displaced in the dispersion direction. The spectral dispersion is great enough to separate monchromatic images of the torus in several wavelengths. Several of these will be strong enough to be analyzed as a snapshot of emission morphology. The spatial resolution over the disk of the planet will separate polar and equatorial emissions of H and H_2.

REFERENCES

1. R. Longo, R. Stalio, R.S. Polidan, and L. Rossi, *"Intrinsic UV Spectral Energy Distributions of OB Stars"*, Astrophysical J. 339 (1989) 474-80.

2. J.V. Vallerga, P.W. Vedder, and B.Y. Welsh, *"Intrinsic EUV Emission from the B Star ε CMa"*, Center for EUV Astrophysics (1993), Preprint No. 532.

TABLE I: SENSITIVITY CALCULATIONS

λ	A	Ω	δ	σ	ε	μ	R	S
600	700	2.10^{-10}	.35	.11	.4	.35	3.7	.000017
1000	700	2.10^{-10}	.35	.15	.2	.45	3.3	.000015

THE STAR IDENTIFICATION, POINTING AND TRACKING SYSTEM OF UVSTAR, AN ATTACHED PAYLOAD INSTRUMENT FOR THE SHUTTLE HITCHHIKER–M PLATFORM

Francesco De Carlo, Roberto Stalio, Paolo Trampus
Center for Advanced Research in Space Optics
Area di Ricerca, Padriciano 99, 34012 Trieste, Italy

A. Lyle Broadfoot, Bill R. Sandel
Lunar and Planetary Laboratory, University of Arizona
901 Gould Simpson Building, Tucson AZ 85721

Giovanni Sicuranza
Dipartimento di Elettronica, Elettrotecnica ed Informatica
Università di Trieste, via A. Valerio 10, 34100 Trieste, Italy

ABSTRACT

In this paper we describe an algorithm for star identification and pointing/tracking of a spaceborne electro–optical system and simulation analyses to test the algorithm. The algorithm will be implemented in the guiding system of *UVSTAR*, a spectrographic telescope for observations of astronomical and planetary sources operating in the 500–1250 Å waveband at ≈ 1 Å resolution. The experiment is an attached payload and will fly as a Hitchhiker–M payload on the Shuttle. *UVSTAR* includes capabilities for independent target acquisition and tracking. The spectrograph package has internal gimbals that allow angular movement of $\pm 3°$ from the central position. Rotation about the azimuth axis (parallel to the Shuttle z axis) and elevation axis (parallel to the Shuttle x axis) will actively position the field of view to center the target of interest in the fields of the spectrographs. The algorithm is based on an on–board catalog of stars. To identify star fields, the algorithm compares the positions of stars recorded by the guiding imager to positions computed from the on–board catalog. When the field has been identified, its position within the guiding imager field of view can be used to compute the pointing corrections necessary to point to a target of interest. In tracking mode, the software uses the past history to predict the quasi–periodic attitude control motions of the shuttle and sends pointing commands to cancel the motion and stabilize *UVSTAR* on the target. The guiding imager (guider) will have an 80–mm focal length and f/1.4 optics giving a field of view of $6° \times 4.5°$ using a 385 x 288 pixel intensified CCD. It will be capable of **1)** providing high accuracy (better than 2 arc–sec) attitude determination from coarse ($6° \times 4.5°$) initial knowledge of the pointing direction and **2)** of pointing toward the target. It will also be capable of tracking at the same high accuracy with a processing time of less than a few hundredths of a second.

INTRODUCTION

The determination of the orientation of a satellite or an "attached payload" relative to an inertial reference system, and the correlated functions of acquiring and tracking a target are essential tools for controlling the line of sight of flying electro–optical systems. Among the techniques used for line of sight orientation, automatic identification of stellar fields recorded by one or more dedicated CCD imagers has important applications for delivering space assets to desired locations and/or for pointing spaceborne instruments towards objects of interest. Star field image stabilization with frequent updating of the orientation, using also predictive algorithms, is an additional important function of a modern electro–optical guidance and navigation system. In this paper we describe an algorithm for star identification (Ref. 1, 2) and pointing/tracking of a spaceborne electro–optical system and simulation analyses to test the algorithm. The algorithm will be implemented in the guiding system of *UVSTAR* (Ref. 3). The algorithm is based on an on–board catalog of stars (Ref. 4). To identify star fields, the algorithm compares the positions of stars recorded by the guider to positions computed from the on–board catalog. When the field has been identified, its position within the guider field can be used to compute the pointing corrections necessary to point to a target of interest. In tracking mode, the software uses the past history to predict the quasi–periodic attitude control motions of the shuttle and sends pointing commands to cancel the motion and stabilize *UVSTAR* on the target.

In the next sections we discuss the access to the on–board catalog, the algorithms for automatic star identification and for determining and updating the orientation of the guider, the simulations made and the results obtained in determining the direction of the optic axis of the guider (z axis) under various initial and operating conditions for a system mounted on the Shuttle.

ON – BOARD CATALOG

The on–board catalog used is a subset of the 1991 version of the Smithsonian Astrophysical Observatory (SAO) catalog (1950) (Ref. 4). Only stars with magnitude brighter than 7 are considered. Twenty bytes are reserved to record the parameters of each star: double precision right ascension and declination coordinates and floating point magnitudes. The catalog contains 15935 stars for a total of 318700 bytes.

An access routine to the catalog provides the parameters for the stars contained in a sky zone centered along a given direction. In order to have fast access to any star field, the celestial sphere has been subdivided into 8 "zones" similar to geographic latitude bands. Each zone has been subdivided into "sectors" of equal areas.

Stellar parameters at the beginning and end of each sector are recorded in a table index. The table index is used to quickly select the sector pertaining to the initial direction. Stars of several nearby sectors are also taken into account in order to ensure covering the whole field of view. This accounts for the estimated inaccuracy in the initial estimate of the direction of the guider z axis and for possible guider shifts that may occur during operations.

The simulation of the guider image is generated from the catalogue by projection on the tangent plane. As the polar zones represent a singularity, we treat them independently by means of a reduced catalog. It contains stars north and south of latitudes +45° and -45° respectively. In this catalog the reference celestial coordinates are rotated by 90° around the axis perpendicular to the plane of the celestial pole and vernal equinox axes.

STAR IDENTIFICATION AND ORIENTATION ALGORITHMS

In order to parameterize the rotation of the orthogonal cartesian axes fixed with the guider with respect to an inertial reference frame, we use the rigid body rotation matrix that relates the Shuttle body system to an inertial system. This matrix is expressed in terms of the Euler parameters (quaternions) (Ref. 1, 2), and is initialized to correspond to the estimated direction of the guider z axis. As stated before, the error in this estimate can be as large as a few degrees.

The identification of the stars recorded by the guider is made by comparing these stars with those in the on–board catalog. Before comparison, these last are re–projected on the plane of the guider (a CCD detector) by using the current value of the rotation matrix. The re–projection procedure makes use of the co–linearity formulas (Ref. 2) which, by means of the current value of the rotation matrix, transform stellar celestial coordinates (right ascension and declination) into metric cooordinates (x and y) on the CCD.

The program seeks a one–to–one correspondence between measured inter–angles, i.e. angles under which the guider sees a star pair, and the inter–angles calculated from the catalog stars listed in the appropriate sectors and selected as described above. Two inter–angle tables are constructed: one for the guider stars and one for the catalog stars. An hypothesis of correspondence between the stars listed in the two tables is made. This hypothesis is accepted or rejected by the orientation algorithm. In the case of rejection, another hypothesis is made; and so on.

The algorithm minimizes the distance between guider stars and the hypothezed corresponding ones determined from the catalog. The minimization procedure is made by adjusting the elements of the rotation matrix.

At the end of the procedure we are able

i. to check that the overlap between the catalog and guider stars is achieved (if not, the hypothesis of pair correspondence is rejected; the algorithm then makes another overlap attempt based on a different hypothesis);

ii. to define, starting from the last updating of the rotation matrix, the orientation of the guider rotation relative to the inertial reference system.

An interesting experimental result is that the selection of a large number of stars on the image plane does not raise the algorithm accuracy but, instead, increases calculation time. Therefore a limit of five stars is compared with the catalog stars.

RESULTS OF THE SIMULATIONS

In this section we report our results on the precision in pointing and tracking reached by the algorithm when we add noise to simulate the digitization of star positions. Errors in star position introduced by the optical system are considered negligible and they in fact are with an appropriate choice of the optical system.

In our hypothesis the CCD guider is mounted on a *UVSTAR*–type movable platform on the Shuttle. The requirement is that it must provide autonomous optical fine pointing (± 5 arcsec) within a radius of 3° of the platform nominal view direction, which is near the Shuttle +y axis, i.e. perpendicular to the long axis of the Shuttle and in the plane of the wings. In addition it must provide autonomous tracking for an angular azimuthal movement of $\pm 3°$ around the Shuttle z axis and for an angular elevation movement of $+2°$ to $+8°$ around the Shuttle x axis, measured from the x–y plane.

POINTING

The simulation of the guider image is generated from the catalog on the basis of the following steps:

- access to the catalog in the (nominal) direction of the optical axis of the guider;
- re–projection on a plane tangent to the celestial sphere at the intersection point with the given direction using the "direct" or the "rotated" catalog;
- transformation of star coordinates into pixel coordinates, taking into account the focal length of the guider optics;
- noise addition to the star positions, using a value chosen to simulate the imperfect determination of location on the CCD;

At this point the simulation of the guider image is complete. The algorithm now performs the transformation of star coordinates from pixel into geometrical position on the detector.

The noise in the guider star positions is introduced to simulate the digitization of star coordinates on the CCD. It is expressed as fraction of pixel and represents the interval in which a random variable with uniform distribution is generated. This variable value is algebraically added to the star coordinates. Concerning this last point, one notes that the stars should generally be out of focus and should blur onto several (typically 9) pixels. This allows calculating star positions by centroiding. The adopted perturbations range from ± 0.1 pixel to ± 0.5 pixel, the latter being equivalent to the case in which the stars are focused on a single pixel.

Failure in determining the orientation of the platform occurs when fewer than 3 stars (brighter than 7th magnitude) are in the detector field of view. The probability of this depends on the size of the field of view. One of the fields of view considered corresponds to the design of the guider of the *UVSTAR*. The CCD pixel size considered is 22×22 μm. Table 1 gives the main characteristics

of the electro–optical systems considered. The pixel field of view of about 50 arc–sec represents the theoretical limit of the pointing and tracking method without centroiding; this limit is greatly improved by centroiding.

Figure 1 gives the distribution of number of stars (brighter than $m_V = 7$) for the *UVSTAR* field of view. The diagram has been constructed by simulating 3000 random accesses to different sky zones with the three instruments. The histogram also shows the percentages of times with fewer than three stars, i.e. the percentage of failure in determining the orientation due to insufficient number of stars in the field of view. We detect fewer than three stars only 1.0% of the times. If we adopt two guiding systems with detectors on orthogonal or nearly orthogonal axes, the two percentages become better than 0.01%.

The star identification simulation has been made by random accessing 300 sky zones and running 25 identification cycles per access. At each access the direction of the sky zone was known with a $\pm 3°$ precision. Each cycle has been run by changing in a random way the direction of the optic axis within a circle of 0.2° in order to take into account the maximum perturbation due to the Shuttle movement when it is in "hold mode".

In figure 2 we show the mean error (arc–sec) in the determination of the z–axis direction and the percentage of false identifications ("true failures") as a function of the perturbation. The mean error is better than 4.5 arc–sec and the "true failure" rate is of 2% with a perturbation in 0.2–0.4 pixel range; the error increases almost linearly with the perturbation, i.e. with the added noise. The "true failures" curve displays a strongly increasing slope when the perturbation becomes larger than 0.7, i.e. ± 0.35 pixel. The typical time required to identify the star field is 250 ms using a 25MHz 80386 personal computer with mathematical coprocessor. In figure 3 we show a similar diagram as a function of focal length; it confirms that the best choice for the *UVSTAR* electro–optical system is a 80 mm focal length. In figure 4 we report the mean error (arc–sec) in right ascension and declination as a function of the perturbation.

TRACKING

The goal of tracking is to use the history of the Shuttle attitude, as determined from the guider, to anticipate near–term motions and compute the pointing corrections necessary to cancel them.

In order to generate the simulated CCD images, we have used the parameters of the Shuttle motion recorded during the STS–39 mission. We have considered the temporal variation of the yaw, pitch and roll angles at 1 Hz frequency during 24 hours from MET 475200 s to MET 561600 s; we have extracted and analyzed the data taken when the Shuttle was in inertial hold mode. Given the temporal variation of the yaw, pitch and roll angles in the year 2000 celestial coordinates rest frame, the motion of any vector fixed on the Shuttle body system can be calculated. Figure 5 gives the azimuth (ϕ) and the elevation (θ) variations of the Shuttle vector, in degrees, during the 10 minute interval between MET 542232 to MET 542832 and the absolute value of the differences, in arc seconds, between two successive ($\Delta t = 1$ s) ϕ and θ positions. ϕ and θ are measured in the celestial coordinates reference system.

A recent paper by Neupert *et al.* (1992) on the Orbiter Stability Experiment which has flown on STS–40 shows that the changes in pitch, roll and yaw angles that have been derived from the STS–39 data do not show the real Shuttle motion; these last suffer of jumps with mean amplitude of ≈15 arcsec between two successive (1 Hz) samples which are not recorded by Neupert *et al.* detectors having detection limit of 25 arcsec but sampling frequency larger than 10 Hz. We believe that the STS–39 curves are strongly affected by instrument read–out noise. This effect makes the θ and ϕ curves worse than real curves but, maybe, more interesting for evaluating the performances of the algorithm.

In the tracking mode, once the orientation has been determined with a precision of ±5 arcsec and the sensor is locked on it, the algorithm "follows" the star field by generating "correction curves", $\phi_c(t)$ and $\theta_c(t)$ to the Shuttle motion. Figure 6 gives an example of the calculated $\theta_c(t)$ and the error $\delta\theta(t) = \theta_c(t) - \theta(t)$ using a portion of STS–39 motion record at two perturbation parameters 0.2 and 0.5.

An evaluation of the precision of the method can be obtained by calculating the differences $\delta\theta(t)$, and $\delta\phi(t) = \phi_c(t) - \phi(t)$. Note that interpreting $\delta\phi(t)$, one has to take into account the fact that we are dealing with a dependence on θ. For a particular value of the pointing error δl, measured in the ϕ direction in arc lenght on the sky, $\delta\phi$ is given by $\delta\phi \approx \delta l/\sin\theta$, except near the poles. Therefore $\delta\phi \geq \delta l$, with equality when $\theta = 90°$.

However the division of the celestial sphere into the two parts, polar and equatorial, described above, and their interchanging role, limits the error increment due to the use of angle instead of arc by a safe factor of $\sqrt{2}$. The average values of the errors in ϕ and θ for two different pertubation parameters are reported in Table 2.

The "correction signal" for the motors is derived after the following two steps:

- at a given time t_0 we record the direction of the guider z axis and express it in celestial coordinates;

- at the next step t_1 with the new star field acquisition we calculate the new pointing direction and the new rotation matrix. By means of the co–linearity formulas, we derive the displacement on the CCD plane of the previous z axis direction and express it in microstep pulses to be transmitted to the motor driver.

CONCLUSIONS

The software developed for star field identification and star pointing and tracking demonstrate the capability to reach the high accuracy and precision that are typical characteristics of systems based on stellar sensors. The algorithm has a processing time of less than a few hundredths of a second. This time was in the past the principal limit of this method.

REFERENCES

1. Strikwerda T.E., Junkins J.L., *"Real time spacecraft attitude determination by star pattern recognition: further results"*, 17^{th} Aerospace Science Meeting, New Orleans, 15–17 Jan 1979.

2. Strikwerda T.E., Junkins J.L., *"Star pattern recognition and spacecraft attitude determination"*, Phase II, U.S. Army Corps of Engineers, Engineer Topographic Laboratory, Report for the period Oct. 78–Sep. 79.

3 R. Stalio, B.A. Sandel, A.L. Broadfoot, *"UVSTAR, an Imaging Spectrograph with Telescope for the Shuttle Hitchhiker–M Platform"*, this volume.

4. Documentation for the machine readable version of the S.A.O., version 1984, National Space Data Center, Goddard Space Flight Center

TABLE 1: SIMULATION PARAMETERS OF THE ELECTRO–OPTICAL SYSTEM

Case No.	CCD size (pixel)	Focal length (mm)	Detector FOV	Pixel dimension (arc–sec)
1	385×288	80	6°×4.5°	56

TABLE 2: POINTING PRECISION

Perturbation	$\overline{\delta\theta(t)}$ (arcsec)	$\overline{\delta\phi(t)}$ (arcsec)
±0.2	1.5	1.6
±0.5	8.8	8.5

Fig. 1: Histogram for random accesses to different sky zones at the *UVSTAR* field of view. The vertical axis shows the percentage of the times that n stars brighter than $m_V = 7$ fall in the field of view. The horizontal axis is n.

Fig. 2: The mean error in the determination of the direction of the optical axis and the percentages of failures as a function of the perturbation.

Fig. 3: The ordinate axes give i. the mean value of the error (in arc–sec), ii. the "true failure" rates (in percentage), iii. the percentage of fields with fewer than three stars, iv. the mean time in ms used by the algorithm with the computer system described in the text ($\alpha \approx 50$). The abscissa axis is focal length of the optical system.

Fig. 4: Right ascension and declination errors (in arc–sec) as a function of perturbation.

Fig. 5: Shuttle vector variations during a "hold" period. Top: elevation motion. Bottom: azimuth motion.

Fig. 6: Predictions and prediction errors of the Shuttle motion with two perturbation parameters: 0.2 and 0.5.

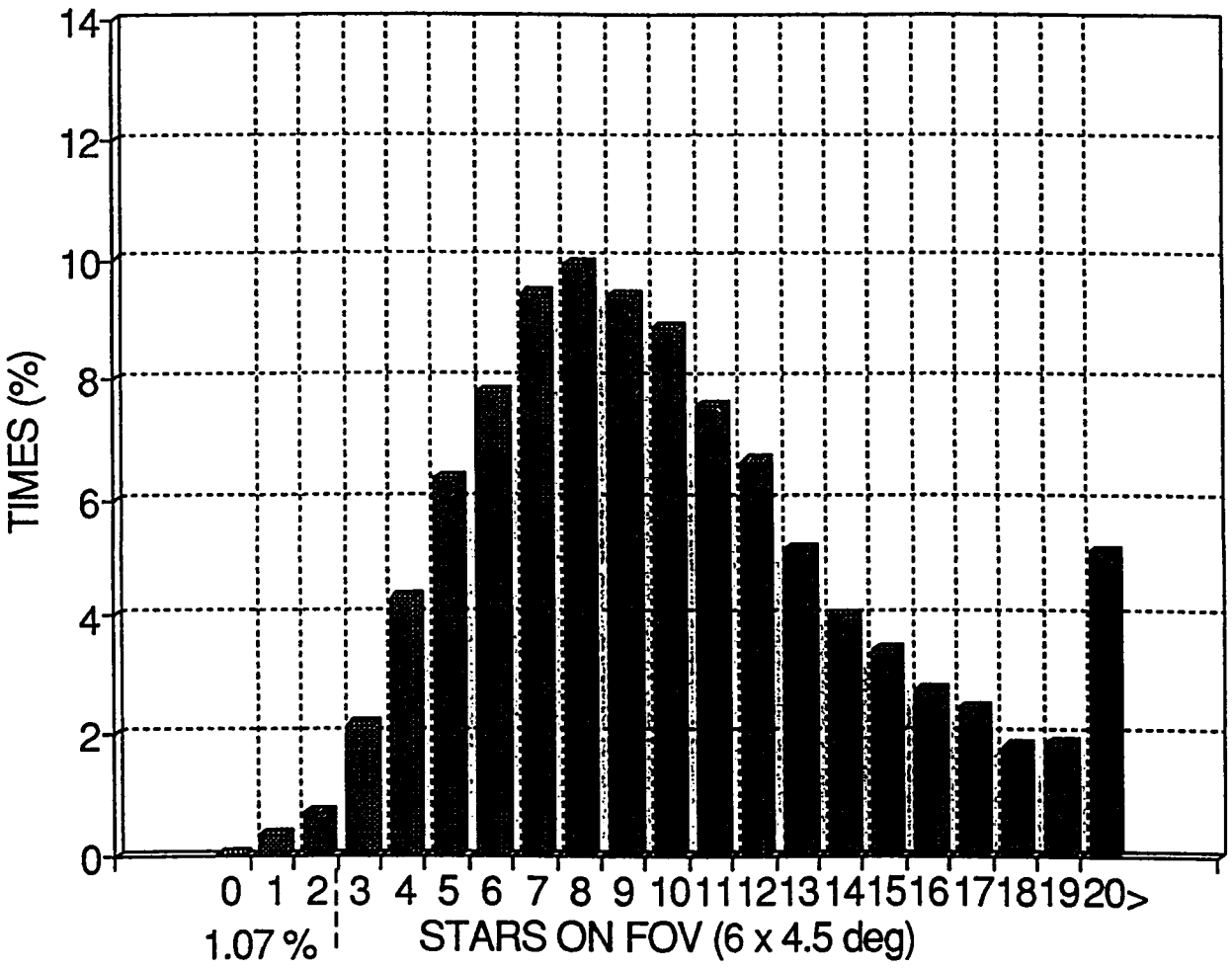

Fig. 1: Histogram for random accesses to different sky zones at the *UVSTAR* field of view. The vertical axis shows the percentage of the times that n stars brighter than $m_V = 7$ fall in the field of view. The horizontal axis is n.

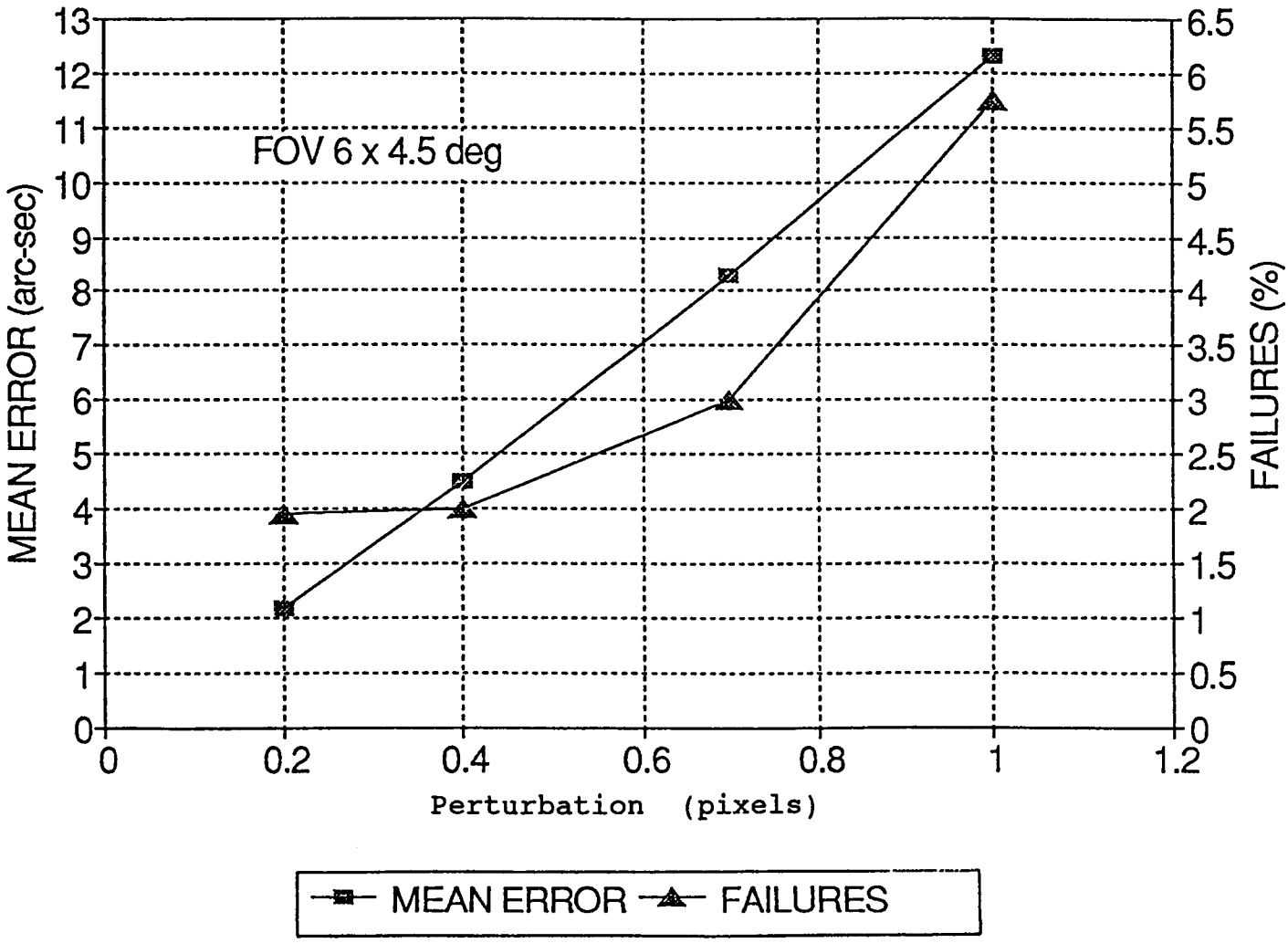

Fig. 2: The mean error in the determination of the direction of the optical axis and the percentages of failures as a function of the perturbation.

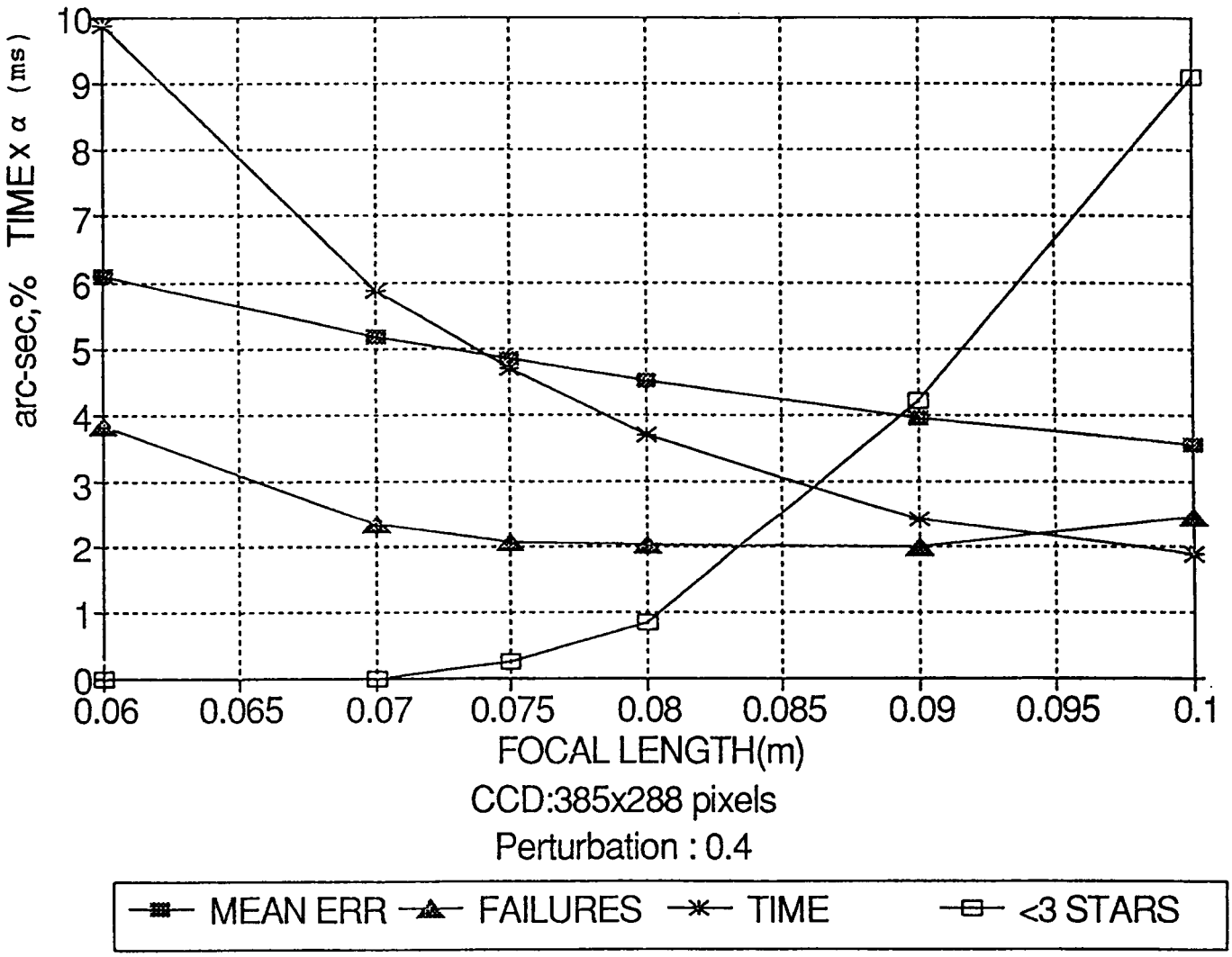

Fig. 3: The ordinate axes give i. the mean value of the error (in arc–sec), ii. the "true failure" rates (in percentage), iii. the percentage of fields with fewer than three stars, iv. the mean time in ms used by the algorithm with the computer system described in the text ($\alpha \approx 50$). The abscissa axis is focal length of the optical system.

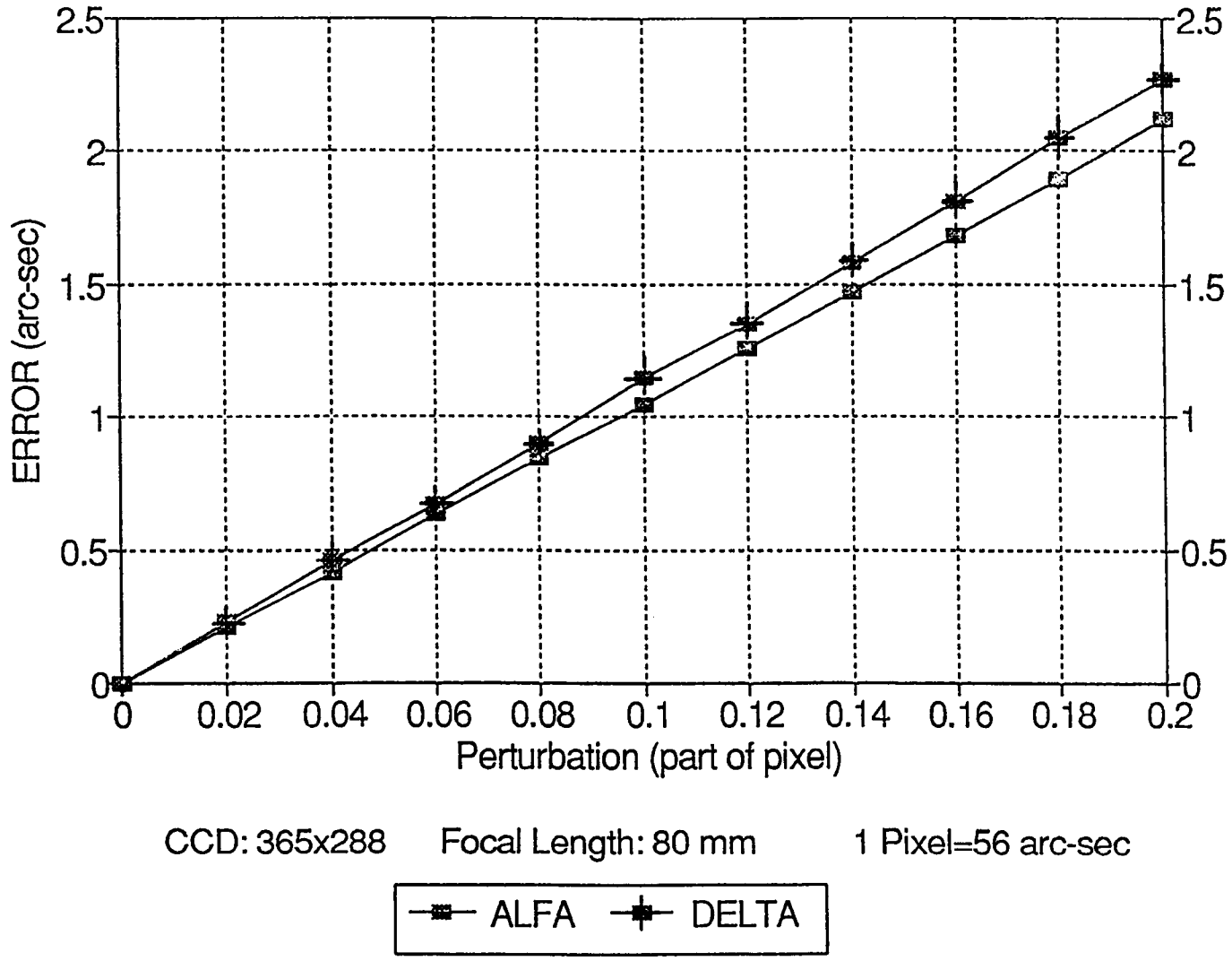

Fig. 4: Right ascension and declination errors (in arc–sec) as a function of perturbation.

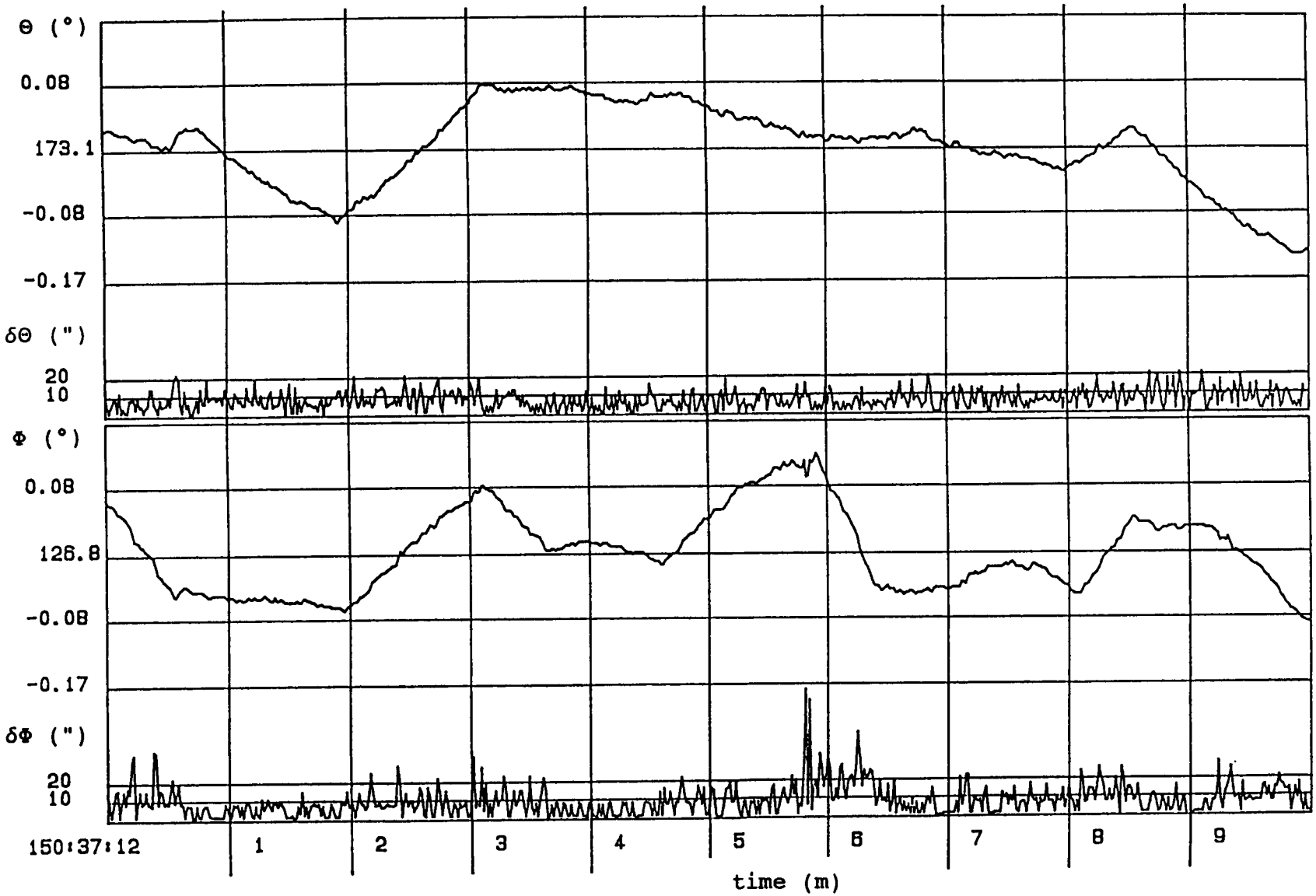

Fig. 5: Shuttle vector variations during a "hold" period. Top: elevation motion. Bottom: azimuth motion.

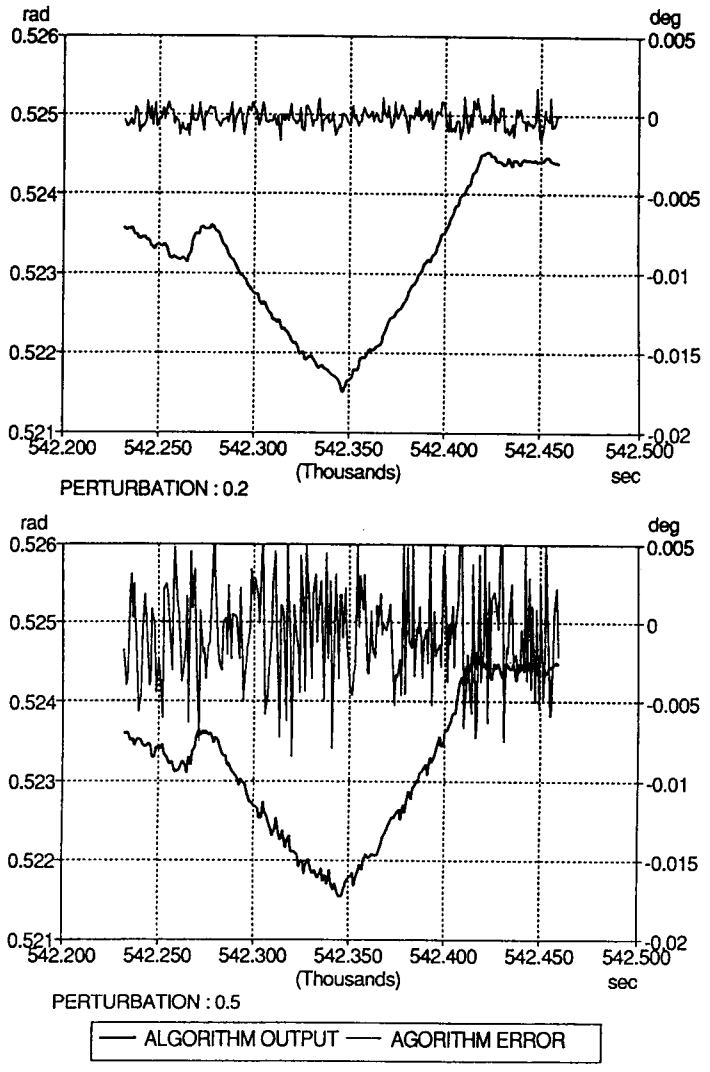

Fig. 6: Predictions and prediction errors of the Shuttle motion with two perturbation parameters: 0.2 and 0.5.

UTILIZATION OF SHUTTLE SMALL PAYLOAD ACCOMMODATIONS IN THE DOD SPACE TEST PROGRAM

Mr. Thomas Hagler
Dr. Eva Czajkowski
ANSER

10 July 1993

This paper reports research sponsored in part by the United States Air Force under Contract No. F49620-91-C-0031. The views, opinions, and findings continued herein are those of the authors and not necessarily those of ANSER or the United States Air Force.

UTILIZATION OF SHUTTLE SMALL PAYLOAD ACCOMMODATIONS IN THE DOD SPACE TEST PROGRAM

Mr. Thomas Hagler
Dr. Eva Czajkowski
ANSER
Arlington, VA 22202

ABSTRACT

Over the past 27 years, the US Air Force, as executive agent for the Department of Defense (DOD) Space Test Program, has flown approximately 325 space experiments for the Army, Navy, Air Force, and other DOD agencies not authorized their own means of spaceflight. These experiments have made significant contributions to the improvement of military technology and operations.

Flight of Space Test Program experiments has been carried out utilizing free flyer spacecraft, the Space Shuttle crew cabin, and the Space Shuttle cargo bay. This paper will concentrate on those experiments which have been flown by the NASA Space Shuttle small payload flight systems, e.g., GAS, uprated GAS (CAP), and Hitchhiker flight systems.

Discussion of Space Test Program experiments flown by Space Shuttle small payloads flight systems will include the experiment objectives, the accommodations and services provided by the flight systems, experiment results, and lessons learned from the planning and conduct of the flight. Particular emphasis will be placed on those experiments which required and were provided with a new and unique capability by the small payloads flight systems. These capabilities include the first use of the GAS opening lid, the first use of the GAS payload ejection capability, and the first use of the Hitchhiker cross bay carrier.

INTRODUCTION

Figure 1 lists the three major categories of experiments that have been conducted by the DOD Space Test Program (STP).

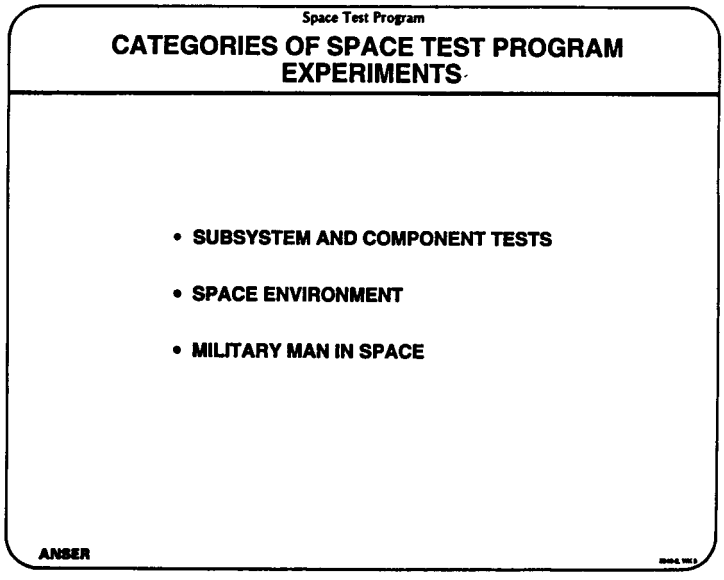

Figure 1

The objective of experiments related to subsystem and component tests is to proof test and demonstrate components which are more reliable, more survivable, or have improved performance. STP has flown 67 experiments related to component and subsystem tests. The purpose of experiments related to the space environment is to understand the environment where

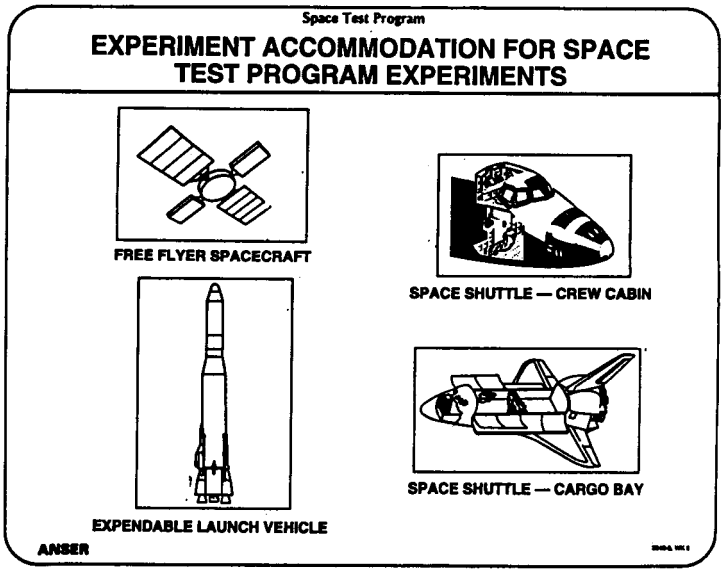

Figure 2

military systems, such as communication systems, must operate. STP has flown 171 experiments related to the environment. Finally, STP has conducted 28 experiments related to military man in space. The objective of these experiments is to determine if there are useful military activities which can be best carried out by a man in space.

Figure 2 illustrates the various types of flight systems which have been utilized by STP to fly experiments. Spacecraft launched by expendable launch vehicles have provided accommodations for STP experiments throughout the life of the program. Frequently the Space Test Program has been able to "piggyback" STP experiments on spacecraft of other flight programs. Approximately 50 experiments have been flown by STP in the Shuttle crew cabin, including all of the experiments related to military man in space. Except for two missions which involved very large payloads, all of the STP experiments which have flown in the shuttle cargo bay have been flown by the Goddard Shuttle small payloads program.

Space Test Program

SUMMARY OF SPACE TEST PROGRAM EXPERIMENTS FLOWN BY SHUTTLE SMALL PAYLOADS PROGRAM

DATE	MISSION	STP EXPERIMENT DESIGNATION	CARRIER
1983	STS 31C	NRL-904A	GAS
1984	STS 41B	SD-301	GAS
	STS 41G	NRL-905	GAS
1985	STS 51B	DARPA-401	GAS
	STS 51G	NRL-904B	GAS
	STS 61A	DARPA-401	GAS
1986	STS 61C	AFA-301	GAS
		AFGL-402	HITCHHIKER G
1988	STS 27	SD-301	GAS
1989	STS 28	AFTAC-402	GAS
	STS 33	SD-301	GAS
1991	STS 39	NRL-904	HITCHHIKER M
		SD-602	
		AFGL-501	
1992	STS 42	NPS-603	GAS
	?	AFGL-502	GAS
	STS 53	WRDC-001	HITCHHIKER G
		GL-601	HITCHHIKER G

ANSER

Figure 3

Figure 3 summarizes the DOD STP experiments that have been flown by the Shuttle small payloads program. STP has utilized this program consistently over the past ten years. These Shuttle small payload experiments have been of a wide variety of types, as will be demonstrated shortly as each of these missions and experiments is presented.

THIE 1983-1984 MISSIONS

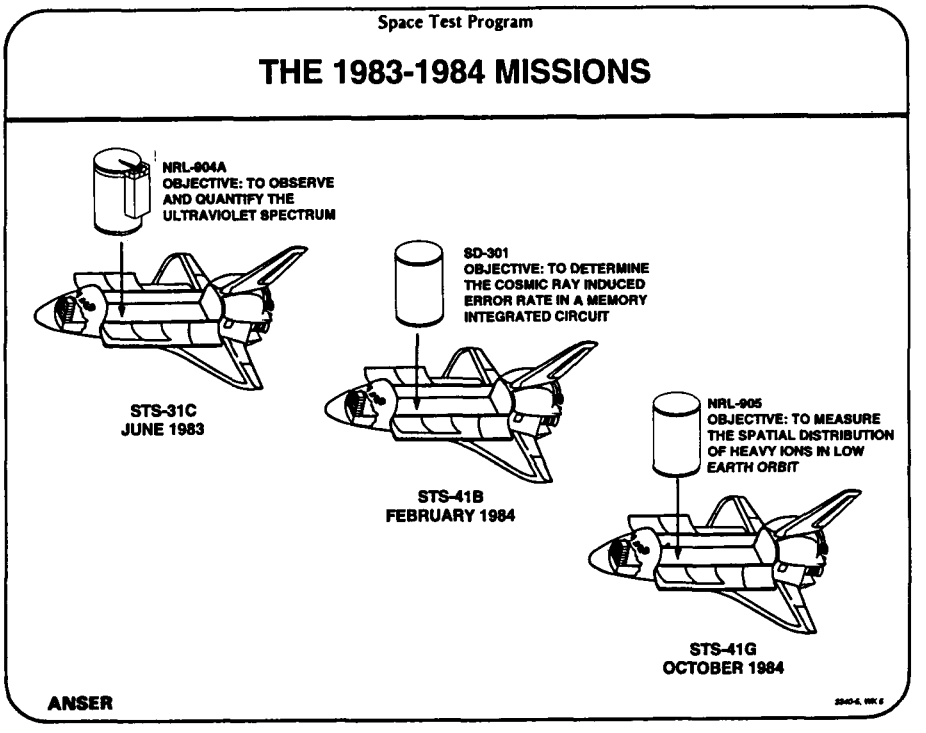

Figure 4

Figure 4 illustrates the accommodations and objectives of the STP experiments flown by the small payload program in the 1983-1984 time frame. All three of these experiments acquired useful experimental data. Of particular interest is the Get-Away Special (GAS) can with the opening lid that was flown in 1983. STP recognized early that the capability of the GAS can for flying experiments could be improved substantially by providing a lid that could be opened in orbit. STP provided advice and assistance, including financial assistance, to the Goddard small payloads program for the design and fabrication of the opening lid. the opening lid has been used for a number of subsequent GAS can experiments. This first group of experiments also gave STP experimenters their first experience with the extensive safety requirements for flight of an experiment on a manned spacecraft.

THE 1985-1986 MISSIONS

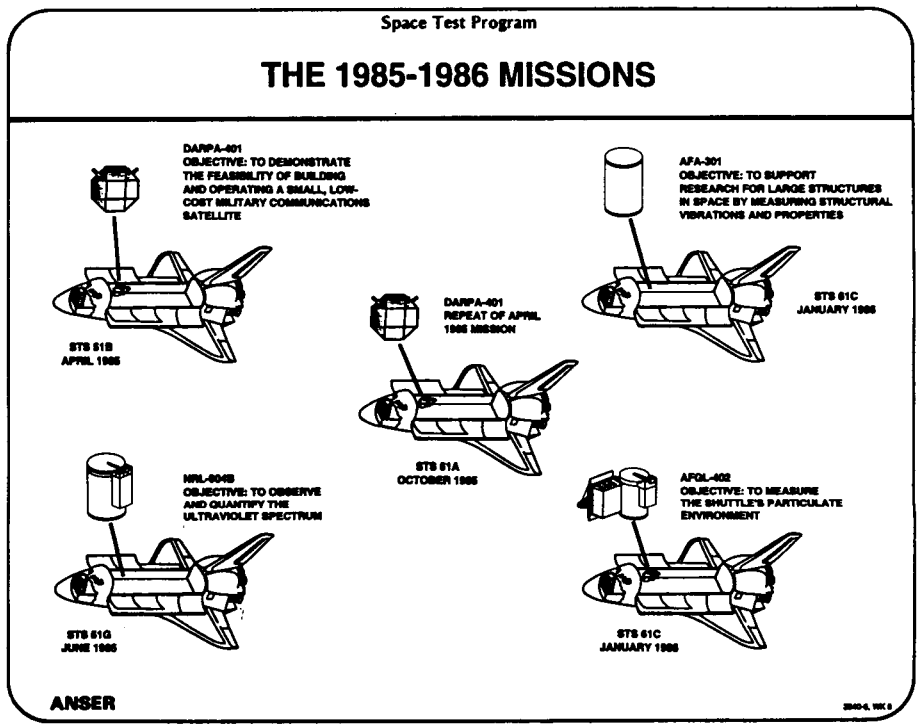

Figure 5

Figure 5 illustrates the accommodation and objectives of the STP experiments flown by the Goddard Shuttle small payloads program in the 1985-1986 frame. This period marked the first use by STP of two new types of Shuttle small payload accommodation. For some time, DOD has been interested in the idea of a battlefield communications system based on space assets. Such a "store and forward" message system would have to be reliable, inexpensive, easy to launch, and have a lifetime of at least several months. Such a system was tested by the DARPA-401 missions in 1985. The first flight failed because malfunction of the GAS can lid did not allow the satellite to deploy. The second flight deployed the satellite properly. It operated satisfactorily for one year. NRL-904B was a repeat of the NRL-904A experiment flown in 1983. No useful data was obtained due to an electronic malfunction. AFA-101 demonstrated that a GAS can can be used to support research for large structures in space by measuring structural vibrations. Finally, AFGL-402 measured the Shuttle's particulate environment in STP's first use of the Hitchhiker G experiment accommodation. This experiment was 100 percent successful.

THE 1988-1989 MISSIONS

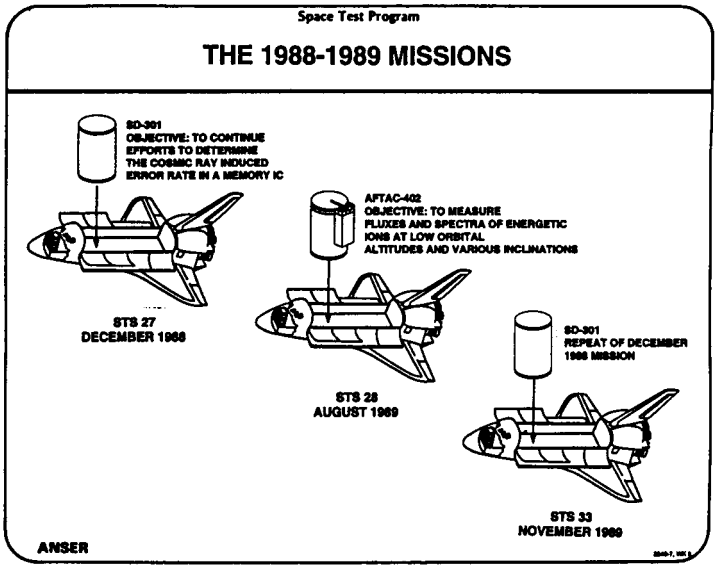

Figure 6

In the 1988-1989 time frame, as the Shuttle began to fly again after the Challenger accident, STP flew three GAS can experiments, as shown in Figure 6. Useful experimental data was obtained from both flights of experiment SD-301. This data was used to validate the analytical model of cosmic ray-induced error rate in a memory integrated circuit. The AFTAC-403 experiment was partially successful. Data from this experiment was used to evaluate detector performance for free flyer spacecraft missions.

THE 1991-1992 MISSIONS

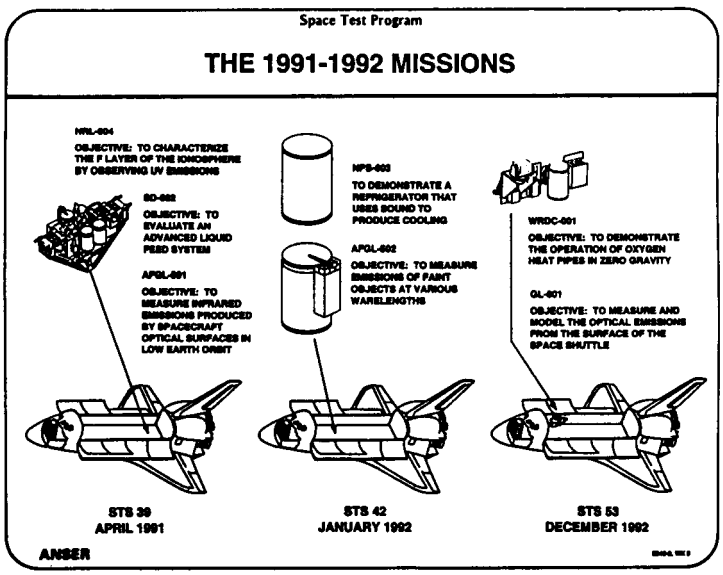

Figure 7

In the 1991-1992 time frame, as illustrated in Figure 7, STP utilized the expanded payload capability of the Goddard Shuttle small payloads Hitchhiker M carrier to fly three substantial experiments. The three experiments together weighed approximately 1,000 pounds. The successful accomplishment of these experiments was aided by the Hitchhiker system's real-time communications with the experiments. Shuttle mission STS-42 flew two successful STP GAS can experiments. One of these experiments demonstrated a space refrigerator which used sound to produce cooling. The other experiment measured the emissions of faint objects in space. Shuttle mission STS-53 carried two successful STP experiments on Hitchhiker G accommodations. One of these experiments demonstrated the operation of an oxygen heat pipe in zero gravity; the other experiment measured the optical emissions from the surface of the Space Shuttle.

POTENTIAL FUTURE MISSIONS

Each year the DOD Space Test Program holds a Tri-Service meeting to discuss and prioritize space experiments which have been proposed for flight. Based on the May 1993 meeting, STP has approximately 50 experiments on the current priority list. After eliminating experiments that require long duration flight or an orbit not achievable by the Space Shuttle, and also eliminating those experiments that require flight in the Shuttle crew cabin, the experiments listed on Figure 8 were selected as good candidates for flight by the Shuttle small payloads program. Detailed analyses of these experiments will be made by the STP office responsible for experiment flight planning.

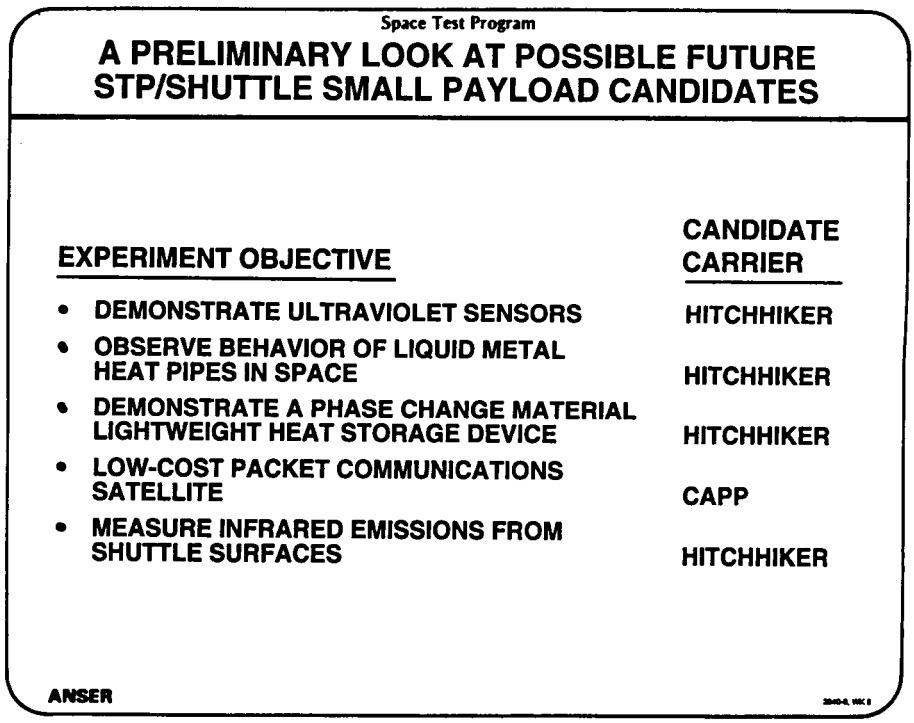

Figure 8

SUMMARY AND OBSERVATIONS

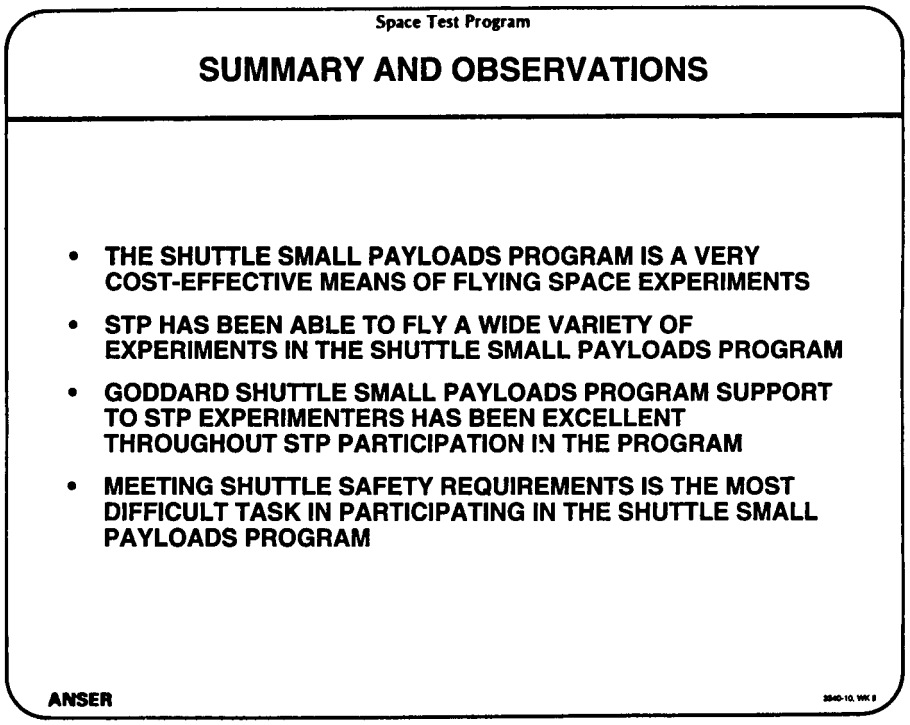

Figure 9

Figure 9 lists some observations relating to STP participation in the Shuttle small payloads program. The program is without doubt the most cost-effective flight program in existence for the flight of space experiments.

As some of the earlier examples indicated, STP has been able to fly experiments in the Shuttle small payloads program, ranging from subsystem tests to environmental measurements. STP has also been able to fly experiments that weigh up to several hundred pounds and experiments that require real-time communications during flight.

STP experimenters have uniformly offered high praise of the members of the Shuttle small payloads office, who frequently have gone the extra mile to make the integration and flight of the experiment a success.

Experimenters considering using the Shuttle small payloads flight accommodations must recognize that their experiment will be flying on a manned flight system, and safety requirements are substantial. Work to support safety analysis must start early and must be completed satisfactorily.

SPNDL: A CONCEPT FOR A SMALL SATELLITE DOPPLER LIDAR WIND SOUNDER

G.D. Emmitt
Simpson Weather Associates, Inc.
Charlottesville, VA

M.M. Sokoloski
Science and Technology Corporation
Washington, D.C.

ABSTRACT

Given current resources and the technical challenges in developing a full coverage space-based Doppler lidar wind measuring system such as LAWS (Laser Atmospheric Wind Sounder), it is not likely that the science community will have data streams with which to work before the end of this decade. Currently, a "fast track" demonstration mission is being seriously considered by several U.S. agencies. Such a mission would have as its primary objectives the demonstration of coherent Doppler lidar technology in space and the delivery of wind observations for science algorithm evaluation and development.

However, for such a mission to be achieved at modest costs and within a short time frame, deviations from the full system design are required. Simulation models have been developed over the last decade to aide in the design of Doppler lidar missions and to provide simulated data for use in wind computation algorithm development. SWA has used both models to examine some options that might be cost-effective for a demonstration mission. Over the past few months, Simpson Weather Associates has been studying SPNDL (Spinning Platform with a Non-rotating telescope Doppler Lidar), a new concept for Doppler lidar wind observations from space. Science and Technology Corporation has an interest in participating in an engineering and shuttle accommodation study for SPNDL.

INTRODUCTION

Knowledge of the tropospheric winds is required for understanding and predicting weather and changes in the earth's climate. With the exception of in situ data obtained within densely populated regions of the globe, today's atmospheric models rely upon estimates of the winds derived from satellite-sensed temperature and moisture fields. Observing System Simulation Experiments (OSSEs) for a space-based Doppler lidar wind sounder have indicated a significant impact of direct wind measurement.

Since the late 1960's, lidar has been studied as a potential means of obtaining these winds. Early in NASA's EOS program, LAWS (Laser Atmospheric Wind Sounder) was identified as an

instrument to provide winds to the global climate study. Phase A/B studies defined a rather demanding system (20 J laser, 1.6 m telescope, 800 kg, 4 kW) to meet the EOS mission requirements. The projected cost and perceived technical risks have contributed to a delayed new start for this ambitious program.

Recognizing that there is a role for a demonstration class wind sounder mission, several proposals have been made. In 1985, NASA (1) considered a shuttle mission (Figure 1) based upon NOAA's WINDSAT study (2) but decided a 7-day mission would not justify the costs. Within the last year, the LAWS Science Team recommended a more modest version of LAWS (5 J, .75 m telescope, 600 kg, 2 kW) which would still provide a significant science return. More recently, a NASA call for "quicker, better, cheaper" space instruments has been made. Emmitt (3), a member of the LAWS Science Team, has proposed SPNDL (.2 J, .6 m telescope, 350 kg, .6 kW) for a techno/science mission that would achieve the following:

- demonstate that a coherent lidar can be launched, aligned, operated and remain aligned for a reasonable period of time;
- obtain data streams that can be used to validate/ calibrate data product algorithms;
- generate low density/high quality soundings that will help build confidence in the feasibility of the "full-up" LAWS.

SPNDL could be launched from a shuttle, boosted into a higher orbit and then left to a lifetime limited by orbit degradation. Another scenario is for the concepts of SPNDL to be tested from the shuttle bay with the instrument returned for post flight evaluation. At this time, both options are considered feasible. The remainder of this presentation describes the measurement concept and identifies key technological and scientific issues that could be addressed with a shuttle mission.

SYSTEM DESCRIPTION

In Table 1, several key design considerations are listed along with their advantages in terms of cost-reduction and performance enhancement. These general considerations are translated into system requirements for the measurement concept called SPNDL, which is outlined in Table 2.

A major departure of SPNDL from the original LAWS design concept is the use of a spinning platform to achieve scanning with a single, fixed (non-rotating) telescope (Figure 2).

While details of the technical feasibility of SPNDL are currently being evaluated, the scan pattern and characterization of the quality and quantity of the resulting wind data have been

simulated. In Figure 3, the horizontal projection of the shot pattern within the earth's troposphere is shown for two revolutions of SPNDL. The prf is 10 Hz and the platform revolution rate is 1 rpm. The plan would be to only pulse the laser near the intersections of scans, resulting in a 3-5% duty cycle.

Using only static lag angle compensation, the optimal range (a fixed distance from the satellite) is located at varying altitudes within the troposphere during a scan (Figure 4). If a 3 dB loss due to uncompensated lag angle is tolerable, then the vertical range of return will be ~ ± 25 km from the optimal range.

The result of the SPNDL pattern of observations is the placement of more than 40 bi-perspective shots into a 50x50 km area. Very accurate (σ_v < .2 m s^{-1}) wind measurements are possible but are spaced ~ 300-400 km along the satellite track. In Figure 5, an example of 24 hours of SPNDL coverage at 1000 mb is shown for a simulation using fields from a global circulation model for input to the LAWS LSM.

CONCLUSION

SPNDL, an SWA concept, offers an alternative to a scaled down version of the full LAWS for use in a wind measuring demonstration mission. Further evaluation of this concept is underway within NASA. Either a smallsat mission or a shuttle small payload mission presently is being considered.

REFERENCES

1. D. Fitzjarrald, R. Beranek, J. Bilbro, and J. Mabry, "Preliminary Plan for a Shuttle Coherent Atmospheric Lidar Experiment (SCALE)", Proc. NASA Sympo. on Global Wind Measurements, (1985), 207-214.

2. NOAA, "Global Wind Measuring Satellite System - WINDSAT", NOAA Final Report under Contract NA79RAC00127, (1981).

3. G.D. Emmitt, "System Simulation Studies in Support of a Technology and Product Demonstration Mission for a Space-Based Coherent Doppler Lidar Wind Sounder", Proc. 7th Conf. Coherent Laser Radar Applications and Technology, (1993), 103-106.

TABLE 1

DESIGN CONSIDERATIONS

SPECIFICATION	ADVANTAGES	PROBLEMS
Daytime operation only	Reduced solar array Reduced battery weight	
Fixed telescope with platform spin	Reduced weight/cost Simplicity in optics Retain bi-perspective measurements	Platform stability(?)
Lag angle compensation	Static only reduces complexity	
5-10% duty cycle operations	Reduced power requirements Eliminate active thermal control	Laser stability(?)
Relaxed pointing control	Reduced subsystem costs	Increased burden on data processing
Trade swath width for observation accuracy	Use nadir angle for maximum SNR	
Target ß(50) = 10 E-8	Obtain aerosol returns from PBL and cloud tops	
Maximize shot density	Reduce random system and atmospheric turbulence Oversampling to be used to define minimum density needed for full LAWS	
Relax mission life requirements	Reduce costs of components	

TABLE 2

DRAFT Requirements for

A LAWS/SMALLSAT CONCEPT
(Based upon SWA's SPNDL Concept)

ORBIT

- 98° inclination
- time of day asynchronous with location [to achieve diurnal sampling]
- 350-400 km altitude at equator (~ 379 at poles)
- 1 yr without reboost (orbit degradation of 50 km is tolerable

PLATFORM

- Rotates (~ 1-10 rpm) on axis perpendicular to orbit plane
- Solar panels deployed have continuous sun exposure (98° orbit) and are edge on to motion vector to minimize drag (see figure)
- Passive thermal radiators directed to dark sky
- Lidar beam exits satellite with a fixed angle ~ 20° from orthogonality to spin axis (exit location not critical)
- Beam scanning achieved from satellite spin

TABLE 2 (cont.)

LASER

- 9.11 or 9.25 μm
- pulse spectrum (TBD)
- output angle jitter (TBD)
- .2-1.0 j (end-of-mission)
- 5% duty cycle
- 10 Hz minimum design = $\sim 2 \times 10^7$ shots/year
- capable of on/off cycling to achieve 5% duty cycle

OPTICS

- .75→1.0 m telescope
- Bearing free scanning (scanning achieved through platform spin)
- Static lag angle compensation [active lag angle compensation is desirable if cost acceptable]
- Pointing accuracy: 10 mrad
  knowledge: 100 μrad
  boresight alignment: 3 μrad

TABLE 2 (cont.)

DETECTOR/RECEIVER

- **HgCdTe at 125°K for 1 detector [active cooling may be needed if 4 detectors are used]**
- **Uniform LO**
- **Broadband for platform motion calibration.**
- **$| V_{search} | = \pm 25$ m s^{-1}**
- **$| V_{max} | = 50$ m s^{-1} (LOS)**
- **Spacecraft to target velocity gross Doppler shift = = 8 km/sec**

POWER SUPPLY

- **Instrument to draw directly from batteries**
- **Solar array to provide a power increment dedicated to battery recharge between shot clusters**
- **Design for multiple battery cycling - dependent upon power increment and instrument duty cycle**

THERMAL CONTROL

- **Passive for laser and detector subsystems [desirable]**

COMPANION INSTRUMENTS (OPTIONS)

- **Passive imager to provide visual context for lidar observations - ± 50 km either side of lidar beam track**

- **IR radiometer to provide complementary data for deriving cloud properties in vicinity of lidar samples - co-sighted with lidar beam**

SCALABILITY

- **Basic measurement principles must be scalable**

  - **laser subsystem**
  - **scanned beam**
  - **detection mode**

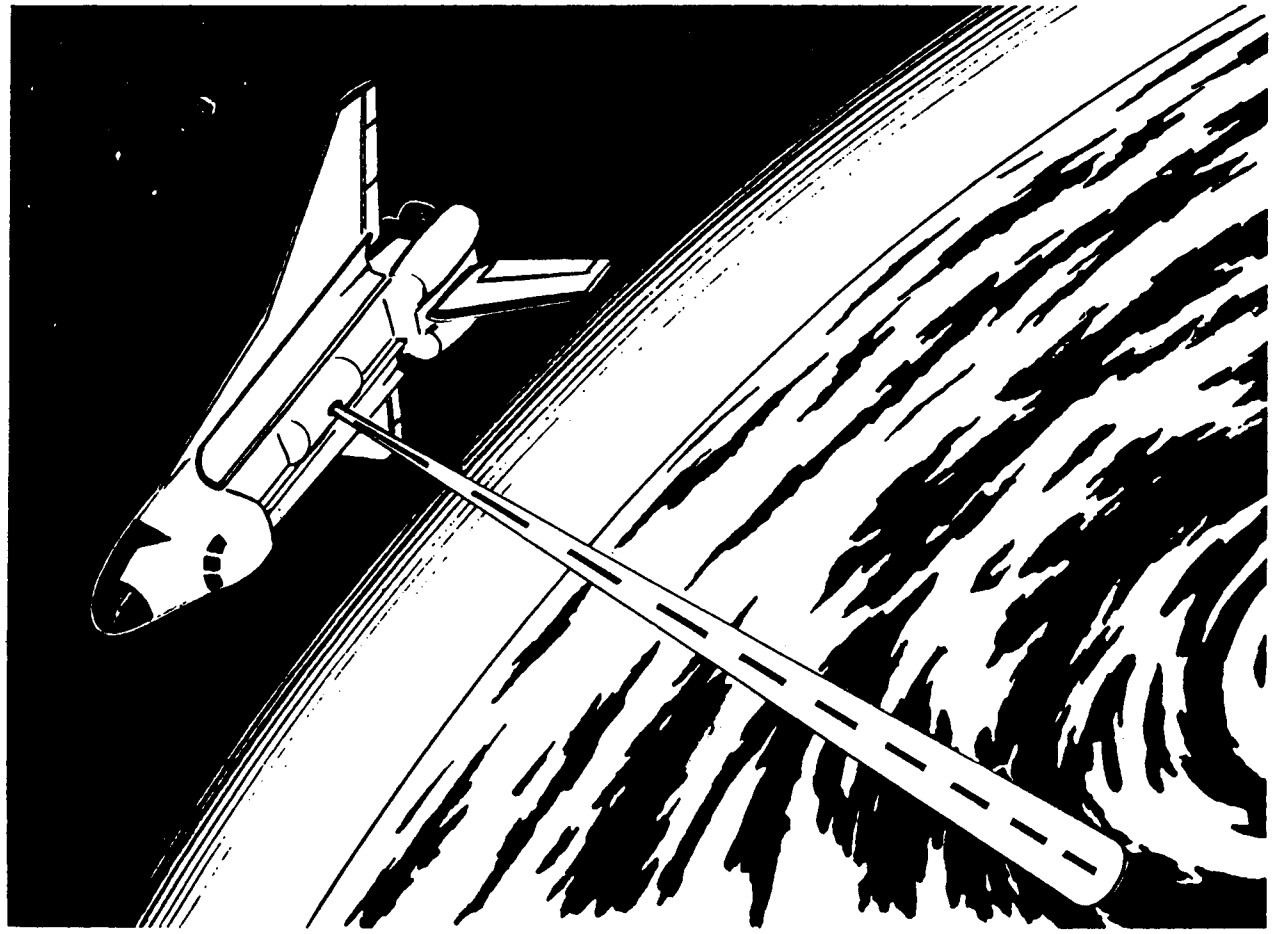

Figure 1. From NASA SP-433, Final Report of Atmospheric Lidar Working Group, 1979.

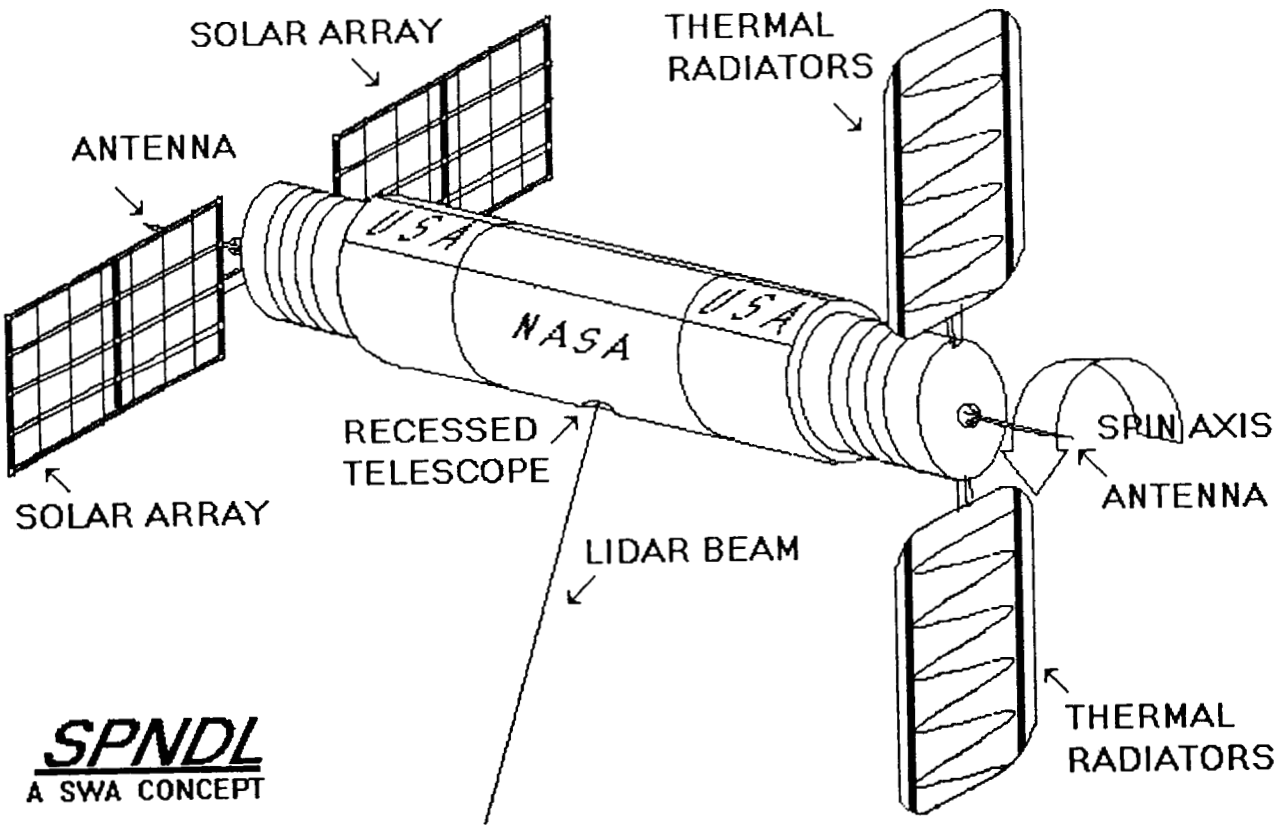
SOLAR ARRAY
THERMAL
RADIATORS
ANTENNA
USA
NASA
USA
RECESSED
TELESCOPE
SPIN AXIS
ANTENNA
SOLAR ARRAY
LIDAR BEAM
THERMAL
RADIATORS
SPNDL
A SWA CONCEPT

FIGURE 2

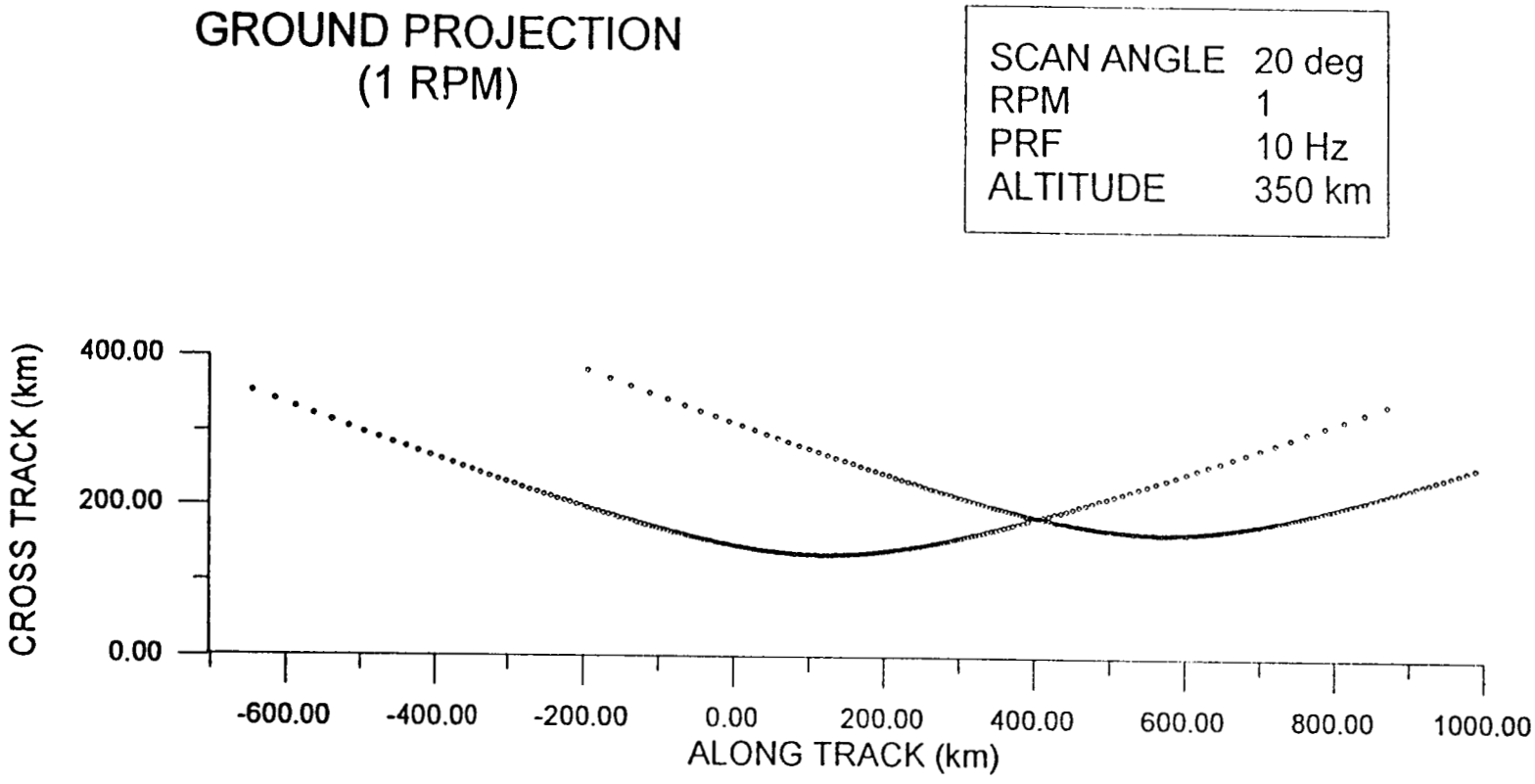
GROUND PROJECTION
(1 RPM)
SCAN ANGLE 20 deg
RPM 1
PRF 10 Hz
ALTITUDE 350 km
CROSS TRACK (km)
400.00
200.00
0.00
-600.00
-400.00
-200.00
0.00
200.00
400.00
600.00
800.00
1000.00
ALONG TRACK (km)

FIGURE 3

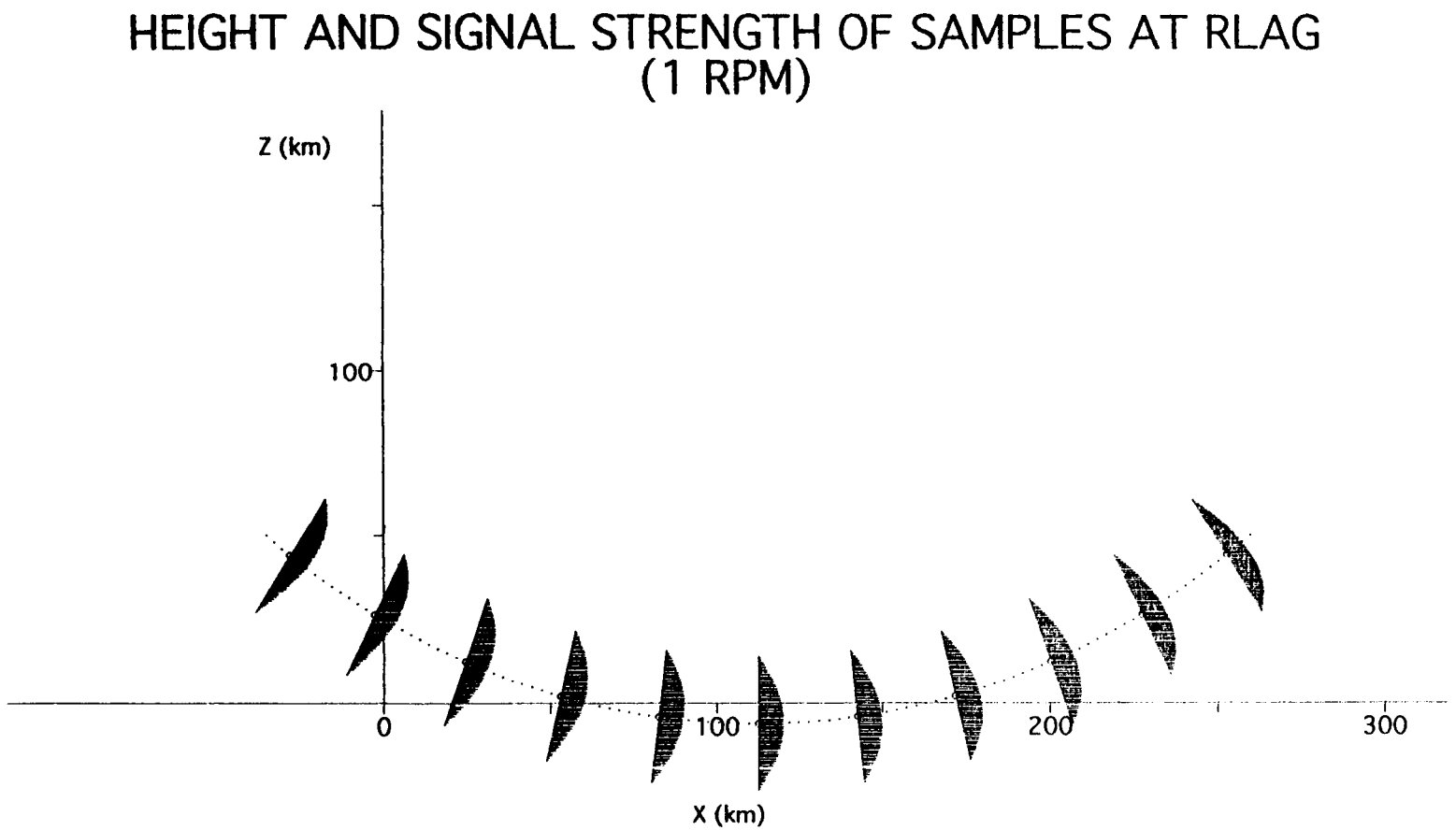
HEIGHT AND SIGNAL STRENGTH OF SAMPLES AT RLAG
(1 RPM)
Z (km)
100
0
100
200
300
X (km)

FIGURE 4

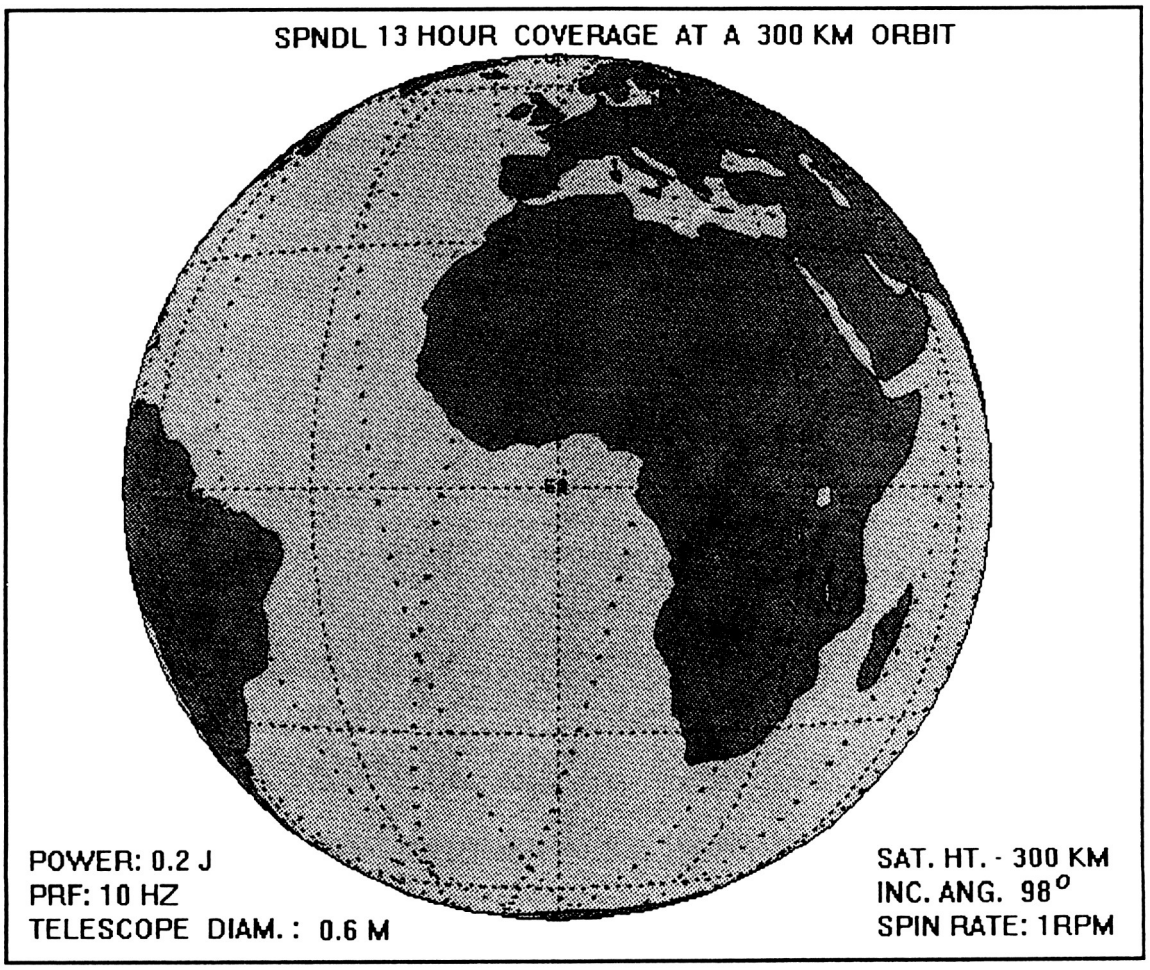
SPNDL 13 HOUR COVERAGE AT A 300 KM ORBIT
POWER: 0.2 J
PRF: 10 HZ
TELESCOPE DIAM. : 0.6 M
SAT. HT. - 300 KM
INC. ANG. 98°
SPIN RATE: 1RPM

FIGURE 5

YOUR GAS EXPERIMENT AND THE MEDIA

or - why does that other can get all of the publicity?

Philip Chien
Earth News
4340 South Hopkins Avenue #40
Titusville, FL 32780

ABSTRACT

NASA has flown almost 100 GAS cans. Only a few of them are remembered by the general public, including the "snowflakes in space" from STS-6, "ants in space" from STS-7, and CanDO from STS-57. Why do some GAS cans get all of the publicity, while others are barely mentioned in press conferences, press kits, and on NASA Select during the mission?

How can you make sure your GAS can gets as much attention as the others on your flight? And why is it important for you to make sure the public finds out about your activities.

Writer Philip Chien has covered the space program since 1983, and is a regular participant in GAS press conferences. This paper will use STS-57 as a case study showing why some GAS cans got more publicity than others. The paper will offer advice for upcoming GAS payloads and how to prepare your press kits and other handouts.

ISOBUS

A New Versatile Spacecraft Platform Using Shuttle Small Payloads

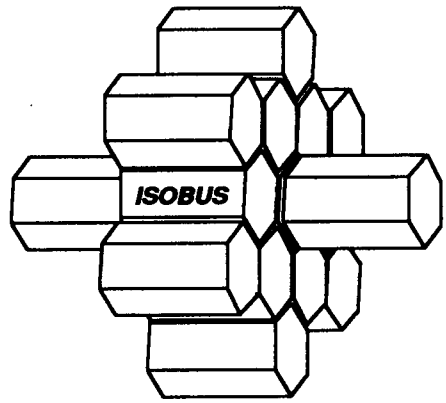

by

David Tamir
Rockwell International Corporation
Space Systems Division

Rex W. Ridenoure
Jet Propulsion Laboratory
Microspacecraft Systems and Technologies Office

R. Gilbert Moore
Space Dynamics Laboratory
Utah State University

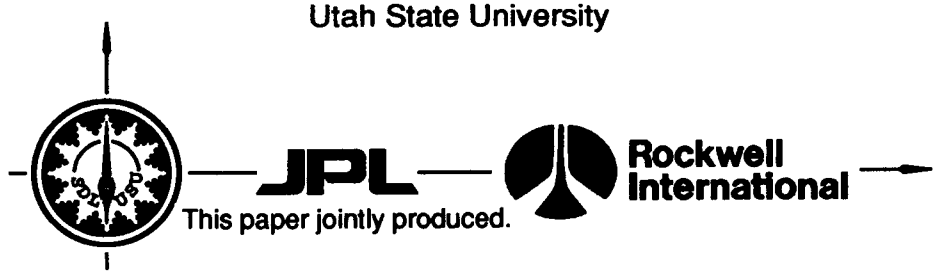

presented at the
Shuttle Small Payloads Symposium

October 4-7, 1993

Annapolis, Maryland

EXECUTIVE SUMMARY

The new NASA credo of "faster, better, cheaper" calls for a new generation of smaller and less complex spacecraft. In response to this challenge, many new spacecraft concepts - generally characterized as mini- or micro-spacecraft to reflect their significantly smaller size - have been generated within NASA, industry, and academia. The Jet Propulsion Laboratory (JPL), Rockwell International Space Systems Division (Rockwell), and the Space Dynamics Laboratory (SDL) / Utah State University (USU) are jointly examining one such new spacecraft concept, hereafter termed ISOBUS, which is derived from recent research and development work in isogrid structures conducted by SDL/USU for JPL's Microspacecraft Development Program. ISOBUS' design is based on a six-sided hexagon shaped structure. Two prototypical products from SDL/USU's work are ISOSPACEPAK (a modular Shuttle Small Payload experiment rack) and ISOSAT (a microspacecraft structure). These hexagon shaped elements serve as building blocks for the ISOBUS spacecraft concept.

ISOBUS pushes the frontier of Shuttle Small Payload applications. Circumventing the limitation posed by the 5 cubic feet user-volume of the single Get Away Special canister (GAS can), ISOBUS employs an assembly of GAS can compatible modules in order to achieve a more capable spacecraft (see Figure-1). Each ISOBUS module may be transported into orbit in a GAS can employing a sealed door assembly, or all the modules could be transported collectively in the Rockwell designed Orbitus carrier employing a mechanized door assembly. Once on orbit, the GAS cans or Orbitus carrier would be opened and the ISOBUS modules, sitting in vacuum and still electrically connected to the Shuttle's Aft Flight Deck (AFD), would undergo functional checks. Key ISOBUS modules with post-launch anomalies would be identified and could possibly be replaced by an on-board spare prior to spacecraft assembly. Assembly of the ISOBUS spacecraft from its individual modules would take place on an "assembly/spin table" employing the cross-bay Mission Peculiar Equipment Support Structure (also known as the GAS Bridge), or the Rockwell developed Lightweight Payload Carrier. On-orbit assembly tasks would be telerobotically performed using the Shuttle's Remote Manipulating System (RMS) with the newly developed Dexterous End Effector (DEE). The Servicing Aid Tool's (SAT) slave robotic arm may also be employed. Finally, an Interface Verification Test (IVT) of the completely assembled ISOBUS spacecraft would be achieved from the AFD to be followed by Shuttle deployment using the RMS-DEE or ejection by the assembly/spin table. The lower end of each ISOBUS module would employ a standardized electrical connector which satisfies interface requirements for on-orbit robotic servicing. The upper end of each ISOBUS module would employ a standardized mechanical interface for grappling by the DEE and perhaps the SAT. The sides of each ISOBUS module would employ standardized mechanical, electrical, and fluid connectors to interface with adjacent ISOBUS modules.

ISOBUS presents new approaches to maximizing Shuttle Small Payload utility. ISOBUS allows better utilization of the Shuttle's precious "real-estate." GAS cans, containing the ISOBUS spacecraft modules, could be mounted in various locations in the Shuttle's cargo bay between the primary payloads (off cross-bay bridge structures or the cargo bay side-wall). The Orbitus carrier option is also flexible and efficient by being compatible with any of bays 2 through 13 and occupying only one full bay. Compatibility of ISOBUS modules with the DEE for on-orbit robotic assembly would improve ground handling and installation of the ISOBUS modules just prior to launch. A ground support version of the DEE could be employed at the launch pad with a ground-based

robotic slave arm. The ISOBUS modules, like Line Replaceable Units (LRU), could be telerobotically slipped-in or changed-out of their GAS cans or Orbitus carrier just prior to launch. This provides flexibility and late payload access not only to the payload-user (i.e. for short-life biological specimens), but also to NASA's cargo integration discipline (i.e. for "Smart Ballast" installation). In addition, the LRU-like nature of the individual ISOBUS modules lends itself to externally mounted Space Station payloads, which can be delivered, installed, and removed using the Shuttle and its RMS-DEE. ISOBUS eliminates large complex integrated spacecraft structures which have to withstand launch vibration and loads; because the individual ISOBUS modules are packed, supported, and protected in their individual GAS cans or collectively in the Orbitus carrier. Lastly, the modular ISOBUS approach lends itself to faster and cheaper development of spacecraft, since each instrumentation package or system would be built by the corresponding contractor directly into the standardized ISOBUS module structure, then delivered to a payload depot at Kennedy Space Center for ground IVTs with other modules, and then launched and assembled on orbit.

The ISOBUS spacecraft would provide a versatile platform for diverse space users and sophisticated missions. Multiple principal investigators requiring lower levels of micro-gravity, cleaner vacuum environments, or longer stays on-orbit could have their individual experiments (each packaged in an individual ISOBUS module) assembled on-orbit into an ISOBUS cluster of experiments. This cluster would then be deployed away from the Shuttle for the duration of the mission (like Spartan) or left on-orbit for an extended stay (like LDEF). In either case, deployment and retrieval of such a cluster of multiple experiments should be cost-effective to both NASA and the experimenters. Other cost-effective applications for the ISOBUS are DoD strategic surveillance missions; civilian Earth observation missions; and with attachment of appropriate propulsion capability, lunar, near Earth objects (asteroids / comets), and perhaps interplanetary probe missions. Moreover, upon arrival at the mission's destination (i.e. a cometary tail or a planet) an ISOBUS spacecraft-cluster could separate into a network of individual science probes (each being an individual ISOBUS module).

ISOBUS introduces a new, innovative, "faster, better, cheaper" approach for space utilization and exploration, using our existing Space Shuttle Program and Shuttle Small Payloads infrastructure. ISOBUS also presents new commercial opportunities for standardizing various spacecraft subsystems for integration into ISOBUS modules (i.e. command & control, power, propulsion, navigation, instrumentation, data collection, communication, etc.). In essence, a large variety of ISOBUS modules could become available, providing cost-effective, off-the-shelf building blocks for future spacecraft. Lastly, ISOBUS provides NASA with an effective, near-term opportunity to gain experience and exercise on-orbit assembly tasks, serving as precursors to more complex future on-orbit assembly of spacecraft such as a manned Earth-to-Mars orbital transfer vehicle.

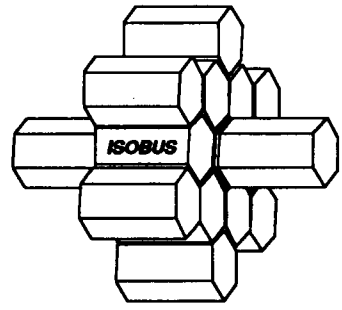

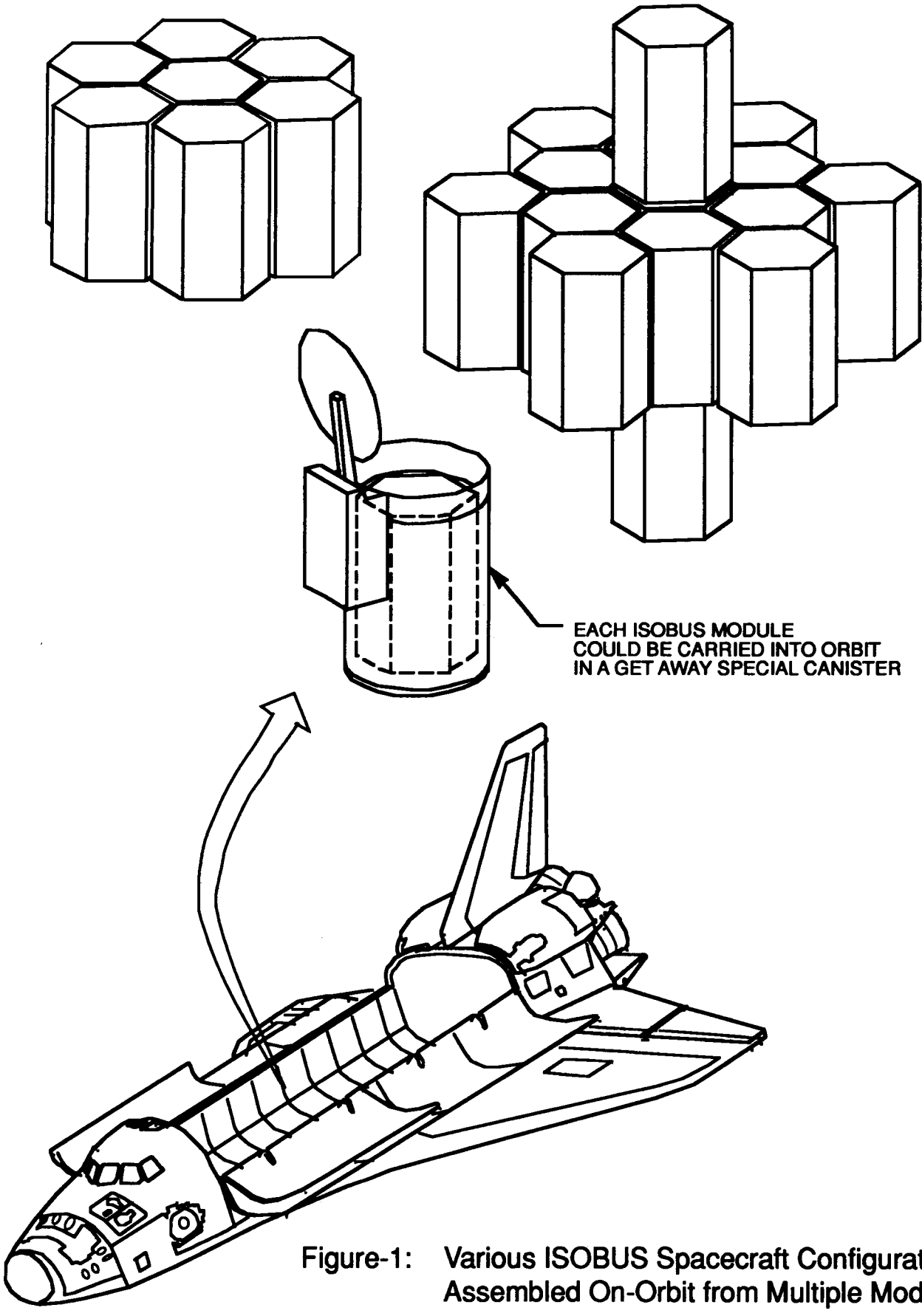

Figure-1: Various ISOBUS Spacecraft Configurations Assembled On-Orbit from Multiple Modules

TECHNICAL ABSTRACT

Radiation Hardened Microprocessor for Small Payloads

Paper classification: unclassified
Sponsored by: Naval Research Lab
Contract number: N00014-91-C-2005

Ravi Shah
MS19-4733
Harris Corporation
P.O. Box 94000
Melbourne, FL 32901

Summary

The RH-3000 program is developing a rad-hard space qualified 32-bit MIPS R-3000 RISC processor under the Naval Research Lab sponsorship. In addition, under IR&D Harris is developing RHC-3000 for embedded control applications where low cost and radiation tolerance are primary concerns. The development program leverages heavily from the commercial development of the MIPS R-3000. The commercial R-3000 has a large installed user base and several foundry partners are currently producing a wide variety of R-3000 derivative products. One of the MIPS derivative products, the LR33000 from LSI Logic, was used as the basis for the design of the RH-3000 chipset.

The RH-3000 chipset consists of three core chips and two support chips. The core chips include the CPU, which is the R-3000 integer unit and the FPA/MD chip pair, which performs the R-3010 floating point functions. The two support whips contain all the support functions required for fault tolerance support, real-time support, memory management, timers and other functions.

The Harris development effort had first passed silicon success in June, 1992 with the first rad-hard 32-bit RH-3000 CPU chip. The CPU device is 30 kgates, has a 508 mil by 503 mil die size and is fabricated at Harris Semiconductor on the rad-hard CMOS Silicon on Sapphire (SOS) process. The CPU device successfully passed testing against 600,000 test vectors derived directly on the LSI/MIPS test suite and has been operational as a single board computer running C code for the past year.

In addition, the RH-3000 program has developed the methodology for converting commercially developed designs to rad-hard designs utilizing logic synthesis techniques based on a combination of VHDL and schematic data bases.

Superfluid Helium On-Orbit Transfer (SHOOT) Flight Demonstration

Peter Shirron, Michael DiPirro and Jim Tuttle
NASA Goddard Space Flight Center
Code 713.1

Steve Volz
NASA Goddard Space Flight Center
Code 704.2

Neal Barthelme
NASA Goddard Space Flight Center
Code 740.3

Abstract

The Superfluid Helium On-Orbit Transfer (SHOOT) Flight Demonstration was an attached Shuttle payload mounted on a Hitchhiker cross-bay carrier which flew on STS-57 in June of 1993. SHOOT successfully demonstrated the handling and transfer of superfluid helium between two containers, called dewars, in low gravity. SHOOT was a class C payload and for the STS-57 mission was termed a complex secondary payload. The primaries were the retrieval of the EURECA carrier and a collection of modular experiments contained in SPACEHAB. Because the liquid helium was continuously boiling off, SHOOT's activities were scheduled for the first three days of the mission, concurrent with some SPACEHAB experiments, but well before the EURECA retrieval. Control of the SHOOT experiment was highly interactive and originated primarily from the Goddard Payload Operations and Control Center (POCC). Transfer and calibration activities required continuous command windows of up to 50 minutes duration and up to 80 minutes out of each orbit. Occasionally the crew controlled the experiment using the Payload General Support Computer (PGSC) when near-real time control and monitoring was required. SHOOT also placed considerable demands on the orbiter, including a pitch rotation of 3°/sec for 15 minutes, and translational burns using both the aft and forward RCS jets to generate accelerations up to 7 milli-g. The basis for these and other requirements will be discussed. Interaction with the crew and timing of crew activity during the mission will be detailed. The processing flow of SHOOT at Kennedy Space Center (KSC) will be described with emphasis on the tradeoffs for vertical, as opposed to horizontal, installation in the orbiter. Finally, some lessons learned will be presented relevant to future cryogenic and Hitchhiker payloads.

REPORT DOCUMENTATION PAGE

Form Approved
OMB No. 0704-0188

1. AGENCY USE ONLY *(Leave blank)*	2. REPORT DATE	3. REPORT TYPE AND DATES COVERED
	October 1993	Conference Publication

4. TITLE AND SUBTITLE

1993 Shuttle Small Payloads Symposium

5. FUNDING NUMBERS

Code 740

6. AUTHOR(S)

Lawrence R. Thomas and Frances L. Mosier, Editors

7. PERFORMING ORGANIZATION NAME(S) AND ADDRESS (ES)

Goddard Space Flight Center
Greenbelt, Maryland 20771

8. PEFORMING ORGANIZATION REPORT NUMBER

93B00119

9. SPONSORING / MONITORING ADGENCY NAME(S) AND ADDRESS (ES)

National Aeronautics and Space Administration
Washington, DC 20546-0001

10. SPONSORING / MONITORING ADGENCY REPORT NUMBER

NASA CP-3233

11. SUPPLEMENTARY NOTES

Lawrence R. Thomas: NASA Goddard Space Flight Center, Greenbelt, Maryland 20771.
Frances L. Mosier: Interstel, Inc., Beltsville, Maryland 20705

12a. DISTRIBUTION / AVAILABILITY STATMENT

Unclassified - Unlimited
Subject Category 12

12b. DISTRIBUTION CODE

13. ABSTRACT *(Maximum 200 words)*

The 1993 Shuttle Small Payloads Symposium is a combined symposia of the Get Away Special (GAS), Hitchhiker, and Complex Autonomous Payloads (CAP) programs, and is proposed to continue as an annual conference. The focus of this conference is to educate potential Space Shuttle Payload Bay users as to the types of carrier systems provided and for current users to share experiment concepts.

14. SUBJECT TERMS

Space Shuttle Small Payloads, Carrier Systems and Experiments--Past, Present, and Future

15. NUMBER OF PAGES
206

16. PRICE CODE

17. SECURITY CLASSIFICATION OF REPORT	18. SECURITY CLASSIFICATION OF THIS PAGE	19. SECURITY CLASSIFICATION OF ABSTRACT	20. LIMITATION OF ABSTRACT
Unclassified	Unclassified	Unclassified	UL